Durham E-Theses

The Crystallisation of Pharmaceuticals Using Tailored Supramolecular Gels

ANDREWS, JESSICA,LAUREN

How to cite:

ANDREWS, JESSICA,LAUREN (2020) *The Crystallisation of Pharmaceuticals Using Tailored Supramolecular Gels*, Durham theses, Durham University. Available at Durham E-Theses Online: http://etheses.dur.ac.uk/13647/

The Crystallisation of Pharmaceuticals Using Tailored Supramolecular Gels

A thesis submitted in partial fulfilment of the

requirements for the degree of

Doctor of Philosophy

In the Department of Chemistry at Durham University

By

Jessica Lauren Andrews

2020

Abstract

Due to ever increasing pressure for pharmaceutical companies to characterise and patent the polymorph landscape of new APIs, it is important that as many forms as possible are identified in the early stages of drug development. Novel polymorph screening techniques are required to expand the scope of traditional solution-phase methods, and access highly metastable or difficult to nucleate solid forms. This work exemplifies a modern polymorph screen, using a wide variety of experimental and computational methods to comprehensively characterise the polymorph landscape of mexiletine hydrochloride. Instead of the six forms described in previous literature, this screen revealed seven: an enantiotropic pair of anhydrous polymorphs that are stable at different temperatures, one anhydrous metastable form, three families of isostructural channel solvates, and a fourth solvate of unknown structure. Two new channel solvates, and new routes to three known forms were discovered by crystallising mexiletine within drug-mimetic supramolecular gels. As gelation was often turned off when a new polymorph crystallised within the gel, these changes in solid form are likely driven by strong interactions between the drug and gelator. The crystallisation of high temperature stable Form 2 from a gel at room temperature is a particularly striking example of the powerful stabilising effect of these tailored supramolecular gels. A complementary study into the gel-phase crystallisation of diatrizoic acid showed that the drug followed the same two-step crystallisation regime as the gelator, leading to the formation of two novel drug-gelator salt solvates. These results suggest that the polymorph landscape of the gelator has influenced the drug crystallisation, which may provide a new avenue of inquiry for the design of supramolecular gelators for pharmaceutical crystallisation. From this work, it is clear that supramolecular gels are a valuable tool for pharmaceutical polymorph screening.

Declaration

The work described in this thesis was carried out in the Department of Chemistry and the Department of Medicine, Pharmacy and Health at Durham University between October 2015 and April 2020, under the supervision of Professor Jonathan W. Steed, Dr Katharina Edkins, Dr David Berry of Durham University, and Dr James McCabe of AstraZeneca, Macclesfield. This work has not been previously submitted for a degree at this or any other university.

In Chapter 2, the Type A methanol solvate of mexiletine was first crystallised by Dr Stefanie Frietag-Pohl. Crystallographic data for the Type A solvent-free form and Type B EMK solvate were collected and processed by Drs Dmitry Yufit and Andrei Batsanov using beamline I19 of the Diamond Light Source synchrotron. Dr Andrei Batsanov also obtained the crystal structure of the Type A diethyl ether solvate. Dr Dmitry Yufit collected crystallographic data for the Type A solvates crystallised from methanol, DCM/hexane and 2-butanol/octane although, the crystal structures of the alkane solvates were solved and refined by the author. Dr Yufit also assisted in refining the crystal structure of Form 2. Solid-state NMR experiments were carried out by Dr David Apperley. The crystal structure prediction calculations were carried out by Dr Sten Nilsson Lill at AstraZeneca in Gothenburg, and high-pressure crystallography experiments were carried out by Dr Matthew Mulvee, in collaboration with Dr Michael Probert at Newcastle University. In Chapter 3, compounds **1** and **2** were first synthesised by Dr Stuart Kennedy, who also carried out gel screens of these molecules. SEM images of the xerogels of compounds **1** and **2** were collected by Dr Matthew Mulvee. Crystallographic data for the Type C 12,4-trchlorobenzene solvate were collected and processed by Drs Dmitry Yufit and Andrei Batsanov using beamline I19

of the Diamond Light Source synchrotron. Finally, in Chapter 4, the gelation behaviour of I-TPI was first discovered during a polymorph screen carried out by Emma Pearson. The crystal structures of Forms SI and SII of I-TPI were obtained by Dr Katharina Edkins. All other results are the product of independent work and investigation by the author.

Statement of Copyright

Funding

Publications

J. L. Andrews, E. Pearson, D. S. Yufit, J. W. Steed and K. Edkins, *Crystal Growth & Design*, 2018, **18**, 7690-7700.

Acknowledgements

On a personal note, I would like to thank my fellow students from the SOFI CDT, for an excellent first six months spent getting to grips with the world of soft matter, and for their continuing support over the years. Whilst there have been many highlights of my PhD, I am most grateful for the friends I have made along the way. In particular, I would like to acknowledge James, Brette, Amy, Lottie, Phil, Tash, Rebecca and Scott, whose friendship has given me solace more times than I can remember. I would like to thank my parents, Nic and Kath, my brother Jason, and my grandparents Gladys, Judith and Stan, whose unshakeable faith in me has, and always will be, the foundation which underpins my whole life. And finally, I would like to express my deepest gratitude to Dr Sarah Jordan and Frances Maw of Bishop Auckland Hospital, who are the only reason I did not surrender my scientific dreams to Crohn's disease.

This thesis is dedicated to my Grandmother, Judith. She was the first scientist I ever knew, and I am honoured to walk in her footsteps.

Table of Contents

1. Introduction

1.1   The solid-form landscape of small molecules

Famously defined by McCrone in 1965, the term polymorph refers to "a solid crystalline phase of a given compound resulting from the possibility of at least two different arrangements of the molecules of that compound in the solid state".[1] The term was first coined by Mitscherlich in 1822, during his study of the solid forms of various inorganic salts.[2] The first example of polymorphism in an organic molecule was benzamide, reported by Liebig and Wohler in 1832.[3] This compound has three known forms, which sequentially crystallise from solution in order of increasing thermodynamic stability.[4] The first crystal structure of benzamide was recorded in 1959, belonging to the stable form,[5] but the other metastable structures were not determined until 2005[6] and 2007,[4] following the development of more efficient X-ray diffraction techniques.

Other landmark discoveries in this field include the first reports of conformational,[7] disappearing[8] and concomitant[9] polymorphs, and increased understanding of the thermodynamics of polymorphism[10, 11] and the phase transitions between forms.[12] The application of polymorphism to pharmaceuticals[13] was a further catalyst that rapidly increased interest in this topic. Ground-breaking cases including ritonavir,[14, 15] aspirin[16-18] and the litigation surrounding Zantac's polymorphism[19, 20] led to the development of a wide range of modern theories, practices and applications of polymorphism.

In addition to anhydrous, crystalline polymorphs, there are a wide range of other structures that make up the solid-state landscape of a compound. If the molecules are arranged without any long-range order, the structure is described as amorphous.[21] Due to a lack of structural order, amorphous forms are significantly higher in energy than their crystalline counterparts. Coupled with very low intermolecular interactions within the structure, these properties make amorphous forms extremely soluble.[22] All other solid forms fall under the umbrella of crystalline, multi-component systems (Figure 1.1). There has been significant debate in the literature regarding the classification of multi-component systems, particularly in the context of pharmaceutical regulation.[23] Neutral multi-component crystals are termed solvates if one of the components was used as a solvent during the crystallisation. If the solvent is water, these structures are termed hydrates. When neither component is a solvent, multi-component crystals are called co-crystals.[24] Solvates, hydrates and co-crystals can exhibit different stoichiometries and degrees of interaction between the components. In some cases, the second component is an integral part of the structure with strong interactions between molecules, and a precise stoichiometry. In others, termed inclusion compounds, the components do not interact strongly and do not have a defined stoichiometry. One component is often accommodated in voids or channels within the crystal structure of the other and in some cases, the guest component is highly disordered. These two arrangements lead to very different physical properties.[25] In any of these multi-component systems, if the component molecules are formally charged, the structure is described as a salt. Ionic co-crystals, also known as co-crystal salts, are subtype of charged multicomponent crystals in which a cation, anion and another neutral molecule crystallise together.[26, 27] All types of multicomponent crystal

can also exhibit polymorphism, and there is therefore a very diverse landscape of possible forms to explore for a given compound.[24]

multicomponent crystal classification
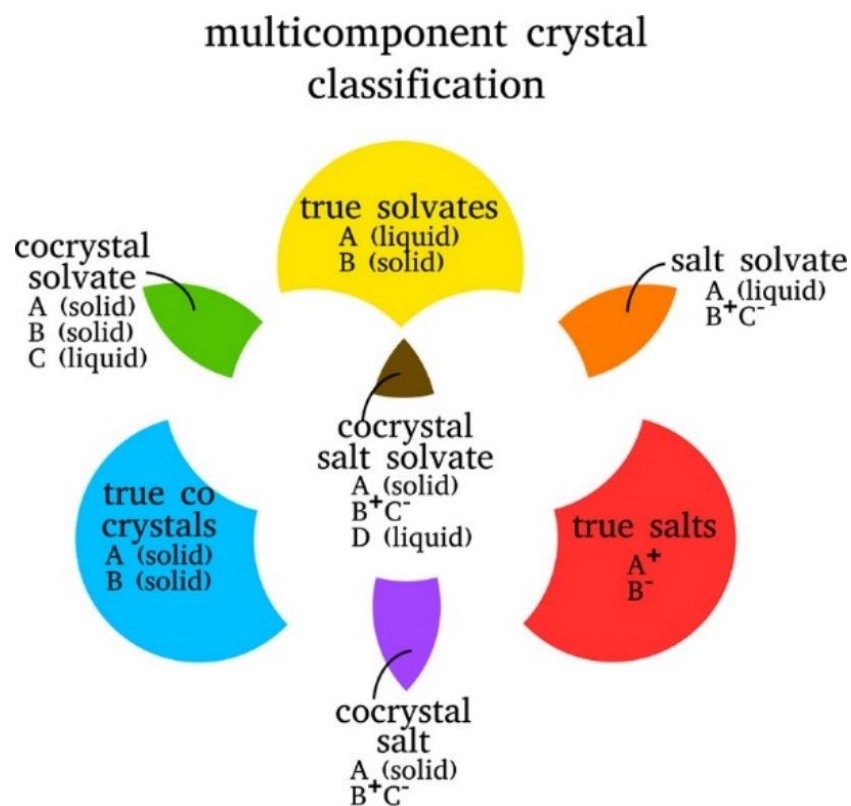
Figure 1.1: Proposed classification system for pharmaceutical solid forms by Grothe et al. Reproduced from reference 24 with permission. Copyright 2016, American Chemical Society.

1.2 Crystallisation Mechanisms

It is widely agreed that crystallisation occurs *via* two main steps: nucleation and growth. Nucleation refers to the aggregation of molecules into an ordered cluster large enough to overcome the tendency to re-dissolve. This step constitutes the spontaneous formation of a new phase, and therefore must occur under non-equilibrium conditions. In solution crystallisation, this means that the solution must be supersaturated.[28] There are two types of nucleation. Primary nucleation occurs where there are no crystals of the product initially present in the solution. It can be divided into two categories:

homogeneous, where nucleation is not influenced by the presence of added solids, and heterogeneous, where the rate of nucleation is increased by the addition of foreign particles. In practise, the former is rare due to the large energy barrier to spontaneous nucleation. Secondary nucleation is initiated by the presence of crystalline seeds in the solution.[29]

Classical nucleation theory assumes that nuclei are formed by the combination of individual molecules, one by one until the cluster reaches the critical radius (Figure 1.2). However, this model ignores the possibility that multiple sub-critical clusters may combine in order to form the nucleus, or that multiple molecules may incorporate at once.[28, 29] Two-step nucleation theory provides a more comprehensive model in which the molecules first aggregate into disordered, liquid-like clusters analogous to a colloid. In the second, rate-determining step, these clusters then rearrange to produce an ordered, crystalline nucleus (Figure 1.2). This model has since been supported by theoretical calculations, computation and experiments.[28, 30]
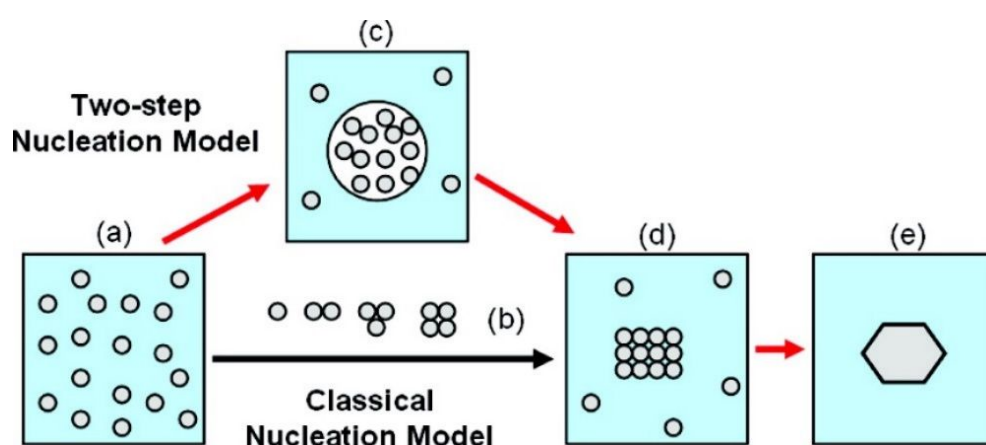
Figure 1.2: Classical and two-step nucleation pathways: (a) supersaturated solution; (b) ordered sub-critical cluster of solute molecules, proposed by classical nucleation theory; (c) liquid-like cluster of solute molecules, proposed by two-step nucleation theory; (d) ordered crystalline nuclei; (e) solid crystal. Reproduced from reference 28 with permission. Copyright 2009, American Chemical Society.

Once a stable nucleus has formed from a supersaturated solution, a macroscopic crystal begins to grow by continuously incorporating molecules from the solution into the lattice. There are several factors that influence crystal growth: the rate of diffusion within the solution, the rate of adsorption onto the surface of the crystal, and the surface energy of the crystal. Crystal growth occurs by the continual deposition of solute from solution into a loosely bound adsorption layer on the crystal surface, in which molecules are free to move over the surface of the crystal, before binding into the crystal lattice where attractive forces are highest.[31, 32] Therefore, the kinetics of crystal growth are controlled by which step is slower, the transport of molecules through solution to the face of the crystal, *i.e.* diffusion, or the incorporation of these molecules into the lattice, *i.e.* adsorption. Which of these is the slower, rate-determining step depends on the degree of supersaturation of the surrounding solution.[33] The morphology of the resulting crystal is controlled by its surface energy, as well as the kinetics of long-range transport processes within the solution. The equilibrium morphology of a crystal is the shape with the lowest possible surface energy and therefore, the minimum Gibbs free energy. This morphology can be derived from the classical Wulff construction although in reality, equilibrium morphologies are observed rarely, and the kinetically controlled growth morphology is more common.[34]

Classical nucleation theory states that the dominant factors determining the rate of crystal nucleation are temperature, interfacial tension, and degree of supersaturation. The importance of supersaturation indicates that there is a link between the solubility of a polymorph and its rate of nucleation.[29] The most thermodynamically stable polymorph has the lowest solubility in the surrounding liquid. Plotting the solubility curves of a compound's polymorphs reveals whether the system is enantiotropic or

monotropic (Figure 1.3). Two polymorphs are monotropic if their solubility curves do not cross each other. In this case, the one with lowest solubility is most stable. Conversely, the system is enantiotropic if the solubility curves cross at a transition temperature, Tr, lower than the melting point of the two polymorphs. In this case, the relative stability of the two polymorphs depends on the temperature and concentration of the solution.[35]
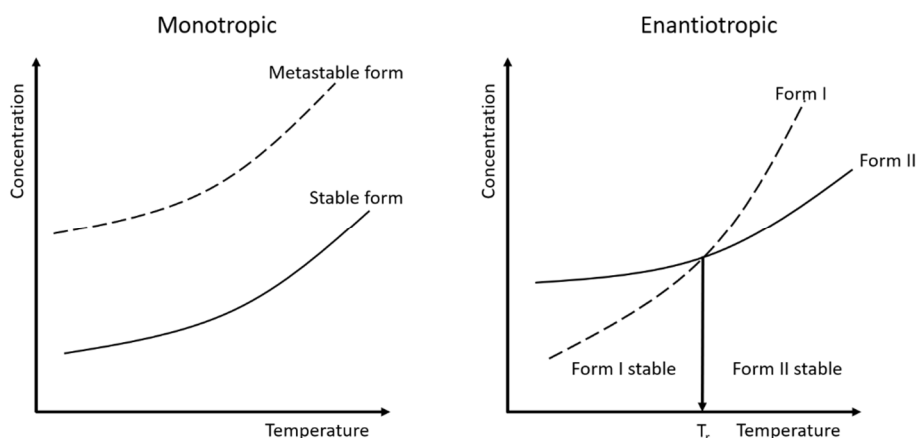
Figure 1.3: Solubility curves for a monotropic and an enantiotropic system.

This stability relationship means that, due to its lower solubility, a supersaturated solution of a given concentration will be most supersaturated with respect to the thermodynamic form. Thus, the critical nucleus size will be lower and the rate of nucleation will increase.[29] However, nucleation is a kinetic process, so in practise, this statement is not always true.[36] In fact, Ostwald's rule of stages says that a chemical system does not necessarily tend towards equilibrium, but towards the metastable state closest in energy to its current form. Therefore, crystallisation of the thermodynamic form occurs in steps *via* a series of metastable forms, with each step inducing a minimal change in free energy.[37, 38] This behaviour has often been observed experimentally.[39-41]

6

Solubility curves can also be helpful to understand the conditions under which nucleation is possible (Figure 1.4).
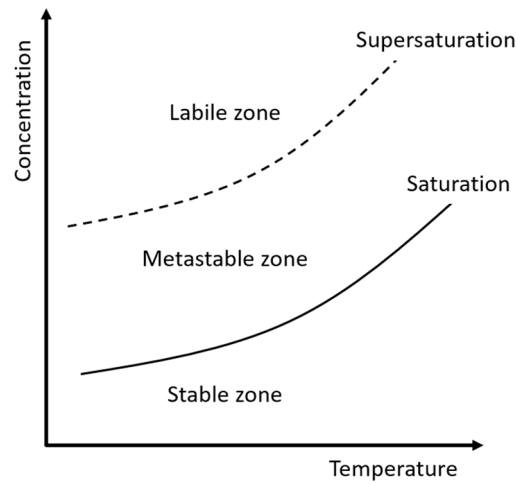
Figure 1.4: Schematic solubility and supersolubility curves for one crystal form.

Spontaneous primary nucleation is only possible in the labile zone. The number of nuclei formed corresponds to the proximity of the experimental conditions to the boundary of the labile zone (Figure 1.5). Few nuclei are formed close to the boundary, whereas many can be formed if the system is more supersaturated. Nucleation stops when the concentration crosses the supersolubility curve, and crystal growth then occurs in the metastable zone. Once sufficient solute has been incorporated into crystals, the system enters the stable zone where the crystal and solution are in equilibrium, and no further transformation occurs. The thermodynamic stability of the target polymorph dictates the most effective strategy for its production. Crystallisation of a thermodynamically stable form requires the system to remain at, or close to, equilibrium at all times. Few nuclei are formed by concentrating the solution just over the supersolubility limit, and the crystals are then allowed to grow slowly by gradual cooling of the solution, ensuring a lot of time is spent in the metastable zone. These are referred to as "thermodynamic conditions" and produce few, large crystals (Figure

1.5). Conversely, metastable forms are produced under "kinetic conditions", in which the system is far from equilibrium. In this method, the solution is highly supersaturated, producing many nuclei of the kinetic form, and then crash cooled, limiting the time in the metastable zone and preventing a transition into the thermodynamic form. These conditions typically produce a larger number of smaller crystals (Figure 1.5).[42, 43] In any crystallisation experiment, Ostwald ripening can take place after the first crystals have formed. In this process, smaller crystals dissolve and the solute molecules incorporate into the existing larger crystals, causing them to grow further, and often favouring the production of the thermodynamic form. This process reduces the surface energy of the system and therefore its overall free energy.[44]
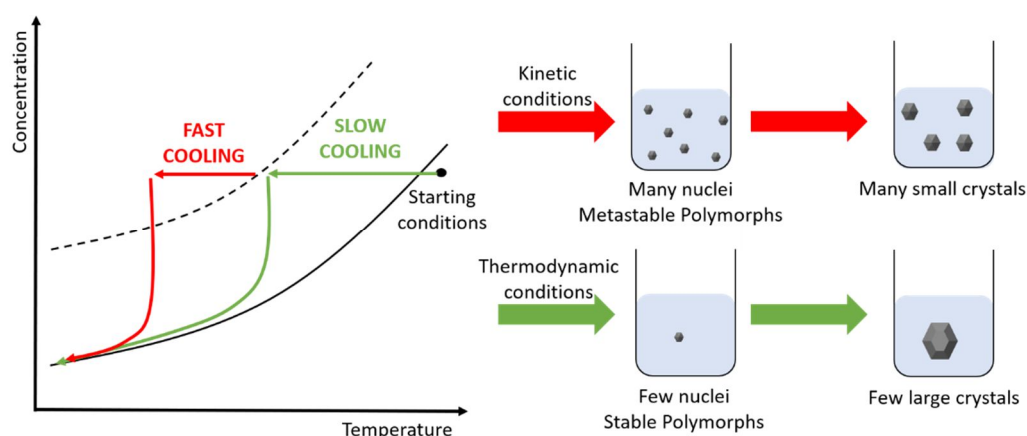
Figure 1.5: Thermodynamic vs. kinetic crystallisation.

Although there are numerous theories to describe the driving forces behind crystal growth and polymorphism, less is understood about the formation of solvates. A recent computational study suggests that the key criterion for solvate formation is the presence of a solute-solvent affinity, in excess of the solute-solute and solvent-solvent affinities. The affinity between solute and solvent does not have to be particularly high, so long as it is greater than the others. Even solvent-phobic molecules can be

encouraged to form solvates if this results in a decrease in Gibbs potential, due to an increased packing efficiency or high atmospheric pressure.[45]

1.3   Characterising solid form

As with any problem of structure determination, single-crystal X-ray diffraction remains the gold standard.[46] However, significant challenges are encountered in growing diffraction-quality crystals. Most common approaches to growing large single crystals involve crystallising the substance very slowly.[47] Clearly this method is unsuitable for metastable polymorphs because they will transform into a more stable structure over time.[48]

A more widely applicable method is powder x-ray diffraction (PXRD), which provides a unique fingerprint of a polymorph without demanding the growth of single crystals. This technique is appropriate for metastable forms as any crystallisation procedure can be applied, and the experimental run-time is relatively short, meaning that metastable forms have less time to transform.[48-51] In addition to the identification of different polymorphs, PXRD can also be used to quantitatively determine the degree of crystallinity and the composition of mixtures. This technique is particularly useful in the pharmaceutical industry because drug formulations are typically mixtures.[52]

Spectroscopic analyses such as infra-red (IR) and Raman give information on the chemical nature and environment of molecules in a crystal. They benefit from being non-destructive and highly sensitive to changing intermolecular interactions such as hydrogen bonds. However, their resolution is often insufficient to distinguish between polymorphs. If two polymorphs are distinguishable by spectroscopy, valuable kinetic

information can be gained by monitoring the spectral changes that correspond to the transition between forms.[48, 50, 51, 53]

Solid-state NMR (SS NMR) facilitates a more quantitative analysis. Although ^{1}H SS NMR is not feasible due to extreme line-broadening caused by homonuclear coupling, ^{13}C, ^{15}N and ^{31}P SS NMR allow precise compositional analysis of mixtures and can be used to distinguish between polymorphs. This technique can even be used to characterise an API within the final dosage form.[54-57]

The relative stability and transitional behaviour of a polymorphic system can be characterised using thermal techniques, predominantly differential scanning calorimetry (DSC) and thermogravimetric analysis (TGA). TGA records changes in the mass of a sample with heating. It is useful for characterisation of solvates and hydrates, as the mass deficit corresponds to the proportion of solvent originally incorporated in the crystal. Sublimation and decomposition can also be identified by a much larger mass loss. DSC measures the difference in power required to maintain a sample and a standard at the same temperature, which can be used to identify phase transitions within the sample, including melting, crystallisation, glass transitions, crystal-crystal transformations, and desolvation. These transitions appear as peaks in the DSC thermogram and the area under these curves corresponds to the enthalpy change of the transition. DSC is the predominant method used to establish the thermodynamic relationships between polymorphs.[48, 50, 51, 58, 59]

Hot-stage microscopy is often used in conjunction with thermal analyses and offers a quick and simple route to both the production and characterisation of polymorphs that are accessible by a change in temperature.[60, 61] Temperature cycling can be used to identify solvates, transition temperatures, stability relationships and crystallisation

kinetics, giving physical context to the thermodynamic data obtained by DSC. Similarly, structural information such as crystal habit and dimensions can be gained from observation of the crystals under crossed polarisers.[48, 50, 51]

1.4   Polymorphism in Pharmaceuticals

The polymorphs of a compound can display different physical and chemical properties including heat capacity, density, hardness, crystal habit, colour, thermal phase transitions, solubility, dissolution rate, stability and hygroscopicity.[62] In a pharmaceutical context, the majority of active pharmaceutical ingredients (APIs) are produced using some kind of crystallisation process, so controlling polymorphism is of particular importance to drug development. The uncontrolled emergence of a new solid form can significantly impair the processing, manufacture, storage, administration and efficacy of the drug as a result of different physical and chemical properties.[63, 64] Changing the solid form of an API can also be used to improve the performance of a formulation.[65] Modern drug candidates are often poorly water-soluble,[66] so using a different polymorph can overcome this problem without having to change the chemistry of the molecule.[67] Some drug polymorphs have been shown to display more than a four-fold increase in solubility compared to the least soluble form,[68] and amorphous forms can offer even more.[22]

A classic example showing the importance of polymorph control in pharmaceuticals concerns the HIV-protease inhibitor ritonavir, marketed by Abbott in 1996 (Figure 1.6). During development only one polymorph, the structure now termed Form I, was known. After two years on the market, Form II was discovered when the capsules began to fail quality assurance tests due to decreased solubility. The large difference in solubility between these two forms derives from a difference in crystal

packing.[14] The molecule adopts a different conformation in each form, and they are therefore termed "conformational polymorphs".[69] In Form I, the amide bonds are arranged in a trans conformation whereas in Form II they are cis. Due to a stronger hydrogen-boding network, the cis structure is more stable, and therefore less soluble. However, this form is extremely difficult to nucleate because it is preceded by an unfavourable conformation in solution, which explains how it remained undiscovered throughout the entire drug development process.[15] Due to the high thermodynamic stability of Form II, once it did nucleate, all samples of Form I began to transform into Form II, and this process was irreversible due to the formation of seeds of Form II throughout the manufacturing facility.[8] These difficulties resulted in the product being withdrawn from the market and reformulated, at an extremely significant cost and with widespread disruption to the treatment of HIV patients.[14] In 2003, a high-throughput polymorph screen of ritonavir identified five solid forms, three of which were previously unknown. It was also shown that a new solvate could easily be converted to the disappearing polymorph, Form I.[70] These results show the importance of thoroughly polymorph screening any new API before releasing it to market, to ensure the most desirable solid form is used, and any stability problems have been addressed.
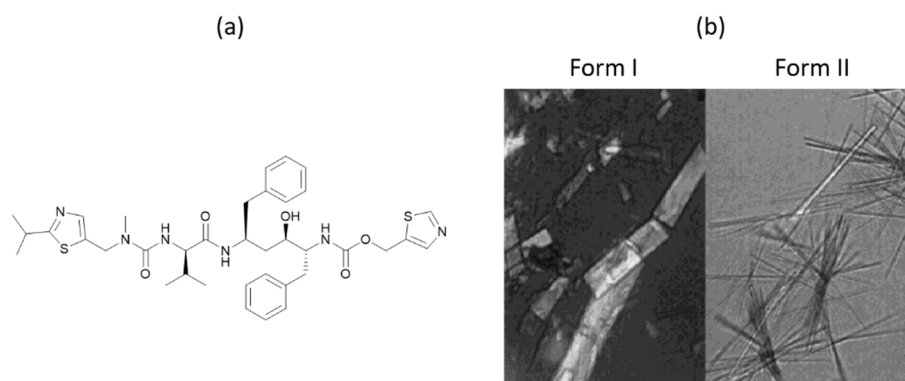
Figure 1.6: (a) The structure of ritonavir, and (b) crystals of Form I and II of ritonavir. Image (b) was adapted from reference 15 with permission. Copyright 2001, Springer Nature.

Ritonavir was the first example of this phenomenon to occur whilst a product was on the market, and it rapidly drew attention to the topic of drug polymorphism. As a result, significantly stricter regulations were implemented surrounding the production of polymorphic pharmaceuticals, and companies are now required to exhaustively screen the solid-form landscape of all potential drugs.[71, 72] Due to the Hatch-Waxman Act, which allows generic drug companies an expedited application process when reproducing a previously approved product,[73] pharmaceutical companies face significant pressure to legally protect their inventions. Given the increased regulatory requirements surrounding solid forms, it has become common practise for companies to patent not only the drug substance itself, but its individual solid forms. These patents can be extremely valuable, and infringement cases surrounding the polymorphism of competing formulations are common.[74]

In addition to the increased interest in drug polymorphism, there has also been a more recent focus on the use of co-crystals[75] and amorphous forms[76] to improve the properties of a pharmaceutical formulation. Novel drug candidates frequently suffer from poor water solubility,[66] so using a co-crystal[77-79] or amorphous form[22, 80] offers a route to improving the bioavailability of an API when none of its polymorphs have suitable properties. Traditionally, poor water solubility was overcome by formulating the API as a salt, so the use of other solid forms offers an alternative for molecules with no ionisable groups.[25, 81, 82]

A key method of increasing the bioavailability of poorly water-soluble drugs is to generate and maintain a supersaturated solution of the drug within the GI tract, a concept commonly described as the "spring and parachute" approach. The high solubility of the amorphous form generates a rapid increase in supersaturation of the

API, and this is termed "the spring". Excipients are then used to prevent crystallisation and maintain the supersaturated solution for long enough to allow the drug to be absorbed, and this is termed "the parachute".[83] This model can also be adapted to explain the increased solubility of pharmaceutical co-crystals (Figure 1.7). The co-crystal first dissociates into amorphous or nanocrystalline drug clusters, which exhibit extremely high solubility and provide "the spring". These clusters then transform into crystalline states of increasing thermodynamic stability, according to Ostwald's rule of stages. These transformations result in a gradual reduction in solubility, which maintains the supersaturated solution for as long as possible and allows more time for the drug to be absorbed. [84]
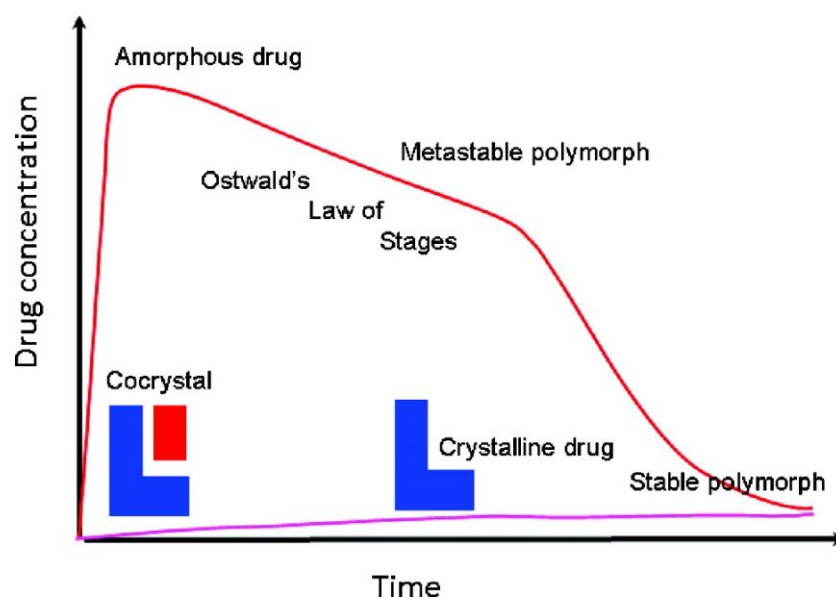
Figure 1.7: Dissolution profiles for a crystalline (pink) and co-crystalline (red) drug, showing the spring and parachute effect that is responsible for the greater solubility of co-crystalline pharmaceuticals. Reproduced from reference 84 with permission. Copyright 2011, American Chemical Society.

The first co-crystalline drug, Entresto, was launched by Novartis in 2015.[85] Since then, the FDA have developed new regulations regarding pharmaceutical co-crystals

that classify them as equivalent to a polymorph of the API for regulatory purposes.[86] This change has made the approval of co-crystalline drugs significantly easier and has encouraged the development of many of these formulations.[87, 88] Co-crystals containing multiple APIs are also emerging, and function as dual-purpose formulations[89] that have shown superior performance in early clinical trials.[90]

Amorphous drugs are thermodynamically unstable, and whilst this can be extremely beneficial for improving the solubility of an API, it also means they have a tendency to transform into a much less soluble crystalline polymorph. Therefore, amorphous drugs must be stabilised in order to ensure their properties remain constant throughout their shelf life. Stabilisation methods typically rely on the physical separation of drug molecules, which prevents them aggregating to form a crystal. Typical methods include the formation of solid dispersions with an inert matrix, coating the amorphous particles in a thin layer of an inert polymer, and adsorbing the amorphous material onto a porous substrate.[91-94] The presence of a secondary amorphous material, whose molecules are strongly bound to the drug by intermolecular interactions, can also provide a barrier towards recrystallisation by preventing the drug molecules from aggregating together. These are termed co-amorphous forms.[95, 96] Due to their inherent instability, there are very few drugs formulated as a pure amorphous API, but stabilised amorphous formulations are common and set to increase.[97]

Due to the direct relationship between the solid-form landscape of an API and its pharmaceutical properties, manufacturability, shelf life, patentability and financial value, there has been significant research into the understanding and control of pharmaceutical solid form. The end goal of this research is to predict and control the

solid form of a new API. Achieving this goal would ensure that a new pharmaceutical product contains the most desirable polymorph, and that the formulation is optimised to overcome any shortcomings in the properties of that solid form. A key area of research towards this goal concerns new polymorph screening techniques, which can be used to characterise the solid-form landscape of an API accurately and efficiently.

1.5   Traditional Polymorph Screening Techniques

The aim of any polymorph screen is to thoroughly explore the solid-form landscape of the target compound by recrystallisation under as many conditions as permitted by the available time, material and resources.[98] By varying experimental conditions, the speed of crystal nucleation[29] and growth[32] can be controlled, and the resulting crystals should represent a range of thermodynamic and kinetic products, ensuring the most suitable form can be selected for the desired application.

Solution crystallisation is the most common technique used in polymorph screening, due to its experimental simplicity. Typical solution-phase methods include cooling crystallisation, evaporation, and anti-solvent addition.[99] Although the nature of the solvent is often the dominant factor in determining the outcome of a crystallisation,[100-103] other parameters can also be varied to generate different solid forms, including the drug concentration, crystallisation temperature, the rate of cooling, evaporation or anti-solvent addition, the pH, and whether the system is agitated during crystallisation.[104-107] As a general rule, slow crystallisations involving mild conditions are more likely to yield a thermodynamically stable form, whereas, rapid crystallisations involving harsh conditions are more likely to produce metastable solid forms.[99] Metastable structures can be converted to the stable form by slurrying in an inert solvent *via* the process of solvent-mediated polymorphic transition. This

mechanism involves three consecutive steps. First, the metastable form dissolves in the solvent until its concentration exceeds the solubility limit of the stable form. At this point, the stable form spontaneously nucleates from solution and then begins to grow. The growth step occurs concurrently with dissolution and continues until the metastable form has completely transformed. This process can be used to transform a wide range of solid forms including polymorphs, solvates and salts, and can also be used to crystallise amorphous forms. As such, it is commonly used in polymorph screening to assess the stability of a particular form.[108, 109]

Mechanochemistry, or "chemical reactions that are induced by the input of mechanical energy", is another common technique for the production and interconversion of specific polymorphs (Figure 1.8). Although the definition encompasses reactions in any state of matter, the most common application of this method involves solid reagents.[110] There are two major mechanochemical techniques used in pharmaceutical solid form screening: neat and liquid-assisted grinding. On a small scale, these processes can be carried out in a mortar and pestle. In neat grinding, the pure solid reagents are ground together, whereas liquid-assisted grinding involves the addition of a small volume of solvent, which increases the rate of reaction by increasing the conformational freedom of the molecules and the opportunity for collisions between components.[111] On a larger scale or for greater efficiency, a ball mill can be used to undertake these reactions. There are a wide range of parameters that can be varied to change the polymorph obtained by mechanical grinding, including the stoichiometry of starting materials, the temperature, the volume and type of solvent, the grinding time, frequency and force, and for ball milling, the size, shape and composition of the ball.[112-115]
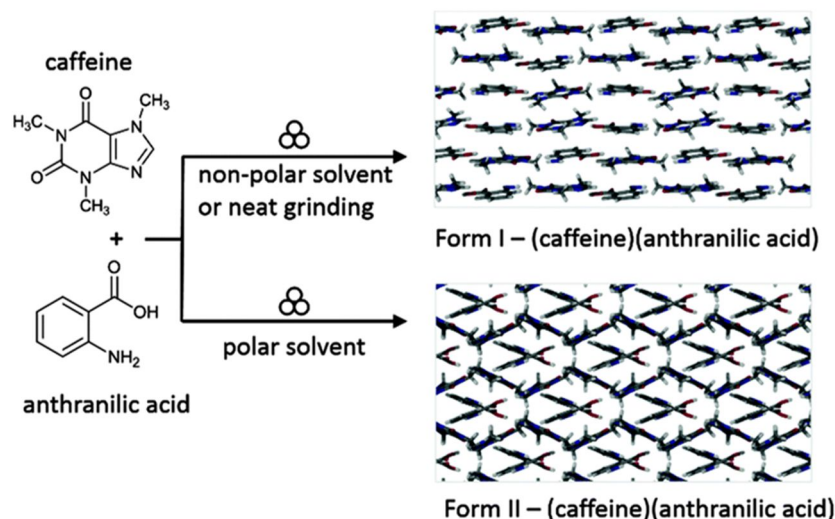
Figure 1.8: Forms I and II of the caffeine-anthrailic acid co-crystal produced by liquid-assisted grinding, originally published by Madusanka et al.[115] Image adapted from reference 110 with permission from The Royal Society of Chemistry.

Thermal techniques are crucial in polymorph screening, both for the characterisation and discovery of new solid forms. DSC and hot stage microscopy can be used to identify crystal-to-crystal transitions.[116] If the system is enantiotropic, there are two forms that are thermodynamically stable at different temperatures. The high temperature stable form can be obtained by heating the low temperature stable form above its transition temperature. If the system is monotropic, only one polymorph is thermodynamically stable at all temperatures. In this case, heating a metastable polymorph at any temperature will generate the stable form.[36] Thus, heating each known polymorph can be a valuable method of discovering new forms. Sometimes, the same crystal can be used for subsequent characterisation of the new polymorph but often, molecular reorganisation causes the crystal to crack.[117] A better-quality crystal can be grown using solution-phase methods at a temperature above the crystal-to-crystal transition temperature.[107] The applicability of this method is limited by the fact that the boiling point of the solvent must exceed the transition temperature so the solvent does not boil off.

If no suitable solvent can be found, sublimation provides an alternative method to access high temperature stable polymorphs (Figure 1.9). Approximately two thirds of all organic compounds display a direct transition from the solid to gas phase upon heating.[118] For these compounds, the vapour can recrystallize as a different polymorph. The polymorphic outcome of this crystallisation predominantly depends on the sublimation temperature. Other important factors include the heating rate, pressure, the presence or absence of solvent vapour, and the distance and temperature gradient between the sublimation and crystallisation surfaces.[99, 119]
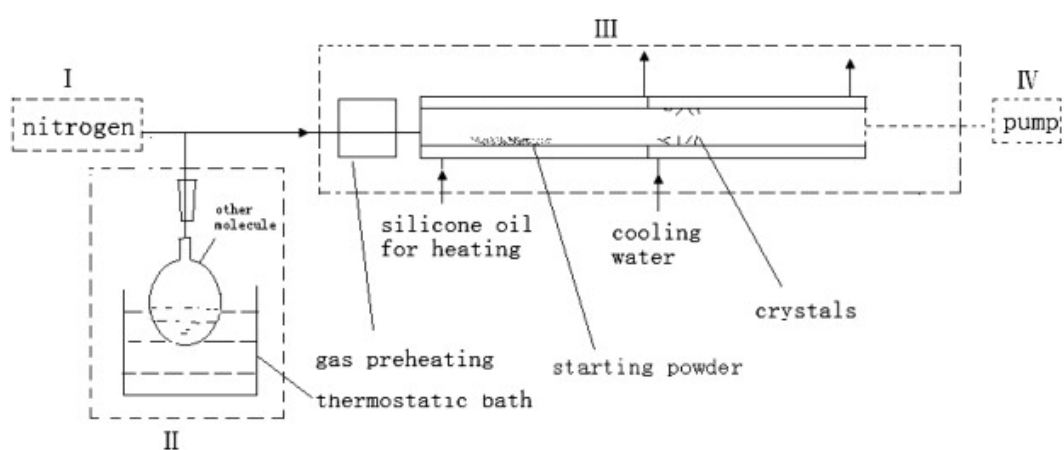
Figure 1.9: Apparatus used to selectively crystallise the two polymorphs of succinic acid both under a nitrogen atmosphere and in the presence of solvent vapour. Reproduced from reference 119 with permission. Copyright 2012, Elsevier.

In general, metastable forms are favoured by lower crystallisation temperatures, as the gas crystallises immediately upon contact with the cool surface, which kinetically traps the metastable structure.[37] Often, crystals grown by sublimation do not contain solvent because the sublimation temperature exceeds the boiling point of the solvent. This technique can therefore offer a route to pure forms of a compound that typically exists as a solvate. However, crystals formed by sublimation often have many defects and can be of low quality due to the high temperature causing increased molecular

motion. A slow growth rate and an extremely clean crystallisation surface (to decrease nucleation) can help to grow fewer, better-quality crystals.[120] For compounds that do not sublime, crystals can also be grown from the melt by controlled heating and cooling. As with sublimation, the polymorphic outcome is strongly influenced by the heating and cooling rate. Rapid cooling can kinetically trap metastable polymorphs, whereas slow cooling allows time for the molecules to reorganise into the thermodynamic form.[121] Cooling too quickly can entirely prevent the self-assembly of molecules into a defined crystal lattice and generate an amorphous form.[122]

Incorporation of these thermal techniques into the polymorph screen of an API can provide insight into the relative stability of the known polymorphs and facilitate the discovery of further high-energy forms. This knowledge is important to minimise the risk of an unwanted change in polymorph later in the product lifetime. Solvated forms are also common in pharmaceutical development, where the pure API has undesirable properties. It is therefore important to include experiments targeting these forms in a comprehensive polymorph screen. The stability of a solvate is dependent upon its environment therefore, changing its environment can bring about a change in solid form. For example, a solvate may be the most thermodynamically stable form whilst in contact with its solvent, but once removed from the liquor, the structure could become highly metastable, causing it to transform. Important variables in solvate stability include the nature and concentration of solvent in the environment, the temperature, pressure, and for hydrates, the relative humidity.[123] Solvated and anhydrous polymorphs can be interconverted by varying these parameters to either add or remove solvent from the structure.

The most obvious method of hydrate formation is crystallisation from water,[124] but this is not always possible due to poor water solubility. An alternative method is to crystallise a metastable polymorph from an organic solvent and to expose it to water vapour to initiate a transformation to the more stable hydrate. This transition can sometimes be reversible, in which case the anhydrate is re-formed by heating the hydrate to remove water.[125] Solvate formation is an analogous process and can be achieved directly by crystallisation from the desired solvent. Other forms can also be transformed into a solvate by slurrying in the solvent or exposure to its vapour.[126] Solvent molecules can be removed from solvates and hydrates by heating the material, exposing it to reduced pressure or decreasing the relative humidity. Depending on how the solvent is incorporated into the crystal structure, the desolvate may sometimes retain the structure of the solvate (Figure 1.10). These structures are often highly metastable due to the loss of stabilising intermolecular interactions with solvent molecules, and the introduction of voids within the structure.[127] It is common for desolvates to retain a structure analogous to that of the solvate,[128] but this is not necessarily the case, and they can adopt completely different packing arrangements. Desolvation, especially when done very quickly, can also generate amorphous forms when the crystal structure permanently breaks down following the removal of stabilising solvent molecules.[129]
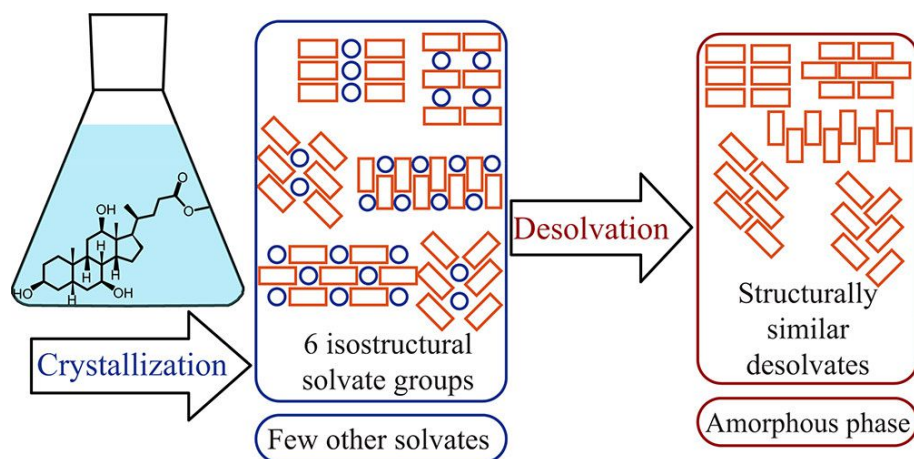
Figure 1.10: Crystallisation of desolvated forms of methyl cholate that bear a structural resemblance to their solvated analogues. Reproduced from reference 128 with permission. Copyright 2017, American Chemical Society.

A pharmaceutical polymorph screen typically incorporates a selection of experiments from each of these areas to address all aspects of the solid-form landscape and give a reliable estimation of the API's behaviour under a range of conditions. The most simple and reliable experiments are often selected to give a comprehensive characterisation using as little time and material as possible. However, there is a range of more sophisticated crystallisation techniques that can be used to access highly metastable or difficult to nucleate solid forms that may not be accessible using traditional methods. As these modern methods develop, it is likely they will become more common in industry, widening the scope of current polymorph screening methodology.[130]

1.6   Modern Crystallisation Techniques

In the pharmaceutical industry, the most favourable of an API must be identified as quickly as possible to minimise delays in marketing the product. For this reason, it is important to develop efficient polymorph screening techniques. The largest development in this field has been the advent of automated, high-throughput screening techniques. Although they are predominantly applied to the discovery of novel polymorphs, these methods can also be used to characterise a wide range of solid forms including salts, hydrates, solvates and co-crystals. A high-throughput crystallisation system typically consists of hardware and software that is used for the design of experiments, handling of materials, execution of crystallisation protocols, characterisation of results, and analysis of data.[131] They typically rely on the same solution-phase crystallisation techniques as traditional polymorph screening, but high-throughput systems can rapidly access a larger parameter space using less material. This method is significantly more efficient and can generate a wider range of solid forms.[132] The small sample size required for high-throughput screening makes it particularly suitable for the early stages of pharmaceutical development. However, the wide range of accessible parameter space means a large library of data can be generated for the target API, allowing the successful crystallisations to be optimised and scaled up for subsequent stages of development.[133-135]

In addition to solution-phase methods, there are several alternative techniques to control the polymorphic outcome of a crystallisation. Based on the suggestion that different polymorphs form structurally distinct nuclei,[136] many techniques focus on controlling the nucleation step of the crystallisation. Homogeneous or soluble additives can promote, impede or inhibit the nucleation of a particular form, and

determine which polymorph is produced.[137] Polymorph selection can be achieved by a range of different mechanisms, and more than one is generally observed in each crystallisation. Common mechanisms include influencing the structure of a pre-nucleation cluster, stabilising a particular nucleus once it is formed, and promoting the growth of one crystal face over another in order to influence the resulting crystal habit (Figure 1.11).[138, 139] The strength of interaction between the solute and the additive is a key factor in determining its ability to influence nucleation. The additive must be able to disrupt the formation of solute clusters and therefore requires a strong interaction with the solute. Often, this interaction is achieved by mimicking a structural feature of the solute in the additive.[140] In addition to polymorph selection, additives can also be used to influence the habit, solvent content and stereochemistry of a crystal, all of which are extremely important in determining the physical and chemical properties of the resulting material.[141, 142]
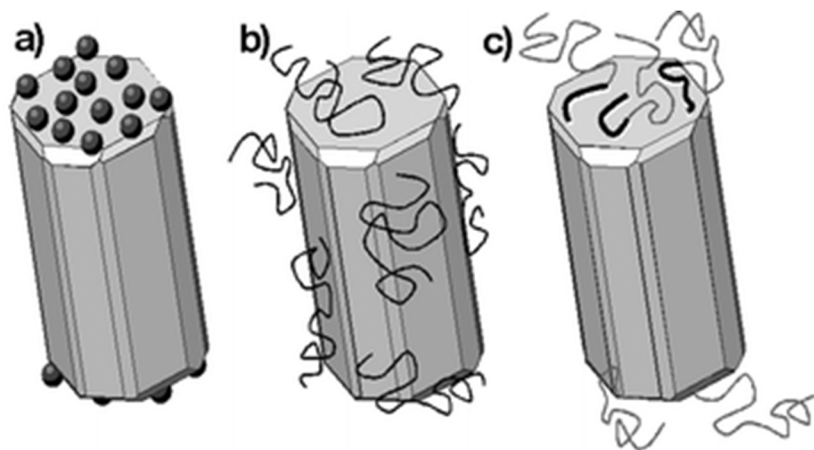
Figure 1.11: Schematic diagrams to show the adsorption of various face-selective, soluble additives onto a crystal. (a) The specific adsorption of ions of low molar mass additives, (b) the unspecific adsorption of polyelectrolytes and, (c) the specific adsorption of block copolymers with a short polyelectrolyte block. Reproduced from reference 139 with permission from The Royal Society of Chemistry.

As well as homogeneous systems, the addition of heterogeneous impurities has been shown to offer polymorph control *via* selective nucleation of a specific form. Seeding a supersaturated solution with crystals of the target form is a well-known method of polymorph control that is commonly used in large-scale manufacture. The polymorphic purity of the seeds is an extremely important factor in determining the success of this technique, as a small trace of an unwanted polymorph can induce crystallisation of that form.[143] This problem is particularly serious if the seeds are introduced unintentionally, as was the case with ritonavir.[15] However, simply adding seeds to any crystallisation is not sufficient to generate the desired polymorph reliably and with high purity. Instead, the conditions must be tightly controlled to ensure that the secondary nucleation rate of the desired form exceeds the primary nucleation rate of any unwanted forms.[144] In addition to seeding with crystals of the solute, the same effect can be produced using a different compound that is isostructural with the desired polymorph.[145]

A range of other heterogeneous additives can also be used to initiate nucleation and exert control over the polymorphic outcome of a crystallisation. Most commonly, these additives are insoluble polymer beads (Figure 1.12). The ability of the polymer to initiate nucleation is determined by the complementarity of the surface and the solute. Hence, the nature of the polymer is tailored to the structure of the solute and the crystallisation conditions. This specificity requires the use of large libraries of chemically diverse polymers, often accessed using combinatorial synthesis.[146, 147] Studies report the use of this method for polymorph-selective crystallisation of various drug compounds, even accessing a previously unknown form of cabamazepine.[146-148] Some homogeneous additives that were successful in controlling nucleation can subsequently be polymerised to produce effective heterogeneous additives, and this

can simplify the process of identifying useful polymers.[149] Phase-selective nucleation has also been observed using other additives including porous frameworks and functionalised glass surfaces. Once again, the polymorphic outcome is directed by the surface chemistry of the substrate.[150, 151]

Figure 1.12: Form II, the metastable orthorhombic polymorph of acetaminophen growing from isotactic polypropylene beads. Reproduced from reference 147 with permission. Copyright 2002, American Chemical Society.

When using a heterogeneous additive, whose crystalline structure complements that of the solute, the energy barrier to nucleation is lowered due to a reduction in the interfacial free energy required to form a new solid phase. The product grows as a crystalline film on top of the substrate, and this process is termed epitaxy.[152] Polymorph selection can be achieved using this method because interaction with the substrate promotes ordering of molecules within a pre-nucleation cluster. This behaviour is thought to derive from one of two mechanisms. Either the lattice parameters of the substrate could match those of one polymorph of the solute, or a topological feature on the surface could mirror those of a specific solid form. Either mechanism would lead to preferential growth of the polymorph whose structure

matches that of the surface.[153, 154] If a chiral surface is used as a template, it is even possible to achieve enantioselective crystallisation.[155]

Instead of incorporating an additive into the crystallisation, it is also possible to influence nucleation and control polymorphism by physical methods. Nonphotochemical laser-induced nucleation is used to induce crystallisation by exposing a supersaturated solution to laser light. This method is most commonly applied to small organic molecules, and although the exact mechanism is unknown, it is thought that molecules within existing pre-nucleation clusters align with the applied electric field, which reduces the entropic barrier to crystallisation. The pre-nucleation clusters corresponding to each polymorph may also have different polarisabilities, which means they will align differently with the electric field, and thus the polymorph with best alignment will crystallise preferentially. This theory is supported by the fact that the resulting polymorph is dependent on the polarisation of the incident light.[156]

Another common strategy is to carry out the crystallisation in a confined space. A glass capillary can serve as a simple crystallisation vessel in which traditional solution-phase techniques can be carried out in a small volume (Figure 1.13). Often, these confined crystallisations are used to produce metastable solid forms, which may not be accessible using other methods. There are two mechanisms behind this effect. Firstly, the small volume limits convection and provides a quiescent environment in which the nucleation rate is low. As a consequence of reduced nucleation, the supersaturation increases and permits nucleation of metastable solid forms. At this elevated concentration, Ostwald ripening is suppressed, as there is sufficient solute to allow the growth of multiple forms without the stable form progressing at the expense of the others.[157, 158]
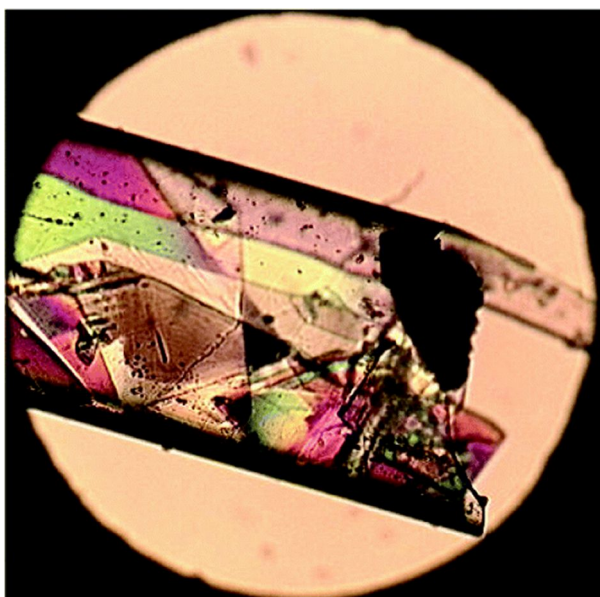
Figure 1.13: Capillary grown crystals of a novel polymorph of nabumetone, Form II. Reproduced from reference 158 with permission. Copyright 2002, American Chemical Society.

A recent study reports a novel confinement technique in which an inert oil is used to encapsulate a nanolitre-sized droplet of a concentrated analyte solution. The oil coating leads to slow, controlled evaporation of the solvent and a very gradual increase in concentration, up to the point of supersaturation. Due to the very limited droplet size, nucleation is reduced, and both of these factors promote the growth of high-quality single crystals (Figure 1.14). This technique has been used to crystallise fourteen structurally diverse substrates, most notable of which are the crystallisation of the agricultural fungicide dithianon, which was previously thought to be "uncrystallisable", and the discovery of a thirteenth polymorph of ROY, which was not predicted by any simulation. The extremely low mass of analyte required for each crystallisation makes this technique well-suited to high-throughput screening, which allows a wide parameter space to be accessed using very little material.[159]

Figure 1.14: Encapsulated nanodroplet crystallisation of ROY: (a) solution of solvated analyte under oil, (b) evaporative solvent loss to supersaturation, (c) onset of crystal growth, and (d) crystallisation complete. Adapted from reference 159. Use permitted under the Creative Commons Attribution License (CC BY-NC-ND 4.0).

Microemulsion crystallisation is a similar technique in which droplets are used for confinement. However, in this case the thermodynamic form can be crystallised preferentially. Within the small volume of an emulsion droplet, the supersaturation will decrease significantly with the formation and growth of a nucleus, which leads to a minimum in the free energy, F_{min}, at a particular radius, r_{min}. If the crystallisation conditions are tightly controlled to ensure F_{min} is below k_BT (k_B = Boltzmann constant, T = temperature) for only the stable polymorph, then any viable nuclei above size r_{min} will correspond to this form, and only the stable form will grow (Figure 1.15).[160] Selective crystallisation of the thermodynamic form of various organic molecules has been reported using this method, including the antibiotic drug isoniazid.[161-163] Aside from microemulsions, small liquid droplets produced by techniques such as inkjet printing can also offer polymorph control. However, these droplets are typically on the picolitre scale and are therefore too large to give thermodynamic control, like in a microemulsion. In this case, the metastable polymorph is produced most often due to size limitation of the growing nucleus.[164]
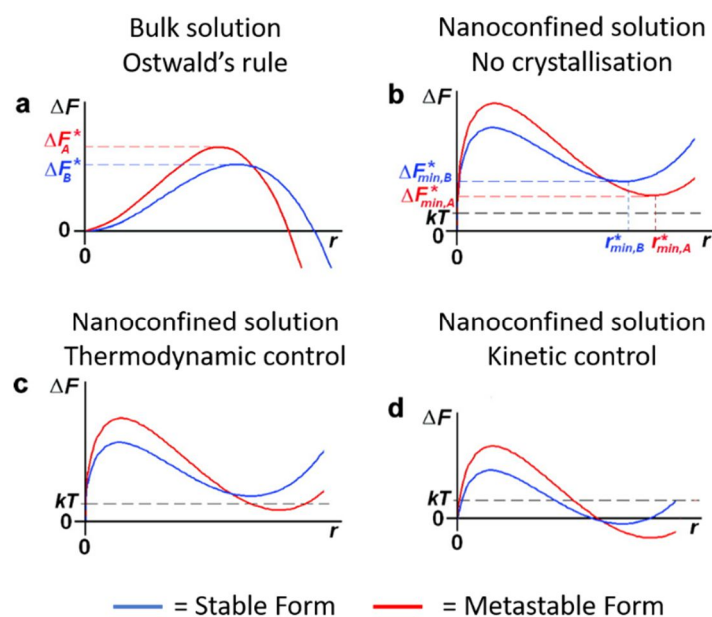
Figure 1.15: Representative plots of free energy vs. nucleus size for systems crystallizing from (a) bulk solution and (b), (c), (d), a 3D nanoconfined solution. Adapted from reference 160 with permission. Copyright 2011, American Chemical Society.

A similar effect can also be achieved by nanoconfinement within a range of porous structures such as polymer gels, mesoporous silicas, controlled pore glass, self-assembled polymer matrices and etched plastics. The properties of the pores can be tuned to preferentially deliver either stable or metastable crystal forms. Systems with pore dimensions close to the radius of a critical nucleus can crystallise one polymorph preferentially because the nuclei of each form differ in size. Similarly, the large surface area of these materials offers significant opportunity for heterogeneous nucleation using the pore walls, which can be functionalised to favour one particular form. Finally, at the nano scale, the relative stability of a given polymorph has been shown to depend on the size of the crystal and thus, limiting the crystallisation volume can lead to polymorph selectivity.[165, 166]

Patterned self-assembled monolayers (SAMs) allow the formation of a highly specific microenvironment, with tightly controlled dimensions and chemical

functionality. These factors allow control over the nucleation and growth of a crystallising substance. A SAM consists of an organic monolayer, which is spontaneously adsorbed onto a surface in an organised array. Each molecule contains a head-group, which anchors it to the surface, and a tail-group, which is functionalised to interact with the solute.[152] Often, long-chain thioalkanes are attached to a gold surface to form a SAM, *via* a sulphur-gold covalent bond.[167] In these systems, polymorph control occurs by a range of mechanisms. The pattern, density, and size of structural features on the surface of a SAM, in addition to the chemical functionality of the tail groups, can all be tuned to alter the way in which the solute interacts with the surface. As a result, the structure of pre-nucleation clusters and post-critical nuclei, the local supersaturation within surface features, the rate of nucleation, and the orientation and dimensions of growing crystals can all be adjusted to facilitate control over polymorphic form. This technique is particularly valuable because it allows the production of many identical crystals (Figure 1.16).[152, 168-171]
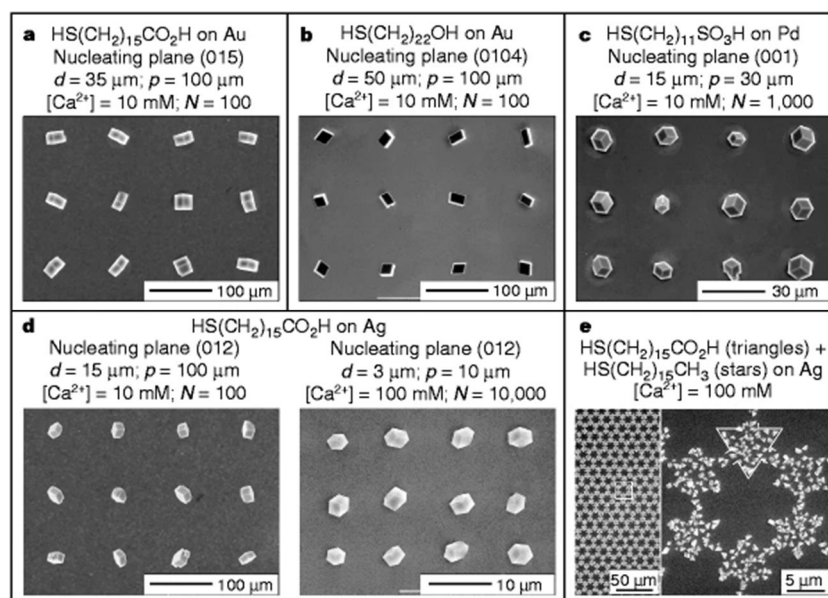
Figure 1.16: Ordered 2D arrays of calcite single crystals grown on patterned, self-assembled monolayers. Reproduced from reference 169 with permission. Copyright 1999, Springer Nature.

In addition to the development of more efficient experimental techniques such as high-throughput screening, there has also been significant effort towards the improvement of theoretical techniques such as crystal structure prediction. Crystal structure prediction aims to calculate the crystal structure of a molecule, starting from its chemical structure. There are many different approaches, but the most common is to calculate the lattice energy of all possible crystal-packing arrangements. The one with the lowest energy is the most likely crystal structure, and any arrangements with comparable energies are possible polymorphs. This strategy includes three main steps: firstly, building a three-dimensional model of the molecule from its chemical structure, secondly, calculating all possible close-packed structures and finally, calculating the lattice energy and physical properties of each of these structures to determine which are most likely.[172] The wide range of alternative methods to achieve crystal structure prediction were displayed in the most recent CCDC Blind Test, which received the largest number of entries to date. All five target structures were successfully predicted despite being extremely challenging targets, which is testament to the significant progress that has been made in this field.[173]

In the pharmaceutical industry, accurate crystal structure prediction would be an extremely useful tool to support experimental polymorph screens by suggesting whether a molecule is likely to be polymorphic and if so, which experimental conditions are required to access those forms.[174, 175] Whilst there has been some progress towards this goal, particularly in calculating the likelihood that a stable form has been missed by an experimental screen,[176] computational methods struggle to model flexible molecules, high Z' structures and multi-component systems, and continue to predict more forms than can be found experimentally.[177] One reason that not all predicted forms crystallise experimentally is that they do not nucleate under

standard conditions. To combat this, a templating approach can be used in which the crystallisation is seeded using a crystal of a different compound, whose packing is isostructural with the predicted form. This method has been used to discover new forms of carbamazepine[178] and tolfenamic acid,[179] which shows that the combination of experimental and computational techniques can be extremely powerful. Current pharmaceutical polymorph screens typically utilise this combination of theory and experiment,[180-182] but as crystal structure prediction becomes increasingly advanced, it is likely that computational methods will play a larger role, as shown by the increasing development of in-house CSP methodologies by large pharmaceutical companies.[183]

1.7   An Introduction to Supramolecular Gels

Gels are applied in many fields, including medicine, food and materials science, finding diverse applications from simple commercial products such as shampoos and shower gels to high-tech, stimuli-responsive gels. The widespread use of these materials derives from their unique physical properties. Sitting on the boundary between a liquid and a solid, gels are able to support their own weight but can also flow or deform under stress.[184] The term "gel" was defined by Flory as "a two component, colloidal dispersion with a continuous structure with macroscopic dimensions that is permanent on the time scale of the experiment and is solid-like in its rheological behaviour".[185, 186] Gels are composed mostly of a fluid phase, supported by a solid-like network, formed by the aggregation of gel-forming or gelator molecules. The fluid phase is most often a liquid, including water, organic solvents and ionic liquids, which produce hydrogels,[187] organogels[188] and ionogels,[189] respectively. Alternatively, gels can contain a gas, which are called aerogels.[190] These

are not to be confused with xerogels, which are formed by the removal of solvent from a gel by evaporation.[191, 192]

Gels are traditionally polymer-based,[193-198] but more recently, supramolecular or low molecular weight gelators have come to the fore.[188, 199-201] Supramolecular gels are formed through the self-assembly of gelator molecules into one-dimensional fibres[187] or scrolled sheets[202] (Figure 1.17). These molecular architectures are termed the primary structure of the gel[187] and can often be modelled by the supramolecular motifs in the crystal structure of the gelator.[203, 204] Indeed, a recent study has shown that successful gelators typically produce high aspect-ratio crystals, suggesting that molecules preferentially assemble into one-dimensional supramolecular architectures.[205] These molecular aggregates come together to form nanoscale fibrils, which entangle to give the three-dimensional gel network: the secondary and tertiary structures of the gel, respectively (Figure 1.17).[187] This network immobilises the solvent by surface tension, producing a solid-like material despite the very high dilution of the system.[206] It is extremely difficult to characterise the secondary and tertiary structures of a gel because of their small size and dynamic nature. Their properties are therefore approximated from the bulk properties of the material, using techniques such as rheology, electron microscopy, spectroscopy and calorimetry.[207] Supramolecular gels have found applications in diverse fields by virtue of their tuneable properties, reversibility, and response to external stimuli.[201, 208-213]
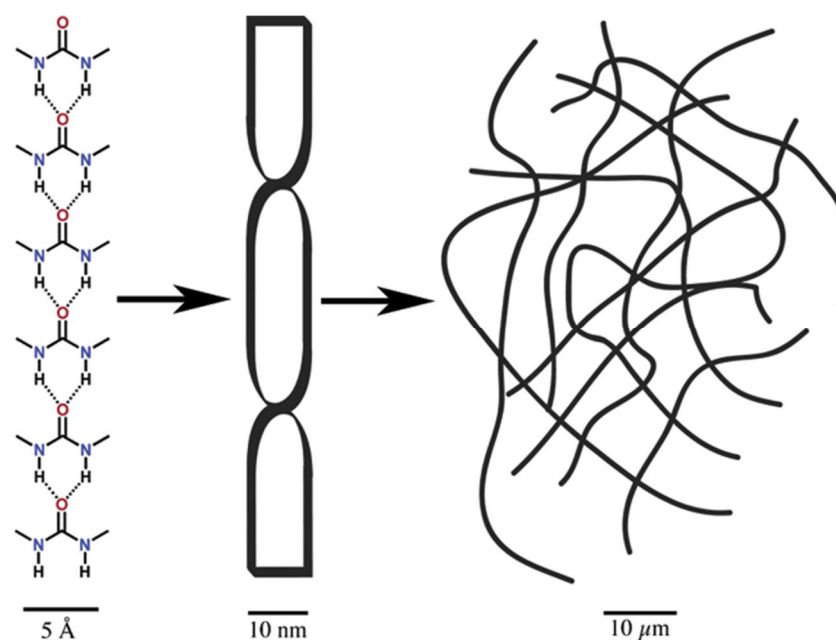
Figure 1.17: The primary, secondary and tertiary structure of a supramolecular gel. Reproduced from reference 187 with permission. Copyright 2004, American Chemical Society.

Supramolecular gelation is promoted by uni-directional non-covalent interactions between molecules, which drive the formation of one-dimensional fibres. In a technique akin to crystal engineering, structural motifs that self-assemble into known supramolecular synthons can be incorporated into gelator molecules to tune gelation behaviour.[214, 215] These synthons are based on a variety of non-covalent interactions including halogen bonding,[216-218] halogen-halogen interactions,[219, 220] π-stacking,[221-223] and coordination interactions,[224-226] but by far the most common is hydrogen bonding. Amides and ureas are commonly used building blocks that form low molecular weight gels due to their strong, directional hydrogen bonds.[227] In amide-based gelators, molecular stacking is driven by NH⋯O=C hydrogen bonds.[228-232] Incorporating an extra NH group to produce urea-based gelators typically strengthens this interaction, resulting in stronger gels.[233, 234] Urea groups form intermolecular hydrogen bonds between the carbonyl oxygen in one molecule, and the two NH groups in another. This interaction encourages linear stacking of molecules

35

into the so-called α-tape arrangement, which promotes the formation of one-dimensional fibres and encourages gelation (Figure 1.17).[235, 236] By increasing the number of amide or urea groups in a molecule, this interaction can be strengthened, meaning bis-ureas and bis-amides are often better gelators than their mono-functionalised equivalents.[233, 234, 237-240] An anti-parallel arrangement of urea groups has been shown to further enhance the gelation behaviour of bis-ureas. The arrangement of the urea groups is influenced by the structure of the linking group that connects them. In a homologous series of alkyl-linked bis-ureas, gelation was shown to alternate with the number of methylene groups in the linker (Figure 1.18). Odd-membered chains did not gel, whereas even-membered chains did, because the linker ensured that the urea groups were anti-parallel.[241]

Figure 1.18: Alternating gel (even n) and sol (odd n) formation in a series of alkyl-linked bis-urea gelators. Reproduced from reference 241 with permission from The Royal Society of Chemistry.

Whilst structure-property correlations of the gel-forming groups have been widely studied, less is known about the impact of the linking groups or the peripheral functionality known as end-groups. In urea-based gelators, intermolecular hydrogen bonds can be promoted over intramolecular ones by the incorporation of a methylene group between the urea and the end-group (Figure 1.19). The addition of the methyl group reduces steric hindrance around the carbonyl oxygen atom, which encourages the formation of the α-tape arrangement, known to support gelation.[242]
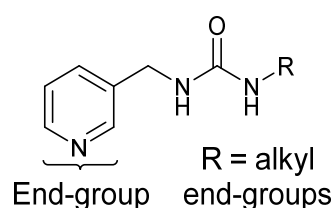
Figure 1.19: Structure of the gelators investigated by Offiler et al.[242]

Similar behaviour has been observed in a series of N-aryl-N′-alkyl urea gelators, in which intramolecular hydrogen bonding between the aryl group and the urea group inhibited gelation by disruption of the α-tape motif (Figure 1.20).[243]
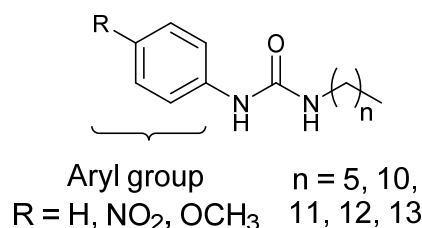
Figure 1.20: Structure of the gelators investigated by Piana et al.[243]

Finally, a detailed study into the gelation behaviour of three structurally related bis-urea compounds highlighted the importance of both the structural and electronic features of the linkers and end-groups (Figure 1.21). π-π interactions between the central aromatic groups were reinforced by the presence of an electron-withdrawing nitrogen atom in the ring. Further functionalisation of the central ring with methyl

groups also improved gelation behaviour by promoting an interlocked packing arrangement that supports a more favourable hydrogen-bonding motif.[244]
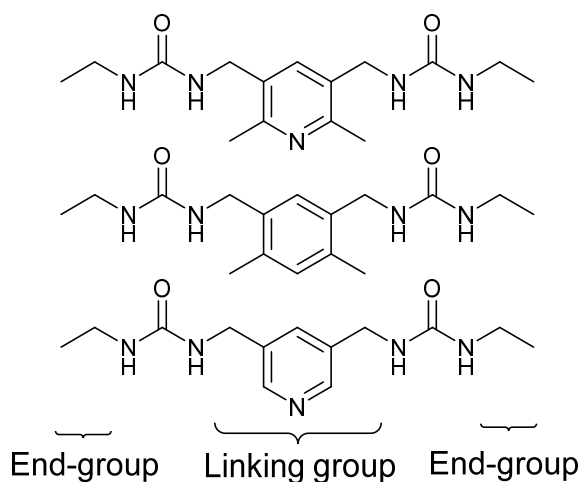
Figure 1.21: Structure of the gelators investigated by Baddeley et al.[244]

Whilst the structural and electronic properties of the molecule are both extremely important, its solubility and supramolecular interactions with solvent molecules also play a key role in determining its success as a gelator, and these characteristics have also been taken into consideration throughout most structure-property correlations.[245] Despite these studies, the discovery of low molecular weight gelators remains predominantly serendipitous. Until the effect of each structural component on the gel-forming ability of a molecule can be fully understood, it will remain impossible to achieve the rational design of a supramolecular gelator.

The most common method used to identify a supramolecular gel is visual inspection. Termed the "inversion test", a gel is defined by the ability to hold its shape in an upturned vial. Although this test is the easiest and quickest method of identifying gel formation, its lack of sophistication presents significant drawbacks. The size, shape and composition of the container all affect the ability of a gel to resist inversion, which can lead to inconsistent results. A weak or partial gel with a very low yield stress may

give a false negative result, and similarly, this technique cannot distinguish between a gel and a suspension or viscous liquid.[246] It is more reliable to identify a gel based on its rheological properties. Gels are viscoelastic and display both an elastic storage modulus, G′, which corresponds to "solid-like" behaviour and an elastic loss modulus, G″, which corresponds to "liquid-like" behaviour. Gels are usually solid-like and therefore can be identified by a value of G′ approximately an order of magnitude greater than G″. Similarly, when a small stress is applied, the storage modulus (G′) of a gel should be invariant with frequency (Figure 1.22). The magnitude of G′ gives an indication of the relative strength of a gel, which can be further quantified by measurement of the yield stress. This term refers to the point at which the gel begins to flow under the applied shear forces. At this point, the material has liquefied and G″ will become larger than G′. A large yield stress therefore corresponds to a stronger gel.[186, 206] The potency of a gelator can be characterised by measurement of the critical gelation concentration (CGC), defined as the lowest concentration of gelator that results in a stable gel. The lower the CGC, the more potent the gelator. The critical gelation temperature (T_{gel}) is an analogous quantity that describes the maximum temperature at which a gel is stable, above which it dissolves.[247]
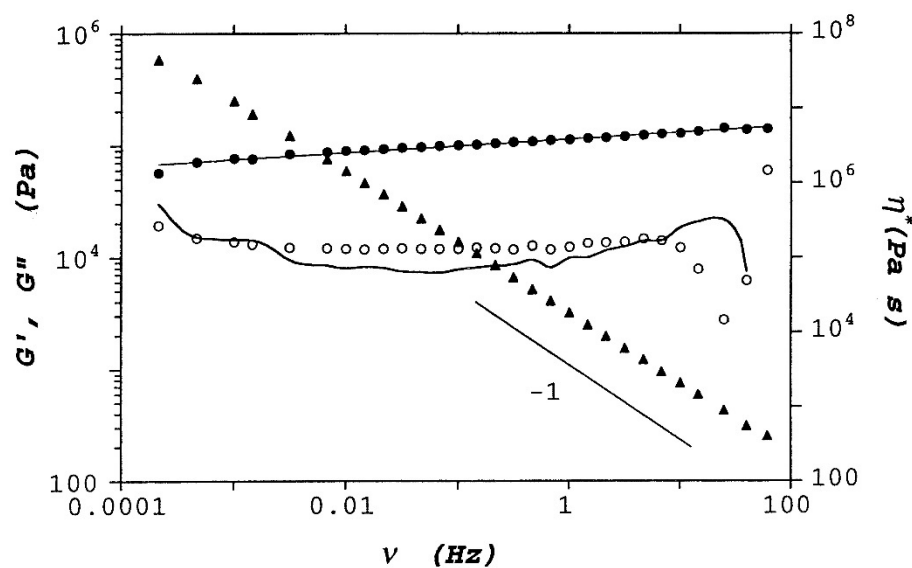
Figure 1.22: Typical rheological behaviour of a supramolecular organogel: 4 % wt 12-hydroxystearic acid in dodecane. · = G′, ○ = G″, ▲ = η*. Reproduced from reference 206 with permission. Copyright 2000, American Chemical Society.

1.8   Gels as Selective Crystallisation Media

Since the late 19th century, gels have been as crystallisation media. Termed gel-phase crystallisation, this technique is used for the study and modification of solid-state materials. Traditionally, this method was used for growing large single crystals for X-ray diffraction. A particularly common example is the use of silica and agarose hydrogels to grow diffraction-quality single crystals of proteins, a technique still in use today.[248-250] Gel-phase crystallisation first arose from the observation of concentric circles of solid silver chromate, formed when silver nitrate was dropped onto a potassium dichromate-containing gel. This pattern, now referred to as "Liesegang rings", derives from the periodic precipitation of a weakly soluble salt in a process akin to an oscillating chemical reaction.[251, 252] From this point, early gel-phase crystallisations primarily involved inorganic metal salts in silica or agarose gels, and were often used to study the mechanism of chemical reactions, and to explore

40

alternative crystallisation media.[253] In these techniques, the use of a gel-phase crystallisation medium produced higher-quality crystals because the rigid network of fibres decreased diffusion in the liquid phase, limiting the rate of nucleation and promoting the slow, controlled growth of single crystals.[254, 255]

More recently, this method has been applied to polymorph-selective crystallisation. In this case, the interaction between the gel and the solute may also be important. The gel can act as a high-energy surface to encourage crystallisation *via* heterogeneous nucleation. As with traditional solid substrates, the surface can be tuned to favour the production of a particular polymorph, and can even lead to epitaxial growth in which a structural feature of the gel fibre is transferred to the growing crystal.[256] An example of this gel-solute interaction is the preferential formation of vaterite, the metastable form of calcium carbonate, when crystallised from a chitosan hydrogel. Carbonate anions formed hydrogen bonds to the chitosan polymer in a periodic array, which acted as a template to encourage the formation of vaterite crystals.[257]

One advantage of polymeric gels is that they are very sturdy and can withstand having solutions diffused into the gel network or being stored for a long time. Both of these properties make them suitable for crystallisation experiments, which can take several weeks. A common format for gel-phase crystallisation involves the formation of a gel column into which a supersaturated solution can be diffused. A different solution can be diffused into either end of the column, in a technique termed counterdiffusion, which is often applied to protein crystallisation. This method allows the controlled mixing of two solutions, or a solution and an anti-solvent, to limit nucleation and encourage the growth of high-quality single crystals (Figure 1.23).[258]
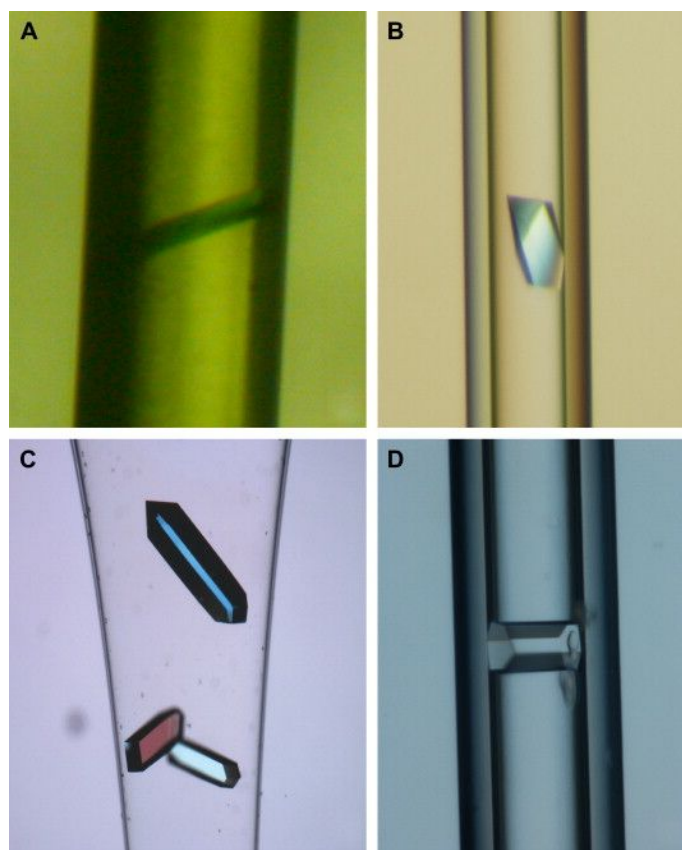
Figure 1.23: Protein crystals grown by capillary counterdiffusion: (a) membrane protein PSIIcc from *Pisum sativum*, (b) hydantoin racemase from *Sinorhizobium meliloti,* (c) PDZ domain of the mammalian PSD95 protein and (d) PurE. Reproduced from reference 258 with permission. Copyright 2009, Elsevier.
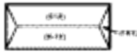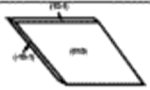
In this technique, polymorph selection is possible by varying the concentration of solute along the column. The polymorph-selective crystallisation of paracetamol has been reported using this technique. Paracetamol has three forms: monoclinic Form I, which is thermodynamically stable, orthorhombic Form II, which is metastable, and an uncharacterised Form III, which is highly metastable. Form I is currently used in tablet formulations, but it requires an excipient to bind the tablets as the crystal lattice has a low compressibility. Form II would be much easier to formulate into tablets due the presence of slip planes in the crystal structure, which increase compressibility. Therefore, a crystallisation technique to selectively produce high-quality crystals of

Form II is of great interest to industry. When a solution of paracetamol was diffused into a pre-formed column of silica gel, a concentration gradient was formed along the column due to more rapid evaporation of solvent from the surface of the column compared to the bulk. This concentration gradient caused selective nucleation of Forms I and II at different heights along the column, allowing easy separation of the two polymorphs.[259]

An alternative method of polymorph selection using polymeric gels is to tune the size and properties of pores within the gel network to encourage nucleation of a particular form. Studies report the polymorph-selective crystallisation of aspirin, paracetamol, carbamazepine and ROY within polymeric microgels whose well-defined pores ranged from angstroms to nanometres. The solute preferentially partitions into the gel pores, which leads to an increased concentration, stronger solute-solute interactions, and therefore an increased likelihood of cluster formation. The structure of these pre-nucleation clusters is directed by interactions with the polymer chains. The solute molecules adopt a specific arrangement to maximise favourable interactions with the polymer, which therefore reduces the entropic barrier to formation of the polymorph whose structure is most similar to the cluster.[260, 261] A similar effect was observed when crystals of the amino acid L-asparagine monohydrate were grown in biopolymer hydrogels of agarose, carrageenan and gelatin. In this case, striking differences in habit were observed from crystallisation within the different gels (Table 1.1). Polymer-solute interactions were thought to be responsible for this effect, although it was difficult to be specific given the diversity of functional groups in these gelators.[262]

Table 1.1: Asparagine monohydrate crystal morphologies observed from gel and solution. Reproduced from reference 262 with permission. Copyright 2006, American Chemical Society.

Media	Morphology	Major face	Minor faces
Aqueous solution		{012}	{101}, {111} {011}, {010}
Agarose (aqueous or binary H₂O / DMSO mixtures)		{012}	{101}
ι-Carrageenan		{101}	{012}
κ-Carrageenan	Ill-defined habits	{012}	?
Gelatin	Dendrites Clusters of tiny crystals	?	?
DMSO/Water		{010}	{101}, {012}
NaCl Na₂SO₄ K₂SO₄		{101} or {001}	{012}, {111}

A particularly impressive result deriving from the interaction between solute and gel has been reported for the crystallisation of sodium chlorate in an agarose hydrogel. Agarose is chiral in both its primary and tertiary structures. Sodium chlorate is achiral in terms of its molecular structure, but crystallises in a chiral space group, giving rise to *d* and *l* forms. Typically, the ratio between these forms is 1:1, but crystallisation within the gel alters the distribution due to interaction with the helical agarose fibres. The exact ratio depends on experimental parameters such as temperature and solvent.[263] Development of a gel capable of selectively crystallising pure enantiomers from a racemic compound would be extremely valuable to the pharmaceutical industry, given that many drugs are chiral and the properties of each enantiomer can vary significantly.[264]

In addition to using known gelators such as silica or agar, it is also possible to design or modify the polymer structure to enable specific gel-solute interactions and encourage heterogeneous nucleation. For example, surface-modified nanocellulose organogels have been used for the crystallisation of a group of poorly water-soluble antibiotics. Cellulose contains many alcohol groups, which can be used as a handle for surface modification. Attaching long alkyl chains to the cellulose polymer leads to a gel with a hydrophobic surface. The hydrophobic drug molecules are drawn to these surfaces, and this attraction increases the local drug concentration and encourages nucleation (Figure 1.24). In this case, gel-phase crystallisation led to a variety of changes in the API solid form, including amorphisation of a previously crystalline product, a change in crystal habit, a change in polymorphism, and the formation of a novel solvate.[265, 266]
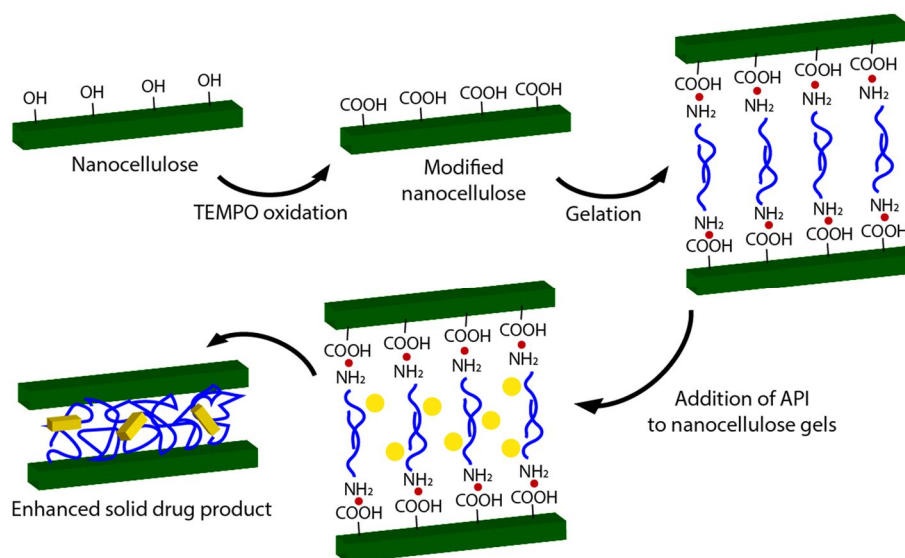
Figure 1.24: Schematic representation of the function of surface-modified nanocellulose organogels in pharmaceutical crystallisation. Reproduced from reference 265 with permission from The Royal Society of Chemistry.

1.9 Supramolecular Gels as Pharmaceutical Crystallisation Media

Recent interest has turned to the use of supramolecular gels as crystallisation media by virtue of their reversibility and tunability. The use of small-molecule gelators allows the structure of the fibres to be modified more easily, so they can bind to a growing crystal through non-covalent interactions. Once bound, they can promote crystallisation of a particular solid form through preferential heterogeneous nucleation, or by inhibiting the growth of a certain crystal face.[267] In 2004, Estroff et al. reported the first gel-phase crystallisation using a supramolecular gelator (Figure 1.25). Calcite crystals were grown in the resulting hydrogel and their morphology was found to be dependent upon the time spent in the gel. Carboxylic acid groups on the gel fibres bind to Ca^{2+} ions in the calcite, facilitating polymorph-selective crystallisation by heterogeneous nucleation.[268]
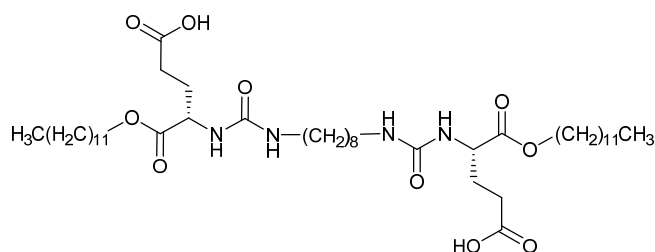
Figure 1.25: The ion-binding gelator published by Estroff et al.[268]

A recent study has shown that the presence of a solute can affect the nucleation of gel fibres. This effect is determined by the concentration of each component in the system. Typically, there is little interaction between the two components, and the self-assembly processes of the gel and the crystal have little effect on each other. Under the right conditions, nucleation of the crystal and gel occur simultaneously, the interaction between solute and gel impairs fibre formation and gelation is suppressed. Given that it is not currently possible to predict when or how a gel will form, these

conditions are likely to be system-specific and discovered through trial and error. Even if nucleation of the crystal and gel do occur simultaneously, the kinetics of each process is often very different, which leads to the formation of one phase before the other.[269]

As described in section 1.4, solid form-selective crystallisation is of great interest to the pharmaceutical industry, where the solid form of a drug can have a significant impact on its physical and biological properties. As a result, the gel-phase crystallisation of pharmaceuticals is becoming an increasingly active field of research. Supramolecular gel-phase crystallisation is particularly well-suited to the pharmaceutical industry because the gels are often reversible, which means they can be handled in liquid form and easily be incorporated into a high-throughput screening methodology. The addition of anions has been a common method of modifying the physical properties of supramolecular gels for some time.[270] Both a strengthening and weakening effect has been observed, based on the nature of the gel and the anion. One theory suggests that the anion-strengthening effect depends on the Hofmeister series, with chaotropic or "salting-in" ions favouring gelation.[271] However, anion-induced weakening of the gel is more common, and is thought to derive from a disruption of the supramolecular interactions that support gelation. The addition of anions, even in non-stoichiometric quantities, can cause complete dissolution of the gel, or a less significant weakening, which is visible as a reduction in the yield stress and elastic and viscous moduli (Figure 1.26).[241, 272-274] A gel-strengthening effect can also be induced by the incorporation of cations that are capable of acting as a template for the self-assembly of gel fibres, such as the co-ordination of silver ions to a pyridyl ligand.[275, 276]
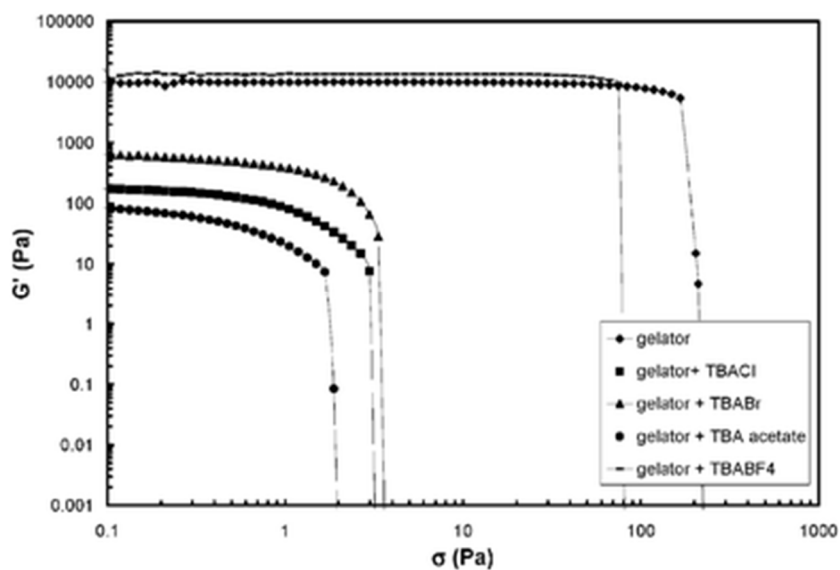
Figure 1.26: Influence of different anions (0.1 equiv. of anion added as their NBu_4^+ salts) on the storage modulus (G′) of a 1 % wt bis-urea gel. Reproduced from reference 241 with permission from The Royal Society of Chemistry.

Anion-induced weakening is particularly common in urea-based gels, given that strong urea-anion hydrogen bonds have been exploited in supramolecular chemistry for some time.[277] A key example of this behaviour is the development of switchable bis-urea gels applied for the crystallisation of pharmaceuticals. A variety of APIs were used in this study, chosen because they cover a wide range of chemical functionality, and are either polymorphic, form hydrates or have unusual crystal packing. Rheology studies showed that the addition of acetate ions, in the form of tetrabutylammonium (TBA) acetate, strongly weakened the gel. Addition of one molar equivalent of TBA acetate was enough to completely dissolve the gel without affecting the crystals within, allowing them to be retrieved by a simple filtration (Figure 1.27). The majority of crystallisations yielded the same solid form as from solution, apart from the drug piroxicam, which produced a different polymorph in one particular gel. Other key results include the habit modification of carbamazepine, an alteration in the supersaturation level required to induce nucleation for carbamazepine and aspirin, and

48

preferential crystallisation of the thermodynamic form of a model urea compound. Although little control over solid form was observed in this study, the anion-switchability of these gelators offers a valuable mechanism for the retrieval of crystals from gels. This method is much more gentle than heating or hydrolysis, which are used to remove traditional, polymeric gels, and is therefore less likely to destroy the crystals within.[278]
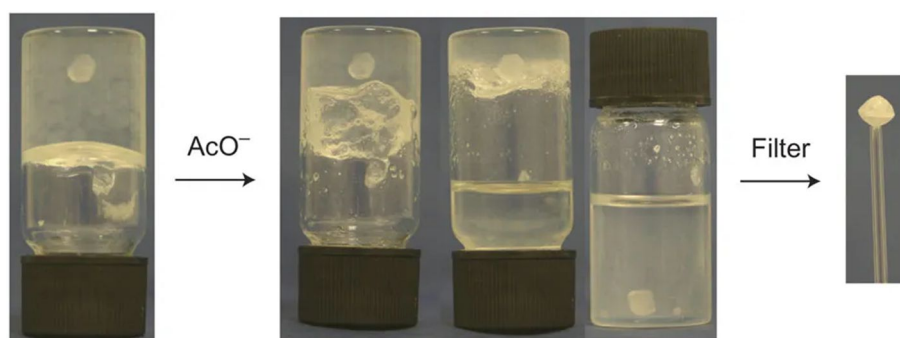
Figure 1.27: Recovery of a single crystal of thermodynamically stable Form III of carbamazepine by acetate anion-triggered gel dissolution of a bis-urea supramolecular gel. Reproduced from reference 278 with permission. Copyright 2010, Springer Nature.

The development of solid form-selective supramolecular gels has been the focus of significant work in recent years. Depending on the design of the system, this technique can have a number of outcomes, including the crystallisation of a specific polymorph, the discovery of new polymorphs and the modification of crystal habit. The mechanism of polymorph control in this technique is based on the degree of interaction between the drug and the gel. If there is little interaction between the two components, the self-assembly processes of gelation and crystallisation proceed as if they were separate. In this case, any change in solid form is likely due to physical confinement within the gel network. Larger degrees of interaction lead to the two processes having a greater influence on one another, which can cause differences in the nucleation and

growth of both the crystals and the gel fibres.[267] In a typical gel-phase crystallisation, the drug and gelator are dissolved in the same solvent, sealed and then left to stand, allowing the gel and crystals to form over time. The ideal scenario is to have minimal interaction between the two components, such that the gel forms unhindered by the solute. The gel should form faster than the crystals to provide a high-energy surface capable of modifying crystal growth. To achieve solid-form modification, a small degree of interaction between the solute and the pre-formed gel network is required, and this interaction is easily tuned using supramolecular gels.

An example in which the self-assembly processes of the gel and drug did not interact with each other concerned the growth of common APIs aspirin, caffeine, indomethacin and carbamazepine in an amide-based supramolecular gel (Figure 1.28).[279]
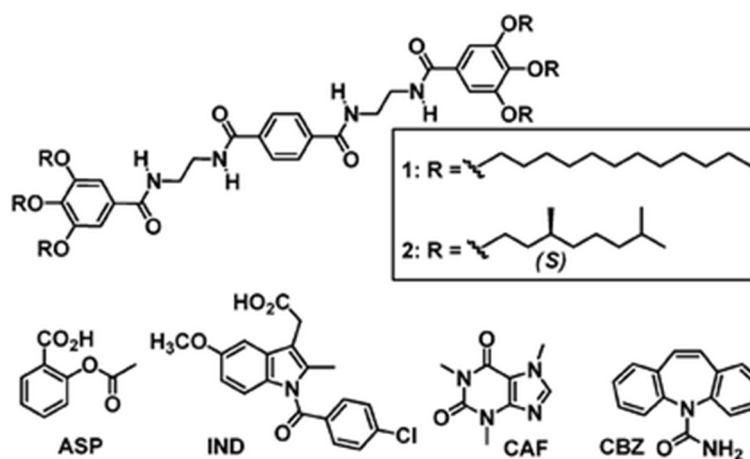
Figure 1.28: The achiral (R1) and chiral (R2) gelators published by Aparicio et al. with the drugs that were used for crystallisation experiments: aspirin, indomethacin, caffeine and carbamazepine. Reproduced from reference 279 with permission from The Royal Society of Chemistry.

50

The only solid-form modification observed in this study was the concomitant crystallisation of carbamazepine Forms II and III in the gel, whilst only Form III was formed in the corresponding solution. This modification was attributed to the viscous environment provided by the gel, given that the crystallisation of carbamazepine is strongly affected by rate of cooling and agitation.[280] The gelator in this study displayed interesting chiral behaviour. With the end-group R_1, the gelator is achiral and the molecules stack into helical columns, driven by π-stacking, hydrogen bonding between amide groups, and Van der Waals interactions between alkyl chains. If a small amount of the R_2-containing, chiral gelator is added, this molecule intercalates into the columns, causing preferential formation of one helix and giving the system an overall chirality. In this case, the chirality was found to have no effect on the outcome of crystallisation, further reinforcing that the drug and gel display very little interaction.[279] However, a similar technique has been used to achieve enantioselective crystallisation using polymeric gels.[263] Chiral resolution using supramolecular gels remains a goal in this field.

In contrast, a recent example shows greater interaction between the drug and gel, resulting in control of solid form. Four APIs were crystallised within a novel benzotriazole-based gel (Figure 1.29), yielding two examples of solid form modification. Niflumic acid displayed a change in crystal habit, from needles in solution to blocks in the gel, and sulfathiazole was crystallised as thermodynamically stable Form II in solution and metastable Form I in the gel. The production of a metastable polymorph in the gel suggests that the crystallisation process deviates from its typical solution-phase mechanism due to the presence of the gel fibres. This mechanism may include a reduction in the nucleation rate of Form II or an increase in the nucleation rate of Form I.[281]
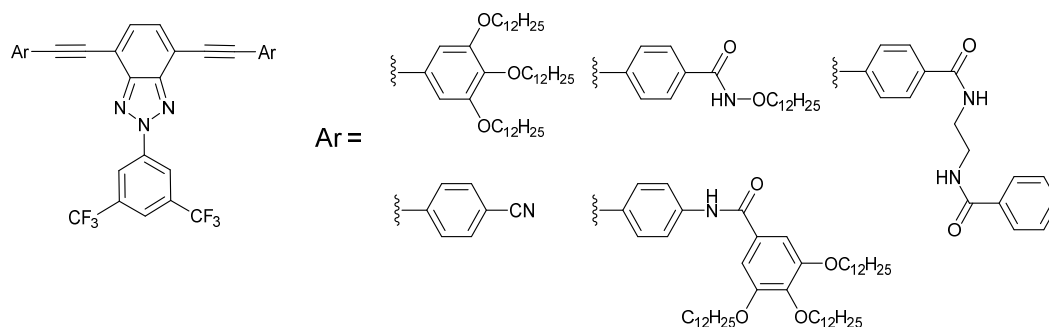
Figure 1.29: Benzotriazole gelators used by Torres-Moya et al.[281]

Similar results were obtained from the crystallisation of caffeine, carbamazepine and piroxicam from a tannic acid-Ti(IV) metallogel.[282] Tannic acid is a natural polyphenol that has previously been shown to form metallogels by co-ordination to group four transition metals.[283] Gelation was observed with a variety of solvents and over a range of conditions, concentrations, and metal-ligand stoichiometries. Unlike most supramolecular gelators, which require heating and cooling to trigger gelation, these materials can be formed by room temperature mixing of metal and acid solutions. For gel-phase crystallisation, the conditions were optimised to ensure that gelation preceded crystallisation, allowing the drug to interact with pre-formed gel fibres. All gel-grown crystals differed in size and habit, compared to those grown in solution, and the polymorphic drugs carbamazepine and piroxicam also differed in polymorphism (Figure 1.30).
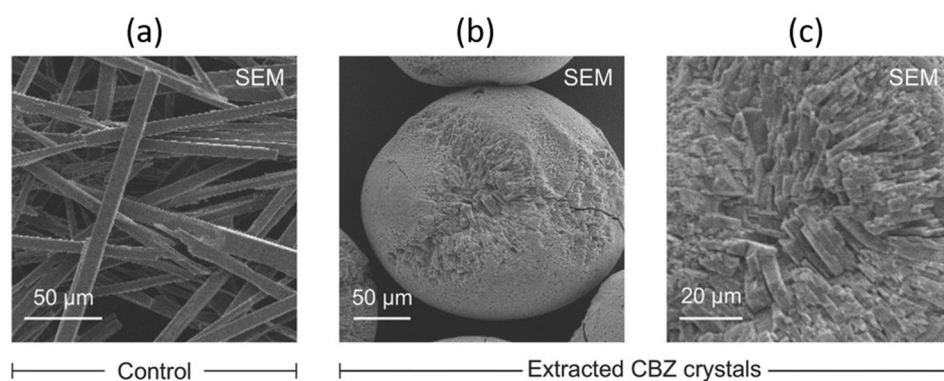
Figure 1.30: The varied morphologies of carbamazepine crystals grown (a) in solution and (b,c) in tannic acid–Ti^{IV} metallogels. All crystals were a mixture of the dihydrate and Form III of carbamazepine, but Form III was the dominant phase in solution and the dihydrate was the dominant phase in the gel. Adapted from reference 282 with permission. Copyright 2018, John Wiley and Sons.

Changing the gel composition and introducing additives to the system both led to changes in crystal size and morphology, which suggests that interaction with the gel network is responsible for the modification of solid form in this case. Interestingly, these systems have been proposed for potential use in sustained-release drug delivery formulations, as release of the API was found to be much slower from a gel containing crystalline, rather than molecular, caffeine. This observation reinforces the importance of the gel network in determining the properties of the crystallising API.[282]

The first example of a supramolecularly assembled two-component organogel used for pharmaceutical crystallisation showed that the interaction between the drug and gel can either support or impair gelation. The gelators were composed of a lysine-based dendron co-ordinated to an alkyl amine by the formation of an acid-base complex. This complex self-assembles into gel fibres *via* the formation of amide-amide hydrogen bonds between dendrons. APIs including carbamazepine, caffeine, aspirin, and indomethacin were crystallised within these gels. Results showed a

difference in crystallisation behaviour depending on whether the drug contained a carboxylic acid (Figure 1.31).
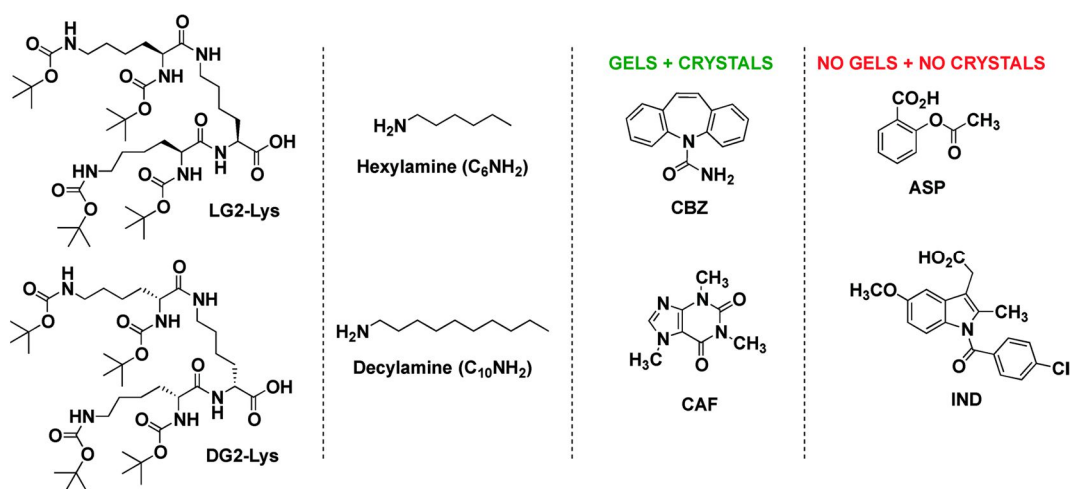
Figure 1.31: Lysine-based dendrons used by Buendia et al. to crystallise four APIs: carbamazepine, caffeine, aspirin and indomethacin. Reproduced from reference 284 with permission from The Royal Society of Chemistry.

Acid-containing molecules aspirin and indomethacin did not crystallise at all, whereas their non-acid-containing counterparts carbamazepine and caffeine, crystallised in every case. This result was attributed to the acid-amine hydrogen bonds between the API and the alkyl amine being stronger than those between the dendron and the alkyl amine. Thus, the two components could no longer self-assemble and form a gel. This theory was reinforced by the calculation of binding energies for the amine with both indomethacin and the dendron. The API-amine pair displayed a higher binding energy, showing that these interactions were in fact the strongest. The opposite effect was reported for the non-acid-containing APIs, which instead enhanced gelation. The enthalpy and entropy of gelation, calculated from variable-temperature ^{1}H NMR studies, further confirmed this effect with both parameters increasing in the presence of carbamazepine, and suggesting increased ordering of the gel. For the drugs that did crystallise, a change in polymorphism was

only noted for carbamazepine when crystallised from the gel. Form III is obtained from solution whereas a mixture of Forms II and III was produced in certain gels. These results highlight the competitive interactions present in gel-phase crystallisation and show that it is possible to tune the structure of the gelator to promote the crystallisation of substrates containing specific functionalities.[284]

A key development in this field has been the rational design of gelators, tailored to interact with a crystallising drug substrate. One method of ensuring an interaction between the two components is to incorporate known host-guest chemistry into the choice of drug and gelator. A characteristic example is the use of calixarene-based gelators for the crystallisation of hydrophobic drugs. Once self-assembled into a gel network, the calixarene cavities offer hydrophobic binding sites along the fibres. Binding of drug molecules to these sites promotes nucleation, facilitating the production of difficult to crystallise polymorphs. Two different gelators were used, with one- and two-component structures. The one-component approach uses directional hydrogen bonding units that are covalently attached to the calixarene to promote gelation behaviour (Figure 1.32).
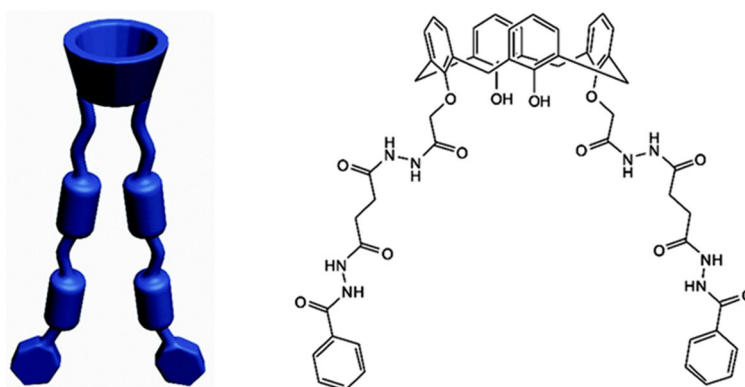
Figure 1.32: The one-component calixarene gelator published by Kaufmann et al., with a schematic representation of the molecule. Adapted from reference 285 with permission from The Royal Society of Chemistry.

The two-component approach uses the cation-binding ability of crown ethers to connect ammonium-terminated calixarene units and aromatic linking groups to produce a supramolecular polymer capable of forming gel fibres. (Figure 1.33).
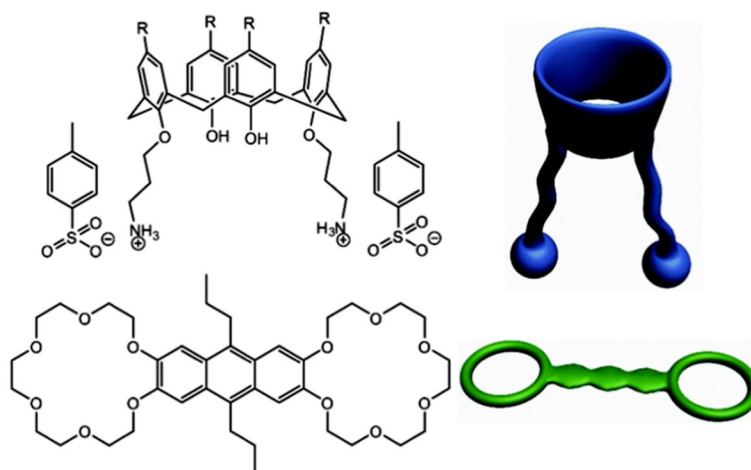
Figure 1.33: The two-component calixarene gelator published by Kaufmann et al., with schematic representations of the molecules. Adapted from reference 285 with permission from The Royal Society of Chemistry.

This interaction can be overcome by the addition of KPF_6, which causes breakdown of the gel, as the crown ether preferentially binds the potassium cations and the supramolecular polymer disassembles. (Figure 1.34). This behaviour is extremely useful for the recovery of crystals from the gel.
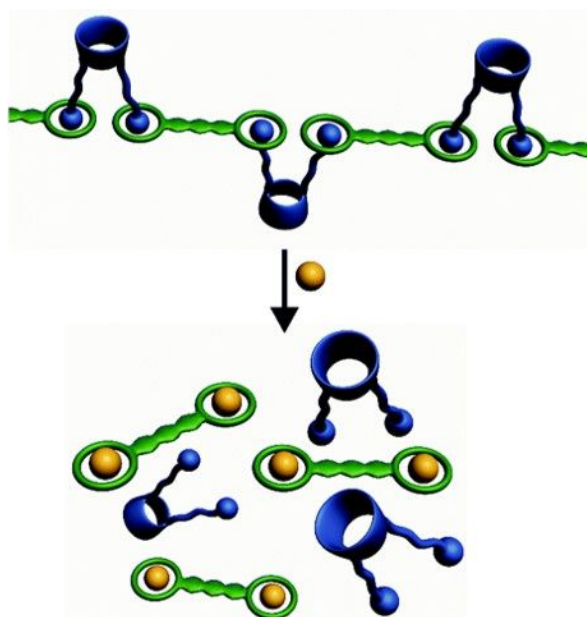
Figure 1.34: Schematic representation of the mechanism of gel breakdown, induced by addition of KPF$_6$. Adapted from reference 285 with permission from The Royal Society of Chemistry.

A range of model drug substances—paracetamol, fenbufen, monobenzone and chlorphenesin—were crystallised within the calixarene-based gels. Most experiments yielded the same polymorph as was formed in solution. The exception was chlorphenesin, for which a novel polymorph was discovered from the two-component gelator in 1,2,4-trichlorobenzene. An interesting feature of this polymorph is the presence of two molecules per asymmetric unit, which likely derives from a large hydrogen-bonded network within the structure. Although these specific gelators are not applicable to a wide range of chemical systems, they serve as proof of concept for the nucleation of hydrophobic drugs using classical host-guest chemistry.[285]

A similar strategy for gel-phase crystallisation of pharmaceuticals is the design of gelators whose structures mimic that of the drug. This technique encourages a templating interaction between the drug and gel fibres, analogous to epitaxy. This strategy was first used to crystallise the highly insoluble anti-cancer drug cisplatin.

The gelators all contained a central platinum complex co-ordinated to functionalised pyridine ligands, and connected by spacers of varying length to a bis-urea (Figure 1.35). Gel formation is driven by the self-assembly of these urea groups into one-dimensional tapes. The ethylene-linked analogue was found to be the best gelator, evidenced by a high yield stress and well-defined fibres under SEM. This behaviour was thought to derive from the greater conformational freedom of the longer linker, which could allow the gel-forming and platinum-binding groups more freedom to adopt the most favourable orientation.
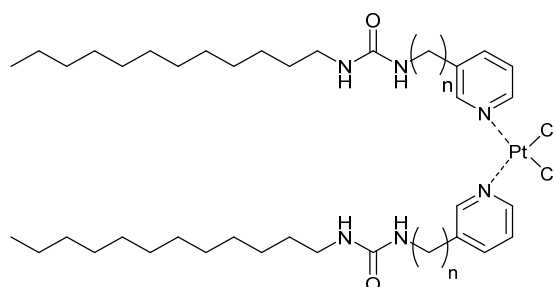
Figure 1.35: The cisplatin-mimicking gelator published by Dawn et al., n = 0,1,2.[286]

Unfortunately, the drug and gelator were not soluble in any of the same solvents, so the typical strategy of dissolving both components in the same solvent could not be employed in this case. The issue was overcome with the use of a biphasic sol-gel system in which a cisplatin solution was diffused into a pre-formed gel. These crystallisations led to habit modification of the known triclinic DMF solvate and discovery of a new DMA hemisolvate. The gel fibres were theorised to interact with cisplatin through amine-chloride hydrogen bonds and platinum-platinum interactions. Coupled with a geometric similarity between the drug and gelator, these factors both encourage nucleation of the new solid forms.[286]

Similar results were observed for the crystallisation of isoniazid, a drug suspected to be monomorphic, within a structure-mimetic bis-urea gel (Figure 1.36). Isoniazid

has a very simple molecular structure terminated by a primary amine. This functionality serves as a convenient synthetic handle to attach the drug molecule to a linking group known to form strong gelators. Incorporating the entire drug structure should strengthen its interaction with the gel fibres and increase the templating effect. Gel tests yielded crystals in eight out of nineteen solvents, all of which were identified as the known form of isoniazid. Two crystals displayed a change in habit, with one growing much larger in the gel than in solution. This result is characteristic of the reduced convection and nucleation rate within the gel network. In this case, the gel, which was previously very stable, broke down upon formation of the crystals, which suggests the hydrogen bond network may be disrupted by a drug-gel interaction.[163, 269] These results were compared to a microemulsion crystallisation strategy, which has been reported to selectively generate the thermodynamic form. The same polymorph was obtained in all cases, which suggests isoniazid is truly monomorphic.[163]
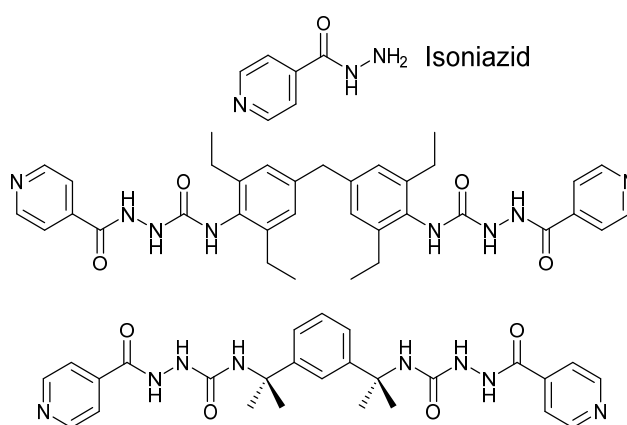
Figure 1.36: Isoniazid-mimetic gelators reported by Kennedy et al.[163]

Instead of mimicking a functional group from the drug in the gelator, polymorph control can also be achieved my mimicking a conformational aspect of the molecule. A recent paper describes the polymorph-selective crystallisation of ROY using a conformationally mimetic gelator. ROY is a drug precursor that is famed for its high

degree of polymorphism. To date, there are thirteen known forms of ROY, ten of which are stable enough to be characterised experimentally,[159, 287-290] although several more have been predicted computationally.[291] Its polymorphs are easily distinguishable by their bright colours, deriving from different molecular conformations. Known gelator cores were functionalised with an ortho-nitroaniline group to mimic the same substituent in the structure of ROY (Figure 1.37).
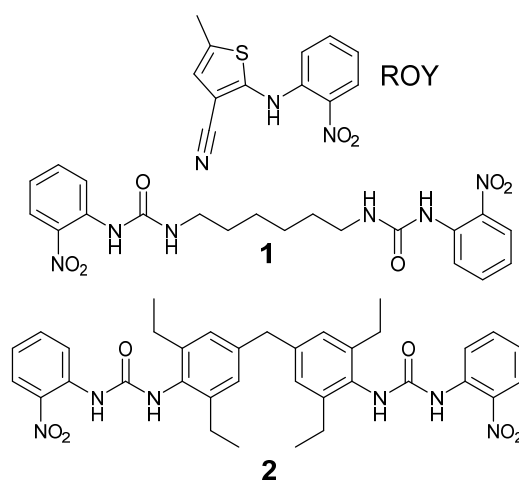
Figure 1.37: ROY-mimetic gelators published by Foster et al.[292]

Gelator **2** could reproducibly crystallise the metastable red form of ROY, whilst the stable yellow form was produced from control experiments in solution, in non-drug-mimetic bis-urea gels, and even with the tailored gelator at a concentration below the gel point (Figure 1.38). This specificity suggests that polymorph selection in this system is caused by interaction with a structural feature of the gel network. Computational structure prediction showed that the nitroaniline group in the successful gelator adopts the same conformation as in the red form of ROY. Coupled with the local periodicity of the gel fibre, this structural matching led to epitaxial nucleation of the metastable form.[292]
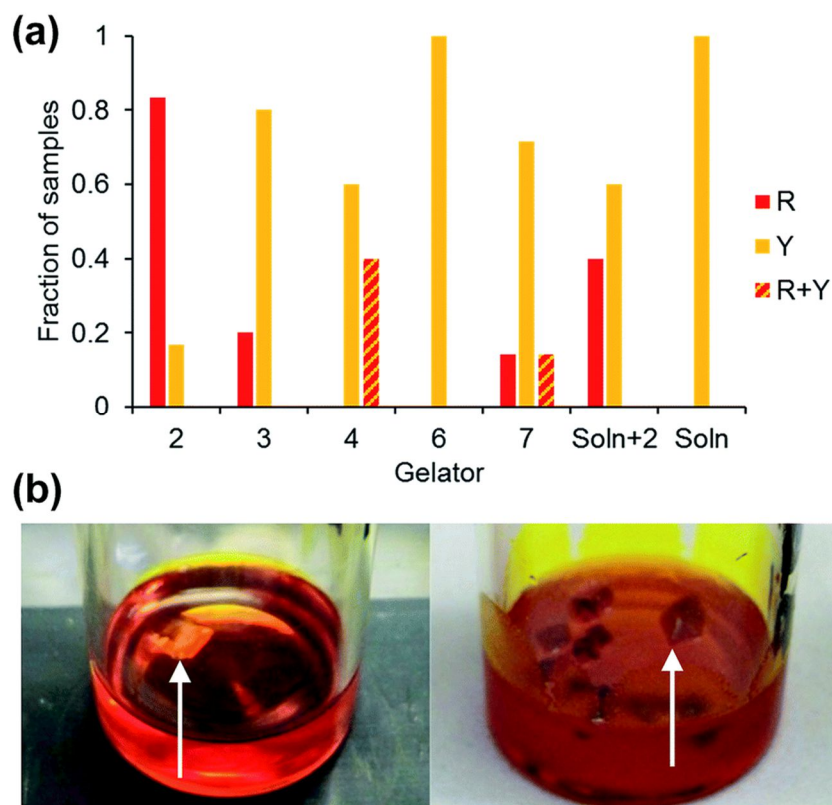
Figure 1.38: (a) A summary of the results of ROY crystallisations in toluene gels of drug-mimetic gelator **2**, non-drug-mimetic gelators **3**, **4**, **6** and **7**, pure toluene solution, and a saturated toluene solution of gelator **2**. (b) Crystallisation of the Y form of ROY in a gel of non-drug-mimetic gelator **7**, and the R form of ROY in a gel of drug-mimetic gelator **2**. Reproduced from reference 292 with permission from The Royal Society of Chemistry.

In addition to use with pharmaceuticals, substrate-mimetic gels have also been applied to the crystallisation of inorganic compounds. For example, habit modification was observed when a copper(II) isonicotinate-N-oxide complex was crystallised using a substrate-mimetic gelator (Figure 1.39). These results were not reproduced in an agarose gel, which once again suggests that interaction with the gel network was the driving force for modification of solid form.[293]
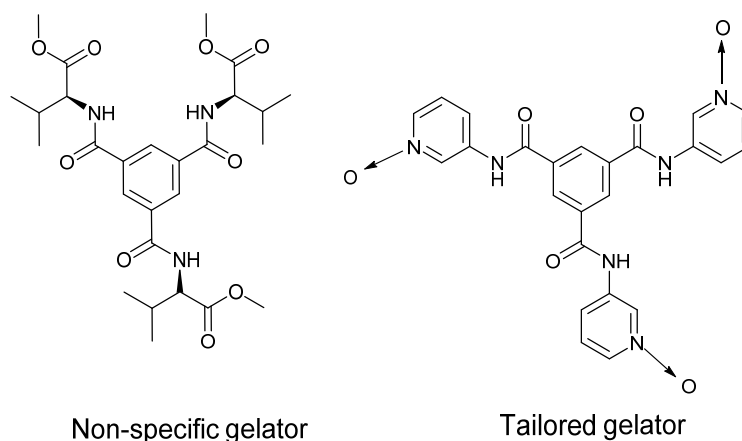
Figure 1.39: The gelators used by Ghosh et al. for crystallisation of copper(II) isonicotinate–N-oxide complexes.[293]

1.10 Project Aims and Overview

This work aims to build on current gel-phase crystallisation strategies for polymorphic pharmaceuticals, and contribute to the development of a universal toolkit of tailored supramolecular gelators, which would be used to expand the scope of traditional solution-phase polymorph screens. In the first part of this work, mexiletine hydrochloride will be the target API. This small-molecule, anti-arrhythmic drug was chosen because its simple molecular structure will make the system easier to understand and to model. Similarly, the terminal amine provides an easy mechanism to synthesise drug-mimetic bis-urea gelators. Firstly, a polymorph screen of mexiletine will be undertaken to fill gaps in the literature data,[294-298] and ensure that the polymorph landscape of the drug is well understood, in order to compare these results to gel-phase crystallisations. A variety of crystallisation techniques will be employed to access the full range of kinetic and thermodynamic solid forms, and each of the resulting polymorphs will be rigorously characterised using X-ray diffraction, spectroscopic and thermal techniques. The experimental polymorph screen will be

supported by computational crystal structure prediction to ensure that the polymorph landscape is complete.

Building on previous work from the Steed group, drug-mimetic gelators will be synthesised to produce tailored crystallisation media capable of stabilising metastable or difficult to nucleate solid forms of mexiletine.[163, 286, 292] In addition to the bis-urea gelators that have been reported previously,[163, 202, 216, 269, 278, 292, 293, 299-304] this work will also incorporate a C_3-symmetric tris-amide gelator. These molecules are reported to stack into helical fibres,[234, 237] rather than the α-tape arrangement that is typical of bis-urea derivatives.[235] It is possible that the different morphology of the tris-amide gel fibres may lead to differences in the interaction between the drug and the gel, which could alter the outcome of the crystallisation. The terminal amine allows the entire mexiletine molecule to be used as an end-group, connected to various gel-forming linkers *via* amide or urea bonds. Results of gel-phase crystallisations of mexiletine will be compared to the solution-phase results to identify any changes in polymorphism.

Finally, experiments using a novel iodo-triphenyl imidazole (I-TPI) gelator aim to highlight a new class of gelators that can be applied to pharmaceutical crystallisation. In this case, the target drug is diatrizoic acid, an X-ray contrast agent that has limited structural similarity to the gelator, but a very diverse polymorph landscape.[305] The varied solid-state behaviour of the I-TPI gelator[306] may alter the thermodynamic landscape of the drug crystallisation within the gel. It is unusual to characterise the polymorphism of a gelator, so these experiments may highlight new mechanisms for solid-form modification of pharmaceuticals using gel-phase crystallisation.

1.11 References

1. W. McCrone, in *Physics and Chemistry of the Organic Solid State*, eds. D. Fox, M. M. Labes and A. Weissberger, Wiley Interscience, New York, 1965, vol. 2, pp. 725-767.

2. E. Mitscherlich, *Abhl. Akad. Berlin*, 1822, **1823**, 43-48.

3. J. Liebig and F. Wohler, *Pharm. Anntiinflam.*, 1832, **249**, 514.

4. J. Thun, L. Seyfarth, J. Senker, R. E. Dinnebier and J. Breu, *Angew. Chem., Int. Ed.*, 2007, **46**, 6729-6731.

5. B. Penfold and J. C. White, *Acta Crystallogr.*, 1959, **12**, 130-135.

6. W. David, K. Shankland, C. Pulham, N. Blagden, R. Davey and M. Song, *Angew. Chem., Int. Ed.*, 2005, **44**, 7032-7035.

7. J. Bernstein and A. T. Hagler, *J. Am. Chem. Soc.*, 1978, **100**, 673-681.

8. J. D. Dunitz and J. Bernstein, *Acc. Chem. Res.*, 1995, **28**, 193-200.

9. J. Bernstein, R. J. Davey and J. O. Henck, *Angew. Chem., Int. Ed.*, 1999, **38**, 3440-3461.

10. A. Burger and R. Ramberger, *Microchim. Acta*, 1979, **72**, 273-316.

11. A. Burger and R. Ramberger, *Microchim. Acta*, 1979, **72**, 259-271.

12. J. D. Dunitz, *Pure Appl. Chem.*, 1991, **63**, 177.

13. J. Haleblian and W. McCrone, *J. Pharm. Sci.*, 1969, **58**, 911-929.

14. S. R. Chemburkar, J. Bauer, K. Deming, H. Spiwek, K. Patel, J. Morris, R. Henry, S. Spanton, W. Dziki, W. Porter, J. Quick, P. Bauer, J. Donaubauer, B. A. Narayanan, M. Soldani, D. Riley and K. McFarland, *Org. Process Res. Dev.*, 2000, **4**, 413-417.

15. J. Bauer, S. Spanton, R. Henry, J. Quick, W. Dziki, W. Porter and J. Morris, *Pharm. Res.*, 2001, **18**, 859-866.

16. P. Vishweshwar, J. A. McMahon, M. Oliveira, M. L. Peterson and M. J. Zaworotko, *J. Am. Chem. Soc.*, 2005, **127**, 16802-16803.

17. A. D. Bond, R. Boese and G. R. Desiraju, *Angew. Chem., Int. Ed.*, 2007, **46**, 618-622.

18. A. D. Bond, K. A. Solanko, S. Parsons, S. Redder and R. Boese, *CrystEngComm*, 2011, **13**, 399-401.

19. J. Bernstein, *International Union of Crystallography Monographs on Crystallography*, Clarendon Press, Oxford, 2002.

20. Glaxo Inc. v. Novopharm Ltd., 1993, vol. 830.

21. S. L. S. Lynne S. Taylor, in *Polymorphism in Pharmaceutical Solids*, ed. H. G. Brittain, Informa Healthcare, New York, 2009, ch. 16, pp. 587-630.

22. B. C. Hancock and M. Parks, *Pharm. Res.*, 2000, **17**, 397-404.

23. S. Aitipamula, R. Banerjee, A. K. Bansal, K. Biradha, M. L. Cheney, A. R. Choudhury, G. R. Desiraju, A. G. Dikundwar, R. Dubey, N. Duggirala, P. P. Ghogale, S. Ghosh, P. K. Goswami, N. R. Goud, R. R. K. R. Jetti, P. Karpinski, P. Kaushik, D. Kumar, V. Kumar, B. Moulton, A. Mukherjee, G. Mukherjee, A. S. Myerson, V. Puri, A. Ramanan, T. Rajamannar, C. M. Reddy, N. Rodriguez-Hornedo, R. D. Rogers, T. N. G. Row, P. Sanphui, N. Shan, G. Shete, A. Singh, C. C. Sun, J. A. Swift, R. Thaimattam, T. S. Thakur, R. Kumar Thaper, S. P. Thomas, S. Tothadi, V. R. Vangala, N. Variankaval, P. Vishweshwar, D. R. Weyna and M. J. Zaworotko, *Cryst. Growth Des.*, 2012, **12**, 2147-2152.

24. E. Grothe, H. Meekes, E. Vlieg, J. H. ter Horst and R. de Gelder, *Cryst. Growth Des.*, 2016, **16**, 3237-3243.

25. D. J. Berry and J. W. Steed, *Adv. Drug Deliv. Rev.*, 2017, **117**, 3-24.

26. D. Braga, F. Grepioni, G. I. Lampronti, L. Maini and A. Turrina, *Cryst. Growth Des.*, 2011, **11**, 5621-5627.

27. D. Braga, F. Grepioni and O. Shemchuk, *CrystEngComm*, 2018, **20**, 2212-2220.

28. D. Erdemir, A. Y. Lee and A. S. Myerson, *Acc. Chem. Res.*, 2009, **42**, 621-629.

29. J. W. Mullin, in *Crystallization*, Butterworth-Heinemann, Oxford, 4th edn., 2001, ch. 5, pp. 181-214.

30. W. H. Zurek and W. C. Schieve, *J. Phys. Chem.*, 1980, **84**, 1479-1482.

31. M. Volmer and A. Weber, *Z. Phys. Chem.*, 1926, **119**, 277-301.

32. J. W. Mullin, in *Crystallization*, Butterworth-Heinemann, Oxford, 2001, ch. 6, pp. 216-288.

33. W. K. Burton, N. Cabrera and F. C. Frank, *Philos. Trans. R. Soc., A*, 1951, **243**, 299-358.

34. R. F. Sekerka, *Cryst. Res. Technol.*, 2005, **40**, 291-306.

35. D. Mangin, F. Puel and S. Veesler, *Org. Process Res. Dev.*, 2009, **13**, 1241-1253.

36. J. Bernstein, in *Polymorphism in Molecular Crystals*, Clarendon Press, Oxford, 2002, ch. 2, pp. 29-65.

37. T. Threlfall, *Org. Process Res. Dev.*, 2003, **7**, 1017-1027.

38. W. Ostwald, *Z. Phys. Chem*, 1897, **22**, 289-330.

39. P. Rein ten Wolde and D. Frenkel, *Phys. Chem. Chem. Phys.*, 1999, **1**, 2191-2196.

40. R. A. Van Santen, *J. Phys. Chem.*, 1984, **88**, 5768-5769.

41. J. C. Burley, M. J. Duer, R. S. Stein and R. M. Vrcelj, *Eur. J. Pharm. Sci.*, 2007, **31**, 271-276.

42. S. M. Reutzel-Edens, *Curr. Opin. Drug Discovery Dev.*, 2006, **9**, 806.

43. J. Bernstein, in *Polymorphism in Molecular Crystals*, Clarendon Press, Oxford, 2002, ch. 3, pp. 66-93.

44. K. Sangwal, in *Nucleation and Crystal Growth*, John Wiley & Sons, New Jersey, 2018, ch. 8, pp. 361-421.

45. S. Boothroyd, A. Kerridge, A. Broo, D. Buttar and J. Anwar, *Cryst. Growth Des.*, 2018, **18**, 1903-1908.

46. H. G. Brittain, *Spectroscopy*, 2000, **15**, 34-39.

47. P. G. Jones, *Chem. Br.*, 1981, **17**, 222-225.

48. T. L. Threlfall, *Analyst*, 1995, **120**, 2435-2460.

49. T. G. Fawcett, S. Gates-Rector, A. M. Gindhart, M. Rost, S. N. Kabekkodu, J. R. Blanton and T. N. Blanton, *Powder Diffr.*, 2019, **34**, 164-183.

50. K. Higashi, K. Ueda and K. Moribe, *Adv. Drug Deliv. Rev.*, 2017, **117**, 71-85.

51. E. Pindelska, A. Sokal and W. Kolodziejski, *Adv. Drug Deliv. Rev.*, 2017, **117**, 111-146.

52. G. A. Stephenson, R. A. Forbes and S. M. Reutzel-Edens, *Adv. Drug Deliv. Rev.*, 2001, **48**, 67-90.

53. A. A. Bunaciu, H. Y. Aboul-Enein and V. D. Hoang, *TrAC, Trends Anal. Chem.*, 2015, **69**, 14-22.

54. R. K. Harris, *Analyst*, 2006, **131**, 351-373.

55. P. A. Tishmack, D. E. Bugay and S. R. Byrn, *J. Pharm. Sci.*, 2003, **92**, 441-474.

56.   R. T. Berendt, D. M. Sperger, P. K. Isbester and E. J. Munson, *TrAC, Trends Anal. Chem.*, 2006, **25**, 977-984.

57.   M. Geppi, G. Mollica, S. Borsacchi and C. A. Veracini, *Appl. Spectrosc. Rev.*, 2008, **43**, 202-302.

58.   B. Perrenot and G. Widmann, *Thermochim. Acta*, 1994, **234**, 31-39.

59.   D. Giron, *Thermochim. Acta*, 1995, **248**, 1-59.

60.   H. G. Wiedemann and G. Bayer, *J. Therm. Anal.*, 1985, **30**, 1273-1281.

61.   M. R. Abu Bakar, Z. K. Nagy and C. D. Rielly, *J. Therm. Anal. Calorim.*, 2010, **99**, 609-619.

62.   H. G. Brittain, *Polymorphism in pharmaceutical solids*, CRC Press, 2016.

63.   A. Y. Lee, D. Erdemir and A. S. Myerson, *Annu. Rev. Chem. Biomol. Eng.*, 2011, **2**, 259-280.

64.   E. Hadjittofis, M. A. Isbell, V. Karde, S. Varghese, C. Ghoroi and J. Y. Y. Heng, *Pharm. Res.*, 2018, **35**, 100.

65.   J. Bernstein, in *Polymorphism in molecular crystals*, Clarendon Press, Oxford, 2002, vol. 14, ch. 7, pp. 240-256.

66.   C. A. Lipinski, *J. Pharmacol. Toxicol. Methods*, 2000, **44**, 235-249.

67.   R. Censi and P. Di Martino, *Molecules*, 2015, **20**, 18759-18776.

68.   M. Pudipeddi and A. T. M. Serajuddin, *J. Pharm. Sci.*, 2005, **94**, 929-939.

69.   A. J. Cruz-Cabeza and J. Bernstein, *Chem. Rev.*, 2014, **114**, 2170-2191.

70.   S. L. Morissette, S. Soukasene, D. Levinson, M. J. Cima and Ö. Almarsson, *Proc. Natl. Acad. Sci. U. S. A.*, 2003, **100**, 2180-2184.

71.   G. Saurabh and C. Kaushal, *J. Chem. Pharm. Res*, 2011, **3**, 6-17.

72.   US Department of Health and Human Services, Food & Drug Administration, Center for Drug Evaluation & Research, *ANDAs: Pharmaceutical Solid Polymorphism. Chemistry, Manufacturing, and Controls Information*, Maryland, 2007.

73.   G. Boehm, L. Yao, L. Han and Q. Zheng, *Acta Pharm. Sin. B*, 2013, **3**, 297-311.

74.   J. Bernstein, in *Polymorphism in Molecular Crystals*, Oxford University Press, 2002, vol. 14, ch. 10, pp. 297-307.

75.   S. Kumar and A. Nanda, *Indian J. Pharm. Sci.*, 2017, **79**, 858-871.

76.   H. Grohganz, K. Löbmann, P. Priemel, K. Tarp Jensen, K. Graeser, C. Strachan and T. Rades, *J. Drug Delivery Sci. Technol.*, 2013, **23**, 403-408.

77. I. Sathisaran and S. V. Dalvi, *Pharmaceutics*, 2018, **10**, 108-182.

78. S. Emami, M. Siahi-Shadbad, K. Adibkia and M. Barzegar-Jalali, *BioImpacts*, 2018, **8**, 305-320.

79. R. Thakuria, A. Delori, W. Jones, M. P. Lipert, L. Roy and N. Rodríguez-Hornedo, *Int. J. Pharm.*, 2013, **453**, 101-125.

80. S. Baghel, H. Cathcart and N. J. O'Reilly, *J. Pharm. Sci.*, 2016, **105**, 2527-2544.

81. A. T. M. Serajuddin, *Adv. Drug Deliv. Rev.*, 2007, **59**, 603-616.

82. S. Kalepu and V. Nekkanti, *Acta Pharm. Sin. B*, 2015, **5**, 442-453.

83. J. Brouwers, M. E. Brewster and P. Augustijns, *J. Pharm. Sci.*, 2009, **98**, 2549-2572.

84. N. J. Babu and A. Nangia, *Cryst. Growth Des.*, 2011, **11**, 2662-2679.

85. A. Karagianni, M. Malamatari and K. Kachrimanis, *Pharmaceutics*, 2018, **10**, 1-30.

86. U.S. Department of Health and Human Services, Food and Drug Administration, Center for Drug Evaluation and Research, *Regulatory Classification of Pharmaceutical Co-Crystals*, Maryland, 2018.

87. O. N. Kavanagh, D. M. Croker, G. M. Walker and M. J. Zaworotko, *Drug Discovery Today*, 2019, **24**, 796-804.

88. H. G. Brittain, *J. Pharm. Sci.*, 2013, **102**, 311-317.

89. M. Merlos, E. Portillo-Salido, A. Brenchat, B. Aubel, J. Buxens, A. Fisas, X. Codony, L. Romero, D. Zamanillo and J. M. Vela, *Eur. J. Pharmacol.*, 2018, **833**, 370-378.

90. N. Gascon, C. Almansa, M. Merlos, J. Miguel Vela, G. Encina, A. Morte, K. Smith and C. Plata-Salamán, *Expert Opin. Invest. Drugs*, 2019, **28**, 399-409.

91. K. R Jadhav, S. S Pacharane, P. P Pednekar, P. V Koshy and V. J Kadam, *Curr. Drug Ther.*, 2012, **7**, 255-262.

92. T. Wu, Y. Sun, N. Li, M. M. de Villiers and L. Yu, *Langmuir*, 2007, **23**, 5148-5153.

93. Y. Li, J. Yu, S. Hu, Z. Chen, M. Sacchetti, C. C. Sun and L. Yu, *Mol Pharm*, 2019, **16**, 1305-1311.

94. R. Laitinen, K. Löbmann, C. J. Strachan, H. Grohganz and T. Rades, *Int. J. Pharm.*, 2013, **453**, 65-79.

95. Q. Shi, S. M. Moinuddin and T. Cai, *Acta Pharm. Sin. B*, 2019, **9**, 19-35.

96.   S. J. Dengale, H. Grohganz, T. Rades and K. Löbmann, *Adv. Drug Deliv. Rev.*, 2016, **100**, 116-125.

97.   N. Wyttenbach and M. Kuentz, *Eur. J. Pharm. Biopharm.*, 2017, **112**, 204-208.

98.   A. J. Florence, in *Polymorphism in pharmaceutical solids*, ed. H. G. Brittain, CRC Press, 2nd edn., 2016, ch. 5, pp. 139-184.

99.   P. W. Cains, in *Polymorphism in Pharmaceutical Solids*, ed. H. G. Brittain, 2nd edn., 2016, ch. 4, pp. 76-138.

100.   C.-H. Gu, H. Li, R. B. Gandhi and K. Raghavan, *Int. J. Pharm.*, 2004, **283**, 117-125.

101.   S. Khoshkhoo and J. Anwar, *J. Phys. D: Appl. Phys.*, 1993, **26**, 90-93.

102.   N. Blagden, R. J. Davey, H. F. Lieberman, L. Williams, R. Payne, R. Roberts, R. Rowe and R. Docherty, *J. Chem. Soc., Faraday Trans.*, 1998, **94**, 1035-1044.

103.   M. Mirmehrabi and S. Rohani, *J. Pharm. Sci.*, 2005, **94**, 1560-1576.

104.   A. Getsoian, R. M. Lodaya and A. C. Blackburn, *Int. J. Pharm.*, 2008, **348**, 3-9.

105.   E. H. Lee, *Asian J. Pharm. Sci.*, 2014, **9**, 163-175.

106.   Renuka, S. K. Singh, A. K. Yadav, M. Gulati, A. Mittal, R. Narang and V. Garg, *Int. J. PharmTech Res.*, 2016, **9**, 144-165.

107.   M. Kitamura, *CrystEngComm*, 2009, **11**, 949-964.

108.   R. J. Davey, P. T. Cardew, D. McEwan and D. E. Sadler, *J. Cryst. Growth*, 1986, **79**, 648-653.

109.   C.-H. Gu, V. Young Jr. and D. J. W. Grant, *J. Pharm. Sci.*, 2001, **90**, 1878-1890.

110.   D. Tan, L. Loots and T. Friščić, *Chem. Commun.*, 2016, **52**, 7760-7781.

111.   N. Shan, F. Toda and W. Jones, *Chem. Commun.*, 2002, **20**, 2372-2373.

112.   D. Hasa and W. Jones, *Adv. Drug Deliv. Rev.*, 2017, **117**, 147-161.

113.   A. M. Belenguer, A. J. Cruz-Cabeza, G. I. Lampronti and J. K. M. Sanders, *CrystEngComm*, 2019, **21**, 2203-2211.

114.   A. A. L. Michalchuk, I. A. Tumanov and E. V. Boldyreva, *CrystEngComm*, 2019, **21**, 2174-2179.

115.   N. Madusanka, M. D. Eddleston, M. Arhangelskis and W. Jones, *Acta Crystallogr., Sect. B: Struct. Sci., Cryst. Eng. Mater.*, 2014, **70**, 72-80.

116. H. Wiedemann and G. Bayer, *J. Therm. Anal.*, 1985, **30**, 1273-1281.

117. P. Commins, I. T. Desta, D. P. Karothu, M. K. Panda and P. Naumov, *Chem. Commun.*, 2016, **52**, 13941-13954.

118. J. K. Guillory, in *Polymorphism in pharmaceutical solids*, ed. H. G. Brittain, Ebsco Publishing, New York, 1999, ch. 5, pp. 183-226.

119. Q. S. Yu, L. P. Dang, S. Black and H. Y. Wei, *J. Cryst. Growth*, 2012, **340**, 209-215.

120. J. D. Wright, in *Molecular Crystals*, Cambridge University Press, Cambridge, 2nd edn., 1995, ch. 1, pp. 7-8.

121. J. S. Redinha and A. J. Lopes Jesus, in *Crystallization and Materials Science of Modern Artificial and Natural Crystals*, ed. E. Borisenko, InTech, Rijeka, 2012, ch. 10, pp. 225-248.

122. T. Einfalt, O. Planinšek and K. Hrovat, *Acta Pharm.*, 2013, **63**, 305-334.

123. B. Samas, C. Seadeek, A. M. Campeta and B. P. Chekal, *J. Pharm. Sci.*, 2011, **100**, 186-194.

124. H. Zhu, C. Yuen and D. J. W. Grant, *Int. J. Pharm.*, 1996, **135**, 151-160.

125. R. V. Manek and W. M. Kolling, *AAPS PharmSciTech*, 2004, **5**, 101-108.

126. G. G. Z. Zhang and D. Zhou, in *Developing solid oral dosage forms*, eds. Y. Qiu, Y. Chen, G. Zhang, L. Yu and R. V. Mantri, Academic Press, London, 2nd edn., 2017, ch. 2, pp. 23-57.

127. G. A. Stephenson, E. G. Groleau, R. L. Kleemann, W. Xu and D. R. Rigsbee, *J. Pharm. Sci.*, 1998, **87**, 536-542.

128. A. Bērziņš, A. Trimdale, A. Kons and D. Zvaniņa, *Cryst. Growth Des.*, 2017, **17**, 5712-5724.

129. A. Kavanagh, I. McConvey, J. McCabe, H. Blade and S. Cosgrove, *Am. Pharm. Rev.*, 2012, **15**, 10.

130. J. W. Steed, *Chem. Commun.*, 2018, **54**, 13175-13182.

131. S. L. Morissette, Ö. Almarsson, M. L. Peterson, J. F. Remenar, M. J. Read, A. V. Lemmo, S. Ellis, M. J. Cima and C. R. Gardner, *Adv. Drug Deliv. Rev.*, 2004, **56**, 275-300.

132. Ö. Almarsson, M. B. Hickey, M. L. Peterson, S. L. Morissette, S. Soukasene, C. McNulty, M. Tawa, J. M. MacPhee and J. F. Remenar, *Cryst. Growth Des.*, 2003, **3**, 927-933.

133. R. Hilfiker, J. Berghausen, F. Blatter, A. Burkhard, S. M. De Paul, B. Freiermuth, A. Geoffroy, U. Hofmeier, C. Marcolli, B. Siebenhaar, M. Szelagiewicz, A. Vit and M. von Raumer, *J. Therm. Anal. Calorim.*, 2003, **73**, 429-440.

134. M. L. Peterson, S. L. Morissette, C. McNulty, A. Goldsweig, P. Shaw, M. LeQuesne, J. Monagle, N. Encina, J. Marchionna, A. Johnson, J. Gonzalez-Zugasti, A. V. Lemmo, S. J. Ellis, M. J. Cima and Ö. Almarsson, *J. Am. Chem. Soc.*, 2002, **124**, 10958-10959.

135. P. Y. Chen, *Drug Dev. Delivery*, 2018, **18**, 38-42.

136. M. C. Etter, *J. Phys. Chem.*, 1991, **95**, 4601-4610.

137. M. Lahav and L. Leiserowitz, *J. Phys. D: Appl. Phys.*, 1993, **26**, 22-31.

138. D. Gebauer, H. Cölfen, A. Verch and M. Antonietti, *Adv. Mater.*, 2009, **21**, 435-439.

139. S. H. Yu and H. Colfen, *J. Mater. Chem.*, 2004, **14**, 2124-2147.

140. I. Weissbuch, L. Leisorowitz and M. Lahav, *Adv. Mater.*, 1994, **6**, 952-956.

141. R.-Q. Song and H. Cölfen, *CrystEngComm*, 2011, **13**, 1249-1276.

142. L. Addadi, Z. Berkovitch-Yellin, I. Weissbuch, J. van Mil, L. J. W. Shimon, M. Lahav and L. Leiserowitz, *Angew. Chem., Int. Ed.*, 1985, **24**, 466-485.

143. W. Beckmann, *Org. Process Res. Dev.*, 2000, **4**, 372-383.

144. L. Nicoud, F. Licordari and A. S. Myerson, *CrystEngComm*, 2019, **21**, 2105-2118.

145. K. Chadwick, A. Myerson and B. Trout, *CrystEngComm*, 2011, **13**, 6625-6627.

146. C. P. Price, A. L. Grzesiak and A. J. Matzger, *J. Am. Chem. Soc.*, 2005, **127**, 5512-5517.

147. M. Lang, A. L. Grzesiak and A. J. Matzger, *J. Am. Chem. Soc.*, 2002, **124**, 14834-14835.

148. M. Lang, J. W. Kampf and A. J. Matzger, *J. Pharm. Sci.*, 2002, **91**, 1186-1190.

149. L. Y. Pfund, C. P. Price, J. J. Frick and A. J. Matzger, *J. Am. Chem. Soc.*, 2015, **137**, 871-875.

150. A. Caridi, S. A. Kulkarni, G. Di Profio, E. Curcio and J. H. ter Horst, *Cryst. Growth Des.*, 2014, **14**, 1135-1141.

151. H. Yang, C. L. Song, Y. X. S. Lim, W. Chen and J. Y. Y. Heng, *CrystEngComm*, 2017, **19**, 6573-6578.

152. J. V. Parambil, S. K. Poornachary, J. Y. Y. Heng and R. B. H. Tan, *CrystEngComm*, 2019, **21**, 4122-4135.

153. C. A. Mitchell, L. Yu and M. D. Ward, *J. Am. Chem. Soc.*, 2001, **123**, 10830-10839.

154. S. J. Bonafede and M. D. Ward, *J. Am. Chem. Soc.*, 1995, **117**, 7853-7861.

155. Y. Mastai, *Chem. Soc. Rev.*, 2009, **38**, 772-780.

156. A. J. Alexander and P. J. Camp, *J. Chem. Phys.*, 2019, **150**, 040901.

157. J. L. Hilden, C. E. Reyes, M. J. Kelm, J. S. Tan, J. G. Stowell and K. R. Morris, *Cryst. Growth Des.*, 2003, **3**, 921-926.

158. L. J. Chyall, J. M. Tower, D. A. Coates, T. L. Houston and S. L. Childs, *Cryst. Growth Des.*, 2002, **2**, 505-510.

159. A. R. Tyler, R. Ragbirsingh, C. J. McMonagle, P. G. Waddell, S. E. Heaps, J. W. Steed, P. Thaw, M. J. Hall and M. R. Probert, *Advance online publication. Chem*, 2019, DOI: 10.26434/chemrxiv.11366054.v1.

160. C. E. Nicholson, C. Chen, B. Mendis and S. J. Cooper, *Cryst. Growth Des.*, 2011, **11**, 363-366.

161. C. E. Nicholson and S. J. Cooper, *Crystals*, 2011, **1**, 195-205.

162. C. Chen, O. Cook, C. E. Nicholson and S. J. Cooper, *Cryst. Growth Des.*, 2011, **11**, 2228-2237.

163. S. R. Kennedy, C. D. Jones, D. S. Yufit, C. E. Nicholson, S. J. Cooper and J. W. Steed, *CrystEngComm*, 2018, **20**, 1390-1398.

164. A. B. M. Buanz and S. Gaisford, *Cryst. Growth Des.*, 2017, **17**, 1245-1250.

165. B. D. Hamilton, J.-M. Ha, M. A. Hillmyer and M. D. Ward, *Acc. Chem. Res.*, 2012, **45**, 414-423.

166. Q. Jiang and M. D. Ward, *Chem. Soc. Rev.*, 2014, **43**, 2066-2079.

167. J. C. Love, L. A. Estroff, J. K. Kriebel, R. G. Nuzzo and G. M. Whitesides, *Chem. Rev.*, 2005, **105**, 1103-1170.

168. R. Hiremath, J. A. Basile, S. W. Varney and J. A. Swift, *J. Am. Chem. Soc.*, 2005, **127**, 18321-18327.

169. J. Aizenberg, A. J. Black and G. M. Whitesides, *Nature*, 1999, **398**, 495-498.

170. I. S. Lee, A. Y. Lee and A. S. Myerson, *Pharm. Res.*, 2008, **25**, 960-968.

171. J. Aizenberg, A. J. Black and G. M. Whitesides, *J. Am. Chem. Soc.*, 1999, **121**, 4500-4509.

172. S. L. Price, *Chem. Soc. Rev.*, 2014, **43**, 2098-2111.

173. A. M. Reilly, R. I. Cooper, C. S. Adjiman, S. Bhattacharya, A. D. Boese, J. G. Brandenburg, P. J. Bygrave, R. Bylsma, J. E. Campbell, R. Car, D. H. Case, R. Chadha, J. C. Cole, K. Cosburn, H. M. Cuppen, F. Curtis, G. M. Day, R. A. DiStasio Jr, A. Dzyabchenko, B. P. van Eijck, D. M. Elking, J. A. van den Ende, J. C. Facelli, M. B. Ferraro, L. Fusti-Molnar, C.-A. Gatsiou, T. S. Gee, R. de Gelder, L. M. Ghiringhelli, H. Goto, S. Grimme, R. Guo, D. W. M. Hofmann, J. Hoja, R. K. Hylton, L. Iuzzolino, W. Jankiewicz, D. T. de Jong, J. Kendrick, N. J. J. de Klerk, H.-Y. Ko, L. N. Kuleshova, X. Li, S. Lohani, F. J. J. Leusen, A. M. Lund, J. Lv, Y. Ma, N. Marom, A. E. Masunov, P. McCabe, D. P. McMahon, H. Meekes, M. P. Metz, A. J. Misquitta, S. Mohamed, B. Monserrat, R. J. Needs, M. A. Neumann, J. Nyman, S. Obata, H. Oberhofer, A. R. Oganov, A. M. Orendt, G. I. Pagola, C. C. Pantelides, C. J. Pickard, R. Podeszwa, L. S. Price, S. L. Price, A. Pulido, M. G. Read, K. Reuter, E. Schneider, C. Schober, G. P. Shields, P. Singh, I. J. Sugden, K. Szalewicz, C. R. Taylor, A. Tkatchenko, M. E. Tuckerman, F. Vacarro, M. Vasileiadis, A. Vazquez-Mayagoitia, L. Vogt, Y. Wang, R. E. Watson, G. A. de Wijs, J. Yang, Q. Zhu and C. R. Groom, *Acta Crystallogr., Sect. B: Struct. Sci., Cryst. Eng. Mater.*, 2016, **72**, 439-459.

174. S. L. Price, *Adv. Drug Deliv. Rev.*, 2004, **56**, 301-319.

175. S. L. Price and S. M. Reutzel-Edens, *Drug Discovery Today*, 2016, **21**, 912-923.

176. Y. A. Abramov, *Org. Process Res. Dev.*, 2013, **17**, 472-485.

177. S. Price, *Acta Crystallogr., Sect. B: Struct. Sci., Cryst. Eng. Mater.*, 2013, **69**, 313-328.

178. J.-B. Arlin, L. S. Price, S. L. Price and A. J. Florence, *Chem. Commun.*, 2011, **47**, 7074-7076.

179. D. H. Case, V. K. Srirambhatla, R. Guo, R. E. Watson, L. S. Price, H. Polyzois, J. K. Cockcroft, A. J. Florence, D. A. Tocher and S. L. Price, *Cryst. Growth Des.*, 2018, **18**, 5322-5331.

180. S. L. Price, D. E. Braun and S. M. Reutzel-Edens, *Chem. Commun.*, 2016, **52**, 7065-7077.

181. S. L. Price, *Proc. R. Soc. A*, 2018, **474**, 20180351.

182. R. M. Bhardwaj, J. A. McMahon, J. Nyman, L. S. Price, S. Konar, I. D. H. Oswald, C. R. Pulham, S. L. Price and S. M. Reutzel-Edens, *J. Am. Chem. Soc.*, 2019, **141**, 13887-13897.

183. J. Nyman and Susan M. Reutzel-Edens, *Faraday Discuss.*, 2018, **211**, 459-476.

184. Y. Osada and K. Kajiwara, *Gels Handbook: Applications*, Academic Press, San Diego, 2001.

185. P. J. Flory, *Faraday Discuss. Chem. Soc.*, 1974, **57**, 7-18.

186. K. Almdal, J. Dyre, S. Hvidt and O. Kramer, *Polym. Gels Networks*, 1993, **1**, 5-17.

187. L. A. Estroff and A. D. Hamilton, *Chem. Rev.*, 2004, **104**, 1201-1218.

188. P. Terech and R. G. Weiss, *Chem Rev*, 1997, **97**, 3133-3159.

189. J. Le Bideau, L. Viau and A. Vioux, *Chem. Soc. Rev.*, 2011, **40**, 907-925.

190. A. Du, B. Zhou, Z. Zhang and J. Shen, *Materials*, 2013, **6**, 941-968.

191. D. Adams, *Gels*, 2018, **4**, 32-36.

192. L. L. E. Mears, E. R. Draper, A. M. Castilla, H. Su, Zhuola, B. Dietrich, M. C. Nolan, G. N. Smith, J. Doutch, S. Rogers, R. Akhtar, H. Cui and D. J. Adams, *Biomacromolecules*, 2017, **18**, 3531-3540.

193. A. C. Balazs, *Nature*, 2013, **493**, 172-173.

194. Y. Osada and J.-P. Gong, *Adv. Mater.*, 1998, **10**, 827-837.

195. G. M. Kavanagh and S. B. Ross-Murphy, *Prog. Polym. Sci.*, 1998, **23**, 533-562.

196. M. Annaka and T. Tanaka, *Nature*, 1992, **355**, 430-432.

197. S. Panyukov and Y. Rabin, *Phys. Rep.*, 1996, **269**, 1-131.

198. R. M. Ziff and G. Stell, *J. Chem. Phys.*, 1980, **73**, 3492-3499.

199. J. W. Steed, *Chem. Commun.*, 2011, **47**, 1379-1383.

200. D. J. Abdallah and R. G. Weiss, *Adv. Mater.*, 2000, **12**, 1237-1247.

201. E. R. Draper and D. J. Adams, *Chem*, 2017, **3**, 390-410.

202. C. D. Jones, S. R. Kennedy, M. Walker, D. S. Yufit and J. W. Steed, *Chem.*, 2017, **3**, 603-628.

203. D. J. Adams, K. Morris, L. Chen, L. C. Serpell, J. Bacsa and G. M. Day, *Soft Matter*, 2010, **6**, 4144-4156.

204. H. R. Khavasi and M. Esmaeili, *Langmuir*, 2019, **35**, 4660-4671.

205. G. K. Veits, K. K. Carter, S. J. Cox and A. J. McNeil, *J. Am. Chem. Soc.*, 2016, **138**, 12228-12233.

206. P. Terech, D. Pasquier, V. Bordas and C. Rossat, *Langmuir*, 2000, **16**, 4485-4494.

207. G. Yu, X. Yan, C. Han and F. Huang, *Chem. Soc. Rev.*, 2013, **42**, 6697-6722.

208. N. M. Sangeetha and U. Maitra, *Chem. Soc. Rev.*, 2005, **34**, 821-836.

209. A. R. Hirst, B. Escuder, J. F. Miravet and D. K. Smith, *Angew. Chem., Int. Ed.*, 2008, **47**, 8002-8018.

210. S. Banerjee, R. K. Das and U. Maitra, *J. Mater. Chem.*, 2009, **19**, 6649-6687.

211. T. Christoff-Tempesta, A. Lew and J. Ortony, *Gels*, 2018, **4**, 40-73.

212. C. D. Jones and J. W. Steed, *Chem. Soc. Rev.*, 2016, **45**, 6546-6596.

213. A. Wang, W. Shi, J. Huang and Y. Yan, *Soft Matter*, 2016, **12**, 337-357.

214. J. G. Hardy, A. R. Hirst, I. Ashworth, C. Brennan and D. K. Smith, *Tetrahedron*, 2007, **63**, 7397-7406.

215. T. K. Adalder, U. K. Das, J. Majumder, R. Roy and P. Dastidar, *J. Indian Inst. Sci.*, 2014, **94**, 9-24.

216. L. Meazza, J. A. Foster, K. Fucke, P. Metrangolo, G. Resnati and J. W. Steed, *Nat. Chem.*, 2013, **5**, 42-47.

217. Y. Huang, S. Liu, Z. Xie, Z. Sun, W. Chai and W. Jiang, *Front. Chem. Sci. Eng.*, 2018, **12**, 252-261.

218. A. Pizzi, L. Lascialfari, N. Demitri, A. Bertolani, D. Maiolo, E. Carretti and P. Metrangolo, *CrystEngComm*, 2017, **19**, 1870-1874.

219. S. M. Ramalhete, J. S. Foster, H. R. Green, K. P. Nartowski, M. Heinrich, P. C. Martin, Y. Z. Khimyak and G. O. Lloyd, *Faraday Discuss.*, 2017, **203**, 423-439.

220. L. Arnedo-Sánchez, Nonappa, S. Bhowmik, S. Hietala, R. Puttreddy, M. Lahtinen, L. De Cola and K. Rissanen, *Dalton Trans.*, 2017, **46**, 7309-7316.

221. A. Sikder, J. Sarkar, T. Sakurai, S. Seki and S. Ghosh, *Nanoscale*, 2018, **10**, 3272-3280.

222. N. Cheng, Q. Kang, J. Xiao, N. Du and L. Yu, *J. Colloid Interface Sci.*, 2018, **511**, 215-221.

223. A. P. Sivadas, N. S. S. Kumar, D. D. Prabhu, S. Varghese, S. K. Prasad, D. S. S. Rao and S. Das, *J. Am. Chem. Soc.*, 2014, **136**, 5416-5423.

224. Z. Gao, P. A. Korevaar, R. Zhong, Z. Wu and F. Wang, *Chem. Commun.*, 2018, **54**, 9857-9860.

225. S. C. Zacharias, G. Ramon and S. A. Bourne, *Soft Matter*, 2018, **14**, 4505-4519.

226. A. Y.-Y. Tam and V. W.-W. Yam, *Chem. Soc. Rev.*, 2013, **42**, 1540-1567.

227. M. de Loos, B. L. Feringa and J. H. van Esch, *Eur. J. Org. Chem.*, 2005, **2005**, 3615-3631.

228. F. Fages, F. Vögtle and M. Žinic, in *Low Molecular Mass Gelators*, Springer, Berlin, 2005, ch. 3, pp. 77-131.

229. J. Schiller, J. V. Alegre-Requena, E. Marqués-López, R. P. Herrera, J. Casanovas, C. Alemán and D. Díaz Díaz, *Soft Matter*, 2016, **12**, 4361-4374.

230. D. Ghosh, I. Lebedytė, D. S. Yufit, K. K. Damodaran and J. W. Steed, *CrystEngComm*, 2015, **17**, 8130-8138.

231. A. Pal, Y. K. Ghosh and S. Bhattacharya, *Tetrahedron*, 2007, **63**, 7334-7348.

232. S. V. Raghava, B. K. Srivastava, K. Ramshad, S. Antharjanam, B. Varghese and K. M. Muraleedharan, *Soft Matter*, 2018, **14**, 2357-2364.

233. M. de Loos, J. H. van Esch, R. M. Kellogg and B. L. Feringa, *Tetrahedron*, 2007, **63**, 7285-7301.

234. J. J. van Gorp, J. A. J. M. Vekemans and E. W. Meijer, *J. Am. Chem. Soc.*, 2002, **124**, 14759-14769.

235. J. van Esch, S. De Feyter, R. M. Kellogg, F. De Schryver and B. L. Feringa, *Chem. - Eur. J.*, 1997, **3**, 1238-1243.

236. S. Meng, Y. Tang, Y. Yin, X. Yin and J. Xie, *RSC Adv.*, 2013, **3**, 18115-18127.

237. R. C. Howe, A. P. Smalley, A. P. Guttenplan, M. W. Doggett, M. D. Eddleston, J. C. Tan and G. O. Lloyd, *Chem. Commun.*, 2013, **49**, 4268-4270.

238. A. E. Hooper, S. R. Kennedy, C. D. Jones and J. W. Steed, *Chem. Commun.*, 2016, **52**, 198-201.

239. A. Ghosh, P. Das, R. Kaushik, K. K. Damodaran and D. A. Jose, *RSC Adv.*, 2016, **6**, 83303-83311.

240. S. Wang, K. Liu, S. Gao, J. Wang, R. K. Marella and Y. Fang, *Soft Matter*, 2017, **13**, 8609-8617.

241. M.-O. M. Piepenbrock, G. O. Lloyd, N. Clarke and J. W. Steed, *Chem. Commun.*, 2008, 2644-2646.

242. C. A. Offiler, C. D. Jones and J. W. Steed, *Chem. Commun.*, 2017, **53**, 2024-2027.

243. F. Piana, D. H. Case, S. M. Ramalhete, G. Pileio, M. Facciotti, G. M. Day, Y. Z. Khimyak, J. Angulo, R. C. D. Brown and P. A. Gale, *Soft Matter*, 2016, **12**, 4034-4043.

244. C. Baddeley, Z. Yan, G. King, P. M. Woodward and J. D. Badjić, *J. Org. Chem.*, 2007, **72**, 7270-7278.

245. Y. Lan, M. G. Corradini, R. G. Weiss, S. R. Raghavan and M. A. Rogers, *Chem. Soc. Rev.*, 2015, **44**, 6035-6058.

246. S. R. Raghavan and B. H. Cipriano, in *Molecular gels: materials with self-assembled fibrillar networks*, eds. R. G. Weiss and P. Terech, Springer, The Netherlands, 2005, ch. 8, pp. 241-252.

247. A. McNaught and A. Wilkinson, *IUPAC Compendium of Chemical Terminology*, Blackwell Scientific Publications, Oxford, 2nd edn., 1997.

248. R. Cudney, S. Patel and A. McPherson, *Acta Crystallogr., Sect. D: Biol. Crystallogr.*, 1994, **50**, 479-483.

249. C. Biertumpfel, J. Basquin, D. Suck and C. Sauter, *Acta Crystallogr., Sect. D: Biol. Crystallogr.*, 2002, **58**, 1657-1659.

250. B. Lorber, C. Sauter, A. Théobald-Dietrich, A. Moreno, P. Schellenberger, M.-C. Robert, B. Capelle, S. Sanglier, N. Potier and R. Giegé, *Prog. Biophys. Mol. Biol.*, 2009, **101**, 13-25.

251. R. Liesegang, *Naturwiss. Wochenschr.*, 1896, **10**, 353-362.

252. H. K. Henisch, *Crystals in gels and Liesegang rings*, Cambridge University Press, Cambridge, 2005.

253. H. N. Holmes, *J. Phys. Chem.*, 1917, **21**, 709-733.

254. J. M. García-Ruiz, M. L. Novella, R. Moreno and J. A. Gavira, *J. Cryst. Growth*, 2001, **232**, 165-172.

255. M. C. Robert and F. Lefaucheux, *J. Cryst. Growth*, 1988, **90**, 358-367.

256. A. Dawn, *Int. J. Mol. Sci.*, 2019, **20**, 22.

257. J. Xiao, Y. Zhu, Y. Liu, H. Liu, Y. Zeng, F. Xu and L. Wang, *Cryst. Growth Des.*, 2008, **8**, 2887-2891.

258. F. Otálora, J. A. Gavira, J. D. Ng and J. M. García-Ruiz, *Prog. Biophys. Mol. Biol.*, 2009, **101**, 26-37.

259. C. Sudha, P. Parimaladevi and K. Srinivasan, *Mater. Sci. Eng., C*, 2015, **47**, 150-155.

260. Y. Diao, M. E. Helgeson, A. S. Myerson, T. A. Hatton, P. S. Doyle and B. L. Trout, *J. Am. Chem. Soc.*, 2011, **133**, 3756-3759.

261. Y. Diao, K. E. Whaley, M. E. Helgeson, M. A. Woldeyes, P. S. Doyle, A. S. Myerson, T. A. Hatton and B. L. Trout, *J. Am. Chem. Soc.*, 2012, **134**, 673-684.

262. R. I. Petrova, R. Patel and J. A. Swift, *Cryst. Growth Des.*, 2006, **6**, 2709-2715.

263. R. I. Petrova and J. A. Swift, *J. Am. Chem. Soc.*, 2004, **126**, 1168-1173.

264. L. A. Nguyen, H. He and C. Pham-Huy, *Int. J. Biomed. Sci.*, 2006, **2**, 85-100.

265. M. Banerjee, S. Saraswatula, L. G. Willows, H. Woods and B. Brettmann, *J. Mater. Chem. B*, 2018, **6**, 7317-7328.

266. C. Ruiz-Palomero, S. R. Kennedy, M. L. Soriano, C. D. Jones, M. Valcarcel and J. W. Steed, *Chem. Commun.*, 2016, **52**, 7782-7785.

267. D. K. Kumar and J. W. Steed, *Chem. Soc. Rev.*, 2014, **43**, 2080-2088.

268. L. A. Estroff, L. Addadi, S. Weiner and A. D. Hamilton, *Org. Biomol. Chem.*, 2004, **2**, 137-141.

269. A. Dawn, M. Mirzamani, C. D. Jones, D. S. Yufit, S. Qian, J. W. Steed and H. Kumari, *Soft Matter*, 2018, **14**, 9489-9497.

270. G. O. Lloyd and J. W. Steed, *Nat. Chem.*, 2009, **1**, 437-442.

271. T. Becker, C. Yong Goh, F. Jones, M. J. McIldowie, M. Mocerino and M. I. Ogden, *Chem. Commun.*, 2008, **33**, 3900-3902.

272. C. E. Stanley, N. Clarke, K. M. Anderson, J. A. Elder, J. T. Lenthall and J. W. Steed, *Chem. Commun.*, 2006, **30**, 3199-3201.

273. J. E. A. Webb, M. J. Crossley, P. Turner and P. Thordarson, *J. Am. Chem. Soc.*, 2007, **129**, 7155-7162.

274. G. O. Lloyd, M.-O. M. Piepenbrock, J. A. Foster, N. Clarke and J. W. Steed, *Soft Matter*, 2012, **8**, 204-216.

275. H.-J. Kim, W.-C. Zin and M. Lee, *J. Am. Chem. Soc.*, 2004, **126**, 7009-7014.

276. H.-J. Kim, J.-H. Lee and M. Lee, *Angew. Chem., Int. Ed.*, 2005, **44**, 5810-5814.

277. J. W. Steed, *Chem. Soc. Rev.*, 2010, **39**, 3686-3699.

278. J. A. Foster, M.-O. M. Piepenbrock, G. O. Lloyd, N. Clarke, J. A. K. Howard and J. W. Steed, *Nat. Chem.*, 2010, **2**, 1037-1043.

279. F. Aparicio, E. Matesanz and L. Sanchez, *Chem. Commun.*, 2012, **48**, 5757-5759.

280. C. Rustichelli, G. Gamberini, V. Ferioli, M. C. Gamberini, R. Ficarra and S. Tommasini, *J. Pharm. Biomed. Anal.*, 2000, **23**, 41-54.

281. I. Torres-Moya, B. Saikia, P. Prieto, J. R. Carrillo and J. W. Steed, *CrystEngComm*, 2019, **21**, 2135-2143.

282. M. A. Rahim, Y. Hata, M. Björnmalm, Y. Ju and F. Caruso, *Small*, 2018, **14**, 1801202.

283. M. A. Rahim, M. Björnmalm, T. Suma, M. Faria, Y. Ju, K. Kempe, M. Müllner, H. Ejima, A. D. Stickland and F. Caruso, *Angew. Chem., Int. Ed.*, 2016, **55**, 13803-13807.

284. J. Buendia, E. Matesanz, D. K. Smith and L. Sanchez, *CrystEngComm*, 2015, **17**, 8146-8152.

285. L. Kaufmann, S. R. Kennedy, C. D. Jones and J. W. Steed, *Chem. Commun.*, 2016, **52**, 10113-10116.

286. A. Dawn, K. S. Andrew, D. S. Yufit, Y. Hong, J. P. Reddy, C. D. Jones, J. A. Aguilar and J. W. Steed, *Cryst. Growth Des.*, 2015, **15**, 4591-4599.

287. S. Chen, I. A. Guzei and L. Yu, *J. Am. Chem. Soc.*, 2005, **127**, 9881-9885.

288. L. A. Yu, *Acc. Chem. Res.*, 2010, **43**, 1257-1266.

289. M. Tan, A. G. Shtukenberg, S. C. Zhu, W. Q. Xu, E. Dooryhee, S. M. Nichols, M. D. Ward, B. Kahr and Q. Zhu, *Faraday Discuss.*, 2018, **211**, 477-491.

290. K. S. Gushurst, J. Nyman and S. X. M. Boerrigter, *CrystEngEomm*, 2019, **21**, 1363-1368.

291. M. Vasileiadis, A. V. Kazantsev, P. G. Karamertzanis, C. S. Adjiman and C. C. Pantelides, *Acta Crystallogr., Sect. B: Struct. Sci.*, 2012, **68**, 677-685.

292. J. A. Foster, K. K. Damodaran, A. Maurin, G. M. Day, H. P. G. Thompson, G. J. Cameron, J. C. Bernal and J. W. Steed, *Chem. Sci.*, 2017, **8**, 78-84.

293. D. Ghosh, K. Ferfolja, Z. Drabavicius, J. W. Steed and K. K. Damodaran, *New J. Chem.*, 2018, **42**, 19963-19970.

294. J. Sivy, V. Kettmann and E. Fresova, *Acta Crystallogr., Sect. C: Cryst. Struct. Commun.*, 1991, **47**, 2695-2696.

295. A. Kiss and J. Repasi, *Analyst*, 1993, **118**, 661-664.

296. M. Kuhnert, D. Seidel and G. Unterkircher, *Sci. Pharm.*, 1987, **55**, 13-25.

297. A. M. Namespetra, D. A. Hirsh, M. P. Hildebrand, A. R. Sandre, H. Hamaed, J. M. Rawson and R. W. Schurko, *CrystEngComm*, 2016, **18**, 6213-6232.

298. M. Hildebrand, H. Hamaed, A. M. Namespetra, J. M. Donohue, R. Q. Fu, I. Hung, Z. H. Gan and R. W. Schurko, *CrystEngComm*, 2014, **16**, 7334-7356.

299. A. Cayuela, M. L. Soriano, S. R. Kennedy, J. W. Steed and M. Valcárcel, *Talanta*, 2016, **151**, 100-105.

300. P. Byrne, G. O. Lloyd, L. Applegarth, K. M. Anderson, N. Clarke and J. W. Steed, *New J. Chem.*, 2010, **34**, 2261-2274.

301. M.-O. M. Piepenbrock, N. Clarke and J. W. Steed, *Langmuir*, 2009, **25**, 8451-8456.

302. M.-O. M. Piepenbrock, N. Clarke, J. A. Foster and J. W. Steed, *Chem. Commun.*, 2011, **47**, 2095-2097.

303. K. Q. Liu and J. W. Steed, *Soft Matter*, 2013, **9**, 11699-11705.

304. L. Applegarth, N. Clark, A. C. Richardson, A. D. M. Parker, I. Radosavljevic-Evans, A. E. Goeta, J. A. K. Howard and J. W. Steed, *Chem. Commun.*, 2005, **43**, 5423-5425.

305. K. Fucke, G. J. McIntyre, M.-H. Lemée-Cailleau, C. Wilkinson, A. J. Edwards, J. A. K. Howard and J. W. Steed, *Chem. - Eur. J.*, 2015, **21**, 1036-1047.

306. T. Kitchen, C. Melvin, M. N. Mohd Najib, A. S. Batsanov and K. Edkins, *Cryst. Growth Des.*, 2016, **16**, 4531-4538.

2. The Polymorphism of Mexiletine Hydrochloride

2.1 Introduction

The polymorphs of an active pharmaceutical ingredient (API) can have very different physical and chemical properties, which impact pharmaceutically important parameters such as bioavailability, dissolution rate and tabletability. Therefore, the polymorphism of an API must be tightly controlled to ensure that the properties of the medicine are reliable.[1, 2] The uncontrolled emergence of an unknown or undesirable solid form at any stage in the life-cycle of a pharmaceutical can drastically reduce the efficacy of the drug and incur severe knock on effects for patients and the manufacturer, as famously occurred with ritonavir.[3] For these reasons, pharmaceutical companies face significant pressure to fully characterise and patent the solid-state landscape of new APIs, for example as part of a new drug application (NDA) filing.[4, 5] The most common method used to assess the solid-form landscape of a new API is a solution-phase polymorph screen, in which the drug is crystallised from a wide range of solvents, using a variety of solution-phase crystallisation techniques to access the full range of kinetic and thermodynamic solid forms.[6, 7] These experiments can either be undertaken manually or more recently, using high-throughput robotics that are significantly more efficient.[8] There has also been significant research into computational crystal structure prediction, which can be used to support experimental polymorph screens by identifying missed forms and predicting the conditions that may access new polymorphs.[9]

The API used in this polymorph screen is mexiletine hydrochloride, an anti-arrhythmic drug used to treat patients with an irregular heatbeat[10] (Figure 2.1). It is formulated as a racemate, but the two enantiomers have different pharmacokinetic profiles[11] and there has been significant research into the stereoselective synthesis and crystallisation of the drug.[12-18] Studies have shown that the enantiomeric excess of mexiletine can be determined by ^{1}H NMR spectroscopy using a chiral solvating agent, and that this method is much simpler than traditional chromatographic tehcniques.[19, 20] The chloride counterion has also enabled characterisation using solid-state ^{35}Cl NMR spectroscopy, which has emerged as a powerful method for distinguishing between the polymorphs of chloride-containing drugs.[21, 22]
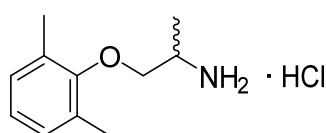
Figure 2.1: The structure of mexiletine hydrochloride.

Mexiletine HCl is reported to have six polymorphs, of which two crystal structures are published in the CSD.[21, 23-25] These forms have been characterised by IR spectroscopy, differential scanning calorimetry (DSC),[24, 25] and in some cases, solid-state NMR spectroscopy.[21] DSC measurements show that mexiletine is an enantiotropic system in which two unsolvated polymorphs, termed Modifikation I and II by Kuhnert-Brandstätter et al.[25] and Forms IV and VI by Kiss et al.,[24] are thermodynamically stable at different temperatures. [24, 25] The structure of the room temperature stable form is known, but the high temperature stable form is yet to be characterised by X-ray diffraction.

The structure of the room temperature stable form of mexiletine was published in 1991 by Sivy et al.[23] Although mexiletine has a chiral centre, the structure is racemic and crystallises in a centrosymmetric space group. There are two molecules per asymmetric unit, which share the same gauche conformation of the aliphatic chain. The terminal ammonium cations hydrogen bond to the chloride counterions of neighbouring molecules, forming a hydrogen-bonded polymer along the crystallographic *a*-axis (Figure 2.2). There are two chloride environments, one that has two NH $\cdots$ Cl hydrogen bonds and one that has four. Previous studies have shown that these two environments can be distinguished by ^{35}Cl solid-state NMR.[22]
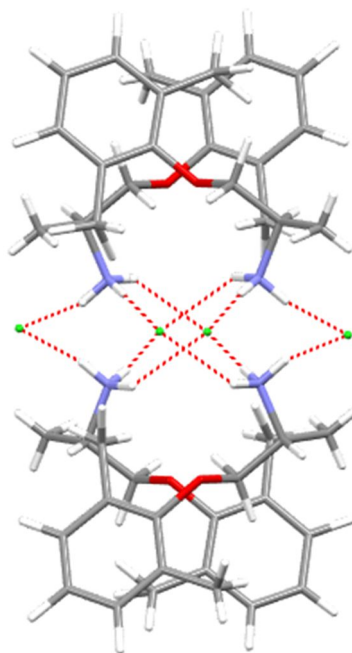
Figure 2.2: The room temperature stable form of mexiletine, viewed along the *a*-axis.

The crystal structure of the first metastable form of mexiletine was published in 2016 by Namespetra et al.[21] This structure is once again a centrosymmetric racemate. There is only one molecule per asymmetric unit, which adopts a gauche conformation. The structure is a salt, with three NH$\cdots$Cl hydrogen bonds per chloride anion. In contrast to the room temperature stable form, all chloride environments in this

structure are equivalent by NMR spectroscopy.[21] Hydrogen-bonded mexiletine polymers run along the crystallographic *c*-axis, in which the molecules are arranged in a square (Figure 2.3). The four molecules making up this motif are related by inversion, whilst the top and bottom layers are related by a *c*-glide plane.
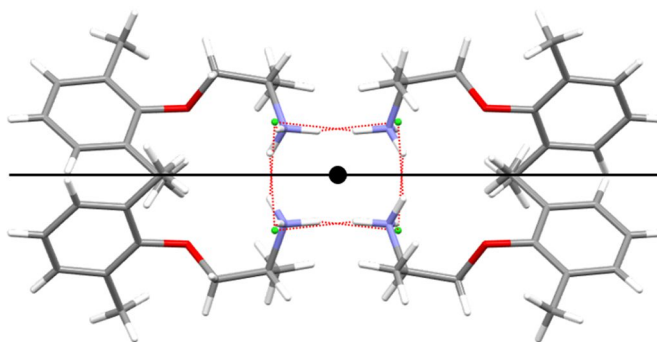
Figure 2.3: The anhydrous metastable form of mexiletine, viewed down the *c*-axis. The centre of inversion is shown by a black circle and the glide plane is shown by a black line.

This work aims to fully characterise the solid-form landscape of mexiletine hydrochloride using X-ray diffraction, alongside spectroscopic and thermal techniques. A rigorous polymorph screen was undertaken using various solution-phase and high-temperature crystallisation methods, designed to access a range of kinetic, thermodynamic, solvated, and anhydrous solid forms. Each form was characterised by IR spectroscopy, PXRD, DSC, TGA and where possible, single-crystal X-ray diffraction. The experimental screen was supported by computational crystal structure prediction, which was used to ensure that the experimental solid-form landscape is complete.

2.2   Polymorph Screening

According to this study, there are five solid forms of mexiletine. An enantiotropic pair of anhydrous polymorphs that are stable at different temperatures, one anhydrous metastable form, and two related families of metastable channel solvates. In the solvate structures, the drug molecules form a porous framework that can accommodate an extensive range of solvents. These solvates can be divided into two broad families, based on the packing arrangement in their mexiletine frameworks. Little change is observed in each of the host structures with a wide variety of guests[26, 27] and in at least one case, the channel arrangement is retained in the absence of any solvent.[28, 29] Eleven solvates of each type were observed in this study, and given this highly prolific solvate formation, it is likely that further solvates of similar structure are possible. Indeed, two further families of channel solvates were identified in Chapter 3. The large number of isomorphic solvates may account for the extra polymorph identified by IR spectroscopy in a previous study,[24] as the incorporation of different solvents within the channels can significantly alter the IR spectrum of the material without inducing any significant structural change.

All previous studies have used different names to refer to the polymorphs of mexiletine. In this work, the non-solvated forms will be named according to their thermodynamic stability. The room temperature stable form is termed Form 1, the enantiotropically related high temperature stable form is termed Form 2 and the non-solvated metastable polymorph is termed Form 3. The previous nomenclature for these forms is summarised in Table 2.1. The two solvate families are termed Type A and B.

Table 2.1: Naming scheme for the polymorphs of mexiletine.

	This work	Kuhnert-Brandstätter et al.[25]	Kiss et al.[24]	Namespetra et al.[21]
Form names	Form 1	Modifikation II	Form IV	Mexi-I
	Form 2	Modifikation I	Form VI	Mexi-III
	Form 3	Not mentioned	Not mentioned	Mexi-II

According to previous literature, Form 1 of mexiletine can be crystallised from ethanol and butanol.[23, 24] In addition to these routes, our polymorph screen revealed that this form could also be accessed by slow and fast cooling (SC and FC), evaporation (EV) and anti-solvent precipitation (PPT) crystallisations, from a range of different solvents (Table 2.2). Single crystals of Form 2 were grown by sublimation at 150 °C, over a period of seven hours. This procedure is similar to the one reported by Hildebrand et al., to access the high temperature form which they referred to as Mexi II.[22] Although in this case, the use of sublimation allows the formation of single crystals rather than a powder. Namespetra et al.[21] crystallised Form 3 by slow evaporation from acetone and in addition to this method, we have also crystallised this form by the evaporation of 1-propanol and fast cooling from nitromethane, acetonitrile and ethyl acetate solutions. In these experiments, Form 3 crystallises concomitantly with Form 1 which suggests that these structures are close in energy (Figure 2.4).
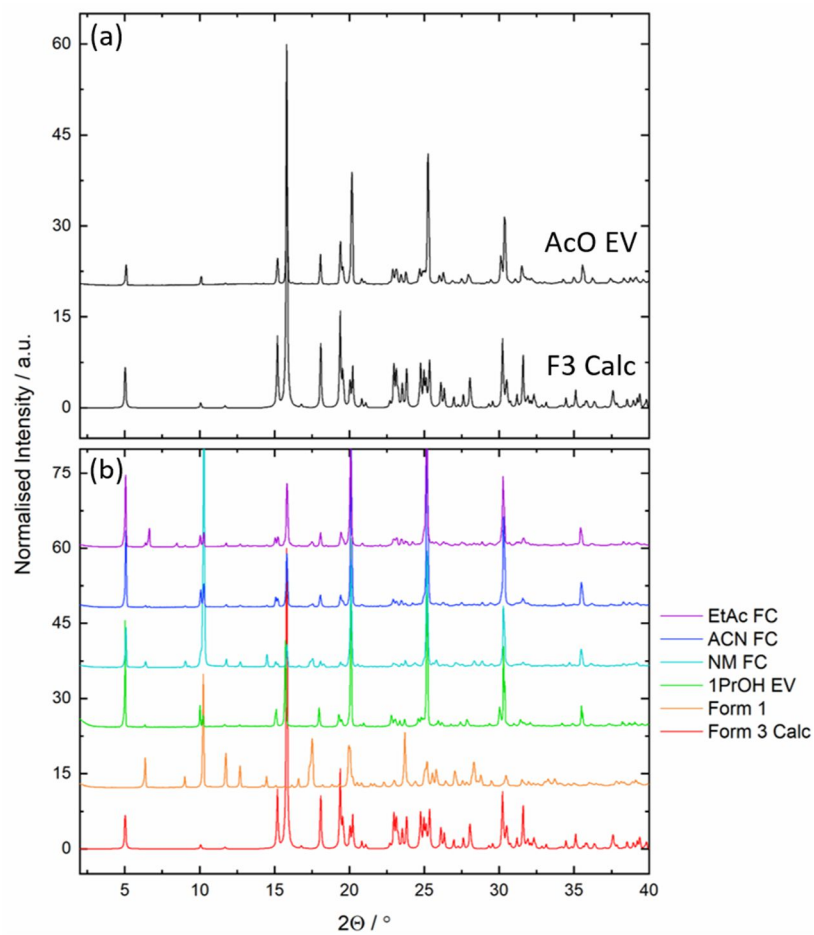
Figure 2.4: (a) PXRD pattern of the pure sample of Form 3, crystallised by evaporation of acetone, compared with the pattern calculated from the single crystal data, showing that they are the same. The experimental pattern exhibits some preferred orientation effects. (b) PXRD patterns of the mixtures of Form 3 and Form 1, crystallised by fast cooling from ethyl acetate, acetonitrile and nitromethane and evaporation of 1-propanol. PXRD patterns of pure Forms 1 and 3 are included for comparison.

The Type A and B solvates were crystallised by slow and fast cooling, evaporation and precipitation from a wide range of solvent systems (Table 2.2). The fast cooling and precipitation methods often involved very rapid crystallisation, which prevented the growth of diffraction-quality single crystals. However, for solvates that were crystallised by precipitation, single crystals could often be grown using vapour diffusion to reduce the rate of anti-solvent addition. In some vapour diffusion experiments, the anti-solvent was changed from hexane to octane as it has a lower vapour pressure and further reduced the rate of anti-solvent addition. Some conditions lead to the concomitant crystallisation of more than one form. Precipitation from chloroform/hexane yields a mixture of a Type B solvate and Form 1. Similarly, a mixture of Type A and Type B solvates crystallise concomitantly by precipitation from DCM/hexane.

Table 2.2: Crystallisation conditions for all polymorphs of mexiletine.

Name	Crystallisation Technique
Form 1	As delivered **Slow cooling from:** chloroform (CHCl$_3$), ethyl acetate (EtAc), acetonitrile (ACN), nitromethane (NM), amyl alcohol (AmOH), 1-butanol (1BuOH), 2-butanol (2BuOH), 1-propanol (1PrOH), 2-propanol (2PrOH), ethanol (EtOH) **Fast cooling from:** CHCl$_3$, AmOH, 1BuOH, 2BuOH, 1PrOH, 2PrOH, EtOH **Precipitation from:** 1BuOH/hexane, EtOH/hexane, MeOH/hexane **Evaporation of:** CHCl3, 1BuOH, 2BuOH, 2PrOH, EtOH, MeOH, ACN
Form 2	Heat any other form above its transition temperature or, sublimation at 150 °C
Form 3	A pure sample can be obtained by evaporation of acetone. A mixture with Form 1 can be obtained by: **Evaporation from:** 1PrOH **Fast cooling from:** NM, EtAC, ACN
Type A Solvates	**Slow cooling from:** Tol, DCM, MeOH **Fast cooling from:** Tol **Precipitation from:** 1PrOH/hexane, AmOH/hexane, DMF/diethyl ether, 2BuOH/hexane, 2PrOH/hexane **Evaporation of:** DCM
Type B Solvates	**Slow cooling from:** AcO, EMK, THF, Dio **Fast cooling from:** AcO, Dio, THF, DCM, EMK **Precipitation from:** CHCl3/hexane (mixture with Form 1)
Both solvated polymorphs crystallise concomitantly by precipitation from DCM/hexane	

The five solid forms of mexiletine were identified by PXRD, using the program PolySNAP[30, 31] to group the patterns together by similarity. To ensure this analysis was accurate, only high-resolution PXRD patterns were used, and mixtures or low crystallinity samples were discounted. The discounted samples include Type A solvates crystallised by precipitation from $CHCl_3$ or DCM/hexane and Type B solvates crystallised by fast cooling from DCM or THF and slow cooling from 1,4-dioxane. At a similarity coefficient of 0.65, the patterns were divided into five distinct clusters, except for the Type A methanol solvate. PolySNAP suggests that the methanol solvate is unrelated to any other form (Figure 2.5), although in fact it is a member of the Type A solvates. At a similarity coefficient of 0.65, the PXRD patterns of Forms 1, 2 and 3 are all unique. However, at similarity coefficient of 0.6, Form 2 falls into the same cluster as the Type B solvates, which shows that these two forms are structurally related. Within both solvate clusters, there are various sub-groups with higher similarity coefficients. The highest similarity sub-groups often contain the same solvate crystallised by different methods whereas more differences are observed between solvates containing different solvents.
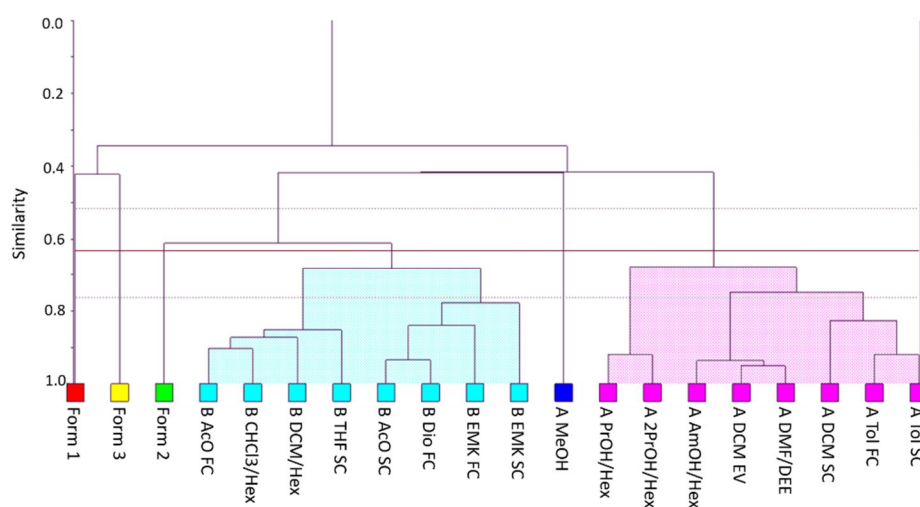
Figure 2.5: The PoySNAP packing similarity dendrogram. The red line at 0.65 shows the similarity coefficient that was used to cluster the patterns into the groups highlighted by different colours.

89

A similar clustering analysis was carried out on the single crystal structures of Forms 1, 2, 3 and seven of the Type A solvates, using the CSD-Materials module in Mercury.[32] The packing similarity analysis generates a cluster of 20 molecules to represent each crystal structure.[33] Pairs of clusters are overlaid and the resulting root mean square deviation (RMSD) can be used to quantify differences between the two forms (Table 2.3). If all of the molecules in both clusters overlap, an RMSD value of less than 0.6 Å shows that the two structures are the same,[34] and based on these results, Mercury separates the crystal structures into groups representing each polymorph.

The packing similarity analysis produced the same clusters as PolySNAP. Compared with all other crystal structures, Forms 1, 2 and 3 have unique packing arrangements and only one or two molecules overlap out of the group of 20. Similarly, all the Type A solvates have the same packing arrangement, except for the methanol solvate. The methanol solvate has the same packing arrangement as the Type A solvate crystallised from DMF/diethyl ether, with 20 out of 20 molecules overlapping and an RMSD value of 0.576 Å. However, differences are observed between the methanol solvate and the four solvates crystallised by precipitation with an alkane anti-solvent. In these comparisons, 19 or 20 out of 20 molecules overlapped, with RMSD values slightly above the cut-off: between 0.65 and 0.79 Å. These results highlight slight structural differences in the drug framework of the methanol solvate, which contribute to differences in the PXRD pattern of this form.

Table 2.3: The number of molecules, out of a group of 20, that overlapped in a packing similarity calculation using all crystal structures of mexiletine. The number in brackets is the resulting RMSD value in Å. The cells are colour coded to denote whether the two forms have the same packing arrangement. Pairs with fewer than 20 molecules overlapping, or an RMSD of greater than 0.6 Å are not the same form and are coloured red. Pairs with 20 molecules overlapping and an RMSD of less than 0.6 Å are the same form and are coloured green. Pairs that show close similarity, but do not meet both criteria, are coloured orange.

	Form 1	Form 2	Form 3	Type A Solvent-free	Type A MeOH	Type A 1PrOH/Oct	Type A 2BuOH/Oct	Type A 2PrOH/Hex	Type A DCM/Hex	Type A DMF/DEE
Form 1	-									
Form 2	1 (0.629)	-								
Form 3	1 (0.629)	2 (0.590)	-							
Type A Solvent-free	1 (0.545)	1 (0.554)	2 (0.862)	-						
Type A MeOH	1 (0.548)	1 (0.560)	2 (0.908)	20 (0.538)	-					
Type A 1PrOH/Oct	1 (0.548)	1 (0.548)	2 (0.682)	20 (0.474)	19 (0.793)	-				
Type A 2BuOH/Oct	1 (0.549)	1 (0.547)	2 (0.865)	20 (0.472)	19 (0.791)	20 (0.008)	-			
Type A 2PrOH/Hex	1 (0.544)	1 (0.549)	3 (1.170)	20 (0.452)	19 (0.759)	20 (0.056)	20 (0.054)	-		
Type A DCM/Hex	1 (0.542)	1 (0.551)	2 (0.667)	20 (0.274)	20 (0.649)	20 (0.211)	20 (0.208)	20 (0.181)	-	
Type A DMF/DEE	1 (0.542)	1 (0.555)	2 (0.864)	20 (0.135)	20 (0.576)	20 (0.348)	20 (0.345)	20 (0.321)	20 (0.144)	-

2.3 Structures of the Non-Solvated Forms of Mexiletine

Single crystals of Form 2 of mexiletine were grown by sublimation at 150 °C. Selected crystallographic information for this structure is given in Table 2.4, along with the other non-solvated forms for reference. Full crystallographic information for Form 2 can be found in Appendix 7.1.

Table 2.4: Selected crystallographic information for the non-solvated forms of mexiletine.

	Form 1[23]	Form 2	Form 3[21]
Space Group	$P\bar{1}$	Pccn	Pbcn
a/Å	8.796(15)	17.874(14)	35.116(2)
b/Å	10.601(18)	18.678(15)	7.740(5)
c/Å	14.229(24)	7.346(7)	9.154(5)
α/°	78.74(13)	90	90
β/°	79.89(14)	90	90
γ/°	68.69(12)	90	90
V/Å^3	1204.3	2452.6(4)	2488.1(3)
Z	4	8	8
ρ_{calc} g/cm^3	1.19	1.17	1.15

As in all previously known structures of mexiletine, Form 2 is a racemic hydrochloride salt. The crystal structure is disordered and the model contains two different conformations of the mexiletine molecule (Figure 2.6).
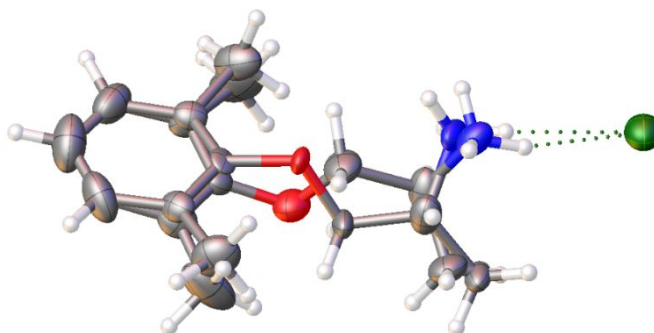
Figure 2.6: Asymmetric unit of Form 2 of mexiletine, showing how the disorder has been modelled.

The anti-periplanar conformer, which has an O-C-C-N torsion angle of 174.5 °, has an occupancy of 0.63. Whereas the gauche conformer, which has an O-C-C-N torsion angle of 47.8 °, has an occupancy of 0.37. There are 56 entries in the CSD containing this R-O-CH$_2$-CHR-NH$_3^+$ fragment, in which the O-C-C-N torsion angles range from 44.1 ° to 75.4 ° (Figure 2.7). These angles all correspond to a gauche conformation, which suggests that the anti-periplanar conformer is less stable.
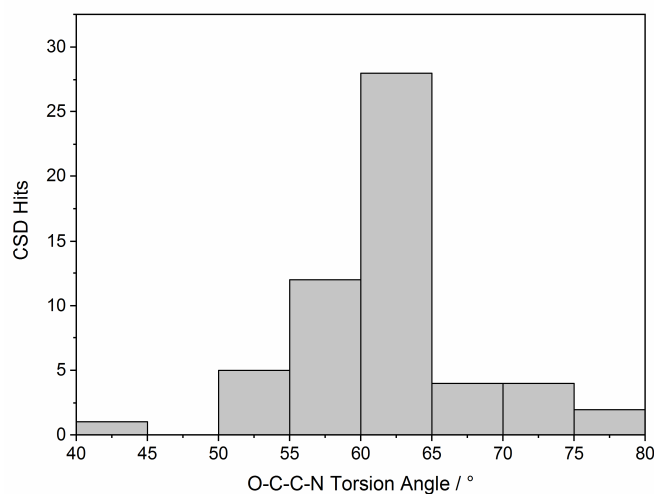
Figure 2.7: O-C-C-N torsion angles in all structures containing the R-O-CH$_2$-CHR-NH$_3^+$ fragment in the CSD.

In Form 2, there are three hydrogen bonds per chloride ion to the ammonium cations in adjacent molecules, forming a hydrogen-bonded polymer along the crystallographic *c*-axis. As in Form 3, the molecules within this polymer are arranged in a square, although the symmetry of this motif is different in Form 2. In this case, the molecules are related by two perpendicular *c*-glide planes, which intersect in the middle of the square (Figure 2.8).
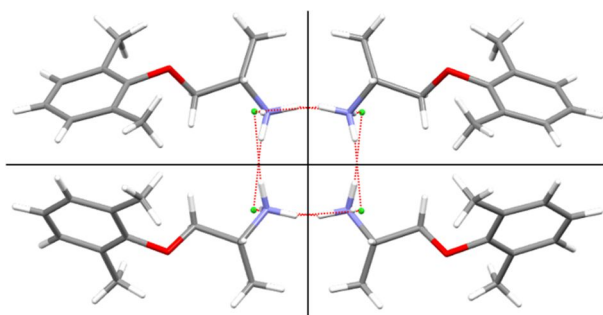
Figure 2.8: Form 2 of mexiletine, viewed down the *c*-axis. The *c*-glide planes are shown by black lines. For clarity, only the higher occupancy anti-periplanar conformer is displayed.

Although Forms 2 and 3 have similar packing arrangements, Form 1 is very different (Figure 2.9). When viewed down the hydrogen-bonded polymers, which corresponds to the *a*-axis for Form 1 and the *c*-axis for Forms 2 and 3, the structures are all layered. In Form 1, the polymers align with each other in the *b*-direction but are offset in *c* due to the shape of the triclinic unit cell. Forms 2 and 3 are both orthorhombic and the molecules align in both the *a*- and *b*-directions. In both of these structures, the layers are shifted such that the chains line up in every other layer.
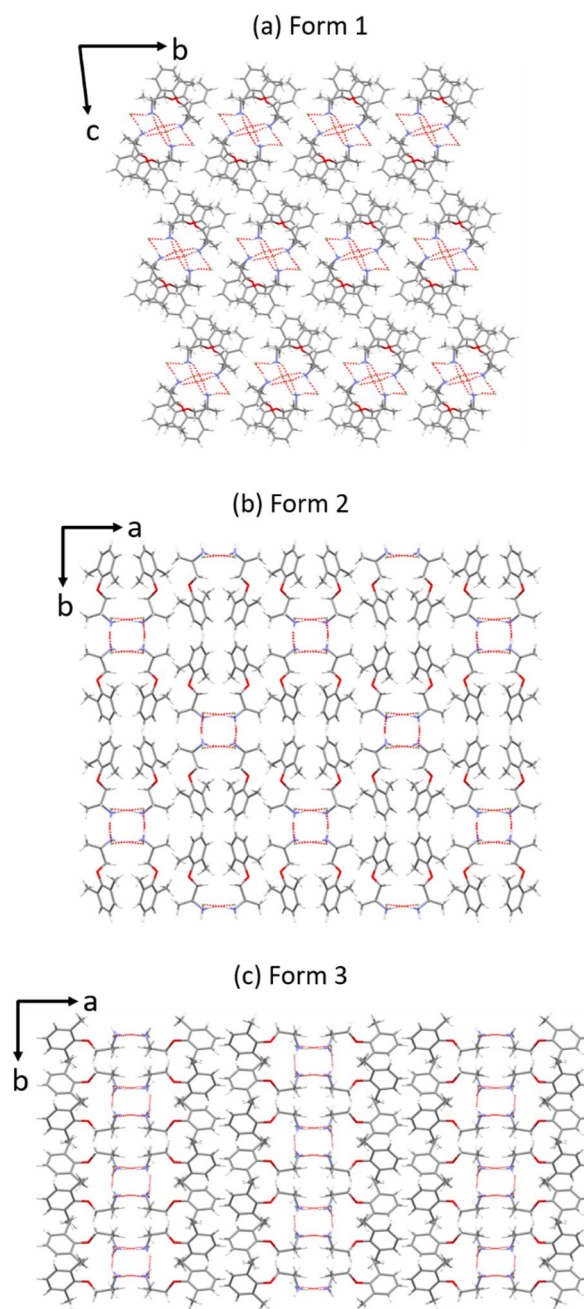
Figure 2.9: The packing arrangements of Forms 1, 2 and 3 of mexiletine, viewed down the hydrogen-bonded chains, which corresponds to the crystallographic (a) *a*-axis and (b,c) *c*-axis. For clarity, only the higher occupancy anti-periplanar conformer in Form 2 is displayed.

IR spectroscopy was also used to characterise the non-solvated forms of mexiletine. The major differences between these spectra occur in the ammonium NH stretching region between 3300 and 2300 cm^{-1}, which is unique for Forms 1, 2 and 3 (Figure 2.10).
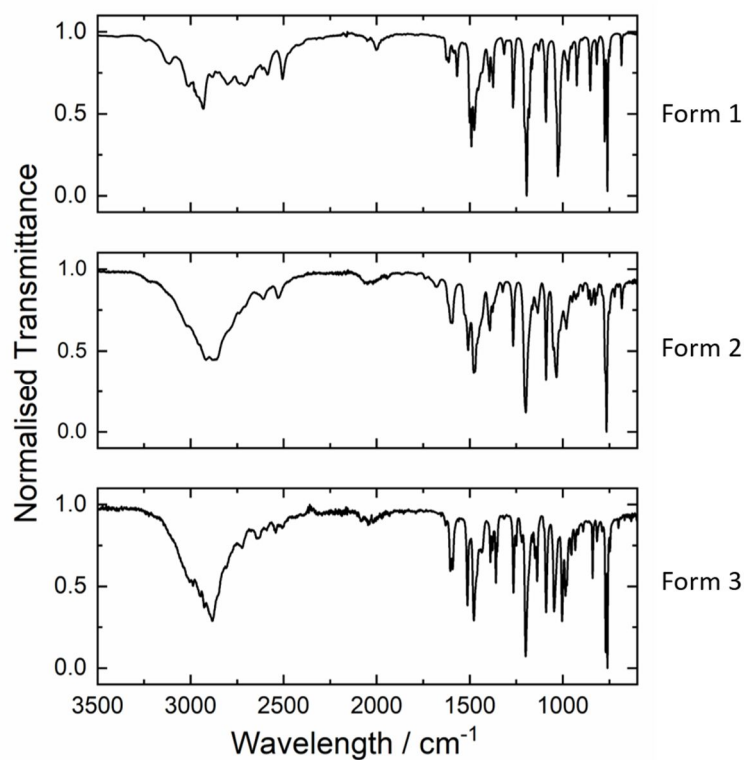
Figure 2.10: IR spectra of Forms 1, 2 and 3 of mexiletine. Form 1 was used as delivered, Form 2 was crystallised by sublimation at 150 °C and Form 3 was crystallised by evaporation of acetone.

2.4 Thermodynamic Relationships Between the Non-Solvated Forms of Mexiletine

The thermodynamic relationships between the three non-solvated forms of mexiletine was investigated by DSC (Figure 2.11, Table 2.5). These findings mirror previous reports[24, 25] in which all polymorphs transform into Form 2 upon heating, which then melts at 202 °C. Hence, Form 2 is the only form that does not display a polymorphic transition or desolvation endotherm. The polymorphic transition in Form 1 has an onset temperature of 148 °C and an enthalpy of 8.4 kJmol^{-1}. Whereas Form 3 transforms into Form 2 at an onset temperature of 167 °C and with an enthalpy of 4.5 kJmol^{-1}. Although Form 3 is metastable at room temperature, it has a higher polymorphic transition temperature than Form 1. Therefore, Form 3 is likely to be the most stable form between the polymorphic transition temperatures of Form 1 and Form 3: between 148 and 167 °C. The enthalpy of the polymorphic transition is lower for Form 3 than Form 1. The structure of Form 3 is more similar to Form 2 and therefore, less molecular reorganization is required to achieve the Form 3 to Form 2 transformation, which is responsible for its lower enthalpy.
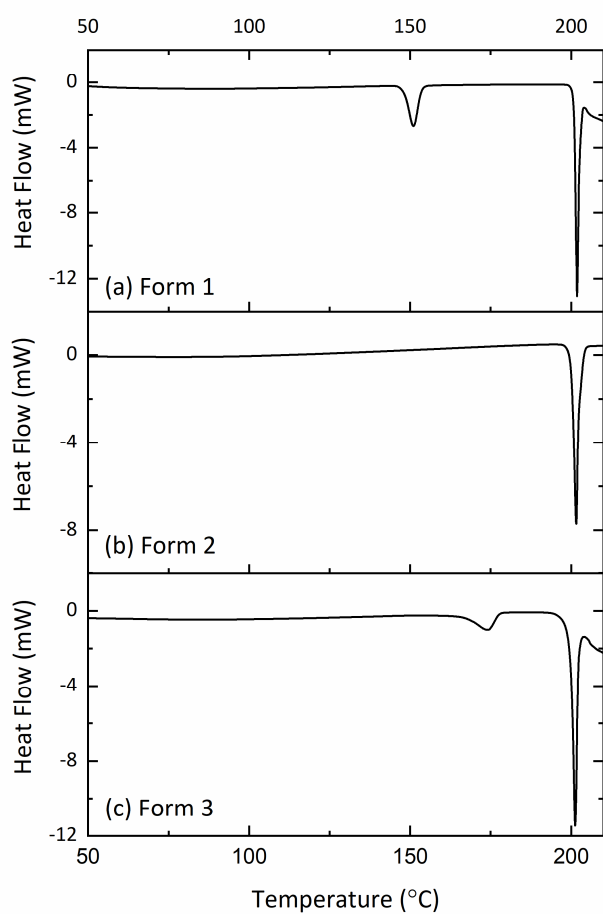
Figure 2.11: DSC thermograms of (a) Form 1, (b) Form 2 and (c) Form 3 of mexiletine.

Table 2.5: The temperature and enthalpy of each transition in the DSC thermograms of Forms 1, 2 and 3 of mexiletine.

	Polymorphic transition			Melting point		
	Onset / °C	Peak / °C	ΔH / kJmol^{-1}	Onset / °C	Peak / °C	ΔH / kJmol^{-1}
Form 1	148	151	8.4	201	202	16.7
Form 2	-	-	-	200	202	18.6
Form 3	167	174	4.5	200	202	16.2

2.5 Structures of the Solvated Forms of Mexiletine

Each family of channel solvates is characterised by a specific series of peaks in their PXRD patterns. These peaks are mostly observed at low angles and are consistent between all solvates of the same family. At higher angles there are some extra peaks or shifts between the patterns, which correspond to changes in the channel dimensions or the presence of different crystalline solvents within the pores. However, the similarities between all members of the same family are sufficient to qualify them as the same structure type.[26, 27]

In the PXRD patterns of the Type A solvates, the characteristic peaks occur in the regions 6-7, 8-10, 13-14 and 15-16 ° and only shift slightly in position between each solvate (Figure 2.12). These patterns match closely at higher angles, except for the solvates crystallised from 1- and 2-propanol, which contain some extra peaks between 17 and 27 °. It was not possible to obtain an experimental PXRD pattern of the Type A methanol solvate because the crystallisation requires such a high degree of supersaturation that when the crystals are removed from the mother liquor, Form 1 immediately precipitates from solution, forming an inseparable mixture. As such, the PXRD pattern calculated from the single-crystal structure was used for comparison and it also matches closely with the rest of the group.
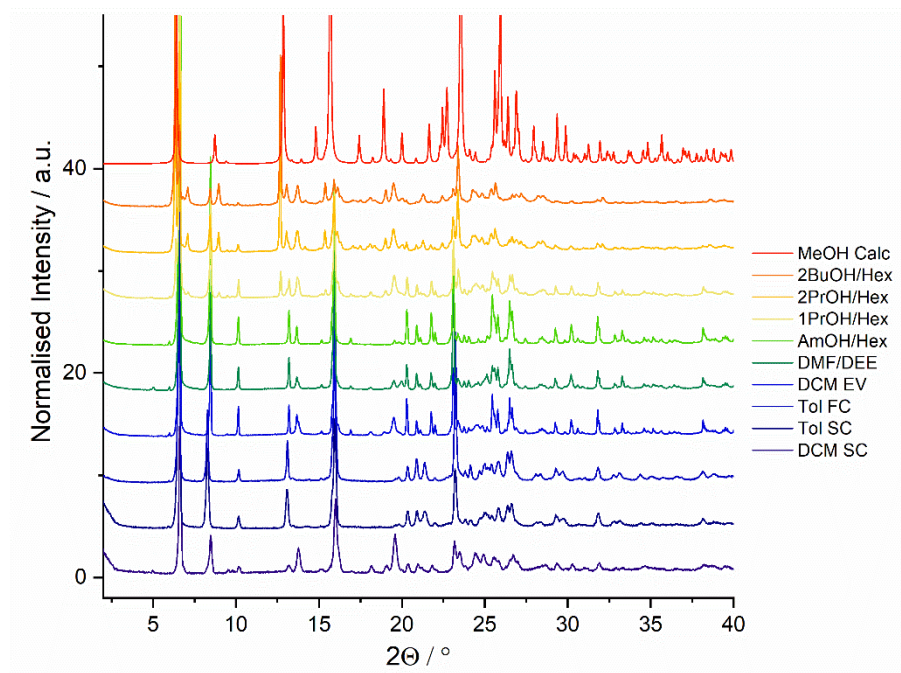
Figure 2.12: PXRD patterns of all Type A solvates. The crystallisation conditions are as follows, from the bottom up: slow cooling from DCM, slow cooling from toluene, fast cooling from toluene, evaporation from DCM, precipitation with diethyl ether from DMF, precipitation with hexane from amyl alcohol, precipitation with hexane from 1-propanol, precipitation with hexane from 2-propanol, precipitation with hexane from 2-butanol and slow cooling from methanol. The methanol pattern was calculated from the crystal structure.

In the PXRD patterns of the Type B solvates, the characteristic peaks occur in the regions 6-7, 9-10, 13-14, 15-17, 19-20 and 23-25 ° (Figure 2.13). However, there is some subtle variation in the shape and position of the peaks at approximately 6 ° and between 15-18 °. The PXRD patterns of the Type B solvates are also strongly affected by preferred orientation, causing the intensity of several peaks to vary widely. This effect is most noticeable for the peaks at approximately 5, 6, 13 and 16 °. As in the Type A solvates, differences are observed between the Type B patterns at higher angles, particularly between 15 and 30 °. Some of the Type B solvates were crystallised by fast cooling, which leads to reduced crystallinity, broadened peaks, and a lower signal to noise ratio in their PXRD patterns. This effect is most noticeable for

the samples crystallised by fast cooling from DCM and EMK. However, the similarities in their key peaks between 13 and 27 °are sufficient to qualify them as Type B solvates.
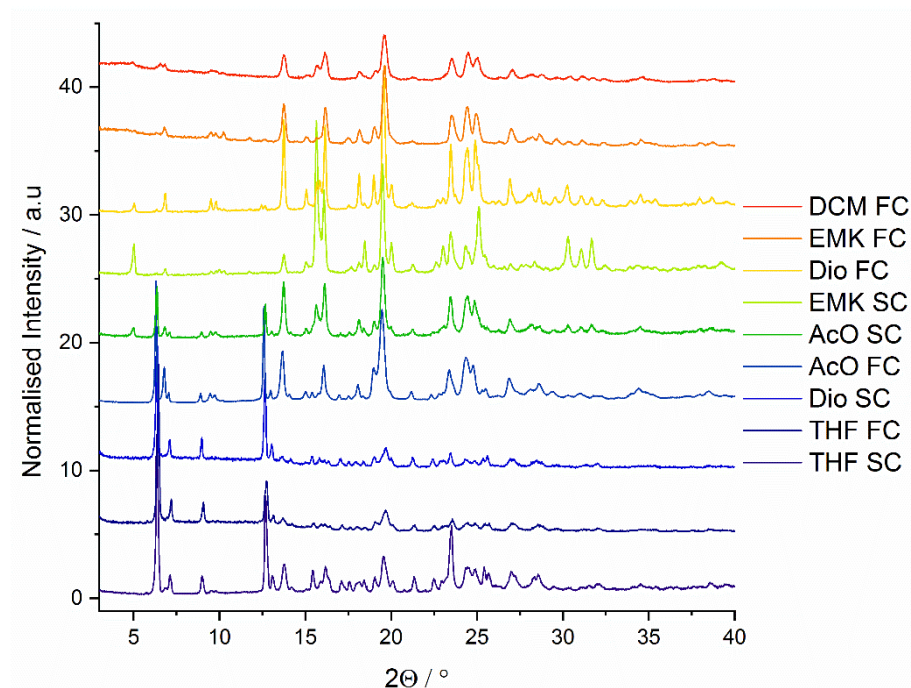
Figure 2.13: PXRD patterns of all Type B solvates. The crystallisation conditions are as follows, from the bottom up: slow cooling from THF, fast cooling from THF, slow cooling from 1,4-dioxane, fast cooling from acetone, slow cooling from acetone, slow cooling from EMK, fast cooling from 1,4-dioxane, fast cooling from EMK, and fast cooling from DCM.

Single-crystal structures of seven Type A solvates were determined. Although the dimensions of the channels and therefore the unit cells (Table 2.6), vary slightly with the incorporation of different guests, their overall packing arrangement varies very little.[26, 27] Full crystallographic information for all of these forms can be found in Appendix 7.1.

Table 2.6: Selected crystallographic information for the Type A solvates.

Crystallisation Conditions	DCM SC slow cooling	MeOH SC slow cooling	1PrOH/octane vapour diffusion	2BuOH/octane vapour diffusion	2PrOH/hexane vapour diffusion	DCM/hexane vapour diffusion	DMF/diethyl ether vapour diffusion
Space group	Pbcn	Pbcn	Pbcn	Pbcn	Pbcn	Pbcn	Pbcn
a/Å	20.857(2)	20.243(7)	21.936(13)	21.924(14)	21.875(17)	21.456(3)	21.125(2)
b/Å	17.378(18)	18.768(6)	17.106(10)	17.110(11)	17.211(13)	17.333(2)	17.358(16)
c/Å	7.565(8)	7.550(2)	7.521(5)	7.520(5)	7.511(6)	7.5478(11)	7.563(7)
α/°	90	90	90	90	90	90	90
β/°	90	90	90	90	90	90	90
γ/°	90	90	90	90	90	90	90
V/Å^3	2741.9(5)	2868.4(15)	2822.3(3)	2820.8(3)	2827.9(4)	2807.0(7)	2773.1(4)
Z	8	8	8	8	8	8	8
ρ_{calc} g/cm^3	1.045	1.147	1.015	1.016	1.013	1.021	1.033

The solvent-free form of the Type A solvates was crystallised by slow cooling a supersaturated solution in DCM. This form is isostructural with the rest of Type A solvates but in this case, the pores are empty, technically making this structure a fourth non-solvated polymorph of mexiletine.[35] As in Forms 2 and 3, the solvent-free structure is a racemate and the asymmetric unit contains one mexiletine molecule. This molecule adopts a gauche conformation, with an O-C-C-N torsion angle of 60.8 °, which is in line with similar structures in the CSD. Each ammonium cation hydrogen bonds to three chloride counterions, forming a hydrogen-bonded polymer along the crystallographic c-axis, in which the molecules are arranged in a square formation with the same symmetry as Form 3. Down the a- and b-axes, the packing arrangement in the solvent-free Type A structure is also very similar to Form 3, although the molecules are oriented differently (Figure 2.14).
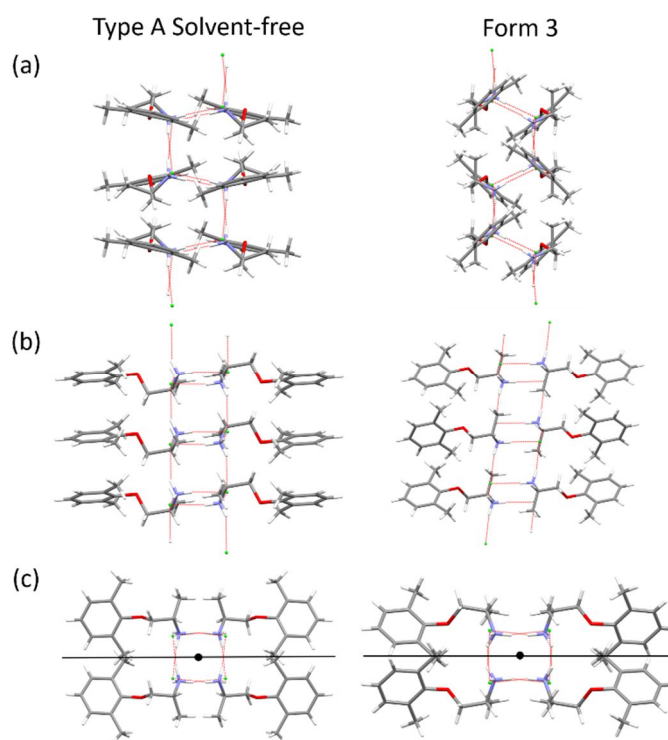
Figure 2.14: The structure of the solvent-free Type A structure of mexiletine, compared to Form 3. Structures are viewed down the (a) a-axis, (b) b-axis and (c) c-axis. The centres of inversion are shown as black circles and the c-glide planes are shown as black lines.

The defining features of the solvent-free Type A structure are the large, continuous voids running along the crystallographic c-axis (Figure 2.15). Calculated using the inward-facing surface of a spherical 1.4 $Å^3$ probe,[36] the voids occupy 255 $Å^3$ per unit cell or, 9.3 % of the crystal volume. This volume reduces to 40 $Å^3$ or 1.5 % when only the solvent-accessible voids, mapped using the centre of the spherical probe, are considered. This estimate of the solvent-accessible volume within this crystal structure is likely to be conservative because Mercury uses hard spheres to model both the host framework and the included solvent. In reality, both the solvent molecules and the host framework have a more nuanced shape and some degree of flexibility, which allow a larger volume of solvent to be included within the channels.[37]
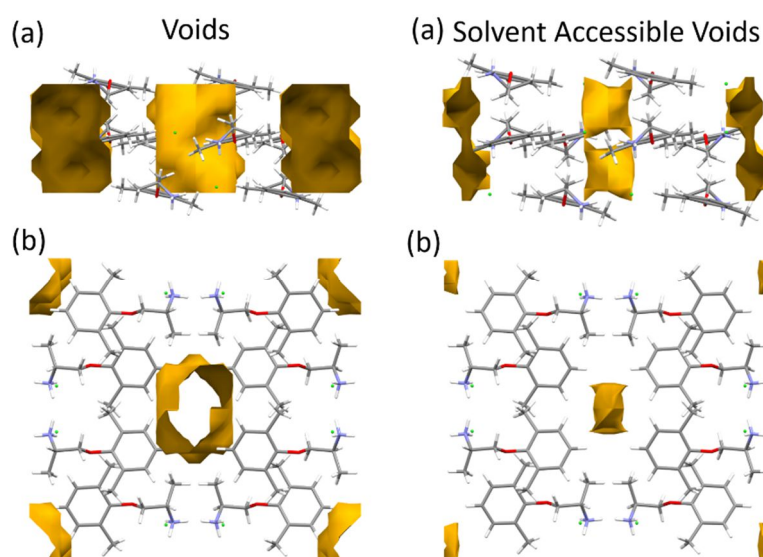
Figure 2.15: The void structure in the solvent-free Type A form of mexiletine, viewed down the (a) a-axis and (b) c-axis. The voids are highlighted in yellow and were calculated in Mercury using a 1.4 $Å^3$ spherical probe.[36]

Both types of void are continuous, but the solvent-accessible voids are small and narrow, which means only small or linear solvents can be included as guests. The surface of the channels is lined by mexiletine's aromatic rings, creating a hydrophobic environment that favours the crystallisation of hydrophobic solvents. It is most likely

the steric bulk of these aromatic groups that promotes a low-density packing arrangement in this form, stabilised by the strong charge-assisted hydrogen bonds from the ammonium groups. No solvent masking procedure was employed during the refinement of the solvent-free structure, and SQUEEZE[38] indicates a residual electron density in the channels of only 6 electrons per unit cell. Hence, the voids really are devoid of crystalline solvent. The experimental PXRD pattern of the solvent-free form matches exactly with the calculated pattern from the crystal structure and is repeatable over several experiments, which further demonstrates the reliability of the single-crystal data (Figure 2.16).
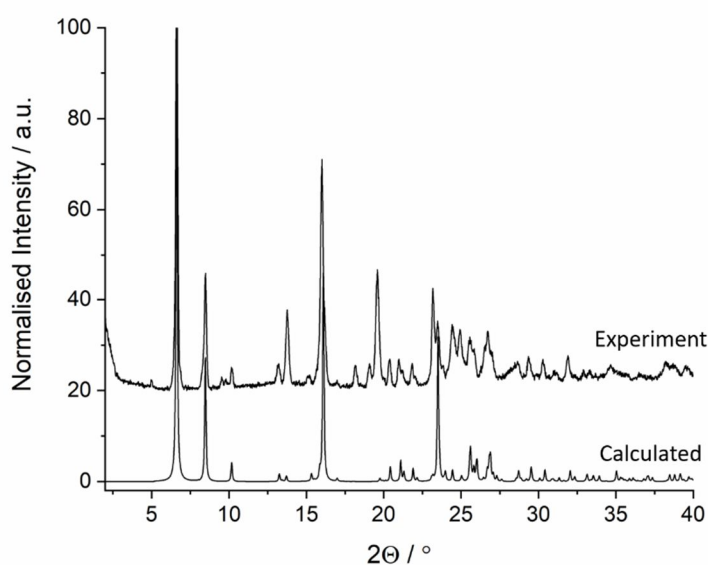
Figure 2.16: Experimental and calculated PXRD patterns of the solvent-free Type A structure, crystallised by slow cooling from DCM. The crystal structure was recorded at 100 K whereas, the experimental PXRD pattern was recorded at room temperature.

The Type A methanol solvate is the only crystal structure of this family that contains well resolved crystalline solvent within the channel, and the only disorder in this structure can be modelled by two positions of the alcohol proton. The methanol molecules do not interact with the host framework and instead hydrogen bond with each other, forming separate chains along the crystallographic *c*-axis (Figure 2.17).

Due to the hydrophobic channel surface, the methanol molecules pack with their alcohol groups facing inwards towards each other and their methyl groups facing outwards towards the channel. Full crystallographic information for this structure can be found in Appendix 7.1.
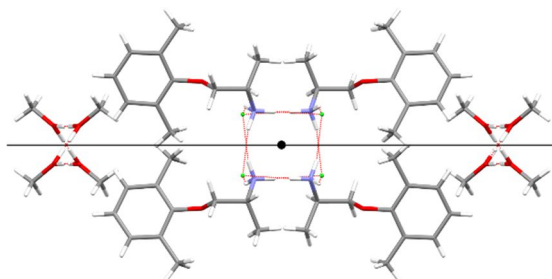
Figure 2.17: The Type A methanol solvate of mexiletine, viewed down the *c*-axis. The centre of inversion is shown as a black circle and the *c*-glide plane is shown as a black line.

The host frameworks in the Type A methanol solvate and the solvent-free form are isostructural. Both structures consist of offset layers, which alternate every half unit cell in both the *a*- and *b*-directions, so that the channels line up every other layer (Figure 2.18). However, there are slight differences in the unit cell dimensions of these two forms. In the methanol solvate, the *a*-axis is shorter and the *b*-axis is longer, showing that the channel dimensions have changed to accommodate the solvent molecules (Table 2.6).
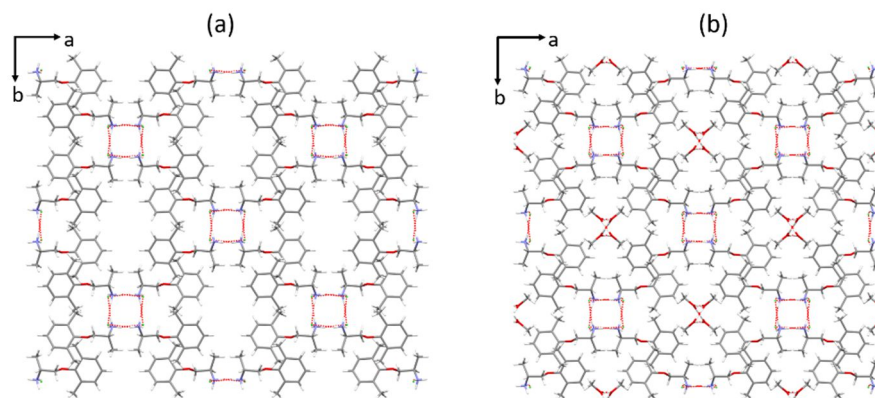
Figure 2.18: The packing arrangement of (a) the solvent-free Type A form and (b) the Type A methanol solvate, viewed down the *c*-axis.

The crystal structures of five more isostructural Type A solvates were determined using crystals grown by vapour diffusion of hexane, octane, or diethyl ether into a supersaturated solution of mexiletine in 1-propanol, 2-propanol, 2-butanol, or DMF. Full crystallographic information for these materials can be found in Appendix 7.1. As with the methanol solvate, slight variations in the cell dimensions of these compounds occur perpendicular to the channels, signifying a change in the channel dimensions to accommodate various solvents (Table 2.6). In all these structures, the solvent molecules are highly disordered and were modelled using a solvent masking procedure. The Mercury packing similarity analysis (Table 2.3) shows that the structure of the host framework in the solvates grown by vapour diffusion is slightly different to the methanol solvate. This difference was likely caused by the crystalline solvent within the pores of the methanol solvate interacting with the channel walls, in contrast to the disordered guests present in the other forms.

One single-crystal structure of a Type B solvate was recorded using a crystal grown by slow cooling from a supersaturated solution in ethyl methyl ketone, EMK. It is extremely disordered (Figure 2.19) and although several attempts were made to grow a better-quality crystal, these solvates crystallised exclusively as tiny needles that were very weakly diffracting. As a result, the precision of this structure is poor, but the approximate model does give insight into the gross structural features. The unit cell dimensions of this structure are given in Table 2.7 and full crystallographic information can be found in Appendix 7.1.
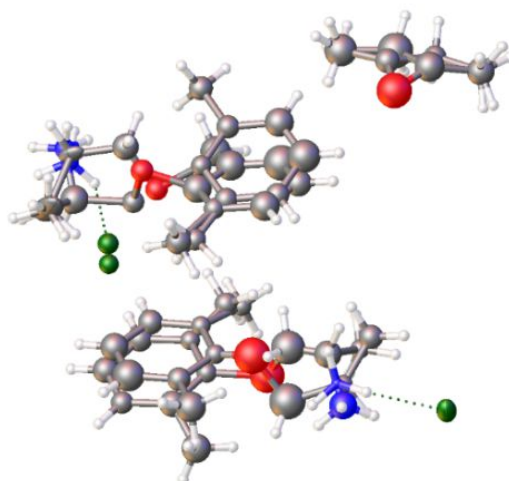
Figure 2.19: Asymmetric unit of the Type B EMK solvate of mexiletine, showing how the disorder has been modelled.

Table 2.7: Unit cell dimensions of the Type B EMK solvate of mexiletine.

Crystallisation Conditions	EMK SC slow cooling
a/Å	27.91(2)
b/Å	27.91(2)
c/Å	7.515(8)
α/°	90
β/°	90
γ/°	90

The Type B EMK solvate is a 2:1 hemisolvate, with two mexiletine molecules per asymmetric unit. As in all other metastable polymorphs, the ammonium cations hydrogen bond to chloride anions, forming a hydrogen-bonded polymer along the crystallographic c-axis (Figure 2.20). However, in contrast to the other metastable forms, there are two different hydrogen bonding motifs in this structure. One consists of four molecules, related by a 4-fold rotation axis, and connected by three hydrogen

bonds per chloride anion. The other contains two pairs of molecules, related by two perpendicular *c*-glide planes, and connected by two hydrogen bonds per chloride anion. The latter motif has the same symmetry as the hydrogen-bonded polymers in Form 2, and although Form 2 has one more hydrogen bond per chloride ion, the arrangement of molecules within the two motifs are the same. The structural similarity between Form 2 and the Type B solvates was also observed in their PXRD patterns, highlighted by the PolySNAP similarity dendrogram (Figure 2.5).
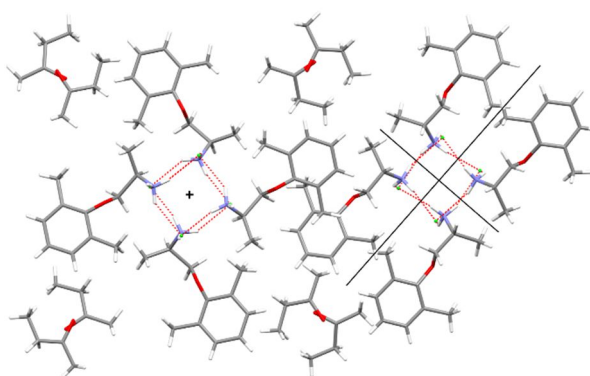
Figure 2.20: The Type B EMK solvate of mexiletine, viewed down the *c*-axis. For clarity, only one disordered component has been displayed. The *c*-glide planes are labelled as black lines and the 4-fold rotation axis is labelled as a black cross.

As in the Type A solvates, the solvent molecules in the Type B EMK solvate are accommodated in channels within the host framework and do not interact significantly with the mexiletine molecules. The surface of these channels is lined with aromatic rings, making them hydrophobic and encouraging the solvent molecules to pack with their hydrophobic functionality facing the channels (Figure 2.21). This structure is layered, with every other layer containing solvent molecules. The layers alternate every quarter unit cell along both the *a*- and *b*-axes, so that the same structural features line up every fifth layer.
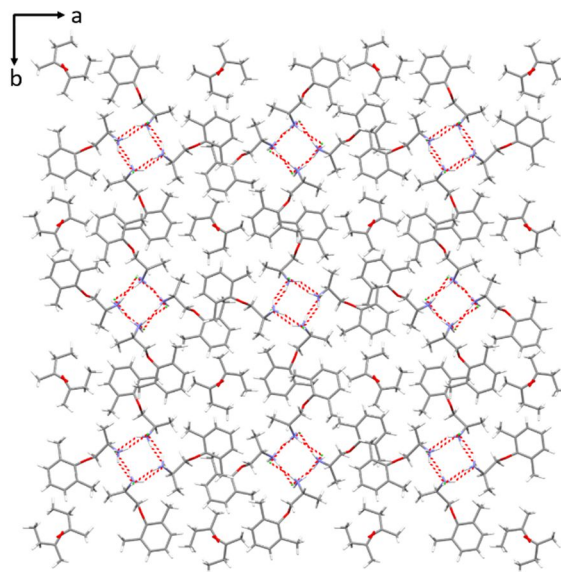
Figure 2.21: Packing arrangement of the Type B EMK solvate of mexiletine, viewed down the *c*-axis. For clarity, only one disordered component has been displayed.

^{13}C solid-state NMR spectroscopy was used to further characterise the channel solvates. Two different methods were used for each sample: cross-polarisation and direct-excitation, which differ in the relaxation times of the nuclei that they detect. Cross-polarisation was used to assess the crystalline, slowly relaxing parts of the structure, whilst direct-excitation was used to probe the more mobile, "liquid-like", and rapidly relaxing components. As the solvates are metastable, the NMR samples were also characterised by IR spectroscopy and PXRD both before and after measurement of the NMR spectra, to ensure they had not transformed during the experiment. The expected mexiletine signals were observed in every cross-polarisation spectrum and for all samples apart from the solvent-free forms, solvent signals were also visible in one or both spectra. These solvent resonances were used to determine the contents of every channel solvate, as shown in Table 2.8 and Table 2.9. A mexiletine signal is observed at approximately 14 ppm in all the direct-excitation spectra, corresponding to the aliphatic methyl group, which has a faster relaxation time than the other carbon atoms due its high rotational freedom.

Table 2.8: Chemical shift values of solvent signals in solid-state NMR spectra of all Type A solvates. SC = slow cool, PPT = precipitation, EV = evaporation, FC = fast cool, * = all solvent signals are significantly stronger in this spectrum, †= solvent peak overlaps a mexiletine peak, ‡= two solvent peaks overlap each other.

Crystallisation conditions	Solvent signals cross-polarisation	Solvent signals direct-excitation	Channel contents
Tol SC	125.8, 128.3, 128.9, 138.0	*125.8, 128.9, 129.2, 138.0	Toluene
DCM SC	- Signal would have been 53-55	- Signal would have been 53-55	Empty
MeOH SC	N/A	N/A	Methanol
1PrOH/Hex PPT	13.9†, 23.6, 32.9	*13.9†, 23.6, 32.9	Hexane
AmOH/Hex PPT	14.0†, 23.6, 32.9	*14.0†, 23.6, 32.9	Hexane
DMF/DEE PPT	15.7, 66.0	*15.8, 66.0	Diethyl ether
2BuOH/Hex PPT	13.9†, 23.5, 32.9	*13.9†, 23.5, 32.9	Hexane
2PrOH/Hex PPT	13.9†, 23.6, 32.9	*13.9†, 23.6, 32.9	Hexane
DCM EV	- Signal would have been 53-55	- Signal would have been 53-55	Empty
Tol FC	125.7, 128.6, 129.2, 138.0	*125.7, 129.0‡, 138.0	Toluene

Table 2.9: Chemical shift values of solvent signals in solid-state NMR spectra of all Type B solvates. SC = slow cool, FC = fast cool, * = all solvent signals are significantly stronger in this spectrum.

Crystallisation conditions	Solvent signals cross-polarisation	Solvent signals direct-excitation	Channel contents
AcO SC	*30.5, 204.5	30.5, 204.6	Acetone
EMK SC	*8.9, 29.3, 36.9, 207.2	9.0, 29.3, 36.9, 207.2	EMK
THF SC	*26.3, 67.9	26.3, 67.9	THF
Dio SC	*67.4	67.4	Dioxane
AcO FC	*30.6, 204.7	30.6	Acetone
Dio FC	*67.4	67.4	Dioxane
THF FC	*26.4, 68.0	26.3, 68.2	THF
DCM FC	- Signal would have been 53-55	- Signal would have been 53-55	Empty
EMK FC	*9.1, 29.5, 36.8, 207.5	9.1, 29.5, 36.8, 207.3	EMK

For most of the Type A solvates, solvent resonances were visible in both types of SS NMR spectra. However, they were much stronger by direct-excitation, which suggests that the solvent is highly mobile but not entirely liquid-like. All precipitation experiments that yielded a Type A solvate involved a polar, hydrogen-bonding solvent and a non-polar, aprotic anti-solvent. In every case, NMR data shows that the anti-solvent is contained within the channels, which is likely caused by the hydrophobic nature of the channel surface. In contrast, no solvent signals were observed in either SS NMR spectrum of the samples crystallised by slow cooling and evaporation of DCM, which highlights that both of these methods result in solvent-free Type A structures and confirms that the pores in this form are truly empty. The Type A solvates crystallised by fast and slow cooling from toluene are a particularly interesting case. The PXRD patterns of both samples match the pattern of the solvent-free form exactly, which suggests that the pores may be empty. However, toluene peaks are observed weakly in the cross-polarisation spectra and strongly in the direct-excitation spectra of these forms, which shows that the channels actually contain highly mobile toluene molecules that are too disordered to diffract X-rays (Figure 2.22).
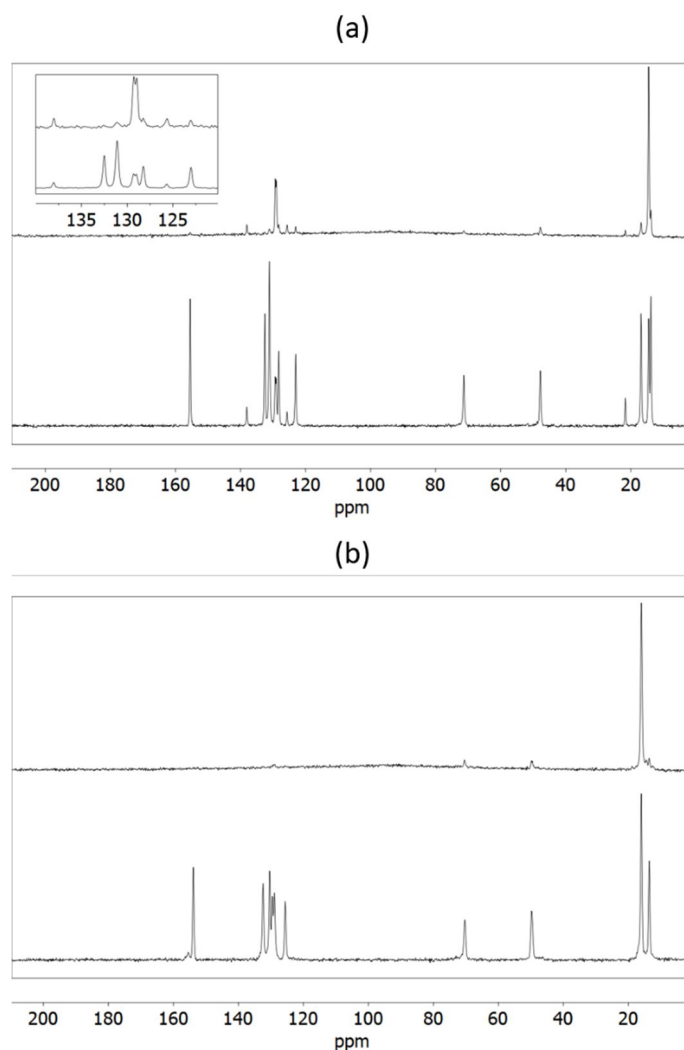
Figure 2.22: Solid-state NMR spectra of the Type A solvates of mexiletine, crystallised by slow cooling from (a) toluene and (b) DCM. In both cases, the top spectra were recorded using direct-excitation and the bottom spectra using cross polarization.

Solvent signals were also observed in the cross-polarisation and direct-excitation spectra of the Type B solvates. The signals were stronger in the cross-polarisation spectra, suggesting that the solvent in these structures is quite crystalline. This trend is reflected in the PXRD patterns of this form, which are much more varied than Type A, suggesting a larger variation in the crystalline components of the Type B solvates. A solvent-free Type B form was also identified by SS NMR, crystallised by fast cooling from DCM. No solvent signals were observed in either NMR spectrum of this

sample, showing that the pores are empty. Since the solvent-free Type A form was also produced by crystallisation from DCM, it is likely that while this solvent facilitates the crystallisation of channel solvates, it is too volatile and interacts with the hydrophobic channels too weakly to be retained.

Solid-state ^{13}C NMR spectroscopy could also be used to distinguish between the Type A and B solvates, and to distinguish them both from Form 1. This technique has previously been applied to distinguish between Forms 1, 2 and 3.[21] All spectra differ in the four fingerprint regions identified by Namespetra et al.: between 154-156, 70-72, 47-49, and 10-20 ppm (Figure 2.23).[21] The spectra of the Type A solvates, which have one molecule per asymmetric unit, are always much simpler than those of Type B and Form 1, which have two molecules per asymmetric unit. For certain nuclei, signals from these two symmetry-independent molecules can be resolved by NMR, as seen at approximately 48 and 72 ppm. At 48 ppm, the two signals overlap and so the peak appears broad, with a small shoulder. There are also significant differences in the aromatic region between 120-135 ppm that are more characteristic of the solvates (Figure 2.23). Once again, the aromatic region is much simpler for the Type A solvates, including only the expected four signals. Whereas, the spectra of the Type B solvates and Form 1 contain more peaks, due to their higher values of Z'. All three forms can be distinguished by differences in the chemical shift, which were used to confirm the polymorphism of the poorly crystalline samples that produced low-resolution PXRD patterns: the Type B solvates crystallised by fast cooling from acetone, DCM and EMK.
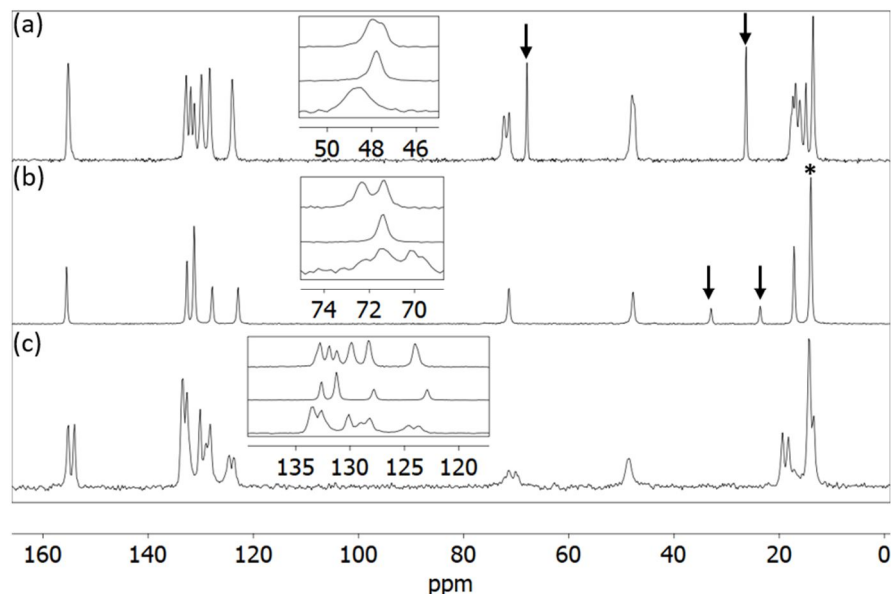
Figure 2.23: Cross-polarisation SS NMR spectra of (a) the Type B solvate crystallised by slow cooling from THF, (b) the Type A solvate crystallised by precipitation from amyl alcohol / hexane, and (c) Form 1 used as supplied. Solvent peaks are highlighted with arrows, corresponding to (b) hexane and (a) and THF. The hexane signal at 14 ppm in spectrum (b), highlighted with an asterisk, overlaps with a mexiletine signal, hence the higher intensity of this peak.

The structure of the mexiletine solvates was also characterised by IR spectroscopy. As with the non-solvated polymorphs, the IR spectra of the Type A and B solvates are very similar, and it was not possible to distinguish the two families by this method. Similarly, there is little variation between different solvates of the same family, showing that any slight changes in crystal packing cannot be resolved by IR spectroscopy. Representative IR spectra of the Type A and B solvates are shown in Figure 2.24 and this data was predominantly used as a convenient method to confirm the polymorphism of a sample before characterising it in more detail using another technique.
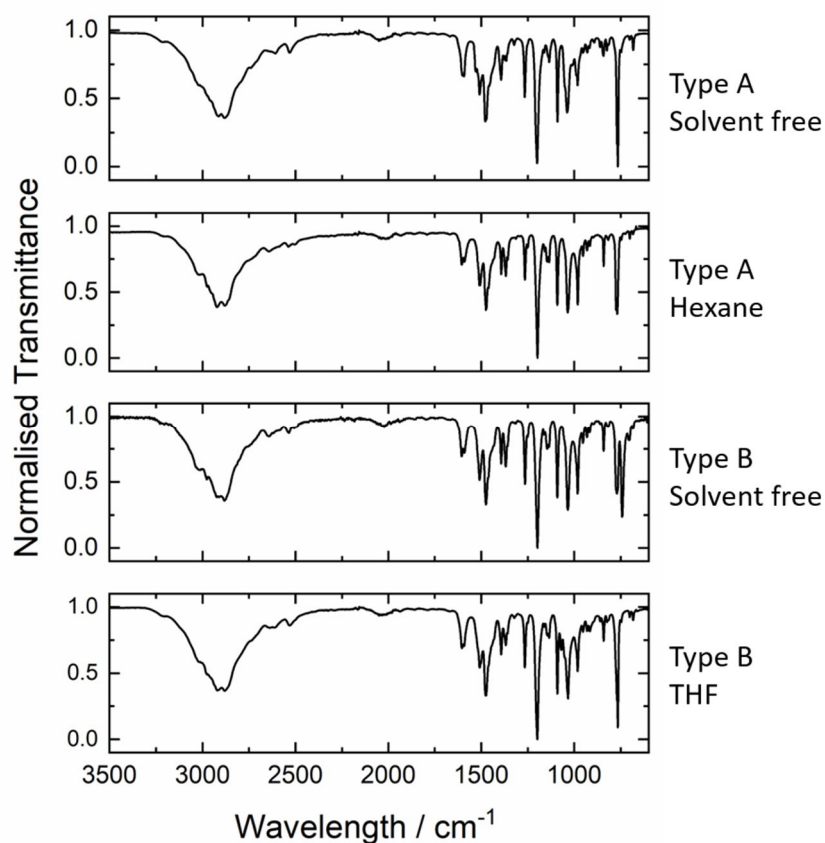
Figure 2.24: Representative IR spectra of the Type A and 2 solvates, crystallised by: slow cooling from DCM (Type A solvent free), precipitation from 1-propanol using hexane (Type A hexane), fast cooling from DCM (Type B solvent free) and slow cooling from THF (Type B THF).

In the Type A solvates, there are no solvent peaks in any of the IR spectra. However, solvent peaks were observed in the spectra of five Type B solvates (Figure 2.25). In the EMK and acetone solvates, the carbonyl stretch of the solvents are observed at 1715 and 1710 cm^{-1} respectively, and in the dioxane solvates, the CH$_2$ twisting vibration of the solvent is observed at 1289 cm^{-1}.[39]
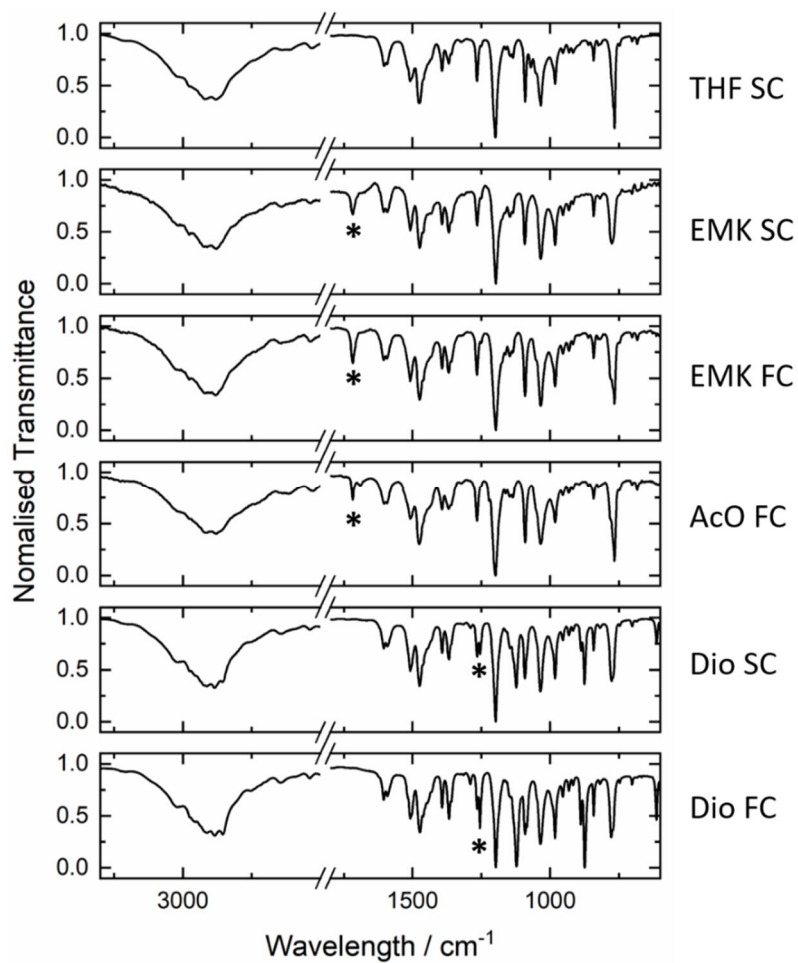
Figure 2.25: IR spectra of the Type B EMK, acetone and dioxane solvates, in which there are extra peaks due to solvent, compared to a representative Type B pattern that contains no solvent signals. The crystallisation conditions are, from the top down: slow cooling from THF, slow cooling from EMK, fast cooling from EMK, fast cooling from acetone, slow cooling from dioxane, and fast cooling from dioxane.

2.6 Thermodynamic Relationships Between the Solvated Forms of Mexiletine

Both solvate families are metastable with respect to Form 1. If removed from the mother liquor and stored under ambient conditions, the solvates transform into Form 1 in a time ranging from one hour to one day, depending on how the sample was crystallised and which solvent is included in the pores. If either of the channel solvates are subject to desolvation at increased temperatures, they transform into the high temperature stable Form 2, which was confirmed using PXRD (Figure 2.26).
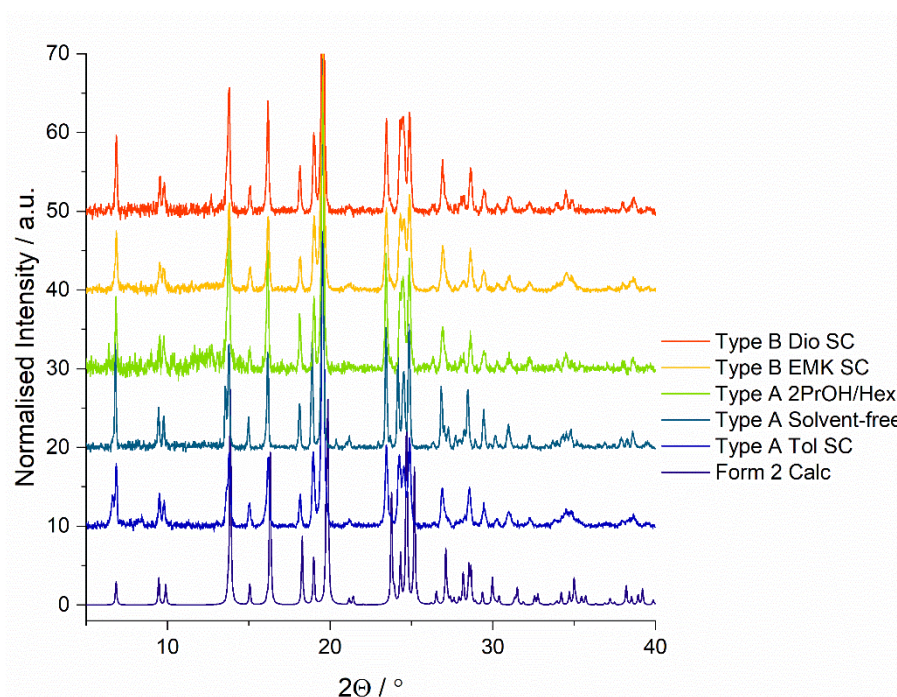
Figure 2.26: PXRD pattern of Form 2 calculated from the crystal structure, compared to experimental PXRD patterns of various Type A and B solvates, heated above their transition temperatures on a hot stage microscope. From the bottom up, samples were crystallised by: sublimation at 150 °C for 7 hours, slow cooling from toluene, slow cooling from DCM, precipitation using hexane from 2-propanol, slow cooling from EMK, and slow cooling from 1,4-dioxane.

DSC measurements showed that the polymorphic transition to Form 2 occurs at a different temperature for each solvate. Representative DSC thermograms of each solvate family are shown in Figure 2.27. In some cases, the polymorphic transition is well defined, whereas in others it is very broad and often, the data is not reproducible. Despite this variation, the melting transition in all solvates occurs at approximately 202 °C, which corresponds to that of Form 2, and confirms that the transition has taken place. The broad peaks and inconsistent desolvation behaviour signify that the solvent is non-stoichiometric and loosely bound within the channels. As a result, the solvent content will vary between different samples and may change over time if the sample was stored prior to measurement, leading to differences in the desolvation endotherm. This effect is compounded in the Type B solvates due to their structural similarity with Form 2, which means that very little molecular rearrangement is required to change between the two forms, and the transition has a low enthalpy. Therefore, the desolvation endotherms are much broader in the Type B solvates than Type A.

Similar inconsistencies were also observed when the solvates were characterised using TGA. The measurement was repeated multiple times for each solvate, and almost never led to consistent results, which is further confirmation that the solvent is non-stoichiometric and loosely bound within the channels. For these reasons, TGA was not a suitable technique to characterise the channel solvates.
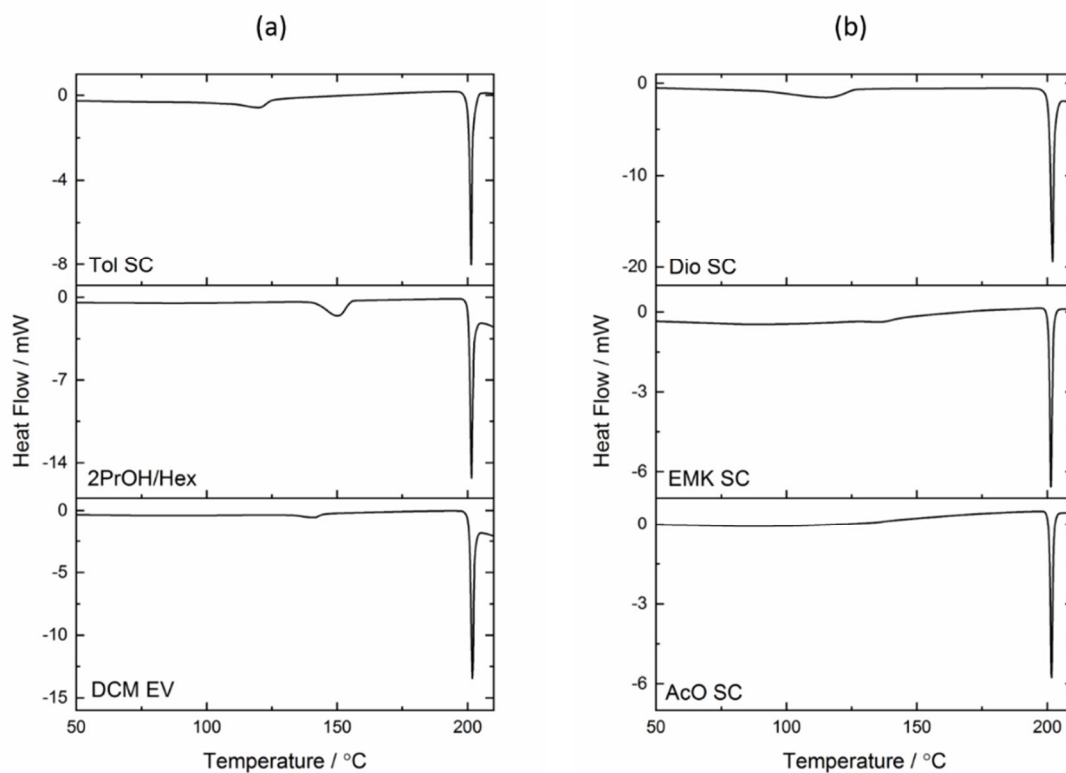
Figure 2.27: DSC thermograms of (a) three Type A solvates, crystallised by slow cooling from toluene, precipitation from 2-propanol/hexane and evaporation from DCM (b) three Type B solvates, crystallised by slow cooling from dioxane, EMK and acetone.

Table 2.10: The enthalpy and onset temperature of each transition in the above DSC thermograms.

	Desolvation			Melting point		
	Onset /	Peak /	ΔH /	Onset /	Peak /	ΔH /
	°C	°C	kJmol^{-1}	°C	°C	kJmol^{-1}
A Tol SC	104	120	7.7	201	201	14.2
A 2PrOH/Hex	142	150	6.3	201	202	13.8
A DCM EV	133	141	3.1	196	202	17.2
B Dio SC	85	115	11.4	201	201	14.2
B EMK SC	-	-	-	201	201	15.6
B AcO SC	-	-	-	201	202	14.0

2.7   Characterisation of Mixtures

Concomitant crystallisation of multiple forms was observed in precipitation experiments from $CHCl_3$/hexane and DCM/hexane. PXRD data shows that the sample crystallised from $CHCl_3$/hexane is a mixture of Form 1 and a Type B solvate (Figure 2.28a). The Type B solvate rapidly transforms into Form 1 and as a result, it was not possible to characterise this form by SS NMR.
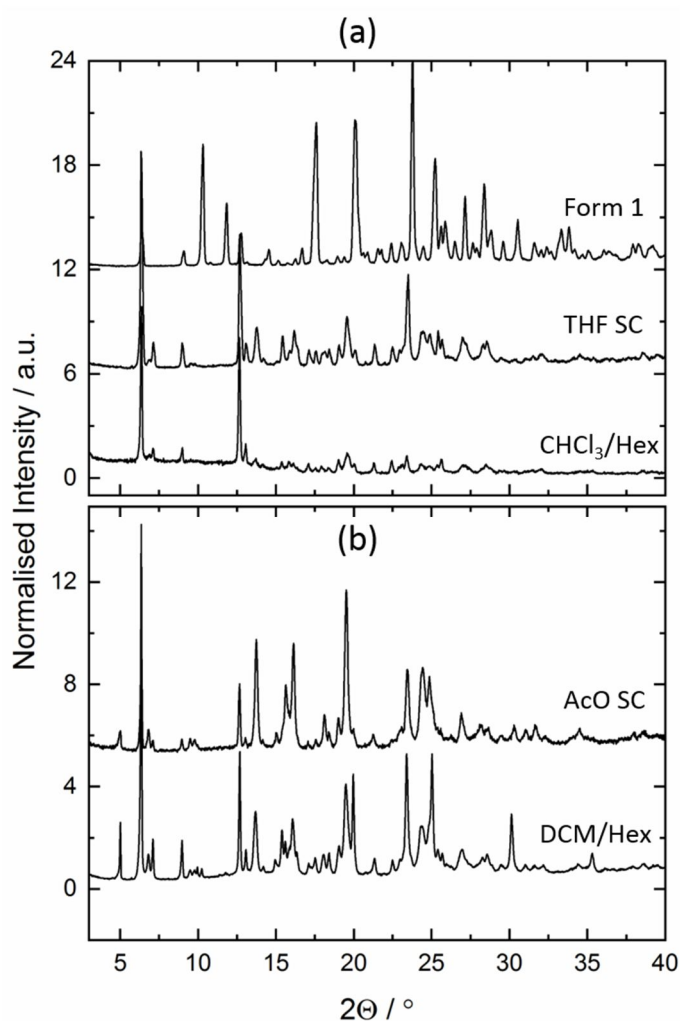
Figure 2.28: (a) PXRD patterns of the Type B solvate crystallised by precipitation from CHCl-₃/hexane, compared with the Type B solvate crystallised by slow cooling from THF, and Form 1. (b) PXRD patterns of the Type B solvate crystallised by precipitation from DCM/hexane, compared with the Type B solvate crystallised by slow cooling from acetone.

The mixture crystallised from DCM/hexane contained large and small crystals. Single-crystal X-ray diffraction revealed the larger crystals to be a Type A solvate containing highly disordered electron density within the pores (Table 2.6). There were no residual peaks large enough to correspond to a chlorine atom and so the solvent was assumed to be hexane, which mirrors the behaviour of other Type A solvates crystallised by precipitation. The smaller crystals did not allow the determination of a full structure, but their unit cell (Table 2.11) and PXRD pattern (Figure 2.28b) showed them to be a Type B solvate.

Table 2.11: Unit cell dimensions of the Type B solvate crystallised by vapour diffusion of hexane into DCM, compared to the Type B EMK solvate crystallised by slow cooling.

Crystallisation Conditions	EMK SC slow cooling	DCM/hexane vapour diffusion
a/Å	27.91(2)	7.473(12)
b/Å	27.91(2)	27.72(2)
c/Å	7.515(8)	27.74(2)
α/°	90	90
β/°	90	90
γ/°	90	90

The cross-polarisation SS NMR spectrum of this mixture contained signals from both DCM and hexane, but only hexane was observed by direct-excitation (Figure 2.29). As the hexane molecules were attributed to the Type A solvate, this data suggests that the Type B solvate contains crystalline DCM within the pores. Given that solvent-free forms of both the Type A and B solvates were crystallised from DCM, it is surprising that crystalline DCM was found within this Type B solvate. Perhaps the addition of hexane to the solvent mixture provides a means to stabilise this unusual structure.
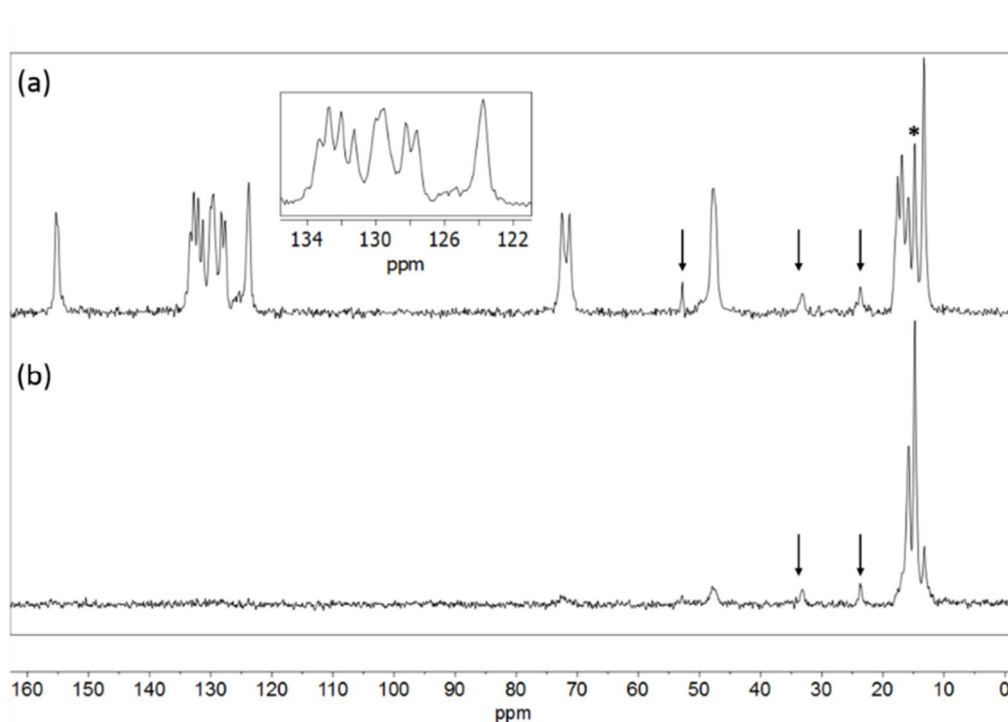
Figure 2.29: (a) Cross-polarisation and (b) direct-excitation ^{13}C SS NMR spectra of mexiletine, crystallised by precipitation from DCM/hexane. The arrows highlight the solvent peaks, corresponding to DCM at 52.8 ppm and hexane at 33.2 and 23.7 ppm. The hexane signal at 14 ppm, highlighted with an asterisk, overlaps with a drug signal and is therefore higher intensity. The inset spectrum highlights the aromatic region of the cross-polarisation spectrum that confirms the sample was a mixture of a Type A and Type B solvate.

2.8   Conformational Polymorphism

The molecular conformation in all polymorphs of mexiletine, except for the highly disordered Type B EMK solvate, are shown in Figure 2.30.
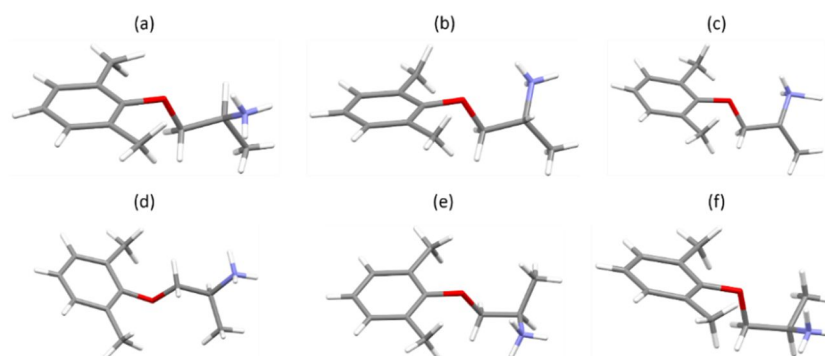
Figure 2.30: The molecular conformation in (a) molecule 1 of Form 1, (b) molecule 2 of Form 1, (c) the gauche conformer of Form 2, (d) the anti-periplanar conformer of Form 2, (e) Form 3 and (f) the solvent-free Type A form.

The differences between these conformations were quantified using Mercury.[32] Two equivalent atoms in a pair of molecules from different crystal structures were overlaid, producing a root mean square deviation (RMSD) for their atomic positions. A review of nearly 3000 crystal structures from the CSD concluded that for two conformations to be considered unique, they require an RMSD greater than 0.375 Å.[40] The results of these comparisons can be found in Table 2.12.

Table 2.12: RMSD values (Å) deriving from a comparison of the molecular conformation in all the crystal structures of mexiletine. The cells are colour coded to denote whether the conformations are the same (green) or different (red), based on whether their RMSD value.

	Form 1 Molecule 1	Form 1 Molecule 2	Form 2 Gauche	Form 2 Anti	Form 3	Type A Solvent-free	Type A MeOH	Type A 1PrOH/Oct	Type A 2BuOH/Oct	Type A 2PrOH/Hex	Type A DCM/Hex	Type A DMF/DEE
Form 1 Molecule 1	-											
Form 1 Molecule 2	0.041	-										
Form 2 Gauche	0.138	0.131	-									
Form 2 Anti	0.635	0.629	0.615	-								
Form 3	0.636	0.629	0.596	0.492	-							
Type A Solvent-free	0.548	0.545	0.517	0.554	0.203	-						
Type A MeOH	0.549	0.548	0.522	0.560	0.222	0.026	-					
Type A 1PrOH/Oct	0.551	0.548	0.521	0.548	0.194	0.028	0.036	-				
Type A 2BuOH/Oct	0.550	0.548	0.522	0.547	0.194	0.028	0.036	0.006	-			
Type A 2PrOH/Hex	0.547	0.544	0.518	0.549	0.199	0.026	0.033	0.010	0.009	-		
Type A DCM/Hex	0.545	0.542	0.514	0.551	0.196	0.023	0.039	0.023	0.023	0.021	-	
Type A DMF/DEE	0.545	0.542	0.515	0.555	0.202	0.014	0.027	0.019	0.019	0.017	0.018	-

These results show that the non-solvated polymorphs of mexiletine, Forms 1, 2 and 3, are conformational polymorphs, producing RMSD values above the threshold (0.375 Å).[40] The lower occupancy, gauche conformer of Form 2 is an exception, and shares its conformation with Form 1. However, as the higher occupancy, anti-periplanar conformer is significantly different to all the other forms, Form 2 can also be considered a conformational polymorph of the other non-solvated forms. The major difference between Forms 1, 2 and 3 is the position of the terminal ammonium group, which is evident from the O-C-C-N torsion angles that range from 47.8 to 67.8 ° (Table 2.13). A slight difference in torsion angle is also observed between the two symmetry independent molecules of Form 1, even though their conformations are the same, producing an RMSD value of only 0.041 Å. The Type A solvates all share the same conformation, with RMSD values less than 0.04 Å, and only a slight variation in O-C-C-N torsion angle of 5–7 ° (Table 2.13). The Type A solvates also have the same conformation as Form 3, with RMSD values around 0.2 Å. Given that these forms share similar structural motifs (Figure 2.14), this conformational similarity suggests that the Type A solvates may be modifications of Form 3, adapted to allow for the incorporation of solvent within the lattice.

Table 2.13: O-C-C-N torsion angles in all crystal structures of mexiletine. The number in brackets is the error on the final digit.

Solid Form	Conformation	O-C-C-N Torsion Angle / °
Form 1 molecule 1	Gauche	57.9(8)
Form 1 molecule 2	Gauche	60.6(8)
Form 2 gauche	Gauche	47.8(15)
Form 2 anti	Anti-periplanar	174.5(6)
Form 3	Gauche	67.8(3)
Type A solvent-free	Gauche	60.8(3)
Type A MeOH	Gauche	61.4(1)
Type A 1PrOH/Oct	Gauche	61.6(2)
Type A 2BuOH/Oct	Gauche	61.7(2)
Type A 2PrOH/Hex	Gauche	62.1(2)
Type A DCM/Hex	Gauche	60.9(4)
Type A DMF/DEE	Gauche	60.8(2)

2.9   Crystal Structure Prediction

Alongside experimental techniques, the polymorph landscape of mexiletine hydrochloride was also investigated by crystal structure prediction, using a force-field approach designed by AstraZeneca, AZ-FF.[34] A detailed description of the calculation procedure can be found in the experimental section, Chapter 5. Of the 1000 predicted structures, 77 were found to be within 10 kJmol^{-1} of the minimum energy form, which corresponds to structures that may be accessible using standard experimental techniques. The relative energies of these forms at 0 K are shown in Figure 2.31, as a function of density. This calculation predicted structures with only one mexiletine molecule per asymmetric unit and did not consider solvated forms. As a result, neither Form 1 nor the Type B solvates could not be found in this CSP search, as they both have two molecules per asymmetric unit. Despite having one molecule per asymmetric unit, neither Form 2 nor the Type A solvates were predicted by the calculation, likely due to their very high relative energy and large voids, respectively. However, Form 2 is closely related to predicted Form 314. Form 3 was successfully predicted by the calculation and is isostructural with predicted Form 973. In Figure 2.31, predicted structures that are isostructural with known forms are highlighted in red. For comparison, the relative energies of the known Forms 1, 2, 3 and the Type A solvent-free form were calculated from their crystal structures and are also plotted in red. The Type A form has a much lower density and so for clarity, its relative energy is shown in a separate plot.
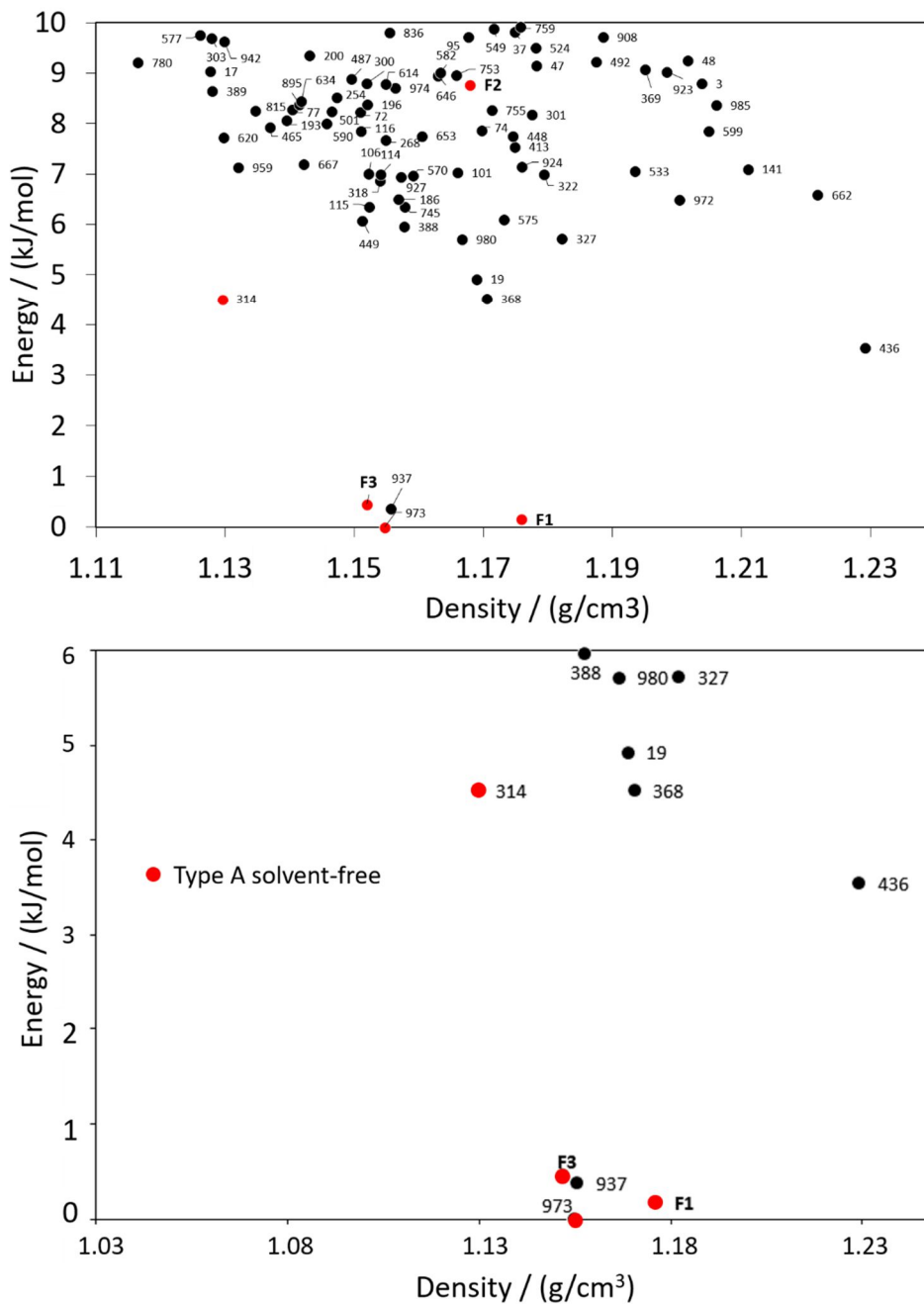
Figure 2.31: The relative energies of the predicted crystal structures of mexiletine, compared to the known forms. The known forms are labelled F1-F3 and the predicted structures are numbered. Known forms, and the predicted forms that are isostructural with known forms, are highlighted in red.

The calculated energies of the known forms reflect the experimental DSC data. Form 1 has the lowest relative energy of the four experimental polymorphs, at 0.2 kJmol^{-1} and Form 3 is close in energy to Form 1 at 0.4 kJmol^{-1}. Likely due to the presence of large voids, the Type A solvent-free form is much higher in energy at 3.6 kJmol^{-1} although, it is still lower energy than most of the predicted structures. Finally, as excepted, Form 2 has the highest relative energy at 8.8 kJmol^{-1}. The very small energy difference between Forms 1 and 3 may explain why they often crystallise concomitantly and DSC data suggest that Form 3 may be more stable than Form 1, above the Form 1 to 2 transition temperature.

There is a very small difference in energy between Form 3 and its isostructural predicted Form 973, which derives from small differences in unit cell dimensions, and is within the accuracy of this technique. However, there is a very large difference in energy between Form 2 and the closely related predicted Form 314. The only structural difference between these two structures is that the molecules in Form 314 are spaced slightly wider apart in the *b*-direction, leading to a lower density. The Mercury packing similarity analysis of Forms 2 and 314 shows that all 20 molecules in the group overlap, with an RMSD of 0.185l Å, indicating that the packing arrangements are essentially the same. Similarly, the molecular conformation in Form 314 is identical to that of the anti-periplanar molecule in Form 2, with an RMSD of only 0.0984 Å. The lower energy of Form 314 may therefore derive from the lack of disorder.

Predicted Form 937 stands out because it is very low energy, at 0.4 kJmol^{-1}. This form was not observed experimentally but is in fact a high symmetry version of Form 3, in which the *a*-axis has been halved (Figure 2.32). The density of Form 937 is slightly higher than Form 3 because the molecules pack more closely together but other than that, the packing arrangements of the two forms are very similar. The molecular conformation in Form 314 is also identical to Form 3, with an RMSD of only 0.0322 Å. It seems that the predicted Form 937 is a more idealized version of Form 3, which is prohibited from crystallising experimentally due to defects during the nucleation or growth step.
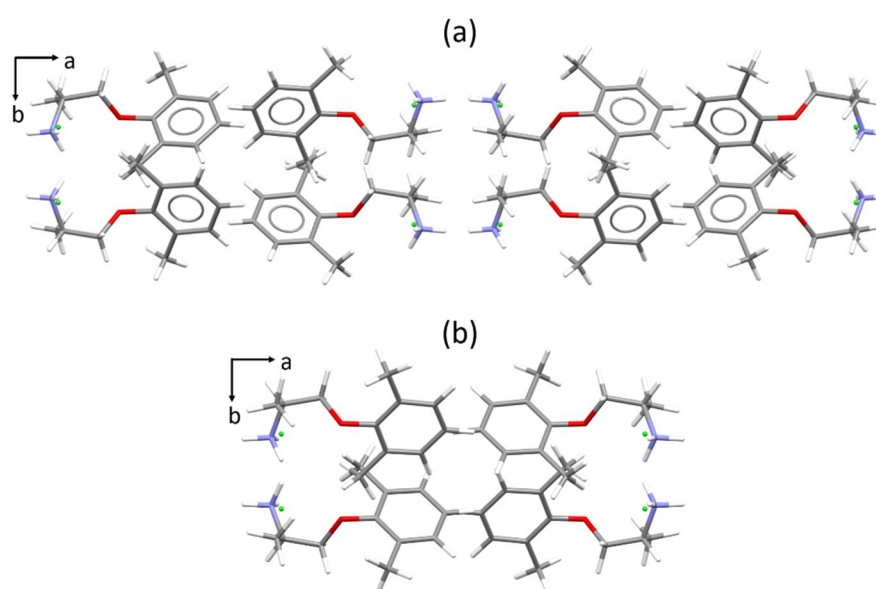
Figure 2.32: Packing arrangement in one unit cell of (a) Form 3 and (b) predicted Form 937 of mexiletine, viewed down the *c*-axis.

Although the Type A solvent-free form was not found in this CSP search, predicted Form 662 has the same space group and similar hydrogen bonding motifs. As in the Type A structures, there are three hydrogen bonds per chloride ion that produce a hydrogen-bonded mexiletine polymer down the crystallographic *c*-axis, in which the molecules are arranged in a square formation (Figure 2.33). However, only 1 out of a

group of 20 molecules overlapped when two structures were overlaid, with an RMSD value of 0.545 Å showing that their packing arrangements are very different.
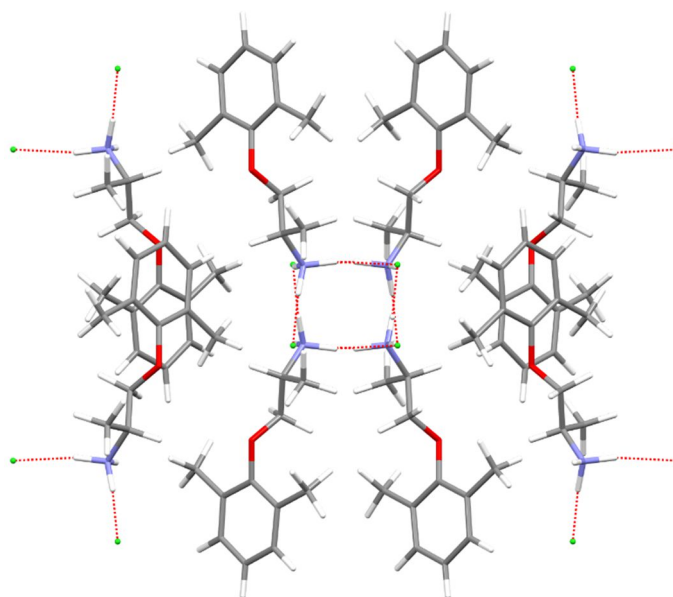
Figure 2.33: Predicted Form 662 of mexiletine, viewed down the *c*-axis.

The main difference between Form 662 and the solvent-free Type A form is the density. Due to a lack of voids, Form 662 is significantly more dense, at 1.22 gcm^{-3}, compared to 1.045 gcm^{-3} for the solvent-free Type A form. Even the Type A methanol solvate, which does not have empty voids, is less dense than Form 662 at 1.15gcm^{-3}. The molecules pack much more closely together in Form 662, which leads to its higher density.

In Form 662, the mexiletine molecule adopts an anti-periplanar conformation that is only observed in the highest energy experimental polymorph, Form 2. This anti-periplanar conformation is observed in all the predicted structures, apart from Form 924, and the two forms that are isostructural with Form 3: Forms 973 and 937. Form 924 is markedly different to all the known forms in terms of both molecular conformation and packing arrangement. The gauche molecule in Form 2 has the most similar conformation to Form 924, although an RMSD value of 0.485 Å shows the

two conformations are statistically different. Similarly, the Mercury packing similarity analysis showed that only 2 or 3 molecules of Form 924 overlap with Forms 1, 2 and 3, out of a group of 20. Although the hydrogen bonding motifs in Form 924 are very similar to Form 3, it is clear that the change in molecular conformation causes the molecules to pack together very differently (Figure 2.34).
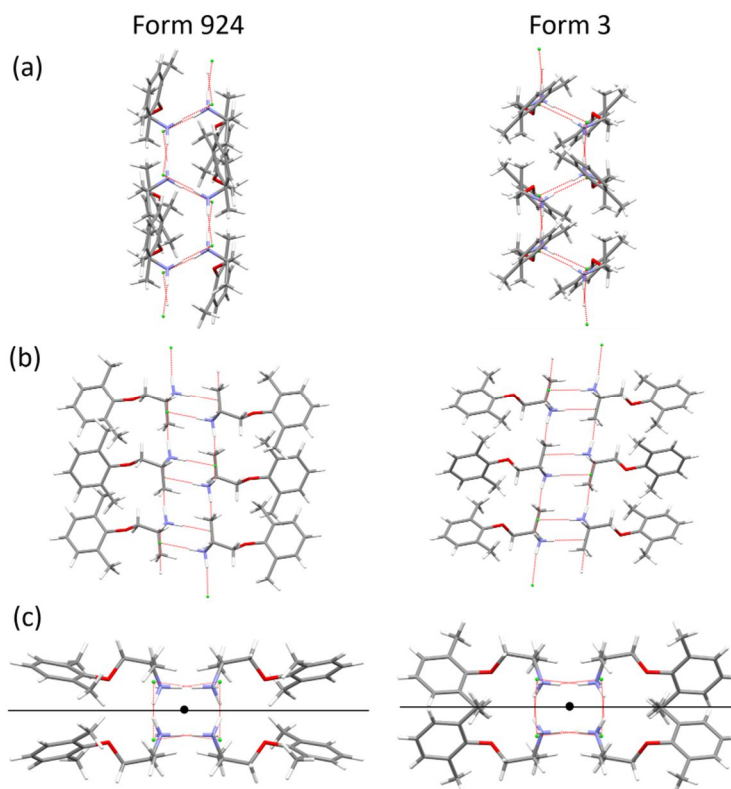
Figure 2.34: The packing arrangement in predicted Form 924 of mexiletine, compared to Form 3, viewed down the (a) *a*-axis, (b) *b*-axis and (c) *c*-axis. In image (c), the centres of inversion are shown as black circles and the *c*-glide planes are shown as black lines. There are more glide planes in Form 924, which have been omitted for clarity.

A gauche conformation is observed in both the lowest energy predicted Forms 973 and 937. All the other predicted structures are significantly higher in energy, and apart from one exception, have an anti-periplanar conformation. These results suggest that the anti-periplanar conformation is higher energy than the gauche one, and mirror experimental observations in which an anti-periplanar conformation is only observed

in the highest energy Form 2. This high energy, anti-periplanar conformation is probably difficult to nucleate under ambient conditions and therefore, it is unlikely that any of the predicted forms would be accessible using standard experimental techniques. The only possible exception is Form 436, which is extremely dense and has a low relative energy of 3.5 kJmol^{-1}. Although this form includes an anti-periplanar conformation, the barrier to nucleating the less stable conformation may be overcome by crystallising mexiletine under high pressure.[41] Taken as a whole, the CSP results come close to correctly identifying Form 3 as the most stable $Z' = 1$ polymorph under ambient conditions. The room temperature stable $Z' = 2$ Form 1 is denser and lower in energy, confirming it as the thermodynamic form at room temperature. The high temperature Form 2 is entropically stabilised and appears high on the CSP landscape. The absence of other low energy polymorphs in the CSP solid-form landscape gives confidence that the experimental screening has identified all the accessible non-solvated forms of mexiletine hydrochloride.

2.10 High-Pressure Crystallisation

Aiming to find predicted Form 436 of mexiletine, which has a high density but low relative energy, a single crystal of Form 2 was compressed to 3.56 GPa in a diamond anvil cell. Form 2 was chosen for this experiment because it has the same anti-periplanar conformation as Form 436, which minimises the molecular rearrangement required to carry out the transformation. Although the crystal remained intact under high pressure, the quality reduced dramatically, and it was no longer birefringent (Figure 2.35).
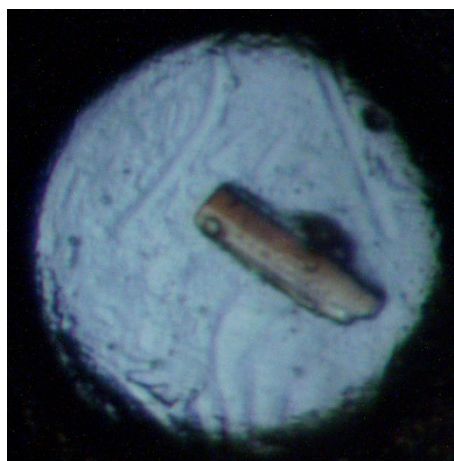
Figure 2.35: A single crystal of mexiletine Form 2, compressed to 3.56 GPa in a diamond anvil cell, photographed under crossed polars.

A slight expansion of the unit cell was observed when the crystal was compressed (Table 2.14). Due to the reduced crystal quality, the diffraction at high pressure was very weak and the resolution was poor, which may have led to the discrepancy in unit cell dimensions. Similarly, the high-pressure data were recorded at room temperature whereas the ambient-pressure structure of Form 2 was recorded at 120 K, which may also have contributed to the expansion of the unit cell. Although predicted Form 436 was not observed in this experiment, these changes in unit cell dimensions suggest that there is significant potential for further study of mexiletine at high pressure.

Table 2.14: Unit cell dimensions obtained by compressing a crystal of Form 2 of mexiletine to 3.56 GPa. Data were recorded at room temperature in a diamond anvil cell.

	Crystal compressed to 3.56 GPa
a/Å	18.680(3)
b/Å	18.125(9)
c/Å	7.398(4)
α/°	90
β/°	90.04(10)
γ/°	90

2.11 Gas Sorption Studies

To further investigate the porosity of the solvent-free Type A and B forms, gas sorption experiments were carried out using I_2 vapour.[36] Iodine is a common choice for these experiments due to its characteristic colour, which provides a visual indication of whether the gas has been absorbed. Tests were carried out by placing a crystalline sample of the solvent-free form of both polymorphs into a sealed vial close to, but not touching a similar mass of solid iodine (Figure 2.36). The experiments were carried out at room temperature, allowing the iodine to sublime gradually and diffuse into the porous crystals. The crystals were monitored for colour changes that would signify iodine absorption, and each sample was also characterised by PXRD to investigate any structural change. A typical vapour diffusion set-up involving two vials placed one inside the other was not effective for this experiment because iodine does not sublime rapidly at room temperature so very little iodine vapour diffused into the inner vial before the crystals transformed to Form 1. The mexiletine and iodine powders were therefore placed on opposite sides of the same vial to maximise iodine exposure. This meant that the front of the drug powder was exposed more directly to the iodine vapour than the back, which led to uneven iodine adsorption in the early stages of the experiment. However, the solvates both became uniformly coloured within one hour of iodine exposure and in each case, the mexiletine-containing powder was thoroughly mixed before PXRD analysis. These tests were also carried out using Form 1, to act as a control, and given the metastability of the solvates, the whole process was undertaken within 24 hours to minimise the transformation to Form 1.

When exposed to iodine vapour, crystals of the solvent-free Type A form began to change colour immediately and darkened significantly over time from light pink, to purple, to brown. When viewed under a microscope, the Type A crystals appeared uniformly coloured, implying that iodine permeates the channels in the structure, rather than simply absorbing onto the crystal surface. Similar results were observed for the solvent-free Type B form, which rapidly darkened in colour when exposed to the vapour (Figure 2.36). Although individual Type B crystals became uniformly brown after 24 hours, the bulk sample remained patchy in colour and did not absorb iodine as efficiently as Type A, which is likely due to a polymorphic transition to Form 1. These observations confirm that both solvent-free structures are porous and suggest that the iodine molecules are accommodated within the channels in the drug framework.
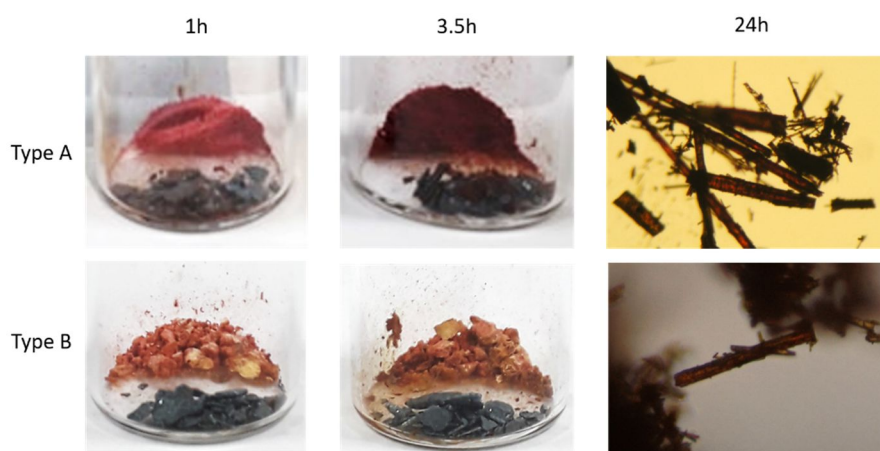
Figure 2.36: Gas sorption experiments showing the colour change of the Type A and B solvent-free forms after 1, 3.5 and 25 hours of exposure to iodine vapour.

In contrast, Form 1 showed a much slower colour change from white to light brown. The colour was more intense on the edge of the powder than in the middle, which suggests this form is not permeable to iodine and the sample undergoes some limited surface sorption (Figure 2.37). If removed from the iodine vapour and stored in air, the purple colour was lost rapidly from all samples, which suggests that the iodine molecules are only loosely bound to the drug structure, mirroring the behaviour of other guests bound within the channel solvates.
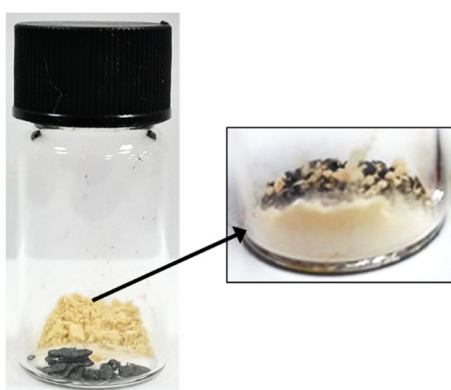
Figure 2.37: Gas sorption experiment showing the colour change of Form 1 after 3.5 hours of exposure to iodine vapour. The inset image is viewed from the back, showing that the colour change is localised to the surface of the powder.

The PXRD patterns of all forms developed a significant amorphous background with increased exposure to iodine vapour, signifying a decrease in crystallinity of the samples as the mexiletine molecules reorganise to maximise favourable interactions with the iodine (Figure 2.38). The solvent-free Type B structure could not be characterised using this method because its PXRD pattern already contains a significant amorphous background, as it is crystallised by fast cooling. The PXRD pattern of Form 1 remained unchanged with exposure to iodine, except for the reduced crystallinity. However, some differences were observed for the solvent-free Type A form. With a short exposure time, some small shifts and extra peaks were observed in

the PXRD pattern, but the key peaks characteristic of the Type A structures remained the same. However, with a longer exposure time, a new PXRD pattern was produced that does not match either the Type A solvates or Form 1, nor is it a mixture of the two.
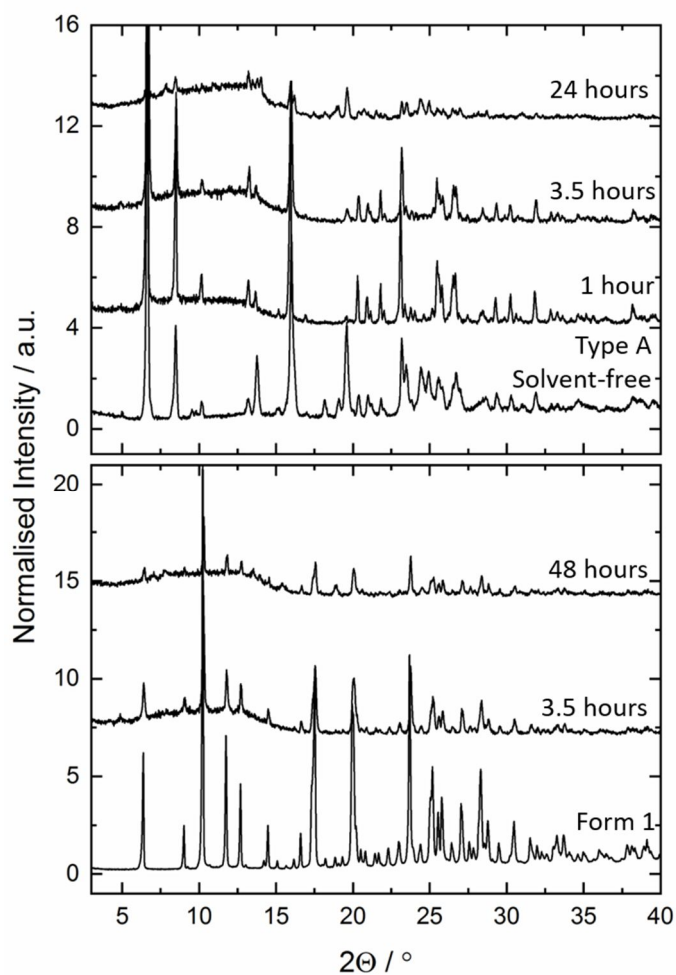
Figure 2.38: PXRD patterns of the solvent-free Type A structure and Form 1, following exposure to iodine vapour for different lengths of time.

To further investigate the co-crystallisation of mexiletine and iodine, a solution-phase crystallisation was carried out by vapour diffusion of hexane into an equimolar solution of mexiletine and iodine in DCM. The resulting structure is a 2:1:1 co-crystal solvate containing mexiletine, I_2 and DCM, respectively (Figure 2.39). Selected crystallographic information for this form can be found in Table 2.15 and the full crystallographic information is given in Appendix 7.1.

Table 2.15: Selected crystallographic information for the co-crystal solvate containing mexiletine, iodine and DCM.

Crystallisation Conditions	Vapour diffusion of hexane into a DCM solution of mexiletine and I_2
Space Group	$P\bar{1}$
a/Å	8.722(9)
b/Å	13.657(14)
c/Å	14.685(14)
α/°	70.816(4)
β/°	76.280(4)
γ/°	78.824(4)
V/Å^3	1592.1(3)
Z	4
ρ_{calc} g/cm^3	1.607

In the co-crystal solvate, both the DCM and iodine molecules are disordered over two positions. Each DCM molecule has an occupancy of 0.5, whereas the iodine molecules have occupancies 0.97 and 0.03. The two mexiletine molecules in the asymmetric unit have identical conformations (Figure 2.39), with an RMSD of only 0.044 Å. This conformation is the same as in Form 1, producing an RMSD of 0.040 Å when the two were compared.
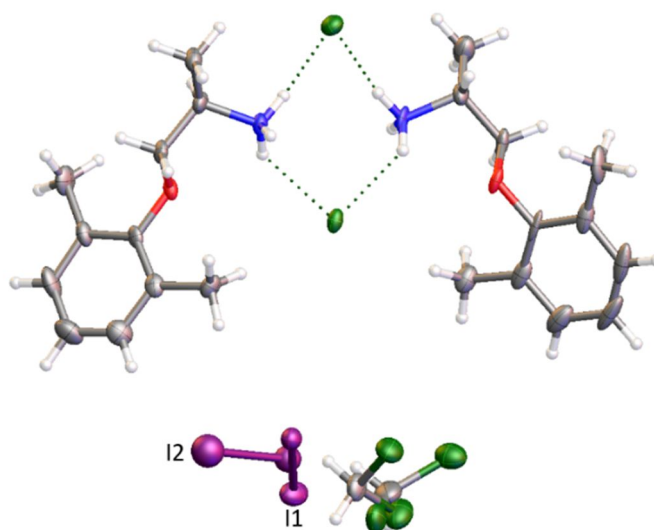
Figure 2.39: The asymmetric unit of the 2:1:1 co-crystal solvate containing mexiletine, I_2 and DCM. Both DCM molecules have an occupancy of 0.5, iodine molecule 1 has an occupancy of 0.97 and iodine molecule 2 has an occupancy of 0.03.

Both the unit cell dimensions and the packing arrangement of mexiletine molecules in the iodine co-crystal solvate are very similar to Form 1 (Figure 2.40). The overlap between the two forms was 12 out of a group of 20 molecules, with an RMSD of 0.357 Å, which signifies a moderate degree of similarity between them. In the co-crystal solvate, there are two chloride environments: one with two NH contacts and one with four, and these NH···Cl hydrogen bonds connect hydrogen-bonded mexiletine polymers along the crystallographic a-axis. Although the hydrogen bonding motifs in co-crystal solvate are very similar to Form 1, the packing

arrangements down the *b*- and *c*-axes are reversed, so that the *b*-axis of one form mirrors the *c*-axis of the other. The molecules are also spaced more widely apart in the co-crystal, to accommodate the iodine and DCM. As is observed in the solvated forms, neither the iodine nor the DCM molecules interact with the drug framework and they are located in between the hydrogen-bonded mexiletine polymers (Figure 2.40).
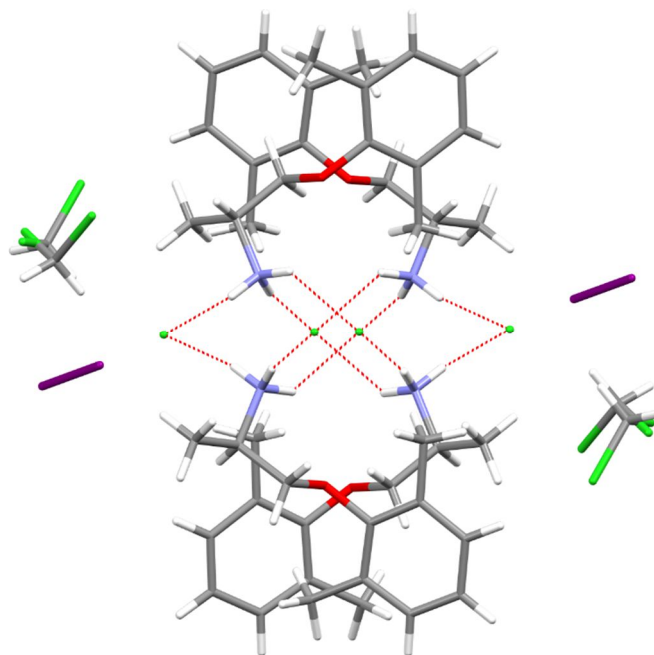
Figure 2.40: Packing arrangement in the 2:1:1 co-crystal solvate containing mexiletine, I_2 and DCM, viewed down the *a*-axis. As they have equal occupancy, both DCM molecules are displayed in full but for clarity, only the higher occupancy iodine molecule is displayed.

The calculated PXRD pattern of the iodine co-crystal solvate is a partial match for that of the solvent-free Type A structure following exposure to iodine vapour for 24 hours. The PXRD pattern of the iodine-exposed sample contains some peaks corresponding to the solvent-free Type A structure and others corresponding to the co-crystal solvate, suggesting that the sample is a mixture of the two forms (Figure 2.41). It is likely that the iodine is first absorbed into the channel solvate, and over a longer exposure time, the structure transforms to the co-crystal. The structure of the co-crystal is very different to both solvates and the high degree of molecular reorganization

required to change between these two forms is likely responsible for the amorphisation of these samples.
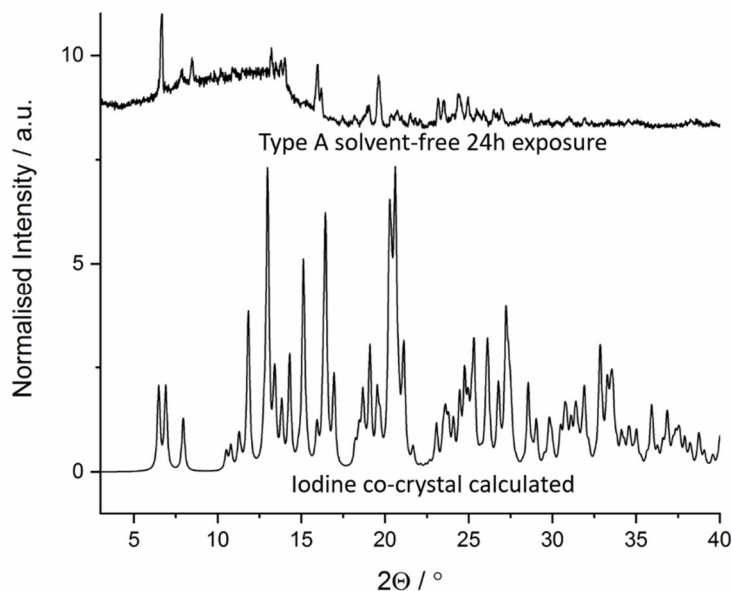
Figure 2.41: PXRD pattern of the solvent-free Type A form, exposed to iodine vapour for 24 hours, compared to the calculated PXRD pattern of the mexiletine-iodine co-crystal solvate.

2.12 Conclusions

In conclusion, this polymorph screen has revealed that the solid-state landscape of mexiletine hydrochloride includes three non-solvated polymorphs, termed Forms 1, 2 and 3 and two families of isomorphic channel solvates, termed Types A and B. In both solvate families, the drug framework acts as a host and remains mostly unchanged with the inclusion of different guests. The solvates differ in their value of Z', with Type A having one molecule per asymmetric unit and Type B having two. The two families are related by similar packing arrangements and hydrogen bonding motifs, but the Type B structure is significantly more complex. We have found eleven modifications of each solvate, including a wide range of different solvents with aliphatic, aromatic, polar and non-polar functionalities. Mexiletine was previously known to be an

enantiotropic system, in which Form 1 is stable at low temperatures and Form 2 is stable at high temperatures. This study reports for the first time, the single-crystal structure of Form 2, which was accessed by sublimation and is structurally related to the Type B solvates. The structure of each polymorph was characterised by PXRD and IR spectroscopy, and the composition of the solvates was also investigated using ^{13}C solid-state NMR spectroscopy, because the solvent was often too disordered to diffract X-rays. The experimental results were supported using computational tools including Mercury and PolySNAP, which compared the structures and quantified their similarity. Finally, a crystal structure prediction study replicated many of the structural and hydrogen bonding motifs seen in the experimental forms, including the prediction of precise structural analogues of Forms 2 and 3. This calculation showed that Forms 1 and 3 are close together in energy whilst Form 2 is significantly less stable at 0 K. This result mirrors experimental trends in which Form 3 crystallised concomitantly with Form 1, and Form 2 was only accessible at high temperatures. Most of the predicted forms include an anti-periplanar conformation of mexiletine's aromatic chain, which was only observed experimentally in the high temperature stable Form 2. The inclusion of this high energy conformation likely explains why very few of the predicted forms crystallised experimentally. The porous Type A and B structures are capable of reversibly including iodine vapour and in the case of Type A, the iodine inclusion complex undergoes a rearrangement to an iodine co-crystal.

2.13 References

1.   H. G. Brittain, *Polymorphism in pharmaceutical solids*, CRC Press, 2016.

2.   J. Bernstein, in *Polymorphism in molecular crystals*, Clarendon Press, Oxford, 2002, vol. 14, ch. 7, pp. 240-256.

3.   J. Bauer, S. Spanton, R. Henry, J. Quick, W. Dziki, W. Porter and J. Morris, *Pharm. Res.*, 2001, **18**, 859-866.

4.   G. Saurabh and C. Kaushal, *J. Chem. Pharm. Res*, 2011, **3**, 6-17.

5.   J. Bernstein, in *Polymorphism in Molecular Crystals*, Oxford University Press, 2002, vol. 14, ch. 10, pp. 297-307.

6.   A. J. Florence, *Eur. Pharm. Rev.*, 2010, **4**, 28-33.

7.   E. H. Lee, *Asian J. Pharm. Sci.*, 2014, **9**, 163-175.

8.   S. L. Morissette, Ö. Almarsson, M. L. Peterson, J. F. Remenar, M. J. Read, A. V. Lemmo, S. Ellis, M. J. Cima and C. R. Gardner, *Adv. Drug Deliv. Rev.*, 2004, **56**, 275-300.

9.   S. L. Price, *Adv. Drug Deliv. Rev.*, 2004, **56**, 301-319.

10.   M. A. Abounassif, M. S. Mian and N. A. Aziz Mian, in *Analytical Profiles of Drug Substances*, ed. K. Florey, Academic Press, 1991, vol. 20, pp. 433-474.

11.   R. Mehvar, D. R. Brocks and M. Vakily, *Clin. Pharmacokinet.*, 2002, **41**, 533-558.

12.   Z. A. Bredikhina, A. V. Kurenkov, D. B. Krivolapov and A. A. Bredikhin, *Tetrahedron: Asymmetry*, 2015, **26**, 577-583.

13.   J. Turgeon, A. C. G. Uprichard, P. M. Belanger, D. W. G. Harron and O. Grechbelanger, *J. Pharm. Pharmacol.*, 1991, **43**, 630-635.

14.   C. Franchini, C. Cellucci, F. Corbo, G. Lentini, A. Scilimati, V. Tortorella and F. Stasi, *Chirality*, 1994, **6**, 590-595.

15.   R. Aav, O. Parve, T. Pehk, A. Claesson and I. Martin, *Tetrahedron: Asymmetry*, 1999, **10**, 3033-3038.

16.   D. Koszelewski, D. Pressnitz, D. Clay and W. Kroutil, *Org. Lett.*, 2009, **11**, 4810-4812.

17.   D. Koszelewski, N. Muller, J. H. Schrittwieser, K. Faber and W. Kroutil, *J. Mol. Catal. B: Enzym.*, 2010, **63**, 39-44.

18. A. Carocci, C. Franchini, G. Lentini, F. Loiodice and V. Tortorella, *Chirality*, 2000, **12**, 103-106.

19. G. Carbonara, A. Carocci, G. Fracchiolla, C. Franchini, G. Lentini, F. Loiodice and P. Tortorella, *Arkivoc*, 2004, **5**, 5-25.

20. H. Y. Aboulenein, R. Rothchild and A. Sinnema, *Spectrosc. Lett.*, 1992, **25**, 1367-1385.

21. A. M. Namespetra, D. A. Hirsh, M. P. Hildebrand, A. R. Sandre, H. Hamaed, J. M. Rawson and R. W. Schurko, *CrystEngComm*, 2016, **18**, 6213-6232.

22. M. Hildebrand, H. Hamaed, A. M. Namespetra, J. M. Donohue, R. Fu, I. Hung, Z. Gan and R. W. Schurko, *CrystEngComm*, 2014, **16**, 7334-7356.

23. J. Sivy, V. Kettmann and E. Fresova, *Acta Crystallogr., Sect. C: Cryst. Struct. Commun.*, 1991, **47**, 2695-2696.

24. A. Kiss and J. Repasi, *Analyst*, 1993, **118**, 661-664.

25. M. Kuhnert, D. Seidel and G. Unterkircher, *Sci. Pharm.*, 1987, **55**, 13-25.

26. G. R. Desiraju, *Cryst. Growth Des.*, 2008, **8**, 3-5.

27. J. Bernstein, *Cryst. Growth Des.*, 2011, **11**, 632-650.

28. G. A. Stephenson, E. G. Groleau, R. L. Kleemann, W. Xu and D. R. Rigsbee, *J. Pharm. Sci.*, 1998, **87**, 536-542.

29. A. Bērziņš, A. Trimdale, A. Kons and D. Zvaniņa, *Cryst. Growth Des.*, 2017, **17**, 5712-5724.

30. G. Barr, W. Dong and C. J. Gilmore, *J. Appl. Crystallogr.*, 2009, **42**, 965-974.

31. G. Barr, W. Dong and C. J. Gilmore, *J. Appl. Crystallogr.*, 2004, **37**, 658-664.

32. C. F. Macrae, I. J. Bruno, J. A. Chisholm, P. R. Edgington, P. McCabe, E. Pidcock, L. Rodriguez-Monge, R. Taylor, J. van de Streek and P. A. Wood, *J. Appl. Crystallogr.*, 2008, **41**, 466-470.

33. J. A. Chisholm and S. Motherwell, *J. Appl. Crystallogr.*, 2005, **38**, 228-231.

34. A. Broo and S. O. Nilsson Lill, *Acta Crystallogr., Sect. B: Struct. Sci, Cryst. Eng. Mater.*, 2016, **72**, 460-476.

35. J. W. Steed and J. L. Atwood, in *Supramolecular Chemistry*, John Wiley and Sons, 2nd edn., 2009, ch. 7, pp. 385-440.

36. L. J. Barbour, *Chem. Commun.*, 2006, **11**, 1163-1168.

37. M. J. Turner, J. J. McKinnon, D. Jayatilaka and M. A. Spackman, *CrystEngComm*, 2011, **13**, 1804-1813.

38. A. L. Spek, *Acta Crystallogr. Sect. C: Struct. Chem.*, 2015, **71**, 9-18.

39. P. Borowski, W. Gac, P. Pulay and K. Woliński, *New J. Chem.*, 2016, **40**, 7663-7670.

40. A. J. Cruz-Cabeza and J. Bernstein, *Chem. Rev.*, 2014, **114**, 2170-2191.

41. M. A. Neumann, J. van de Streek, F. P. A. Fabbiani, P. Hidber and O. Grassmann, *Nat. Commun.*, 2015, **6**, 7793.

3. Tailored Supramolecular Gelators for the Crystallisation of Mexiletine Hydrochloride

3.1 Introduction

Controlling the solid form of an API is paramount in creating a safe and effective medicine[1-5] and there is increasing pressure on pharmaceutical companies to characterise and patent the solid-form landscape of new APIs.[6, 7] As a result, many novel crystallisation techniques have emerged, to increase the scope of traditional solution-phase polymorph screens and ensure the solid-form landscape of an API is fully understood before marketing the product. These include soluble crystallisation additives, heterogeneous nucleation, epitaxy, macro- and nano-scale confinement, microemulsions, self-assembled monolayers and gel-phase crystallisation.[8-10] Gel-phase crystallisation originated from the field of protein crystallography, in which polymeric hydrogels such as silica or agarose were used to increase crystal quality by slowing diffusion and limiting nucleation.[11-13] Small molecule supramolecular gels, held together by non-covalent interactions, are tuneable, reversible and more varied in structure than their polymeric counterparts.[14-17] Several studies report alterations to the size, habit, quality and solid form of crystals grown within supramolecular gels. In some cases, the self-assembly processes of the gel and crystals are orthogonal and changes in solid form derive from reduced nucleation within the gel environment.[10, 18, 19] Whereas in others, the gelators were designed to interact with the target drug. In these systems, the gel fibres can act as a heterogeneous nucleation surface and provide a template to encourage epitaxial overgrowth of highly metastable or difficult to nucleate solid forms.[20-25] If the correct functionality is included, the gelation can even

be switched off by the addition of anions so that the crystals can be retrieved by filtration.[26]

Gelator molecules can interact with a crystallising drug by several different mechanisms. Acid-amine hydrogen bonds between a carboxylic acid containing drug and an amine containing dendron gelator supported the crystallisation of an unusual polymorph of carbamazapeine.[22] Similarly, a novel polymorph of chlorphenesin was crystallised from a calixarene-based gel, in which the drug molecules bound to the hydrophobic cavities along the gel fibres, acting as nucleation sites for the new form.[23] Cis-platin mimicking gelators have shown that incorporating some chemical functionality from the drug structure into the gelator provides a template for the crystallisation of unusual drug polymorphs. In this case, a previously unknown solvate of cis-platin.[24] Similarly, ROY-mimetic gelators containing the same torsion angle as ROY's metastable R polymorph led to the reliable crystallisation of this form, from solvents that would typically crystallise the thermodynamically stable Y form.[20] A recent study suggests that, in systems where there is a significant interaction between the drug and gelator, nucleation of the gel fibres and drug crystals can become competitive rather than orthogonal processes, preventing the formation of a gel network.[27]

This work reports the design of drug-mimetic supramolecular gelators for the crystallisation of the antiarrhythmic drug mexiletine hydrochloride (Figure 3.1). As described in Chapter 2, mexiletine has five known solid forms. Forms 1[28] and 2 are an enantiotropic pair of anhydrous polymorphs that are stable at different temperatures, Form 3[29] is an anhydrous metastable polymorph and there are two related families of metastable channel solvates termed Type A and B.
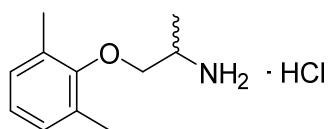
Figure 3.1: The structure of mexiletine hydrochloride.

Mexiletine is a prolific solvate former, with eleven members of each family discovered to date. It is therefore likely that more solvated forms with a similar structure are possible. Several forms of mexiletine also crystallise as mixtures, because two polymorphs are close together in energy. The potential for undiscovered solid forms and the opportunity to separate concomitantly crystallising polymorphs makes mexiletine HCl an ideal candidate for gel-phase crystallisation. Indeed, gel-phase crystallisation of mexiletine has already been attempted by our group, using a nanocellulose gelator that was designed to form hydrogen bonds with the target drugs. However, due to the high solubility of mexiletine in the solvent used to form these gels, the drug did not crystallise.[25] The gelators described in this work gel a much wider range of solvents and therefore present a greater opportunity for drug crystallisation.

3.2 Gelator Design

Two of the gelators used in this study are bis-urea dimers, composed of a central linking group that provides the gelling properties of the molecule, and mexiletine mimetic end-groups that act as a template for the crystallising drug molecules. The linking groups were chosen due to their strong gelling ability, which has been discussed widely in previous work from our group.[20, 26, 27, 30-39] The third gelator is a tris-amide trimer, with a central benzene 1,3,5-tricarboxamide group, derivatives of which have previously demonstrated reliable hydro-[40-43] and organo-gelation[44-48] behaviour. The terminal amine in mexiletine HCl means that the entire drug structure could easily be connected to the linker molecule. Using the whole molecule as an end-group, instead of mimicking one structural feature,[20, 24, 31] is likely to strengthen the templating effect by increasing the structural similarity between the drug and gelator.[31] The three gelators used in this study are shown in Figure 3.2.
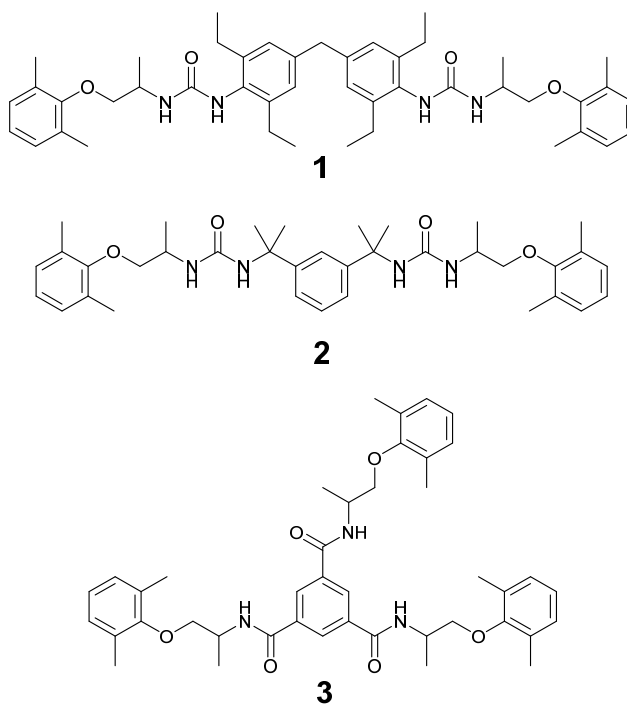
Figure 3.2: Structure of the three gelators, compounds **1**, **2** and **3**.

All three gelators were synthesised using simple, one-step reactions between the linking group and mexiletine HCl, in the presence of triethylamine (Figure 3.3). In the bis-urea syntheses, the isocyanate form of the linking group was used whereas, 1,3,5-benzenetricarbonyl trichloride was used to make the tris-amide gelator.
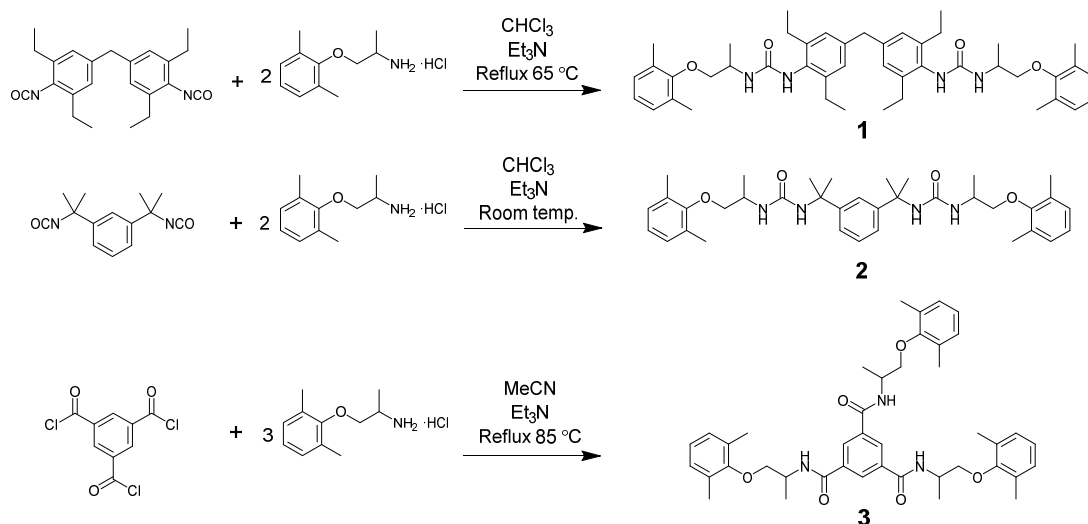
Figure 3.3: Synthetic routes to compounds **1**, **2** and **3**.

The isocyanate form of linker **1** was synthesised according to the literature method; from the corresponding amine and di-tert-butyl dicarbonate[49] (Figure 3.4), whereas the other starting materials could be purchased from standard commercial sources. Full experimental details and characterisation data for all three gelators can be found in the experimental section, Chapter 5.
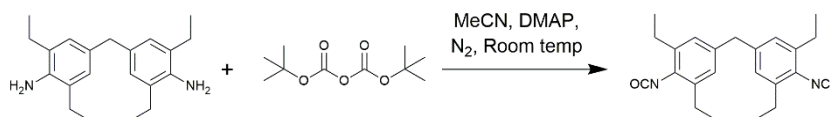
Figure 3.4: Synthesis of bis(3,5-diethyl-4-isocyanatophenyl)methane.

3.3   Gel Characterisation

The gelation behaviour of compounds **1**, **2** and **3** was tested in 46 solvents, spanning a wide range of chemical functionality. A 2 % w/v solution of the gelator was heated to its boiling point in a sealed vial, using a heat gun. The solution was placed in an insulating wooden block at room temperature and monitored for 24 hours. Gelation was identified by the inversion test. If the material supported its own weight and did not flow when the vial was inverted, the material was classed as a gel. The results of gel screening are shown in Table 3.1. Compound **1** was the best gelator, gelling 35 out of the 46 solvents tested, whereas compound **2** gelled 13 solvents and compound **3** gelled 8. This pattern reflects previous studies, in which compounds based on linker **1** were the strongest gelators.[20, 30, 33] Of the 46 solvents used for gel testing, 20 were included in the solution-phase polymorph screen of mexiletine that is described in Chapter 2. Including partial gels, compound **1** gelled 15 of these solvents, compound **2** gelled 3 and compound **3** did not gel any. These solvents were used for most of the gel-phase crystallisation experiments because the solution-phase polymorphism data could be used as a control.

Table 3.1: Gel screening results for Compounds **1**, **2** and **3**. G = gel, PG = partial gel (part of the sample has gelled, but part remains in solution), S = solution, I = insoluble, PPT = precipitate, C = crystals. * = These solvents were included in the solution-phase polymorph screen in Chapter 2.

Solvent	Compound 1	Compound 2	Compound 3
1,2,4-trichlorobenzene	G	G	G
1,2-dibromoethane	G	G	G
Ethyl methyl ketone, EMK*	G	S	I
1,2-dichlorobenzene	G	G	G
1,3-dichlorobenzene	G	G	G
1,4-dioxane*	G	S	PPT
1-butanol*	G	S	PPT
1-pentanol*	G	S	PPT
1-propanol*	G	S	I
2-butanol*	G	S	I
2-Ethyl pyridine	G	S	G
2-Picoline	G	S	PG + C
2-propanol*	G	S	I
3-chloro-1-propanol	S	S	PPT
3-Picoline	G	S	S
4-Ethyl pyridine	G	S	S
4-Picoline	G	S	S
Acetone*	I	S	I
Acetonitrile*	G	PPT	I
Benzene	PPT	G	I
Benzyl alcohol	G	S	S
Chlorobenzene	G	G	G
Chloroform*	S	S	PPT
Cyclohexane	PPT	PPT	I
Cyclohexanone	G	S	PPT
Cyclopentanone	G	S	S
Dichloromethane*	G	S	PPT
Diethyl ether*	I	I	I
Diethylene glycol	G	S	I
Diisopropyl ether	I	I	I
Dimethylacetamide	G	S	S
DMF*	G	S	S
DMSO*	G	S	S
Ethanol*	G	S	I
Ethyl acetate*	PPT	G	I
Ethylene glycol	PPT	G	I
Ethylene glycol butyl ether	G	S	PPT
Mesitylene	PG	G	I
Methanol*	G	S	I
Nitrobenzene	G	PG	G
Nitromethane*	PG	G	PPT
p-xylene	G	G	S
Pyridine	G	S	PPT
THF*	PG	S	PPT
Toluene*	S	G	I
Water	I	I	PPT
Solvents gelled	35/46	13/46	8/46

At a concentration of 2 % w/v, gels of compound **1** were either opaque or contained visible particles of undissolved gelator. Transparent gels of compound **1** could be achieved by reducing the concentration to 1 % w/v although, solid gelator particles were unavoidable in gels of apolar or low boiling point solvents. Compounds **2** and **3** were more soluble and these gels were therefore transparent. SEM images of the dried xerogels prepared from compounds **1**, **2** and **3** in nitrobenzene all showed a fibrillar network characteristic of a supramolecular gel (Figure 3.5).[50]
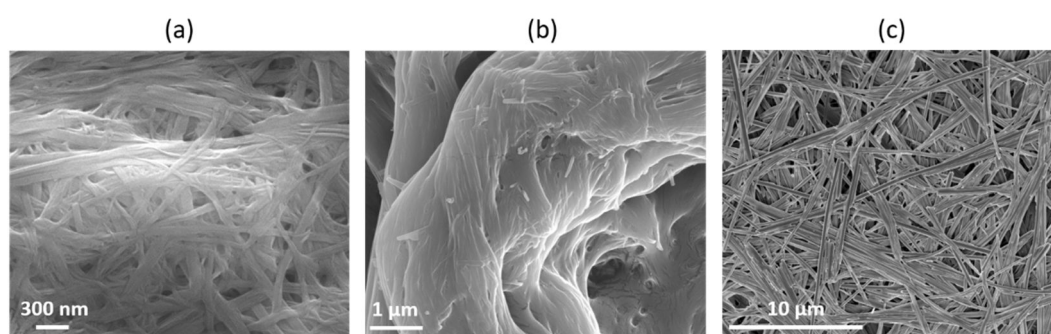
Figure 3.5: SEM micrographs of dried xerogels prepared from: (a) a 1 % (w/v) gel of compound **1** in nitrobenzene (b) a 2 % (w/v) gel of compound **2** in nitrobenzene (c) a 2 % (w/v) gel of compound **3** in nitrobenzene. Samples were coated in 7 nm gold-palladium.

Oscillatory rheology was used to probe the mechanical properties of the gels. A 1 % w/v gel of compound **1**, and 2 % w/v gels of compounds **2** and **3** in 1,2,4-trichlorobenzene were characterised using this technique. This solvent was chosen because its high boiling point and low vapour pressure produced uniform gels that did not dry out during the measurement (Figure 3.6). A lower concentration was used for compound **1** because this gelator has a lower solubility, and gels at 2 % w/v concentration contained undissolved solid that may alter their rheological properties.
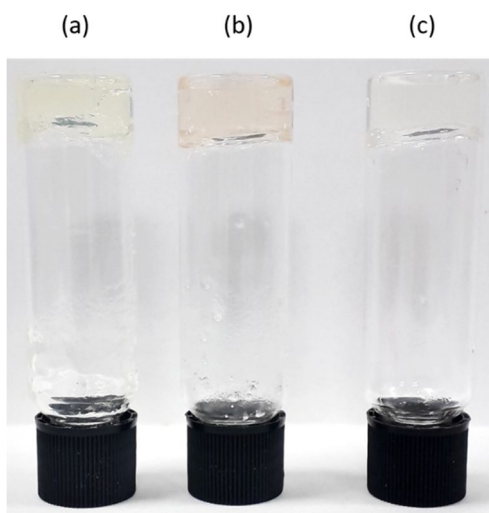
Figure 3.6: (a) 1 % w/v gel of compound **1** in 1,2,4-trichlorobenzene, (b) 2 % w/v gel of compound **2** in 1,2,4-trichlorobenzene and (c) 2 % w/v gel of compound **3** in 1,2,4-trichlorobenzene.

The gel phase can be identified by a storage modulus approximately one order of magnitude greater than the loss modulus, that does not vary with frequency.[51] This linear region was observed in the frequency sweep data for all gels, between 0.6 and 210 rad/s (Figure 3.7a), and confirms that these materials all display the elastic behaviour characteristic of a gel. The yield stress of a gel, which is used to quantify its strength, can be identified from stress sweep data as the oscillation stress at which the storage and loss moduli are equal (Figure 3.7b). The bis-urea gels of compound **1** and **2** were significantly stronger than the tris-amide gel of compound **3**, due to the addition of an extra hydrogen bonding group. Despite the lower concentration, compound **1** produced the strongest gel, with a yield stress of *ca.* 320 Pa. The gel of compound **2** had a comparable yield stress of *ca.* 200 Pa whereas, compound **3** produced a much weaker gel, with a yield stress of *ca.* 70 Pa. This trend mirrors previous reports in which bis-urea gelators containing the linking group in compound **1** are stronger than those based on the linking group in compound **2**.[20, 30, 33] A weak strain overshoot was observed in gels of compound **1**; where the loss modulus, G'',

increases just before the yield stress. This behaviour is indicative of a second mode of aggregation, in which components of the gel fibre align in the direction of the applied shear, forming a weak structure that is capable of resisting deformation for a short time, before it yields and the gel begins to flow.[52] Weak strain overshoot is common in systems containing hard particles.[53, 54] The low solubility of compound **1** may have led to precipitation within the gel, which could have contributed to this behaviour.
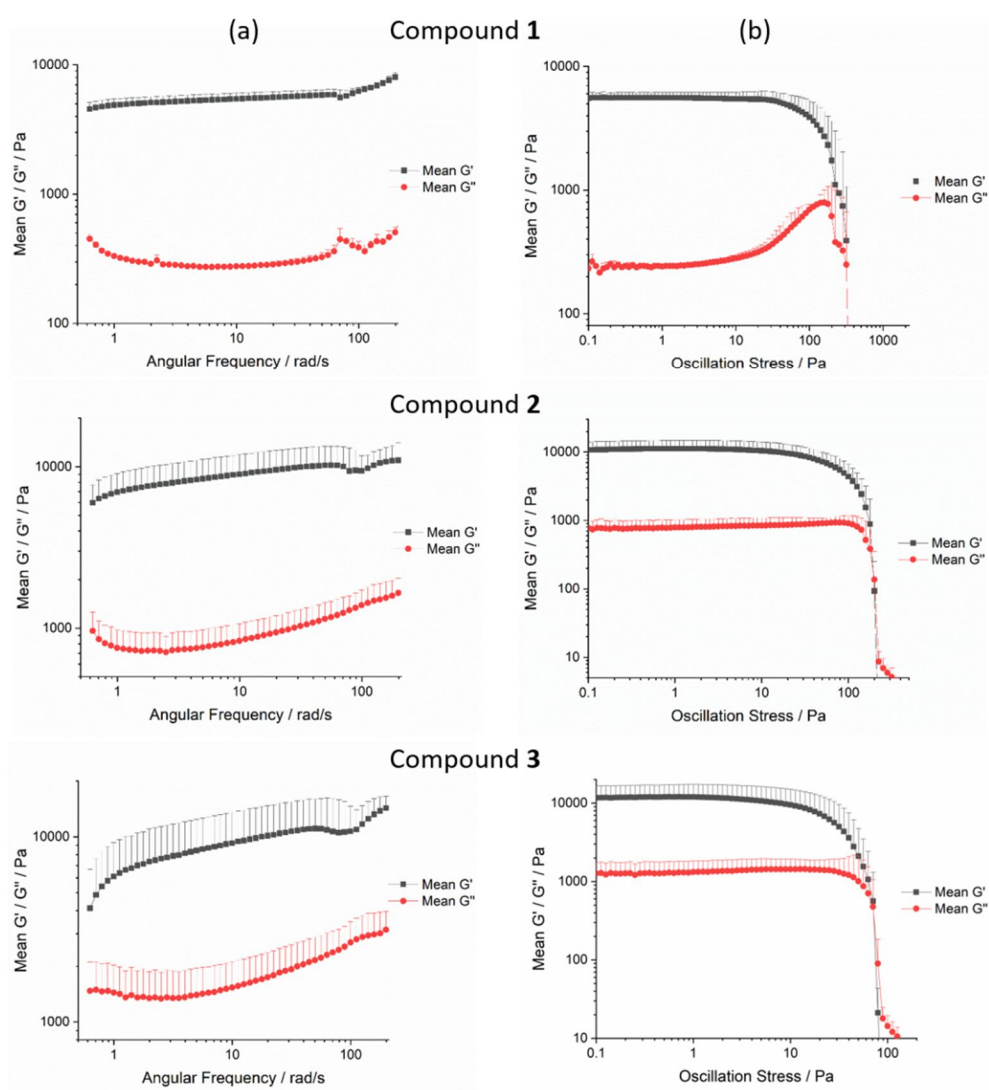
Figure 3.7: Oscillatory (a) frequency and (b) stress sweeps for a 1 % w/v gel of compound **1** in 1,2,4-trichlorobenzene, and 2 % w/v gels of compounds **2** and **3** in 1,2,4-trichlorobenzene. Error bars indicate the standard deviation from repeated measurements. For clarity, only the positive error bars are displayed.

3.4   Solution-Phase Polymorph Screening

Compound **3** did not gel any of the solvents that were included in the polymorph screen described in Chapter 2. Therefore, preliminary solution-phase crystallisations of mexiletine hydrochloride were carried out in the 6 solvents that were gelled by all three gelators, so that these results could be compared to the gel-phase crystallisations. Solution-phase crystallisations were carried out by slow cooling a supersaturated solution of mexiletine, formed by dissolving 20 mg of mexiletine powder in the minimum possible solvent and heating it to boiling in a sealed glass vial. The mixture was allowed to cool to room temperature in an insulating wooden block and monitored for crystallisation over time. PXRD was used to assess the polymorphism of the resulting crystals, as summarised in Table 3.2.

Table 3.2: Polymorphism of the samples crystallised from by slow cooling from a supersaturated solution in 1,2-dibromoethane, chlorobenzene, 1,2-dichlorobezene, 1,3-dichlorobenzne, 1,2,4-trichlorobenzene and nitrobenzene.

Solvent	Solid-Form Outcome
Chlorobenzene (CB)	Type A Solvate
1,2-Dichlorobenzene (12DCB)	Type A Solvate
1,3-Dichlorobenzene (13DCB)	Type A solvate
1,2-Dibromoethane (DBE)	Type B Solvate
1,2,4-Trichlorobenzene (TCB)	Type C TCB Solvate
Nitrobenzene (NB)	Type D NB Solvate

Four of the solution-phase crystallisations led to known forms characterised in Chapter 2. Crystallisation from the chlorinated solvents chlorobenzene, 1,2-dichlorobenzene and 1,3-dichlorobenzene yielded Type A solvates with PXRD patterns that match the Type A diethyl ether solvate crystallised by vapour diffusion of diethyl ether into a saturated solution of mexiletine in DMF (Figure 3.8).
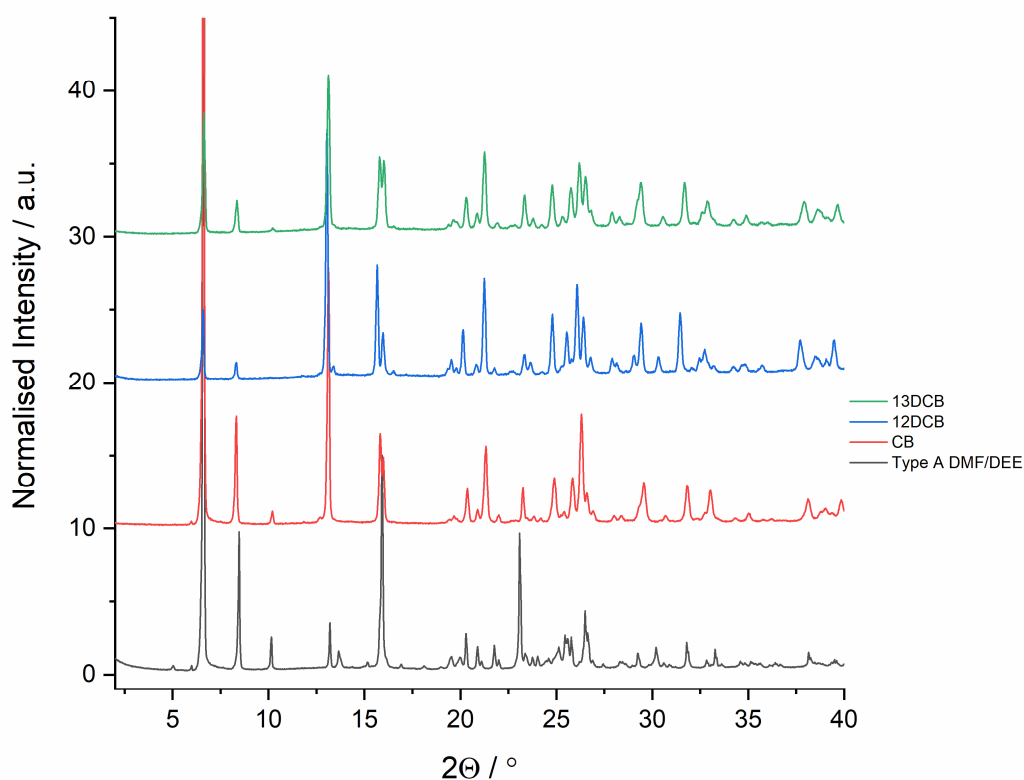
Figure 3.8: PXRD patterns of the Type A solvates of mexiletine crystallised by slow cooling from chlorobenzene (CB), 1,2-dichlorobenzene (12DCB) and 1,3-dichlorobenzene (13DCB), compared to the Type A diethyl ether solvate crystallised by vapour diffusion of diethyl ether into a mexiletine solution in DMF (DMF/DEE).

Crystallisation from 1,2-dibromoethane produced a Type B solvate, with a PXRD pattern that matches the Type B solvate crystallised by slow cooling from EMK (Figure 3.9).
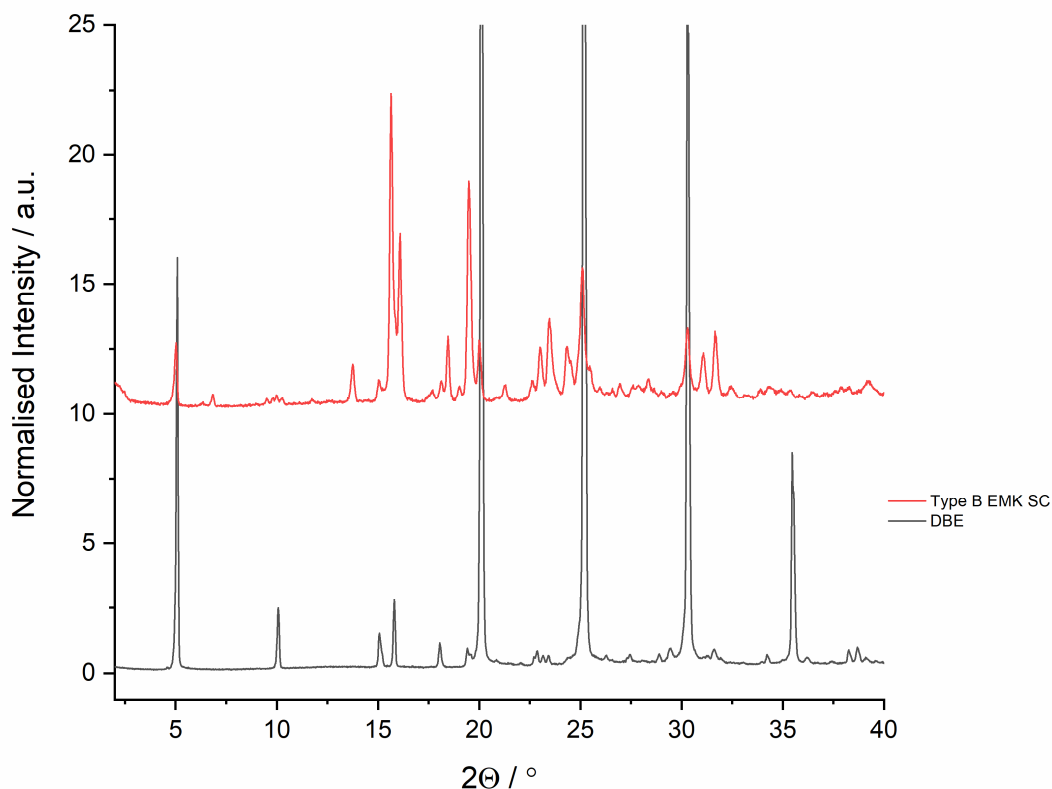
Figure 3.9: PXRD patterns of the Type B dibromoethane (DBE) and ethyl methyl ketone (EMK) solvates of mexiletine, crystallised by slow cooling.

Two new solvated polymorphs of mexiletine were crystallised from 1,2,4-trichlorobenzene and nitrobenzene. Their PXRD patterns are not related and therefore, they will be referred to as the Type C 1,2,4-trichlorobenzene solvate and the Type D nitrobenzene solvate. In addition to the five forms characterised in Chapter 2, the discovery of these new solvates means that mexiletine has seven known solid forms. The PXRD pattern of the Type C polymorph contains unique peaks at 12.9, 15.4 and 16.4 °, that are not observed in any of the forms identified in Chapter 2 (Figure 3.10).
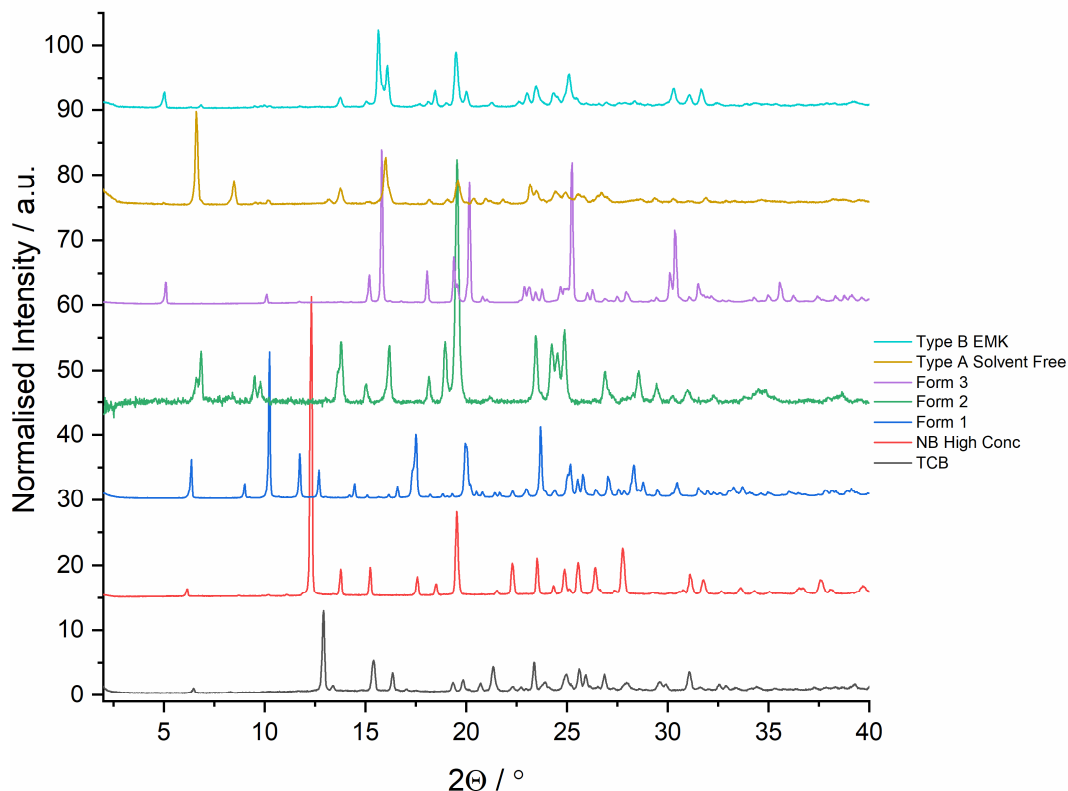
Figure 3.10: PXRD patterns of the form crystallised by slow cooling from 1,2,4-trichlorobenzene (TCB), compared to the Type D nitrobenzene solvate, and the five known forms from Chapter 2. For clarity, one representative example of the Type A and B solvates is shown.

A single-crystal structure of the Type C solvate was recorded using a crystal grown by slow cooling a supersaturated solution of mexiletine in 1,2,4-trichlorobenzene. Full crystallographic information for this structure is given in Appendix 7.1. The Type C structure is a 4:1 tetartosolvate in which the solvent molecules are situated inside channels that run along the a-axis of the mexiletine host framework. The structure is a racemate, with the asymmetric unit containing two identical pairs of mexiletine molecules and one 1,2,4-trichlorobenzene molecule. The two symmetry-independent mexiletine molecules both adopt a gauche conformation, with O-C-C-N torsion angles of 62.2 and 58.1 °, which are in line with other structures containing the R-O-CH$_2$-CHR-NH$_3^+$ fragment in the CSD. Each ammonium cation hydrogen bonds to three chloride counterions, forming a hydrogen-bonded polymer along the

crystallographic *a*-axis. When viewed along this axis, the molecules are arranged in a square formation, versions of which are observed in all forms of mexiletine other than Form 1. In this case, the four molecules making up the square motif are related by inversion, as shown in Figure 3.11a. Although the solvent molecules in this structure are disordered, it was possible to model them without using a mask and they are clearly visible within the channels (Figure 3.11b). A precise solvent model was only obtained for one of the seven Type A solvate structures and this unusual behaviour is most likely caused by the limited number of positions that the large trichlorobenzene molecule can occupy within the small channel.
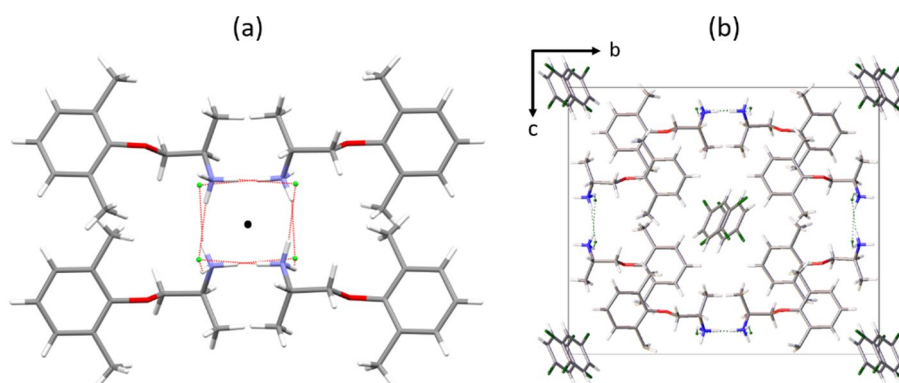
Figure 3.11: The Type C 1,24-trichlorobenzene solvate, viewed down the *a*-axis, showing (a) the square motif with the inversion centre labelled as a black circle and (b) the disordered solvent situated inside one unit cell of the porous mexiletine framework.

Although the Type C solvate has a different symmetry, the packing arrangement, hydrogen bonding motifs and unit cell dimensions are closely related to the Type A solvates. When compared to the Type A methanol solvate, which is the only member of that family in which the solvent molecules are clearly resolved in the crystal structure, several similarities are visible. Viewed down the channels, the packing arrangement of molecules within the mexiletine framework of the two solvates are nearly identical. Both structures consist of offset layers that alternate every half unit

cell, so the channels line up every other layer (Figure 3.12). The molecules are arranged very differently down the other two axes, although the hydrogen bonding motifs between molecules are closely related. There are slight differences in the unit cell dimensions of these two forms, which reflect changes in the channel dimensions to accommodate different solvents (Table 3.3).
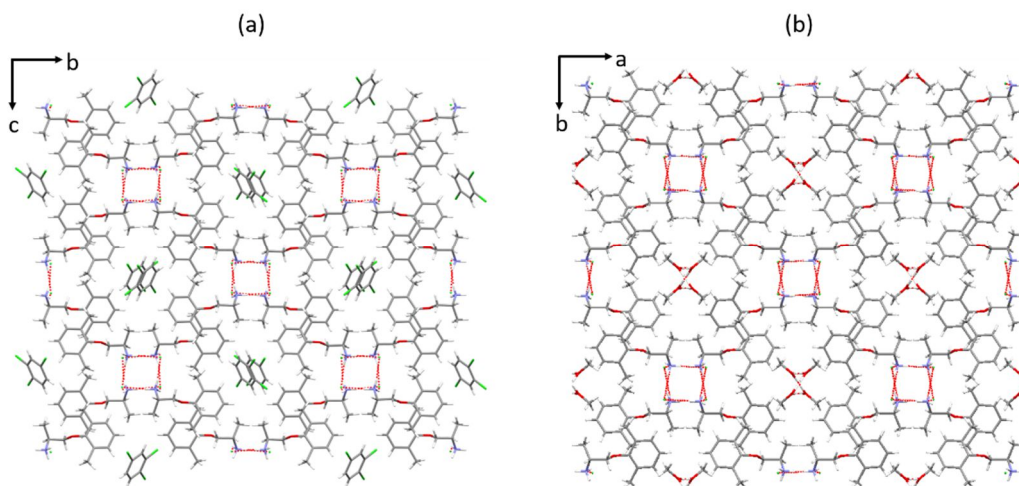
Figure 3.12: Packing arrangements in the Type C 1,2,4-trichlorobenzene solvate of mexiletine, compared to the Type A methanol solvate.

Table 3.3: Selected crystallographic information for the Type C 1,2,4-trichlorobenzene solvate of mexiletine, compared to the Type A methanol solvate.

	Type C TCB	Type A MeOH
Space group	P2$_1$/c	Pbcn
a/Å	7.538(3)	20.243(7)
b/Å	20.972(9)	18.768(6)
c/Å	18.043(8)	7.550(2)
α/°	90	90
β/°	93.725(7)	90
γ/°	90	90
Volume/Å^3	2846.0(2)	2868.4(15)
Z	2	8
ρ_{calc} g/cm^3	1.219	1.147

When stored for 24 hours under ambient conditions, the Type C trichlorobenzene solvate transformed into a Type A solvate, producing a PXRD pattern that closely matched the Type A diethyl ether solvate crystallised by vapour diffusion (Figure 3.13). The Type A solvates are metastable with respect to Form 1 and so this unusual result suggests that the trichlorobenzene solvate may be very close in energy to the Type A solvates. As the two forms are structurally similar, only a small degree of molecular rearrangement is required during the transformation, which is reflected in the high crystallinity of the sample after storage.
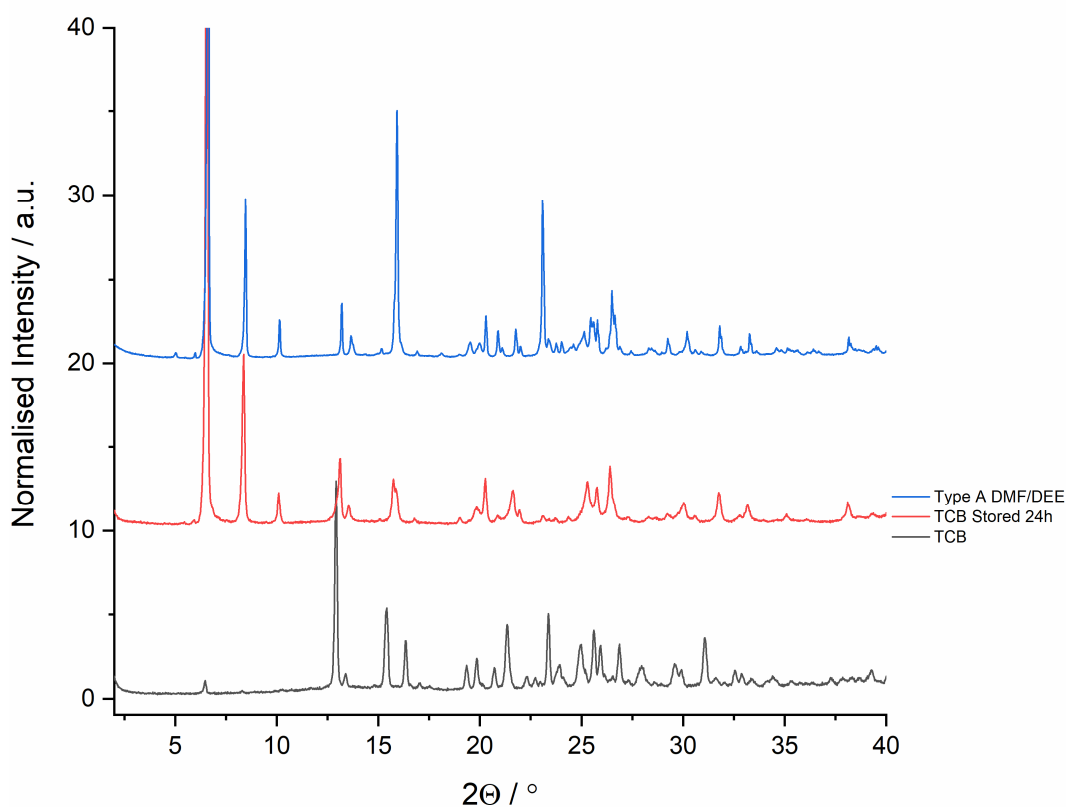
Figure 3.13: PXRD pattern of the Type C 1,2,4-trichlorobenzene solvate of mexiletine, compared with the same sample after being stored for 24 h, and the Type A diethyl ether solvate crystallised by vapour diffusion of diethyl ether into a saturated solution of mexiletine in DMF.

The polymorphic outcome of the crystallisations from nitrobenzene depended on the concentration of mexiletine. Low concentrations produced Form 1 whereas higher concentrations led to the Type D nitrobenzene solvate. The PXRD pattern of this form lacks several key peaks from each of the known forms and contains a unique peak at 12.3 ° (Figure 3.14).
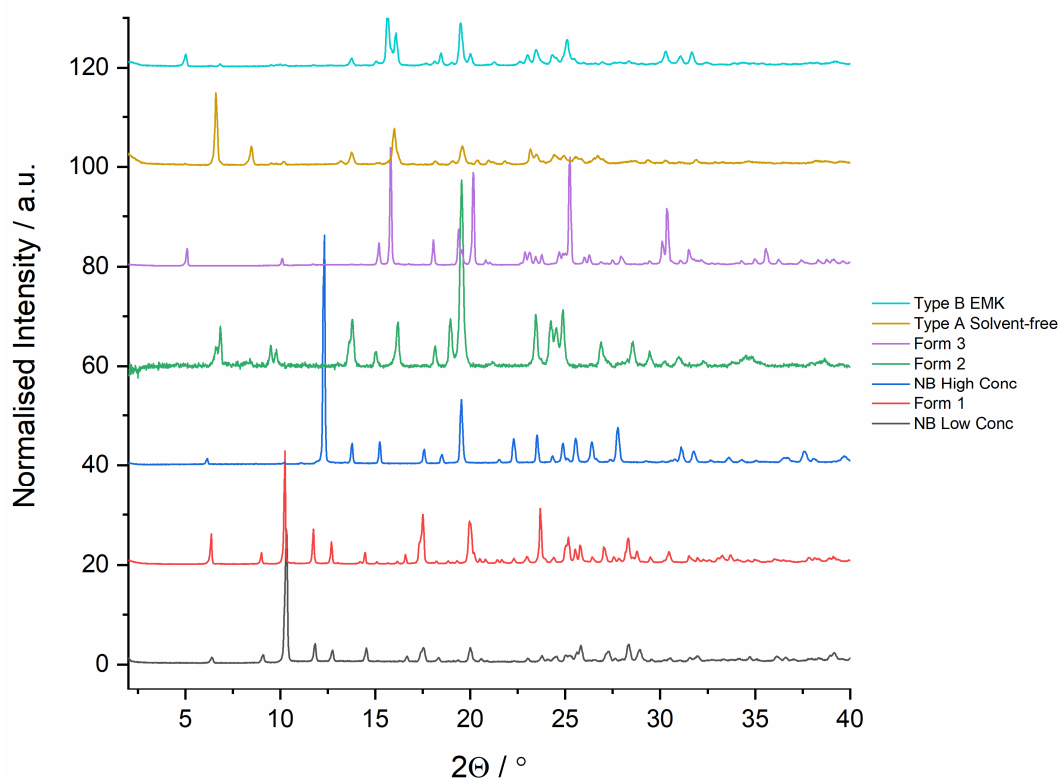
Figure 3.14: PXRD patterns of the two forms of mexiletine crystallised by slow cooling from nitrobenzene, at a high and low concentration, compared with the five known forms from Chapter 2. For clarity, one representative example from the Type A and B solvates is shown.

Form 1 has a very characteristic IR spectrum and so IR spectroscopy was used to identify the concentration that favours the Type D polymorph over Form 1. Seven solutions were prepared, at varying concentrations according to Table 3.4. When 20 mg of mexiletine was dissolved in 0.15 mL of nitrobenzene or less (>13.3 % w/v), the new form was produced. Whereas, solvent volumes of 0.2 mL and above (<10 % w/v) led to Form 1.

Table 3.4: Polymorphic outcome of seven slow cooling crystallisations containing various concentrations of mexiletine in nitrobenzene.

Mass of mexiletine / mg	Volume of nitrobenzene / mL	Concentration of mexiletine / % w/v	Solid-Form Outcome
20	0.05	40	Type D NB Solvate
20	0.1	20	Type D NB Solvate
20	0.15	13.$\dot{3}$	Type D NB Solvate
20	0.2	10	Form 1
20	0.3	6.$\dot{6}$	Form 1
20	0.4	5	Form 1
20	0.5	4	Form1

The Type D form can only be crystallised at high degrees of supersaturation, which suggests that it is metastable, and accordingly, it transformed into a mixture with Form 1 when stored for 24 hours under ambient conditions (Figure 3.15).
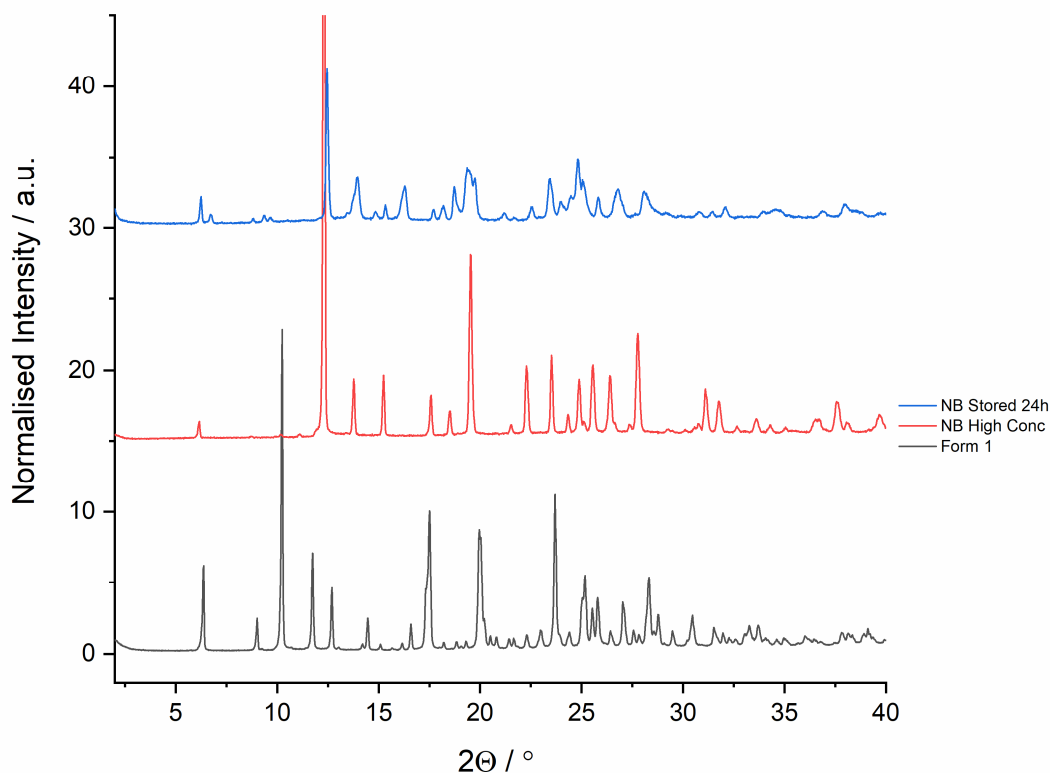
Figure 3.15: PXRD patterns of the Type D nitrobenzene solvate of mexiletine, crystallised at high concentrations from nitrobenzene, compared to the same sample after being stored for 24 h, and Form 1.

The Type C and D solvates were further characterised by IR spectroscopy. Both forms have unique spectra, different to each other and the known forms (Figure 3.16). Both spectra also contained solvent peaks, which confirms that they are solvates. In the Type C 1,2,4-trichlorobenzene solvate, the solvent peaks occur at 1457, 866, 815, and 678 cm^{-1}. Whereas, in the Type D nitrobenzene solvate, these peaks occur at 1527, 1350, 1317, 852, 843, and 682 cm^{-1}. From this data, it is not possible to know how the solvent molecules are incorporated into the Type D crystal structure. However, given that all previous solvated forms are channel solvates, it is likely that this form has a

similar structure. Similarly, there are likely to be more possible Type C solvates, incorporating different solvents into the channels.
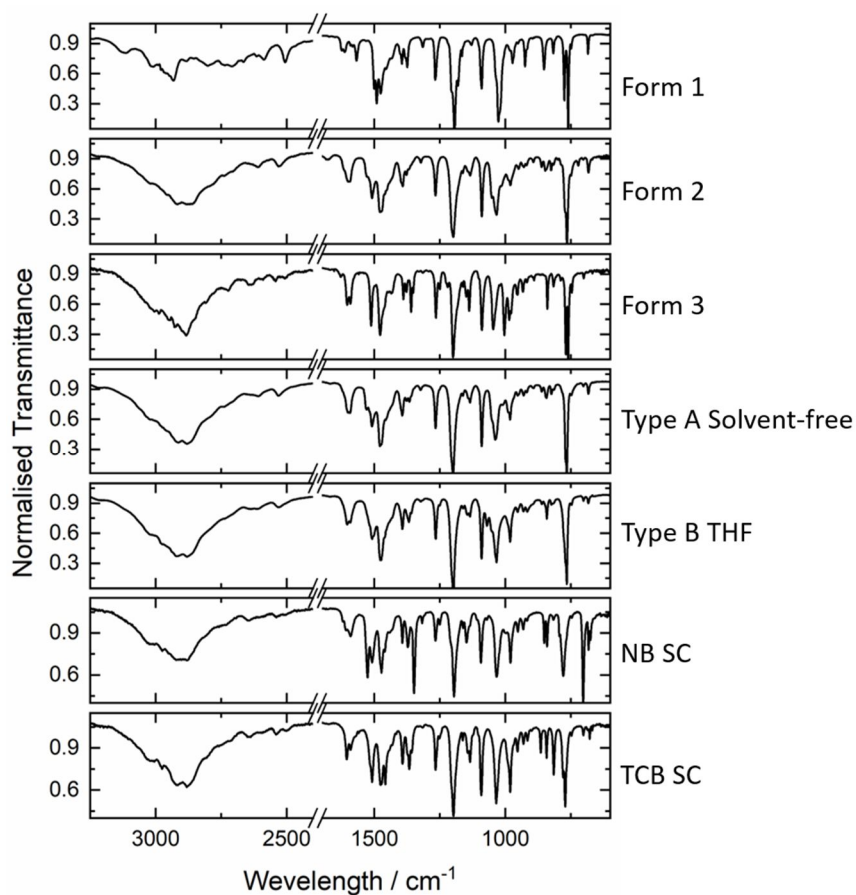
Figure 3.16: IR spectra of the Type C 1,24-trichlorobenzene solvate and Type D nitrobenzene solvate, both crystallised by slow cooling, compared to the five known forms from Chapter 2. For clarity, one representative example from the Type A and B solvates is shown.

It was not possible to characterise the Type C and D solvates by DSC and TGA because the extremely low vapour pressure of the solvents they were crystallised from caused significant amounts of solvent to adsorb onto the surface of the powders, meaning that the thermograms contained mostly solvent peaks. The powders could be dried in a desiccator or a low temperature oven, but by the time the solvent had evaporated, the samples had changed form.

3.5   Gel-phase Crystallisation

Gel-phase crystallisations of mexiletine were carried out using all three gelators, in solvents that were included in the solution-phase polymorph screens. The concentrations of the drug and gelator were optimised to ensure that where possible, gelation occurred before crystallisation, so that the gel network could interact with the crystallising drug molecules. Compound **1** was sparingly soluble in most solvents so a low concentration of gelator was used in these experiments, to avoid large gelator peaks in the PXRD patterns. The drug and gelator were dissolved in 0.5 mL of the required solvent by heating the mixture to the boiling point of the solvent in a sealed glass vial. The vials were placed in an insulating wooden block and monitored for gelation and crystallisation (Figure 3.17). After 24 hours, the vials were emptied onto filter paper, left to dry in air, and the resulting powder was characterised by PXRD. PXRD patterns of the gel-grown samples were compared to the solution-phase polymorph crystallised from the same solvent, to establish whether any change in polymorphism had occurred due to the presence of the gel network.
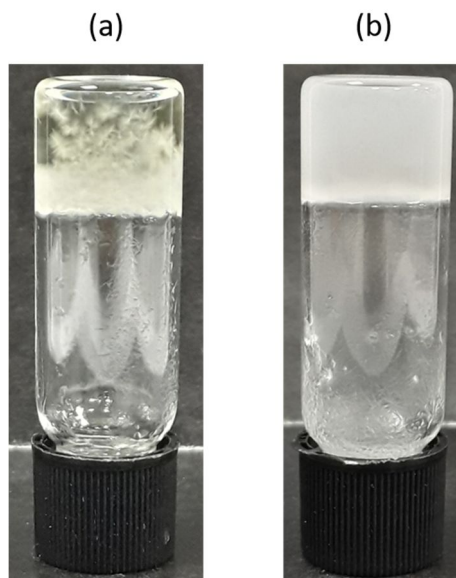
Figure 3.17: Gel-phase crystallisations of mexiletine in (a) a nitrobenzene gel of compound **2**, at concentrations of 2 % w/v gelator 5 % w/v drug, and (b)a 1,2-dichlorobenzene gel of compound **1**, at concentrations of 1 % gelator 5 % w/v drug. In results Tables 3.5, 3.6 and 3.7, samples like image (a) were described as gel + crystals whereas samples like image (b) were described as gel + precipitate.

All gel-phase crystallisations using compound **3** resulted in the same solid forms as in solution (Table 3.5). Crystallisation within gels of 1,2-dichlorobenzene, 1,3-dichlorobenzene and chlorobenzene led to Type A solvates, gels of 1,2-dibromoethane crystallised a Type B solvate and gels of 1,2,4-trichlorobenzene and nitrobenzene produced Type C and D solvates, respectively. Gels of compound **3** were an order of magnitude weaker than both the bis-urea gels, which suggests that they contained fewer gel fibres. The gel network may therefore have been insufficient to encourage the growth of new polymorphs, leading to the same crystallisation behaviour as in solution.

Table 3.5: Results of gel-phase crystallisations of mexiletine using compound **3**. G = gel, C = crystals.

Solvent	Gelator Concentration / % w/v	Drug Concentration / % w/v	Gelation Behaviour	Solid-Form Outcome
1,2-Dichlorobenzene	2	5	G+C	Type A
1,3-Dichlorobenzene	2	5	G+C	Type A
Chlorobenzene	2	5	G+C	Type A
1,2-Dibromoethane	2	5	G+C	Type B
1,2,4-Trichlorobenzene	2	5	G+C	Type C TCB
Nitrobenzene	2	5	G+C	Type D NB

Mexiletine crystallised within 13 of the 15 gel-phase crystallisation experiments using compound **1** (Table 3.6). Due to its high solubility in polar solvents, mexiletine did not crystallise in any gel containing ethanol or methanol and the resulting PXRD patterns matched the gelator. These experiments are therefore omitted from Table 3.6.

Table 3.6: Results of gel-phase crystallisations of mexiletine using compound **1**.
G = gel, C = crystals, P = precipitate, * = gel and solution-phase crystallisations yield different forms.

Solvent	Gelator Concentration / % w/v	Drug Concentration / % w/v	Gelation Behaviour	Solid-Form Outcome
Nitromethane	2	5	G+PPT	Form 1
Nitromethane	1	2	G+C	Form 1
1-Propanol	1	10	G+C	Form 1
2-Propanol	1	10	G+C	Form 1
1-Butanol	1	10	G+C	Form 1
2-Butanol	1	10	G+C	Form 1
Amyl Alcohol	1	10	G+C	Form 1
Acetonitrile	1	2	C	Form 1
Acetonitrile	2	5	C	Form 3
DCM	1	2	G+PPT	Type A
DCM	2	5	G+C	Type A
THF	1	2	G+C	Type B
THF	0.5	1	G+C	Type B
1,4-Dioxane	1	10	G+C	Type B
1,4-Dioxane	0.5	10	G+C	Type B
EMK	1	2	G+C	Type B
EMK	0.5	1	G+C	Form 3*
DMF	2	5	G+PPT	Type A*
DMF	1	10	PPT	Type A*
DMSO	2	5	G+PPT	Type A*
1,2-Dichlorobenzene	1	5	G+C	Type A
1,3-Dichlorobenzene	1	5	G+C	Type A
Chlorobenzene	1	5	G+PPT	Type A
1,2-Dibromoethane	1	5	G+C	Type B
1,2,4-Trichlorobenzene	1	5	G+C	Type C TCB
Nitrobenzene	1	5	G+C	Type D NB

Most gel-phase crystallisations using compound **1** yielded the same solid form as in solution. Form 1 was crystallised form gels of nitromethane, 1-propanol, 2-propanol, 1-butanol, 2-butanol, and amyl alcohol. Type A solvates crystallised from gels in all chlorinated solvents: DCM, 1,2-dichlorobenzene, 1,3-dichlorobenzene and chlorobenzene, and Type B solvates crystallised from gels in THF and dioxane. Similarly, gels of 1,2,4-trichlorobenzene and nitrobenzene produced Type C and D solvates, respectively. Incorporation of mexiletine inhibited the gel formation of compound **1** in acetonitrile and accordingly, the result of these crystallisations was also the same as in solution. At concentrations of 1 % w/v gelator and 2 % w/v drug, mexiletine crystallised as Form 1, as observed in slow cooling crystallisations from pure acetonitrile. At a higher supersaturation, using 2 % w/v of gelator and 5 % w/v of drug, mexiletine crystallised as the metastable Form 3. This result mirrors solution-phase behaviour in which a mixture of Forms 1 and 3 can be crystallised by fast cooling from pure acetonitrile.

In contrast, gel-phase crystallisations using compound **1** in EMK, DMF and DMSO produced different solid forms than in solution. A Type B solvate crystallises from EMK solution and the same form is observed from a gel containing 1 % w/v gelator and 2 % w/v drug. However, when the concentrations are reduced to 0.5 % w/v gelator and 1 % w/v drug, Form 3 is produced (Figure 3.18). Form 3 is a metastable polymorph, very close in energy to Form 1, and pure samples have only been crystallised previously from solution in acetone. The crystallisation of pure Form 3 within this drug-mimetic gel highlights its ability to stabilise and selectively nucleate a metastable solid form.
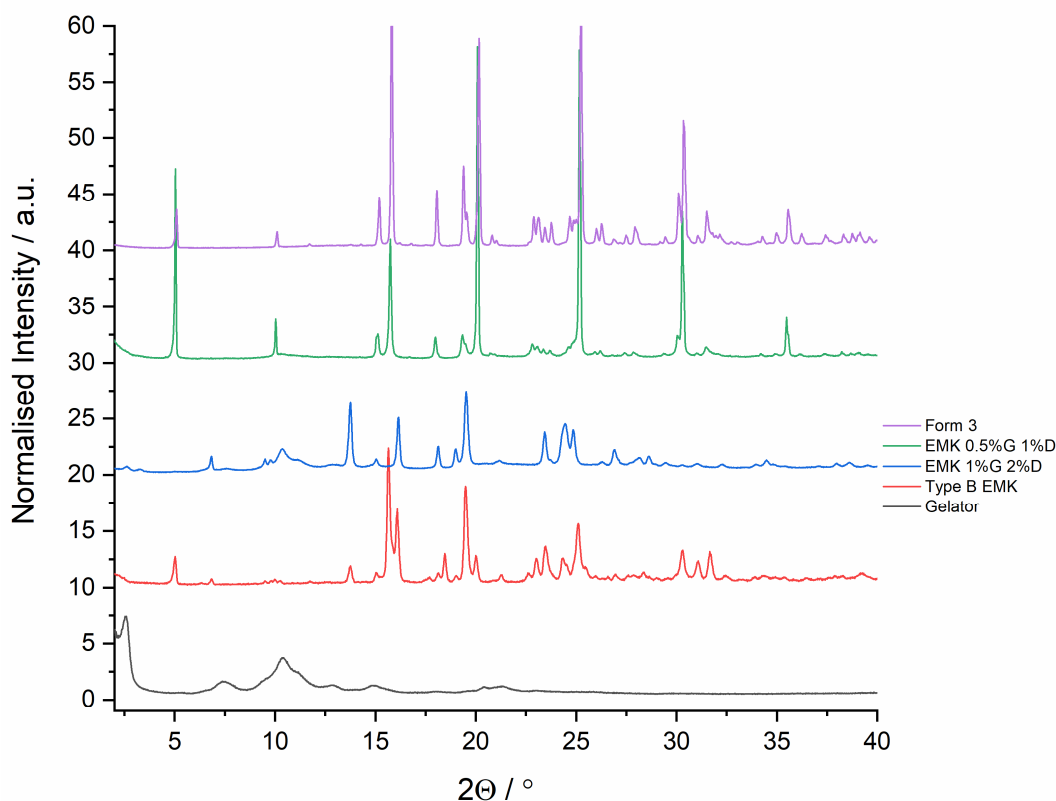
Figure 3.18: PXRD patterns of the two solid forms of mexiletine crystallised within two EMK gels of compound **1**, compared to Form 3, the Type B EMK solvate and compound **1**.

Finally, a crystalline solid form is produced from gels of compound 1 in DMF and DMSO, whereas mexiletine does not crystallise from solution in either of these solvents. The PXRD patterns of the gel-crystallised samples all contain gelator peaks, showing that only a small amount of the drug has crystallised. The crystallinity of the samples increases with drug concentration and at 1 % w/v gelator and 10 % w/v drug, some clear mexiletine peaks are observed at 4.9, 6.4, 19.5, 19.9, 24.4, 25.0, 29.3 and 30.0 ° (Figure 3.19). These peaks match most closely with the Type A diethyl ether solvate, which is crystallised by vapour diffusion of diethyl ether into DMF. Although the low crystallinity of their PXRD patterns means that it is not possible to assign the polymorphism of these gel-grown crystals unequivocally, they are likely to be Type A solvates because that form can also be crystallised from DMF by vapour diffusion.

Similar behaviour was observed when sulfapyridine was crystallised from a nanocellulose organogel in DMSO. Crystallisation was not observed from a solution under the same conditions, even though the solution was highly supersaturated, and the gel network was thought to be acting as a kinetic nucleation promoter.[25] It is therefore likely that in this case, the gel fibres are acting as nucleation sites to enable the crystallisation of a Type A solvate from an unusual solvent.
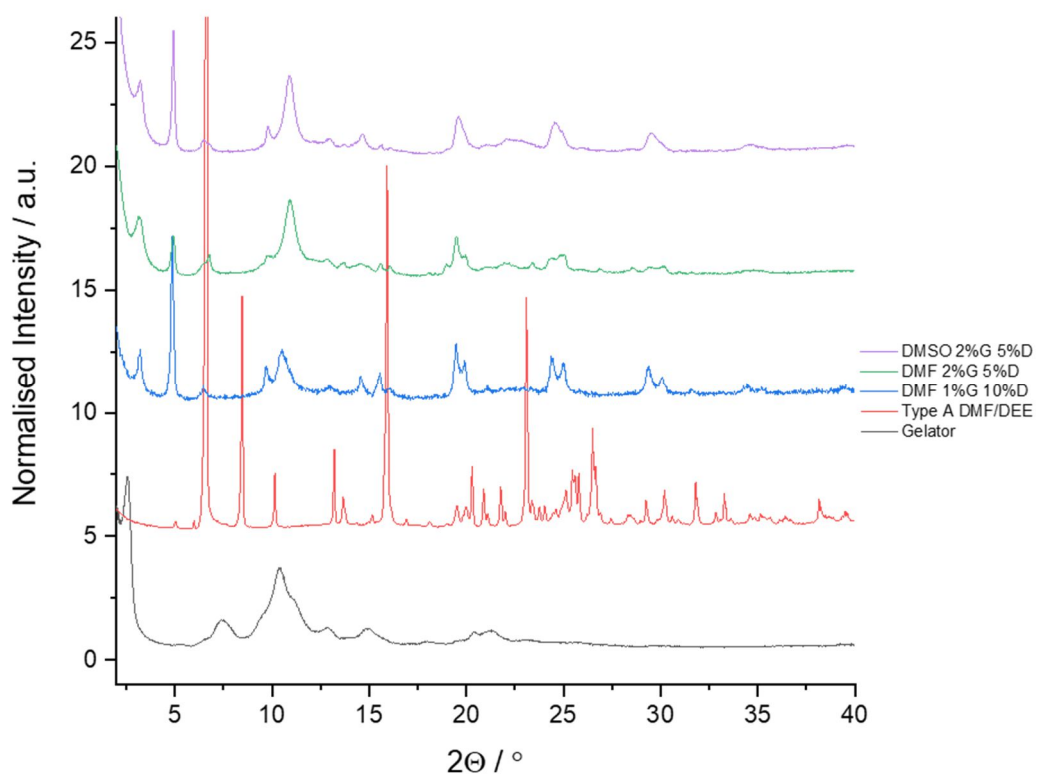
Figure 3.19: PXRD patterns of the mexiletine solid forms crystallised from three DMF and DMSO gels of compound **1**, compared to the gelator, and the Type A diethyl ether solvate crystallised by vapour diffusion of diethyl ether into DMF.

The greatest changes in polymorphism were observed when mexiletine was crystallised using compound **2**. The polymorphic outcome of these crystallisations was dependent on the concentration of mexiletine and in many cases, gelation was switched off in experiments that led to a change in solid form. This behaviour suggests

that there were significant interactions between the drug and gelator molecules that hindered the self-assembly of gel fibres.[27] It is likely that the strong interactions between the drug and gelator molecules played a key role in the nucleation of unusual solid forms. Due to the inconsistent gelation behaviour of this system, several experiments were repeated multiple times, so that a reliable trend could be established (Table 3.7).

Table 3.7: Results of gel-phase crystallisations of mexiletine using compound **2**. G = gel, C = crystals, P = precipitate, * = gel and solution-phase crystallisations yield different forms, Type A′ = the contents of the channels differs between the Type A solvates crystallised from solutions and gels.

Solvent	Gelator Concentration / % w/v	Drug Concentration / % w/v	Gelation Behaviour	Solid-Form Outcome
Nitromethane	2	5	C	Form 1
Nitromethane	2	2	G+C	Form 1
Nitromethane	2	2	C	Form 1
Nitromethane	2	1	Weak G+C	Form 1
Nitromethane	2	1	C	Form 1
Toluene	2	5	C	Type A Tol
Toluene	2	2	C	Type A Tol
Toluene	2	2	G+C	Type A Tol
Toluene	2	1	C	Type A Tol
Toluene	2	1	PG+C	Type A′*
Ethyl Acetate	2	5	C	Type A*
Ethyl Acetate	2	2	C	Type A*
Ethyl Acetate	2	2	C	Form 1
Ethyl Acetate	2	2	G+C	Form 1
Ethyl Acetate	2	1	C	Form 1
Ethyl Acetate	2	1	C	Type A′*
1,2-Dichlorobenzene	2	5	G+C	Type A
1,3-Dichlorobenzene	2	5	G+C	Type A
Chlorobenzene	2	5	G+C	Type A
1,2-Dibromoethane	2	5	G+C	Form 2*
1,2,4-Trichlorobenzene	2	5	G+C	Type C TCB
Nitrobenzene	2	5	G+C	Type D NB

In several cases, the same solid form crystallised from gels as from solution. Form 1 crystallised from gels of compound **2** in nitromethane, and Type A solvates crystallised from gels in 1,2-dichlorobenzene, 1,3-dichlorobenzene and

chlorobenzene. Similarly, Type C and D solvates crystallised from gels of 1,2,4-trichlorobenzene and nitrobenzene, respectively. The majority of crystallisations from toluene also produced the same form as in solution: a Type A solvate. However, in one crystallisation with a low drug concentration of 1 % w/v, a new solid form was produced. The PXRD pattern of this form contains the key peaks characteristic of a Type A solvate and many extra peaks between 12–27 ° that are not present in the pattern of the toluene solvate crystallised from solution (Figure 3.20). The extra peaks in the PXRD pattern of the gel form suggest that the contents of the channels differ from the solution form. This new Type A solvate also crystallised from ethyl acetate at concentrations of 2 % w/v gelator and 1 % w/v mexiletine (Figure 3.20). This result is particularly unusual because mexiletine crystallises as Form 1 from ethyl acetate solution. In both of these cases, gelation was switched off by interactions between mexiletine and the gelator.[27]
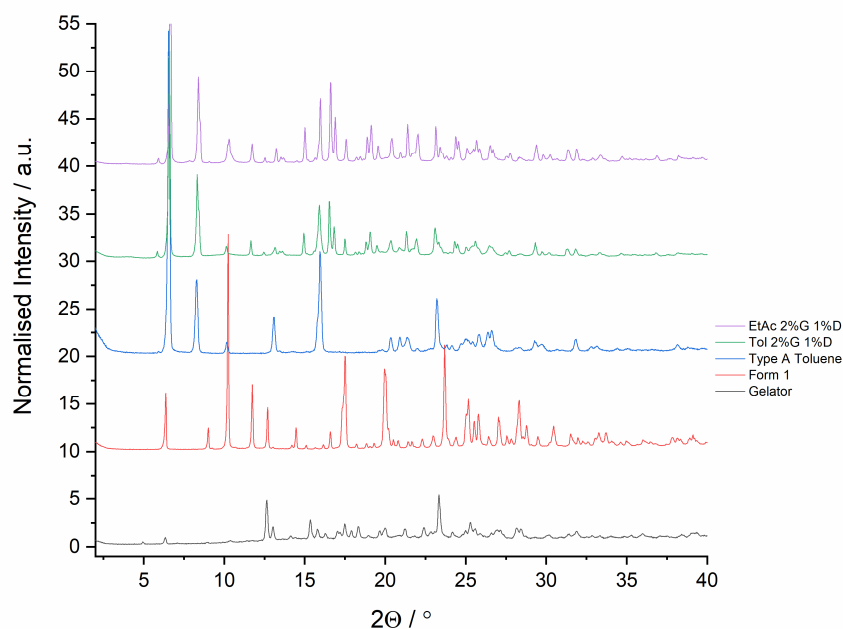
Figure 3.20: PXRD patterns of mexiletine crystallised from toluene and ethyl acetate solutions, at concentrations of 2 % w/v gelator and 1 % w/v drug, compared to Form 1, the Type A toluene solvate, and the gelator.

Two other ethyl acetate crystallisations, with concentrations of 2 % w/v gelator and 2 or 5 % w/v drug, also led to a Type A form, although in these cases the PXRD pattern matched the Type A solvent-free structure (Figure 3.21). In this form, the channels may be empty or, could be filled with highly disordered solvent that does not diffract X-rays. It is clear that compound **2** has a profound effect on the nucleation of the Type A solvates, and the crystallisation of solvent within the channels.
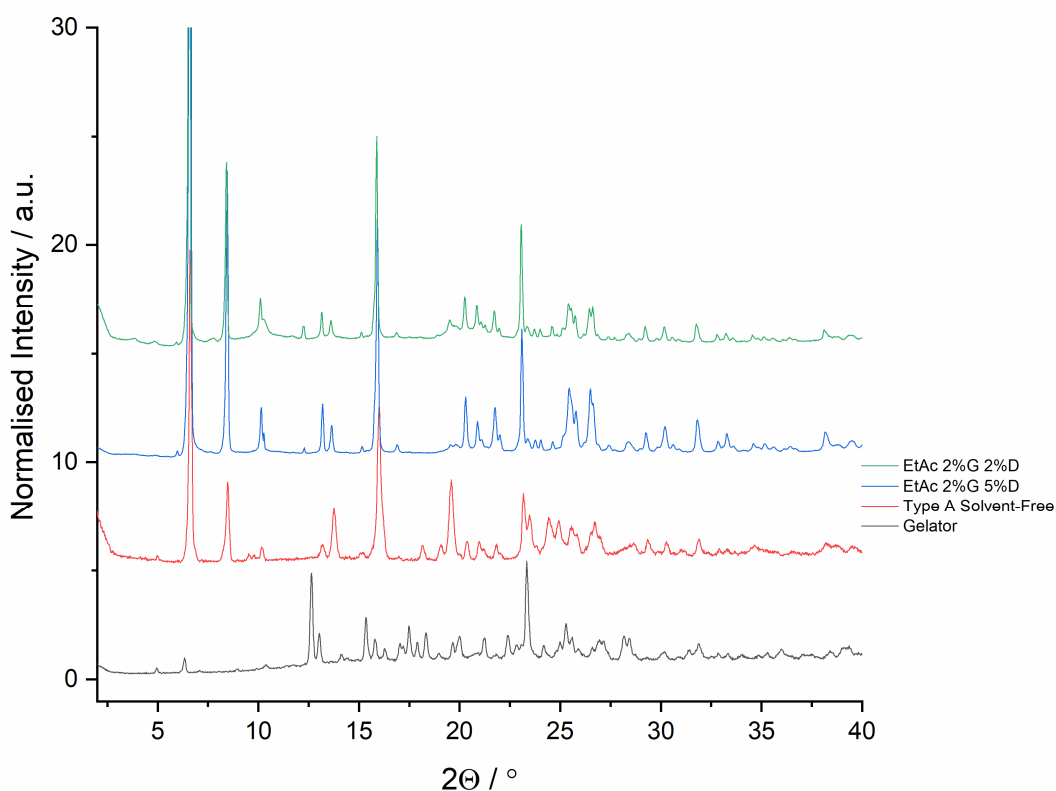
Figure 3.21: PXRD patterns of mexiletine crystallised from solutions in ethyl acetate, at concentrations of 2 % w/v gelator and 2 or 5 % w/v drug, compared to the Type A solvent-free form, and the gelator.

Finally, Form 2 crystallised from a gel of compound **2** in 1,2-dibromoethane (Figure 3.22). Form 2 is extremely high in energy and previously, has only been crystallised by sublimation or by heating another form above its transition temperature. Crystallisation within this gel is therefore the only known method to access Form 2 at room temperature. The sample did gel in this experiment, which suggests that the nucleation processes of the drug and gelator occurred on different timescales, likely driven by the high solubility of mexiletine in 1,2-dibromoethane. As a result, the gel network formed before the crystals began to grow, facilitating epitaxial overgrowth of crystals upon the gel fibres, and stabilising this extremely high energy solid form.
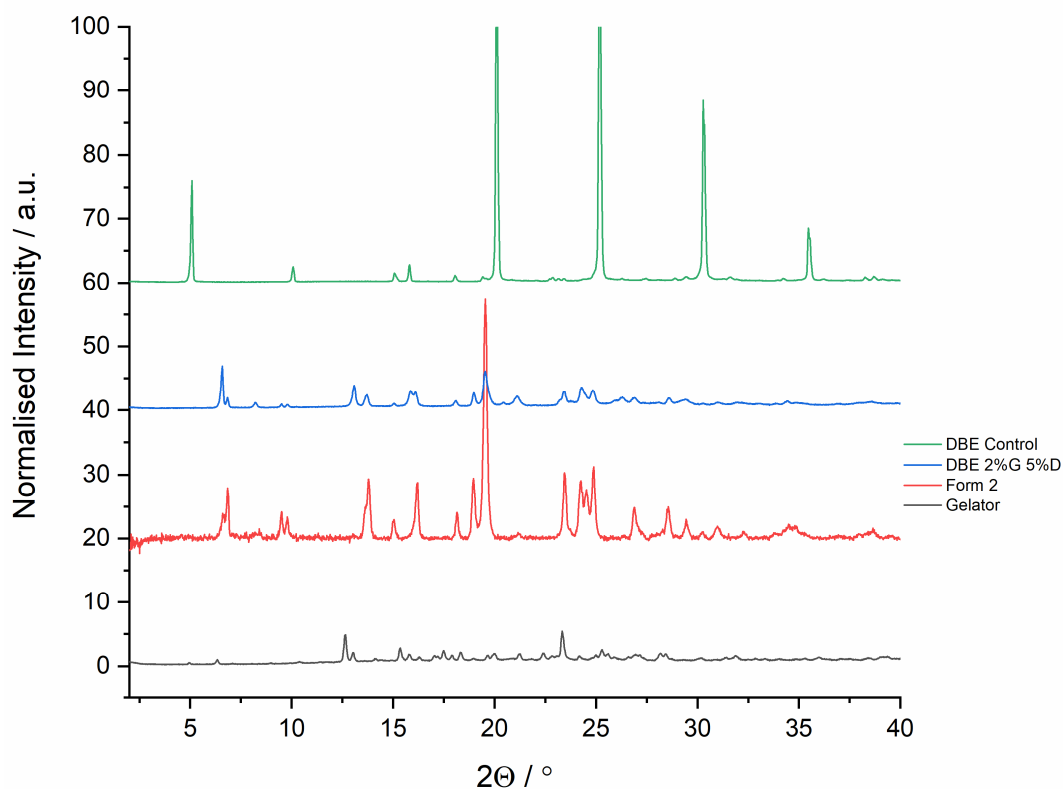
Figure 3.22: PXRD pattern of the mexiletine solid form crystallised from a gel of compound **2** in 1,2-dibromoethane, compared to Form 2, the Type B form crystallised from 1,2-dibromoethane solution, and the gelator.

3.6   Conclusions

In conclusion, this work demonstrates the versatile gelation behaviour of three mexiletine-mimetic supramolecular gelators. Significant changes in polymorphism were observed when the API mexiletine HCl was crystallised within the two bis-urea gels. Gels of compound **1** in DMF and DMSO facilitated the crystallisation of a Type A solvate, in solvents from which mexiletine does not crystallise in solution. Similarly, in an EMK gel of compound **1**, mexiletine crystallised as Form 3, which is metastable and often crystallises concomitantly with Form 1. This gel is only the second known route to access a pure sample of Form 3, which shows that the gel network can selectively nucleate a metastable solid form. Similarly, Form 2 was crystallised from a 1,2-dibromoethane gel of compound **2**. Form 2 is the high temperature stable polymorph of mexiletine and is significantly higher in energy than all the other forms. Crystallisation within this gel is the only known route to access this form at room temperature, which demonstrates the powerful stabilising effect of this gel network. Compound **2** also enabled the crystallisation of unusual Type A solvates. Crystallisation from ethyl acetate solutions of compound **2** at drug concentrations of 2 and 5 % w/v presented new route to a known Type A structure. Whereas, a new Type A solvate was crystallised from the same mixture, at a lower drug concentration of 1 % w/v. This novel Type A solvate can also be accessed from solutions of compound **2** in toluene, at a 1 % w/v concentration of mexiletine. In these experiments, the mixture did not form a gel, which suggests that interactions between the drug and gelator inhibited the self-assembly of gel fibres. It is likely that these interactions are responsible for the changes in polymorphism observed in these experiments. These results demonstrate the versatile ability of drug-mimetic supramolecular gels to achieve solid-from modification of an API. Finally, two additional solvated

polymorphs of mexiletine were crystallised from solutions in 1,2,4-trichlorobenzene and nitrobenzene, which further highlights the prolific solvate-forming behaviour of this compound. A crystal structure of the Type C trichlorobenzene solvate showed that it is another channel solvate, which suggests that there may be more modifications of this polymorph to be found.

3.7   References

1.   H. G. Brittain, *Polymorphism in pharmaceutical solids*, CRC Press, 2016.

2.   A. Y. Lee, D. Erdemir and A. S. Myerson, *Annu. Rev. Chem. Biomol. Eng.*, 2011, **2**, 259-280.

3.   E. Hadjittofis, M. A. Isbell, V. Karde, S. Varghese, C. Ghoroi and J. Y. Y. Heng, *Pharm. Res.*, 2018, **35**, 100.

4.   S. R. Chemburkar, J. Bauer, K. Deming, H. Spiwek, K. Patel, J. Morris, R. Henry, S. Spanton, W. Dziki, W. Porter, J. Quick, P. Bauer, J. Donaubauer, B. A. Narayanan, M. Soldani, D. Riley and K. McFarland, *Org. Process Res. Dev.*, 2000, **4**, 413-417.

5.   J. Bauer, S. Spanton, R. Henry, J. Quick, W. Dziki, W. Porter and J. Morris, *Pharm. Res.*, 2001, **18**, 859-866.

6.   J. Bernstein, in *Polymorphism in Molecular Crystals*, Oxford University Press, 2002, vol. 14, ch. 10, pp. 297-307.

7.   G. Saurabh and C. Kaushal, *J. Chem. Pharm. Res*, 2011, **3**, 6-17.

8.   R.-Q. Song and H. Cölfen, *CrystEngComm*, 2011, **13**, 1249-1276.

9.   J. W. Steed, *Chem. Commun.*, 2018, **54**, 13175-13182.

10.   D. K. Kumar and J. W. Steed, *Chem. Soc. Rev.*, 2014, **43**, 2080-2088.

11.   R. Cudney, S. Patel and A. McPherson, *Acta Crystallogr., Sect. D: Biol. Crystallogr.*, 1994, **50**, 479-483.

12.   C. Biertumpfel, J. Basquin, D. Suck and C. Sauter, *Acta Crystallogr., Sect. D: Biol. Crystallogr.*, 2002, **58**, 1657-1659.

13.   B. Lorber, C. Sauter, A. Théobald-Dietrich, A. Moreno, P. Schellenberger, M.-C. Robert, B. Capelle, S. Sanglier, N. Potier and R. Giegé, *Prog. Biophys. Mol. Biol.*, 2009, **101**, 13-25.

14. J. W. Steed, *Chem. Commun.*, 2011, **47**, 1379-1383.

15. P. Terech and R. G. Weiss, *Chem Rev*, 1997, **97**, 3133-3159.

16. D. J. Abdallah and R. G. Weiss, *Adv. Mater.*, 2000, **12**, 1237-1247.

17. E. R. Draper and D. J. Adams, *Chem*, 2017, **3**, 390-410.

18. F. Aparicio, E. Matesanz and L. Sanchez, *Chem. Commun.*, 2012, **48**, 5757-5759.

19. I. Torres-Moya, B. Saikia, P. Prieto, J. R. Carrillo and J. W. Steed, *CrystEngComm*, 2019, **21**, 2135-2143.

20. J. A. Foster, K. K. Damodaran, A. Maurin, G. M. Day, H. P. G. Thompson, G. J. Cameron, J. C. Bernal and J. W. Steed, *Chem. Sci.*, 2017, **8**, 78-84.

21. L. A. Estroff, L. Addadi, S. Weiner and A. D. Hamilton, *Org. Biomol. Chem.*, 2004, **2**, 137-141.

22. J. Buendia, E. Matesanz, D. K. Smith and L. Sanchez, *CrystEngComm*, 2015, **17**, 8146-8152.

23. L. Kaufmann, S. R. Kennedy, C. D. Jones and J. W. Steed, *Chem. Commun.*, 2016, **52**, 10113-10116.

24. A. Dawn, K. S. Andrew, D. S. Yufit, Y. Hong, J. P. Reddy, C. D. Jones, J. A. Aguilar and J. W. Steed, *Cryst. Growth Des.*, 2015, **15**, 4591-4599.

25. C. Ruiz-Palomero, S. R. Kennedy, M. L. Soriano, C. D. Jones, M. Valcarcel and J. W. Steed, *Chem. Commun.*, 2016, **52**, 7782-7785.

26. J. A. Foster, M.-O. M. Piepenbrock, G. O. Lloyd, N. Clarke, J. A. K. Howard and J. W. Steed, *Nat. Chem.*, 2010, **2**, 1037-1043.

27. A. Dawn, M. Mirzamani, C. D. Jones, D. S. Yufit, S. Qian, J. W. Steed and H. Kumari, *Soft Matter*, 2018, **14**, 9489-9497.

28. J. Sivy, V. Kettmann and E. Fresova, *Acta Crystallogr., Sect. C: Cryst. Struct. Commun.*, 1991, **47**, 2695-2696.

29. A. M. Namespetra, D. A. Hirsh, M. P. Hildebrand, A. R. Sandre, H. Hamaed, J. M. Rawson and R. W. Schurko, *CrystEngComm*, 2016, **18**, 6213-6232.

30. A. Cayuela, M. L. Soriano, S. R. Kennedy, J. W. Steed and M. Valcárcel, *Talanta*, 2016, **151**, 100-105.

31. S. R. Kennedy, C. D. Jones, D. S. Yufit, C. E. Nicholson, S. J. Cooper and J. W. Steed, *CrystEngComm*, 2018, **20**, 1390-1398.

32. C. D. Jones, S. R. Kennedy, M. Walker, D. S. Yufit and J. W. Steed, *Chem.*, 2017, **3**, 603-628.

33. K. Liu and J. W. Steed, *Soft Matter*, 2013, **9**, 11699-11705.

34. L. Meazza, J. A. Foster, K. Fucke, P. Metrangolo, G. Resnati and J. W. Steed, *Nat. Chem.*, 2013, **5**, 42-47.

35. M.-O. M. Piepenbrock, N. Clarke, J. A. Foster and J. W. Steed, *Chem. Commun.*, 2011, **47**, 2095-2097.

36. P. Byrne, G. O. Lloyd, L. Applegarth, K. M. Anderson, N. Clarke and J. W. Steed, *New J. Chem.*, 2010, **34**, 2261-2274.

37. M.-O. M. Piepenbrock, N. Clarke and J. W. Steed, *Langmuir*, 2009, **25**, 8451-8456.

38. D. Ghosh, K. Ferfolja, Z. Drabavicius, J. W. Steed and K. K. Damodaran, *New J. Chem.*, 2018, **42**, 19963-19970.

39. L. Applegarth, N. Clark, A. C. Richardson, A. D. M. Parker, I. Radosavljevic-Evans, A. E. Goeta, J. A. K. Howard and J. W. Steed, *Chem. Commun.*, 2005, **43**, 5423-5425.

40. R. C. Howe, A. P. Smalley, A. P. Guttenplan, M. W. Doggett, M. D. Eddleston, J. C. Tan and G. O. Lloyd, *Chem. Commun.*, 2013, **49**, 4268-4270.

41. N. Shi, G. Yin, M. Han and Z. Xu, *Colloids Surf., B*, 2008, **66**, 84-89.

42. N. E. Shi, H. Dong, G. Yin, Z. Xu and S. H. Li, *Adv. Funct. Mater.*, 2007, **17**, 1837-1843.

43. C. M. A. Leenders, T. Mes, M. B. Baker, M. M. E. Koenigs, P. Besenius, A. R. A. Palmans and E. W. Meijer, *Mater. Horiz.*, 2014, **1**, 116-120.

44. J. J. van Gorp, J. A. J. M. Vekemans and E. W. Meijer, *J. Am. Chem. Soc.*, 2002, **124**, 14759-14769.

45. Y. Yasuda, E. Iishi, H. Inada and Y. Shirota, *Chem. Lett.*, 1996, **25**, 575-576.

46. V. Nagarajan and V. R. Pedireddi, *Cryst. Growth Des.*, 2014, **14**, 1895-1901.

47. N. Malviya, M. Das, P. Mandal and S. Mukhopadhyay, *Soft Matter*, 2017, **13**, 6243-6249.

48. N. Malviya, C. Sonkar, B. K. Kundu and S. Mukhopadhyay, *Langmuir*, 2018, **34**, 11575-11585.

49. H. J. Knolker, T. Braxmeier and G. Schlechtingen, *Angew. Chem., Int. Ed.*, 1995, **34**, 2497-2500.

50. G. Yu, X. Yan, C. Han and F. Huang, *Chem. Soc. Rev.*, 2013, **42**, 6697-6722.

51. K. Almdal, J. Dyre, S. Hvidt and O. Kramer, *Polym. Gels Networks*, 1993, **1**, 5-17.

52.   K. Hyun, S. H. Kim, K. H. Ahn and S. J. Lee, *J. Non-Newtonian Fluid Mech.*, 2002, **107**, 51-65.

53.   T. Domenech and S. S. Velankar, *Soft Matter*, 2015, **11**, 1500-1516.

54.   T. Domenech and S. S. Velankar, *J. Rheol.*, 2017, **61**, 363-377.

4. Supramolecular Gelation as the First Stage in Ostwald's Rule

4.1 Introduction

Throughout many decades of research into the mechanism and applications of crystallisation, a range of empirical rules have emerged, acting as general guidelines to predict and characterise the result of a crystallisation process.[1] A notable example is Ostwald's rule of stages, which refers to the observation that a kinetically favoured, metastable polymorph will often crystallise from solution before the form that is most thermodynamically stable under the same conditions.[2] The classic example is benzamide, in which the least stable form, orthorhombic Form II, is initially produced by crash cooling, followed by the monoclinic Form III, and finally, the most stable form, monoclinic Form I.[3] Because nucleation is the critical step in a crystallisation process, and is kinetically controlled, the crystallisation progresses towards equilibrium *via* a series of kinetically favoured, metastable polymorphs. Traditionally, this rule has been applied to purely crystalline systems, but recent work suggests that the formation of supramolecular materials can also follow Ostwald's rule.[4] It is therefore plausible that the rule holds true for the breakdown of other supramolecular systems, such as low molecular weight gels.

Formation of a small-molecule supramolecular gel requires the organisation of molecules into a low-dimensional aggregate, such as a fibril[5] or scrolled sheet.[6] This behaviour is most commonly displayed by molecules whose non-covalent interactions are strongest in one direction,[5] such as ureas or amides, which provide strong directional NH···O=C hydrogen bonds.[7, 8] It is well known that gelation and

crystallisation are two closely related self-assembly processes.[9] Although this relationship is not sufficiently well understood to allow the rational design of a molecule that will preferentially gel or crystallise, work is underway in this area. Theoretical and computational studies have probed the stability relationships between gels and crystals,[10, 11] and empirical studies on gels that gradually form microcrystals have probed systems sitting right on the boundary between gelation and crystallisation.[12-14] In some cases, crystals have been observed to grow directly from the gel. Despite originally being thought of as extremely rare, this phenomenon has recently been observed with increasing frequency, and within a chemically diverse range of both hydro- and organogels.[15-22] Understanding this phenomenon, and the balance between gelation and crystallisation in general, is important because the ability to precisely control both of these processes would be extremely useful in chemical industry. For example, the antibiotic drug cefpiramide has been observed to form an organogel that is stable for several days before it breaks down and crystallises.[23] This behaviour is by no means unique to this drug,[24] and is highly undesirable for large-scale manufacturing because it reduces the time and cost efficiency of the process.

Sterically hindered 2,4,5-triphenylimidazole (TPI) or, lophine, derivatives have classically been exploited for their luminescence properties, allowing them to be used as versatile analytical probes.[25, 26] Similarly, lophine radicals have been shown to exhibit photo-, thermo-, and piezo-chromism through the formation of reversible dimers.[27] These materials therefore lend themselves to application in display technologies and chemical or molecular switches.[28-30] A previous study of a series of mono-halogenated 2,4,5-triphenylimidazole derivatives (Figure 4.1) showed that changing the halogen substituent in a single position has a significant effect on the

solid-state structure and properties of these materials.[31] A key finding was the much more significant change in properties between the chloro- and bromo- derivatives, than between any other adjacent pair in the series.
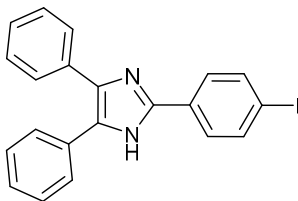
Figure 4.1: Structure of the mono-iodinated 2,4,5-triphenyl imidazole derivative (I-TPI).

The crystal structures of all halogenated TPIs were based on hydrogen-bonded imidazole chains, which is the dominant motif observed in other imidazole derivatives.[31-34] All TPIs formed methanol solvates, in which the solvent intercalates into the imidazole chains.[31] Previous work characterised the methanol solvates of all halogenated TPI derivatives by powder X-ray diffraction (PXRD), and reported single-crystal structures for the fluoro- and bromo-TPI solvates. The layered structures of the two solvates were closely related, but there was a shift in the layers with the larger bromine substituent. Two anhydrous polymorphs of each TPI derivative were also characterised by PXRD, and for the methanol solvates, the desolvated form showed no structural similarity to the solvate.

This work reports the supramolecular gelation behaviour of the I-TPI analogue in methanol. Whilst imidazole functionalities have been incorporated into gelators before,[35-38] they are rarely the functional group solely responsible for gelation. Imidazole derivatives typically prefer to crystallise, often forming NH···N hydrogen bonds between molecules.[34] In the case of I-TPI, gelation is most likely driven by the unidirectional hydrogen bonds between imidazole groups, coupled with weaker interactions perpendicular to the hydrogen-bonded chains, caused by the peripheral

aromatic rings and the large size of the halogen substituent. The I-TPI gel spontaneously crystallised, forming a series of distinct polymorphs, one after the other. This study presents a detailed investigation of the solid-form landscape of I-TPI, probing the delicate balance between gelation and crystallisation. It appears that this system behaves as an unusual example of Ostwald's rule of stages.

4.2   Characteristics of the I-TPI Gel

The gelation behaviour of I-TPI was first noted in methanol, in which a stable and optically transparent gel is formed from a supersaturated solution, when heated to 65 °C and left cool under ambient conditions for ten minutes (Figure 4.2a). The gel is thermoreversible, meaning it will dissolve when heated and reform when cooled a second time. However, it is not thixotropic and will not reform after being broken down by mechanical stress. SEM images of the dried xerogel demonstrate an unusual morphology, composed of short aggregates with dimensions *ca*. 0.5 x 0.05 μm, which explains why the gel is transparent in visible light (Figure 4.2b).
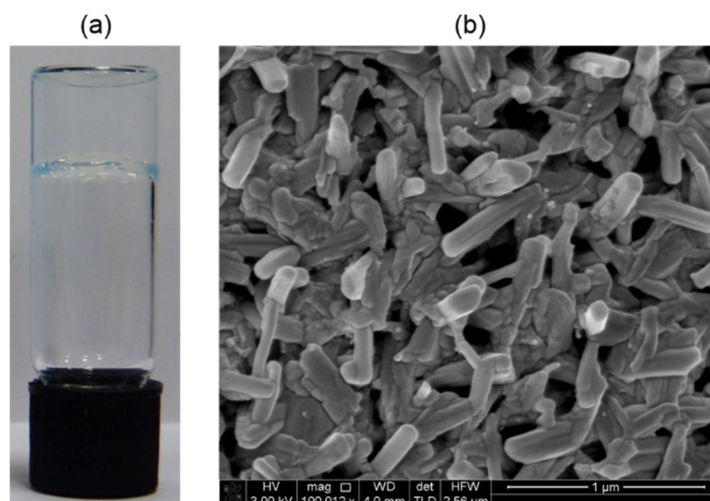
Figure 4.2: (a) Photograph of a 2% w/v I-TPI gel, showing its optical transparency. (b) SEM micrograph of a xerogel prepared from a 2% w/v gel of I-TPI in methanol. Sample was coated in 2 nm platinum.

The blocky morphology in the I-TPI gel differs considerably from the long intertwined fibres typical of a supramolecular gel,[39, 40] but it is possible this may be artefact from drying the native gel.[41, 42] Because this gel was known to crystallise, a series of SEM images were recorded at different magnifications to confirm that the gel morphology was consistent throughout the sample (Figure 4.3a,b,c), and that it differed from that of a crystal (Figure 4.3d,e). Whilst the gel morphology does differ significantly from that of a macroscopic crystal, its blocky appearance suggests some degree of crystallinity. It is possible that the very early stages of the gel to crystal transition occurred during the drying process, leading to this unusual morphology.
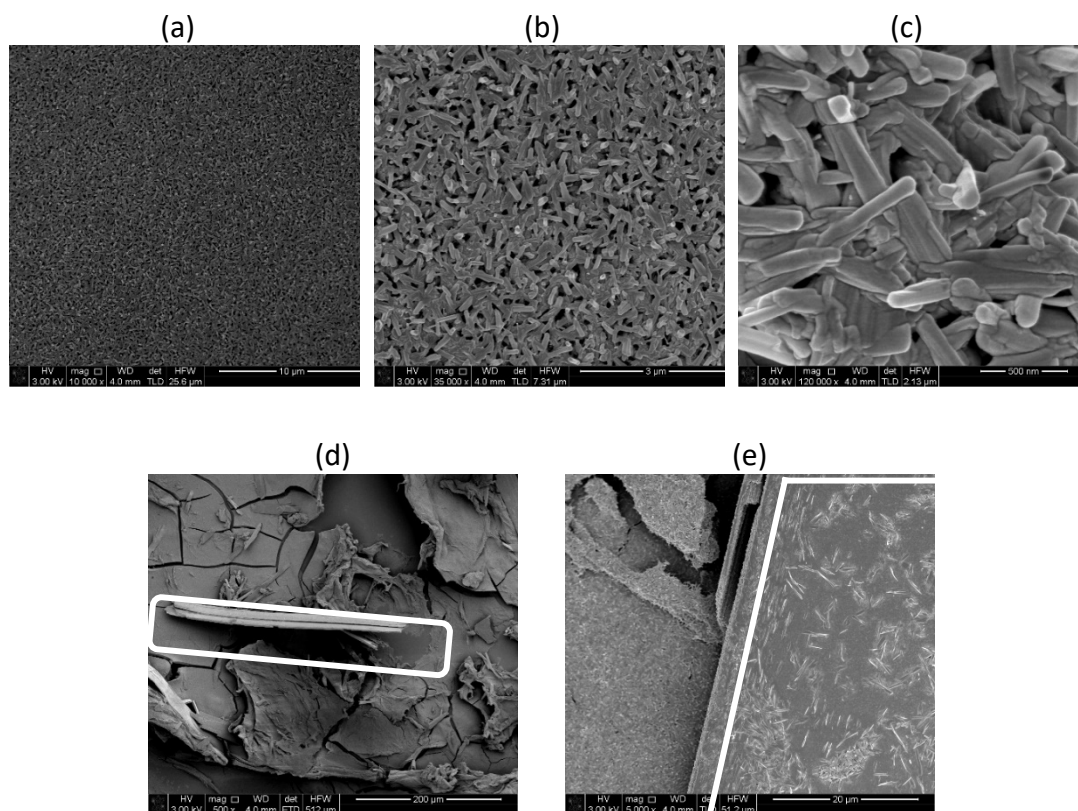
Figure 4.3: SEM images of a xerogel prepared from a 2% w/v gel of I-TPI in methanol. Images a-c show the sample at different magnifications, to confirm that the morphology was consistent. Images d and e compare the morphologies of a gel and a crystal, to confirm they are noticeably different (crystals are highlighted in white). Samples were coated in 2nm platinum.

The gelation behaviour of I-TPI was tested in a wide range of solvents. A 2% w/v solution of I-TPI in the test solvent was heated to the boiling point of the solvent in a sealed glass vial, left to cool to room temperature, and monitored for gelation or crystal growth. Of the 47 solvents tested, gelation was only observed in methanol, over a small range of concentrations. By cooling under ambient conditions, the critical gelling concentration (CGC) in methanol, determined by the inversion test, is 1.9% w/v, but this can be reduced to 1.25% w/v by sonication or crash cooling in ice, in which cases the gel forms in a reduced time of five minutes (Table 4.1). This finding fits well with the hypothesis that the gel is favoured by Ostwald's rule.

Table 4.1: Gel screening results of I-TPI in methanol. G = gel, PG = partial gel (part of the sample has gelled, but part remains in solution), S= solution. Critical gelation concentrations are shaded.

Concentration / mg mL^{-1}	Concentration / mol dm^{-3}	Concentration /% (w/v)	Result from Cooling	Result from Sonication
20	0.047	2	G	G
19	0.045	1.9	G	G
18	0.043	1.8	S	G
17	0.040	1.7	S	G
16	0.038	1.6	S	G
15	0.036	1.5	S	G
12.5	0.030	1.25	S	PG
10	0.024	1	S	S
7.5	0.017	0.75	S	S
5	0.012	0.5	S	S

Oscillatory rheology probes the mechanical properties of the gel. Frequency sweep data from a 2% w/v gel show the storage modulus to be approximately one order of magnitude greater than the loss modulus, demonstrating the elastic behaviour characteristic of a gel (Figure 4.4).[43] The yield stress of the gel, used to quantify its strength, can be estimated from stress sweep rheology as the oscillation stress at which the storage and loss moduli are equal. In the case of a 2% w/v I-TPI gel, a yield stress

of *ca.* 300 Pa proves the material to be quite robust[44] and as expected, the 1.9 % w/v

gel is slightly weaker, with a yield stress of *ca.* 200 Pa (Figure 4.4)
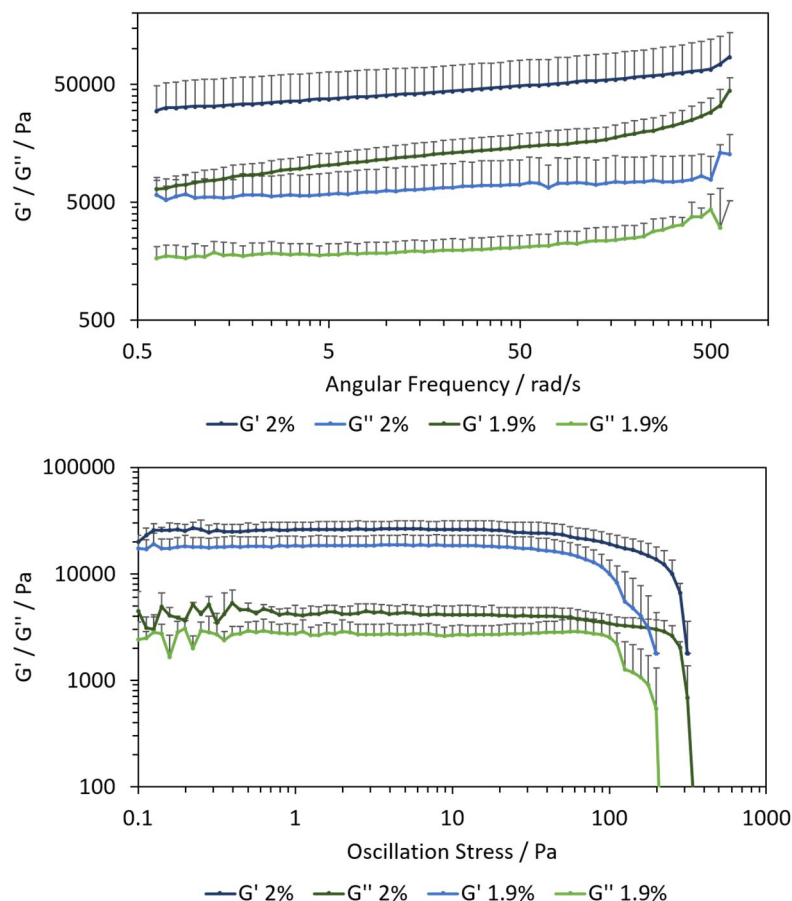
Figure 4.4: Oscillatory frequency (top) and stress (bottom) sweeps for 2 and 1.9 % w/v gels of I-TPI

in methanol. Gels were formed and measurements taken at 10 °C. Error bars indicate the standard

deviation from repeated measurements.

Gelation was observed over a much wider range of concentrations by cooling the

solution to 0 °C, and all of these materials also displayed the elastic behaviour

characteristic of a supramolecular gel (Figure 4.5). Gels formed at 0 °C were stronger

than gels of the same concentration that were formed at 10 °C. The yield stress of a 2

% w/v I-TPI gel increased from *ca.* 300 Pa when formed at 10 °C to *ca.* 1000 Pa when

formed at 0 °C, most likely caused by the precipitation of more gel fibres due to the

increased supersaturation at a lower temperature.
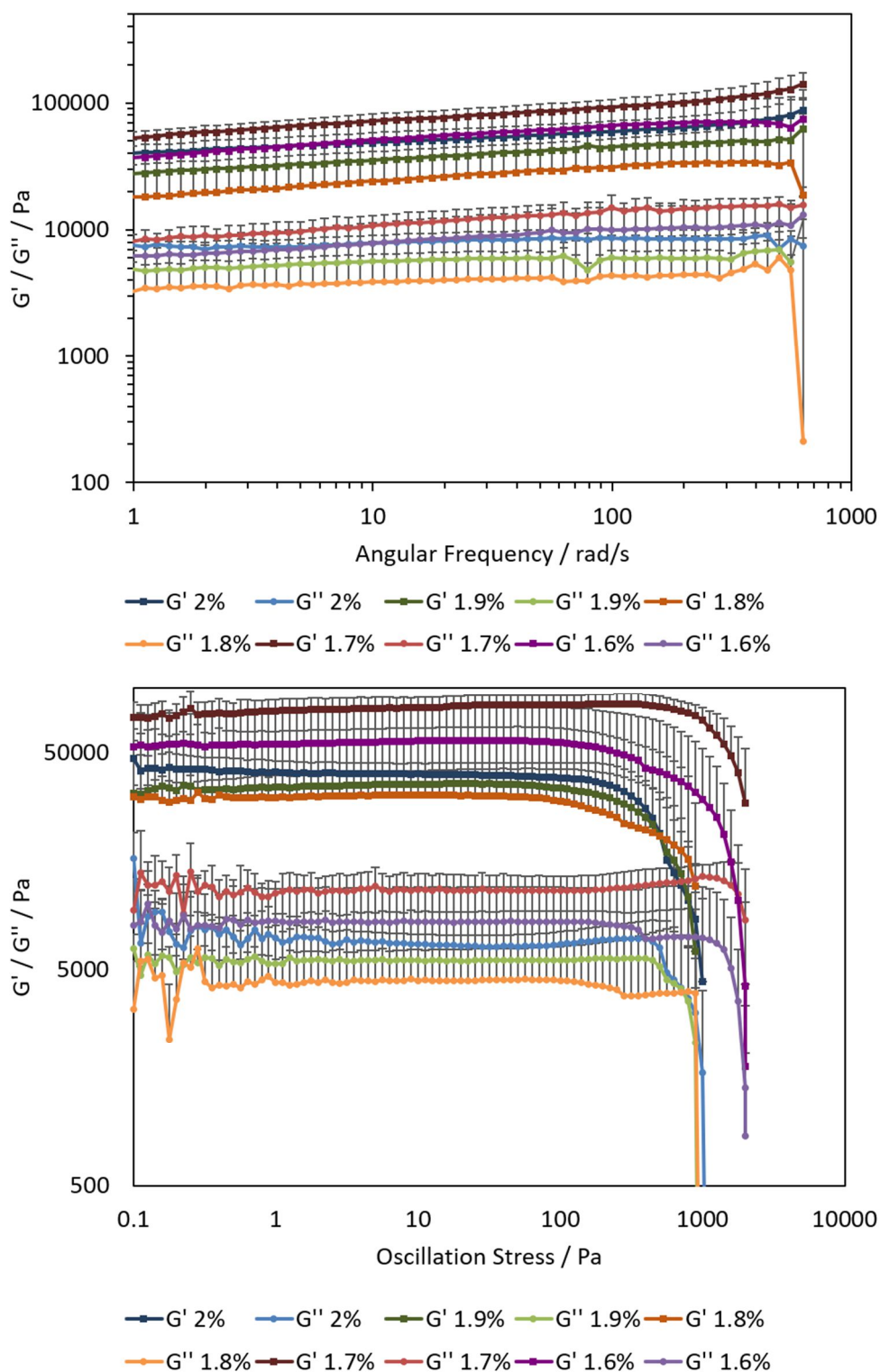
Figure 4.5: Oscillatory frequency (top) and stress (bottom) sweep data for gels of 2-1.6% w/v I-TPI in methanol. Gels were formed and measurements taken at 0°C. Error bars indicate the standard deviation from repeated measurements.

If stored, the I-TPI gel breaks down yielding large, block-shaped single crystals (Figure 4.6). The length of time taken for this crystallisation to occur varies due to the inconsistent nature of the nucleation process, however general trends can be established depending on the storage conditions of the gel. If left undisturbed and at a constant temperature, some gels were stable for several months, whilst crystallisation occurred more commonly between one day and two weeks. The effect could be accelerated to occur between five minutes and three hours through any kind of mechanical agitation of the gel, including shaking, cutting, stirring or an oscillatory rheology experiment. The more the gel was disrupted, the more quickly it crystallised. The crystals forming reproducibly were identified by single-crystal X-ray diffraction as a 1:1 methanol solvate termed Form SI, in which the "S" denotes that the structure is a solvate.
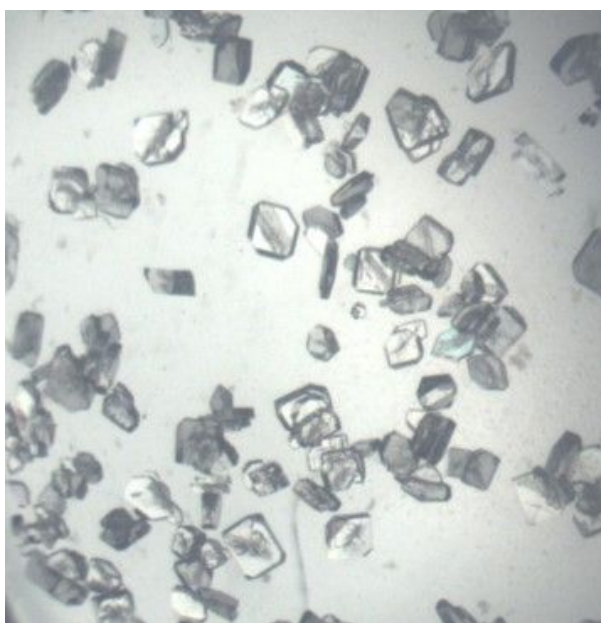
Figure 4.6: Crystals of Form SI of I-TPI.

4.3   Incorporating Crystallisation Additives

Based on a large body of previous work into additive-mediated crystallisation,[45-47] the crystallisation behaviour of the I-TPI gel was investigated further, by incorporating a chemically diverse range of additives. Previous studies have shown that crystallisation additives can have a variety of different effects, notably including suppression of the kinetically stable forms favoured by Ostwald's rule, to promote the production of a desired thermodynamic polymorph.[48-51] The additives used in this study were 1,4-diiodobenzene, pyrene, 1-aminopyrene and tetrabutylammonium (TBA) chloride (Table 4.2), as they have a variety of potential modes of interaction with the gelator, that could lead to the suppression of the kinetically favoured gel phase.[52] For solid additives, gels were prepared by dissolving the required additive at concentrations ranging from 0.4–8 % w/v in a 2 % w/v solution of I-TPI in methanol, before cooling to room temperature. Gelation of solvent mixtures was also investigated, with methanol mixtures containing between 1-14 % v/v of hexane, water or DMSO (Table 4.3).

Table 4.2: Results of gel testing incorporating solid additives. G = gel, PG = partial gel, S = solution, I = insoluble, C = crystals, - = experiment not performed

Additive	1,4-diiodobenzene		Pyrene		1-aminopyrene		TBA Chloride	
Mass / mg	mmol	Result	mmol	Result	mmol	Result	mmol	Result
2	0.006	G	0.010	G	0.009	G	-	-
5	0.015	G	0.025	G	0.023	G	-	-
10	0.030	PG	0.049	C then G	0.046	G	0.007	G
15	0.061	I	-	-	-	-	-	-
20	0.006	G	0.099	C then G	0.092	G	0.018	G
25	-	-	0.124	-	0.115	G	0.036	G
30	-	-	0.148	-	0.138	PG	0.072	G
40	-	-	0.198	-	0.184	S	0.090	G

Table 4.3: Results of gel testing using solvent mixtures. G = gel, PG = partial gel, S = solution, I = insoluble, C = crystals, - = experiment not performed

Additive	Hexane		Water		DMSO	
Volume / µL	mmol	Result	mmol	Result	mmol	Result
5	0.038	G	0.277	G	0.070	G
10	0.076	G	0.555	G	0.141	G
20	0.153	G	1.110	G	0.282	G
30	0.229	-	1.665	G	0.422	-
40	0.306	-	2.220	G	0.563	-
50	0.382	G	2.775	I	0.704	G
60	0.459	I	3.330	-	0.845	PG
70	0.535	I	3.885	-	0.986	S

In all additive-containing gels, except those including TBA chloride, crystallisation was observed within the intact gel over the course of one hour to one week, depending on the nature of the additive. These crystals were large plates; a noticeably different morphology to the block-shaped crystals of Form SI (Figure 4.7a).
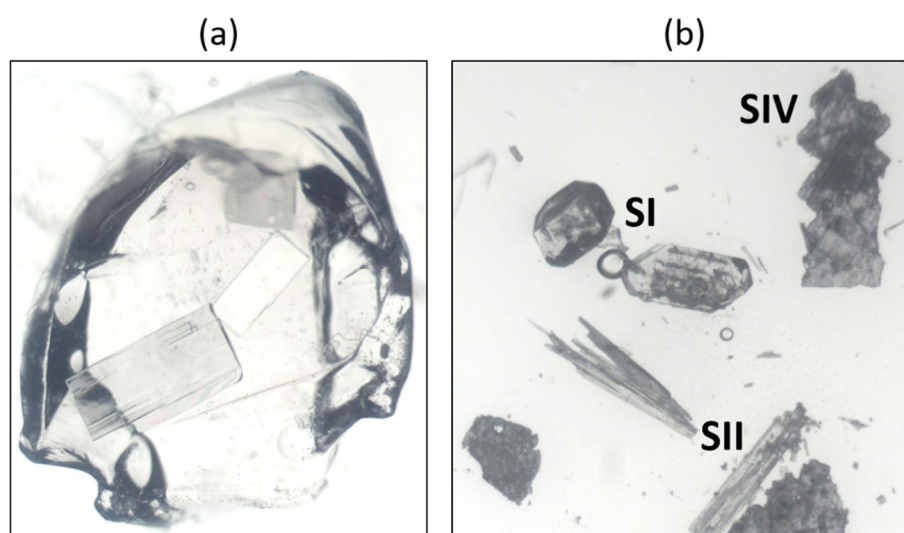
Figure 4.7: (a) crystals of Form SII grown within a gel containing 5 µL of DMSO, (b) the concomitant crystallisation of Forms SI, SII and SIV from a gel containing 10 mg of 1,4-diiodobenzene.

Single-crystal X-ray diffraction was used to characterise a crystal from eighteen different gels and in every case except one, the crystals were identified as a second 1:1 methanol solvate, Form SII. The exceptional case occurred when 1,4-diiodobenzene was incorporated into the gel, which caused concomitant crystallisation of Forms SI, SII and a further unidentified form termed Form SIV (Figure 4.7b). In addition to the incorporation of additives, the growth of Form SII crystals within the gel could be also triggered by forming the gel very quickly in ice, which increases the supersaturation of the solution. Or, by repeatedly heating and reforming the material, which ensures all seeds and nucleation sites for Form SI are removed and allows Form SII to grow. This behaviour points towards the metastable character of Form SII, as per Ostwald's rule.

All gels in which Form SII crystallised broke down over a time period ranging from one hour to three days after crystal formation, which was much quicker than the pure 2% w/v material. The dissolution of these gels was likely caused by the incorporation of gelator molecules into the crystals, causing the solution concentration to drop below the critical point required for gelation. Following the breakdown of the gel, crystals of Form SII consistently transformed into Form SI, either within the mother liquor or when removed and stored under ambient conditions. These observations imply that Form SI is more stable than Form SII.

Rheological characterisation of gels containing DMSO, hexane and TBA chloride allowed the effect of these additives or mixed media to be quantified. DMSO and hexane were selected for more detailed analysis because they have opposite effects on the solubility of the gelator and should therefore represent two extremes of behaviour.[53] Increasing the concentration of DMSO in the solvent mixture from 2 to 6 % v/v caused a decrease in elastic and viscous moduli, G′ and G″ respectively, and a decrease in yield stress (Figure 4.8). This behaviour is consistent with the increasing solubility of the gelator in the DMSO-containing solvent mixture, which inhibits the formation of solid-like gel fibres.
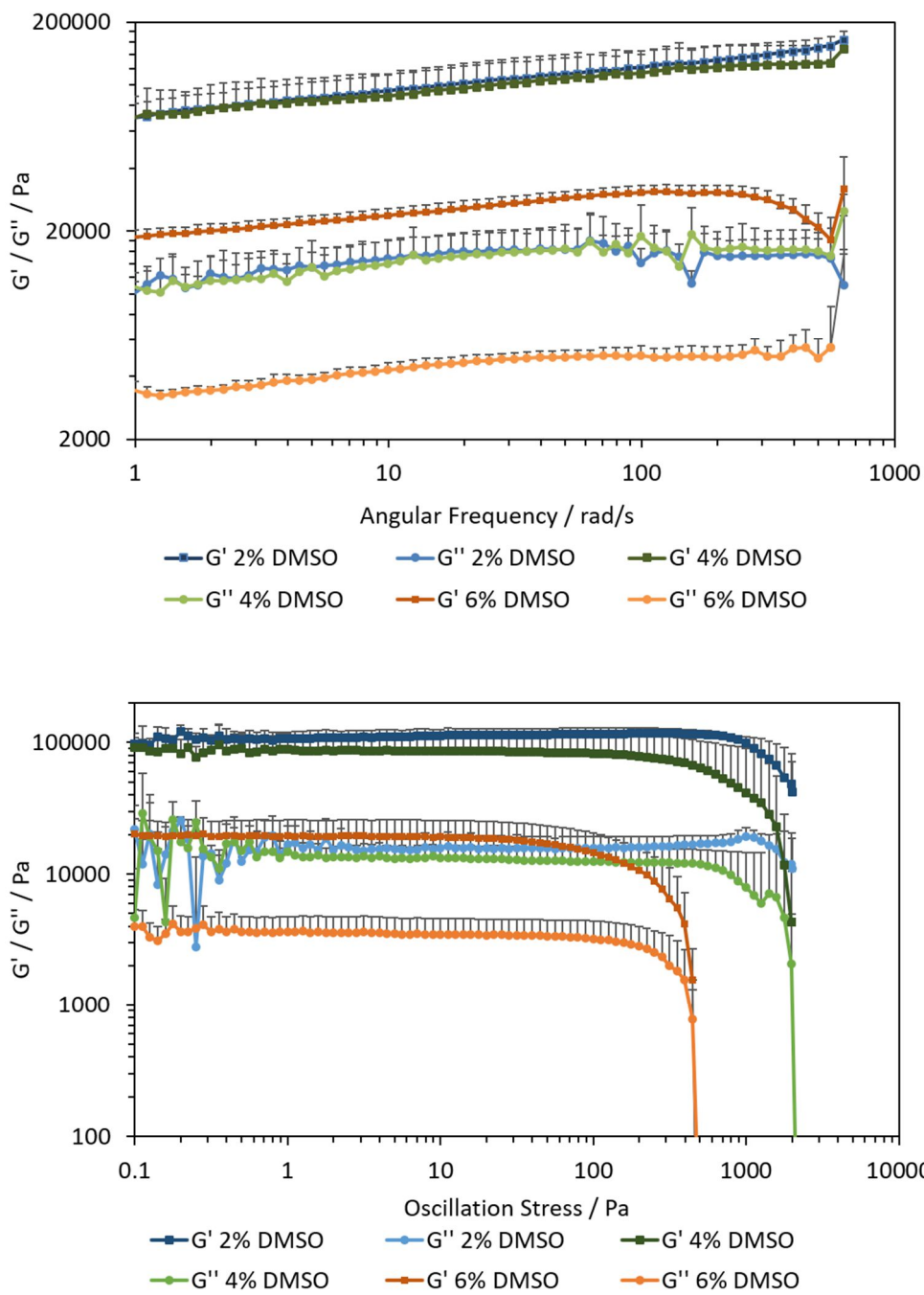
Figure 4.8: Oscillatory frequency (top) and stress (bottom) sweeps for 2% w/v I-TPI gels in methanol containing 2%, 4% and 6% v/v DMSO. Gels were formed and measurements taken at 10 °C. Error bars indicate the standard deviation from repeated measurements.

Increasing the concentration of hexane in the solvent mixture from 2 to 6 % v/v produced little variation in shear moduli, but an increase in yield stress (Figure 4.9). Due to the low solubility of I-TPI in hexane, this gel crystallised on the timescale of a rheology experiment (*ca.* two hours). One possible explanation of this rheological behaviour may be the formation of solid particles within the gel, as small crystallites begin to grow.[54]
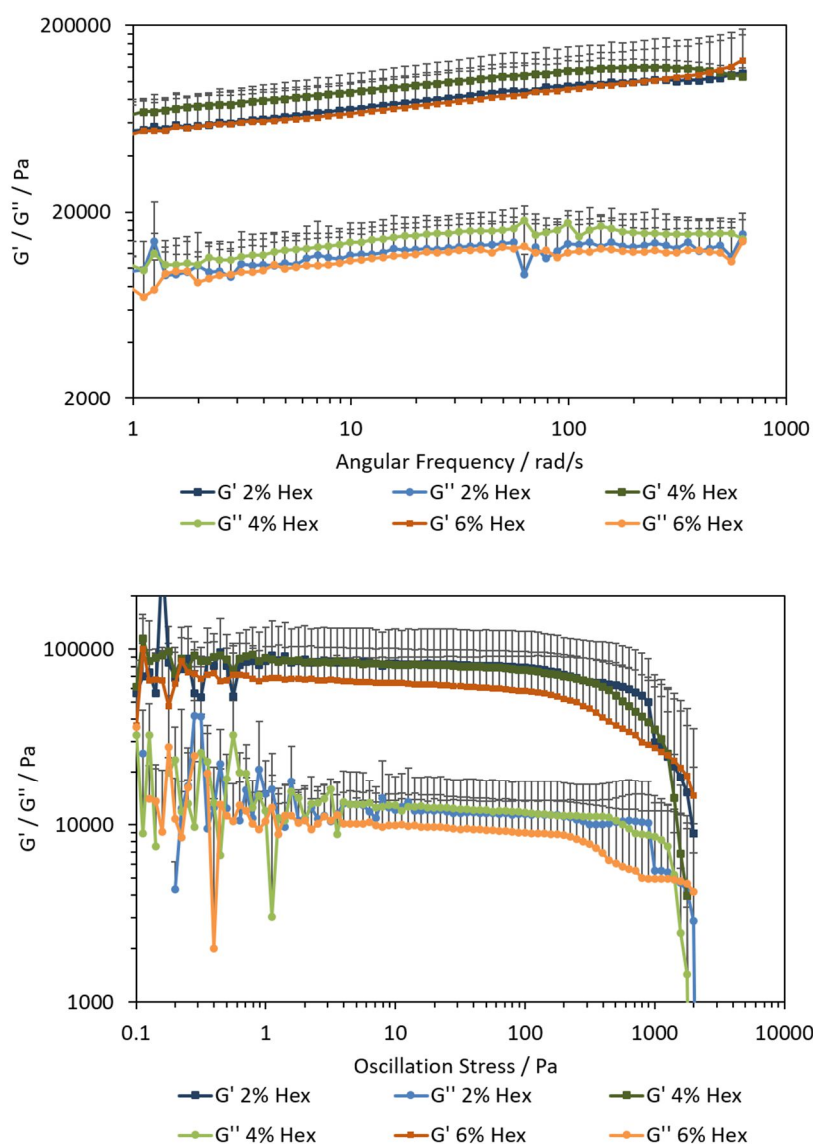
Figure 4.9: Oscillatory frequency (top) and stress (bottom) sweeps for 2% w/v I-TPI gels in methanol containing 2%, 4% and 6% v/v hexane. Gels were formed and measurements taken at 10 °C. Error bars indicate the standard deviation from repeated measurements.

TBA chloride-containing gels were selected for rheological characterisation because the addition of anions has typically been shown to disrupt gelation,[55-58] but the opposite seemed to be true in this case. The chloride-containing I-TPI gels remained stable for much longer than any other gel tested and at sufficient chloride concentration, were not observed to crystallise at all. A decreasing yield stress was observed as the concentration of TBA chloride was increased from 2 to 6 % w/v. This behaviour is consistent with a high concentration of anions disrupting the hydrogen-bonded network as previously reported.[55-58] However, in this case, there was no significant effect on the shear moduli with increasing concentration of chloride (Figure 4.10).

Figure 4.10: Oscillatory frequency (top) and stress (bottom) sweeps for 2% w/v I-TPI gels in methanol containing 2%, 4% and 6% w/v TBA chloride. Gels were formed and measurements taken at 10 °C. Error bars indicate the standard deviation from repeated measurements.

Regardless of the concentration of additive, the inclusion of DMSO, hexane or TBA chloride all produced a small but reproducible trend towards higher shear moduli and yield stress than the pure gelator in methanol. A representative example is shown in

Figure 4.11, comparing the 2% w/v pure I-TPI gel in methanol, to gels containing 2% w/v I-TPI and either 2% w/v TBA chloride or, 2% v/v hexane or DMSO.
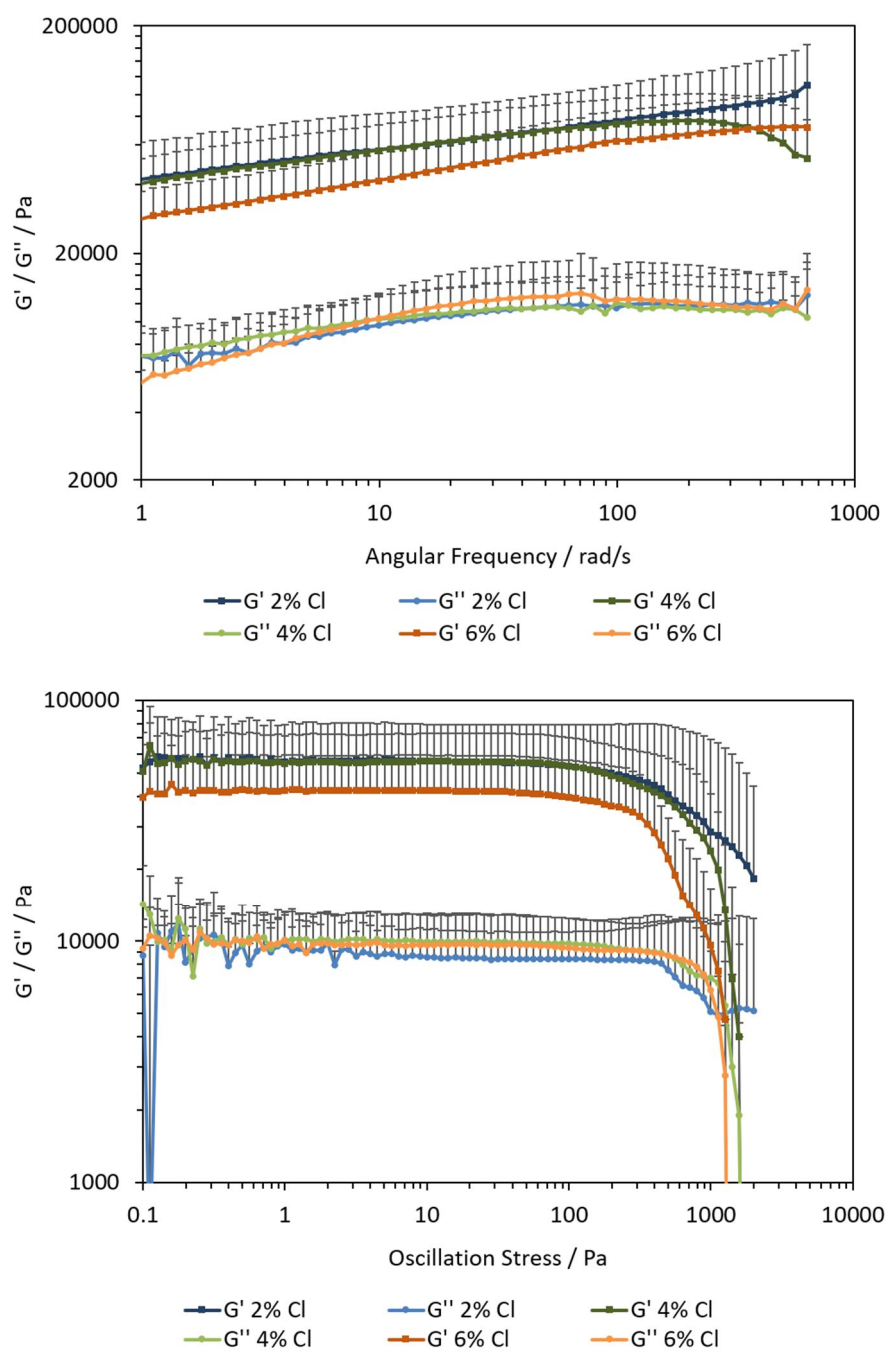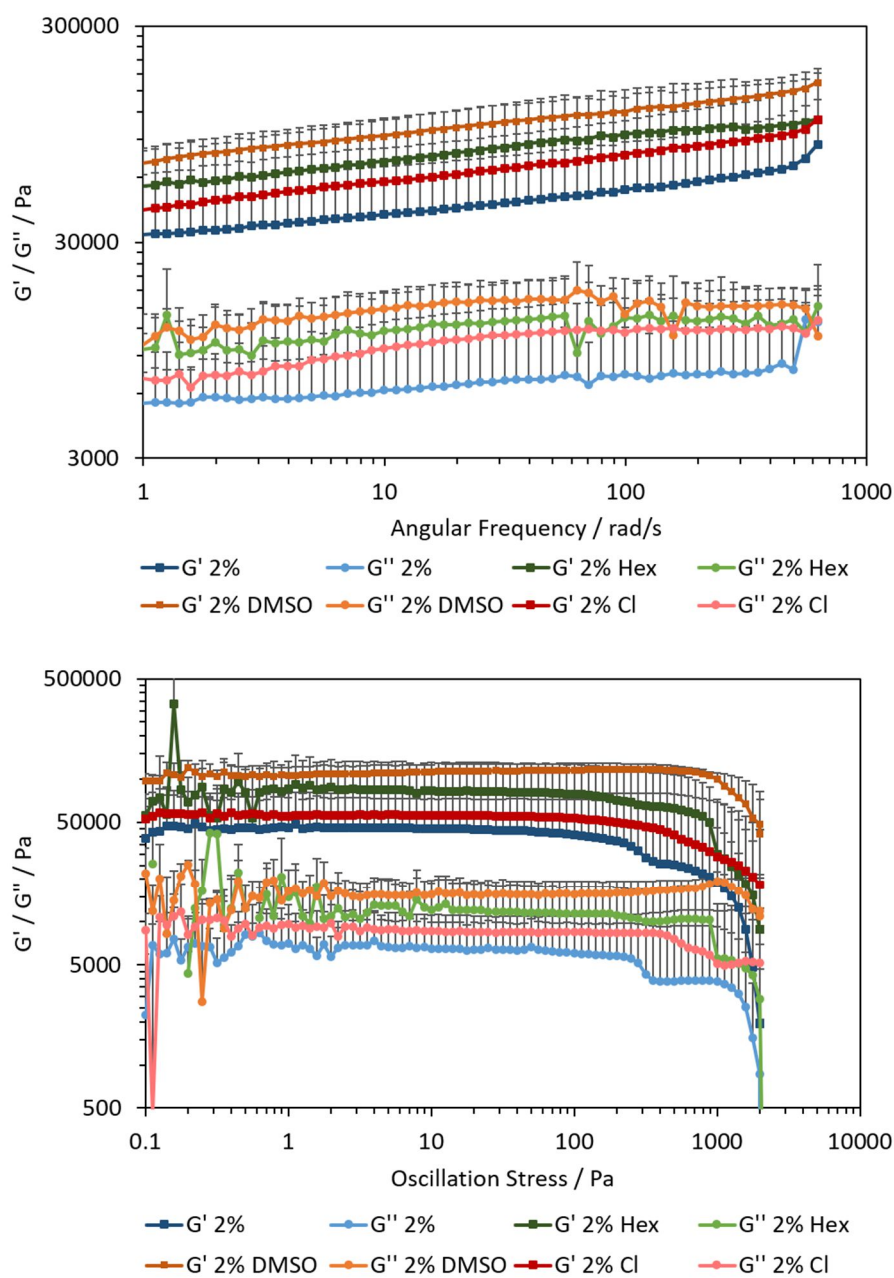

Figure 4.11: Oscillatory frequency (top) and stress (bottom) sweeps for 2% w/v I-TPI gels in methanol containing either 2% w/v TBA chloride or 2% v/v DMSO or hexane, compared to the pure 2% w/v gel in methanol. Gels were formed and measurements taken at 10 °C. Error bars indicate the standard deviation from repeated measurements.

I-TPI is insoluble in hexane, and therefore, the increase in strength of this gel is likely due to the formation of more gel fibres, because the solution is more supersaturated. DMSO can accept multiple hydrogen bonds and may form lateral links between gel fibres, causing greater entanglement of the gel network and increasing its strength relative to the pure material; a phenomenon commonly observed when polymers or surfactants are incorporated into supramolecular gels.[59-62] Finally, the incorporation of anions into supramolecular gels has been reported to have both strengthening[63-65] and weakening effects,[55-58] depending on the gelator in question. This anion-tuning behaviour has commonly been observed in urea-based gelators and has been attributed to the anions either promoting[63, 64] or disrupting[55-58] formation of the urea-tape motif that is responsible for gelation in these materials. One notably different example concerns the anion-triggered gelation of a calix[4]arene derivative, rationalised using the Hofmeister series.[65] In the I-TPI gel, the chloride ions may cause a salting out effect,[66, 67] prompting the formation of more gel fibres and strengthening the gel.

A qualitative assessment, carried out by observing all the additive-containing gels over time, showed that the rate of formation of Form SII crystals within the gels is affected by the chemical nature of the additive. Gels of solvent mixtures containing DMSO crystallised much more slowly, over a minimum of two days, than those containing hexane and water, in which Form SII grew within three hours. This trend is to be expected given the high solubility of I-TPI in polar organic solvents. Hydrogen-bonding additives noticeably slowed the rate of crystallisation, as did the incorporation of TBA chloride. The chloride-containing gels were particularly stable and did not crystallise throughout the entire duration of this work, or about a year.

4.4   Crystal Structures of I-TPI

Further investigation into the crystallisation behaviour of I-TPI led to the discovery of three more solid forms, in addition to the three solvates SI, SII and SIV obtained from the gel phase. Despite several attempts, a full structure of Form SIV could not be obtained due to poor crystal quality. However, the unit cell volume is consistent with a methanol monosolvate,[68] and the cell dimensions also match closely with the other three solvates, which adds weight to this hypothesis. When paper fibres were serendipitously included into a 2% w/v solution of I-TPI in methanol, gelation was inhibited, and large single crystals grew on the fibres. These were identified by single-crystal X-ray diffraction as a third methanol solvate polymorph, Form SIII. Attempts to reproduce this form have been repeatedly unsuccessful, despite the incorporation of a wide range of solid particles to the gel, including paper fibres, microcrystalline cellulose, silica gel, and PVA beads. These difficulties suggest that Form SIII has an extremely high energy barrier to nucleation or is highly metastable, immediately converting to or outgrown by a more stable polymorph.[69]

High-temperature crystallisations aimed to produce the anhydrous forms identified by PXRD in previous work.[31] Two non-solvated forms, Forms V and VI, were successfully identified and fully characterised by single-crystal X-ray diffraction. Form V was crystallised from pure methanol at 50 °C, a condition under which the gel did not form, even at sufficient concentration. Whereas, Form VI was produced by sublimation, a technique that was used to investigate the crystallisation behaviour of I-TPI in the absence of methanol. Selected crystallographic data for the six crystal forms of I-TPI identified in this work are given in Table 4.4 and the full information can be found in Appendix 7.2.

Table 4.4: Selected crystallographic data for the novel polymorphs of I-TPI

Crystal Form	Form SI	Form SII	Form SIII	Form SIV	Form V	Form VI
Space group	P2$_1$/c	P2$_1$/c	P2$_1$	Unit cell only	P2$_1$	P$\bar{1}$
a/Å	12.662(9)	6.086(4)	14.668(12)	6.209(5)	8.922(7)	8.901(8)
b/Å	12.608(11)	11.591(8)	12.091(10)	13.991(8)	32.728(2)	11.904(11)
c/Å	12.750(10)	27.260(16)	17.388(14)	22.072(25)	11.912(9)	33.334(3)
α/°	90	90	90	103.790(3)	90	81.404(3)
β/°	109.050(19)	92.094(19)	110.237(3)	92.300(5)	94.579(3)	82.994(3)
γ/°	90	90	90	91.350(4)	90	85.467(3)
V/Å^3	1923.9(3)	1921.5(2)	2893.5(4)	1910.0(3)	3467.0(5)	3459.5(5)
Z	4	4	6		8	8
ρ_{calc}/g cm^{-3}	1.568	1.570	1.564		1.618	1.621

The crystal structures of imidazole derivatives are typically characterised by chains of imidazole units, connected by NH⋯N hydrogen bonds.[31, 34] This arrangement is observed in both anhydrous polymorphs of I-TPI, Forms V and VI (Figure 4.12).
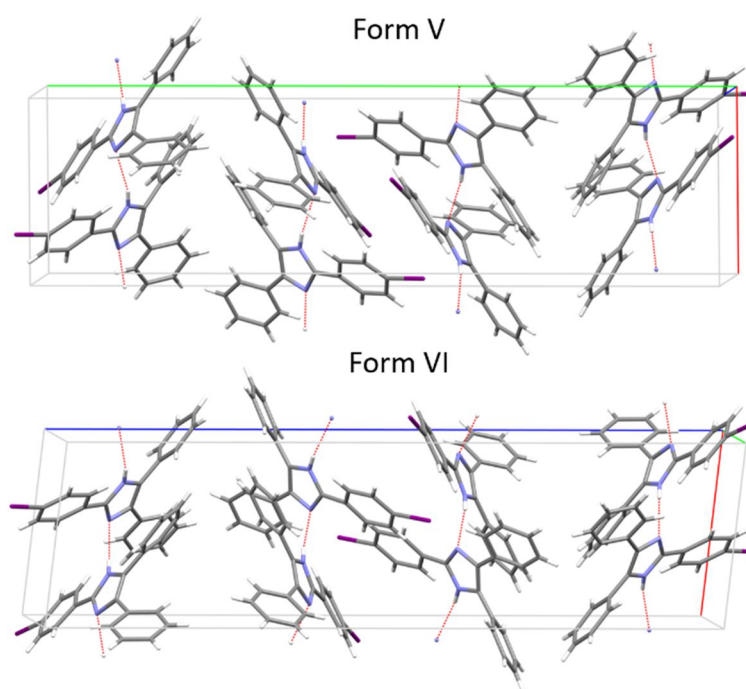
Figure 4.12: Hydrogen-bonded chains in Forms V and VI of I-TPI.

For both structures V and VI, there are four independent molecules per asymmetric unit and there are four different NH⋯N hydrogen bonds in each structure. The average N⋯N distance in both forms is 2.9 Å, which is typical for a substituted imidazole.[70] In I-TPI, steric interactions between the bulky phenyl substituents cause the imidazole rings to twist out of plane with each other, as was observed in other sterically hindered lophine derivatives.[34] Both structures have a high Z' of 4, which suggests some degree of awkwardness in their packing. A significant correlation has been found between $Z' > 1$ "parent" phases and solvate or co-crystal formation, which may explain the prevalence of solvates in this system.[71, 72]

Although the basic packing motif of both anhydrous polymorphs are essentially the same, the stacking of these motifs shows a subtle difference (Figure 4.13).
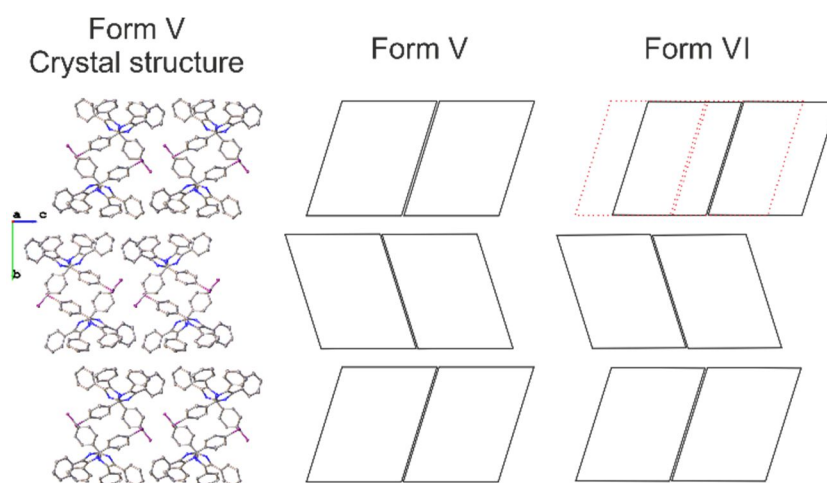
Figure 4.13: Packing arrangement of Form V crystal structure, and schematic representations of Form V and VI, all viewed along the crystallographic *a* axis. The red dotted overlay in the schematic of Form VI represents the deviation in packing observed in Form V.

Both crystal forms display layered packing when viewed along the crystallographic *a*-axis. The layers contain the typical hydrogen-bonded chains, in which two are packed together to form strands stabilised by π-stacking of the iodo-phenyl moieties. In Figure 4.13, each double strand is represented by a rhomboid to simplify the stacking of the crystal structure. This schematic representation shows that a shift in the layers occurs in Form VI compared to Form V, due to the different symmetry of the two crystal forms. In Form V the layers are related through the 2_1-screw axis resulting in the monoclinic cell of the crystal structure, whereas Form VI shows only the inversion centre of the triclinic space group $P\overline{1}$. The latter results in a larger shift of every third layer against the first when compared to Form V. These small differences in the packing arrangement of polymorphs has been shown for other pharmaceutical compounds such as aspirin[73], or larger supramolecular assemblies such as calix[4]arene.[74]

Forms SI–SIII are discrete-site solvates containing 1:1 I-TPI and methanol. In these materials, methanol molecules are incorporated into the imidazole chains, linked by O-H···N and N-H···O hydrogen bonds (Figure 4.14). The same arrangement has previously been reported for other halogenated TPI derivatives.[31]
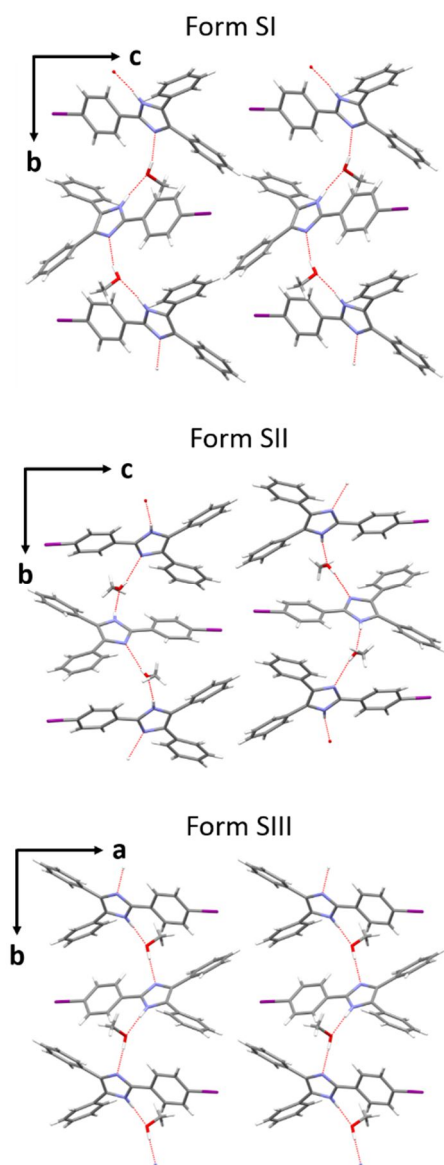
Figure 4.14: Hydrogen-bonded chains in forms SI, SII and SIII of I-TPI.

The formation of solvates from alcohols and water is known in sterically hindered imidazole derivatives, as the incorporation of solvent allows a greater distance between molecules.[34] The large aromatic substituents in I-TPI cause the imidazole rings to deviate from co-planarity with one another, as observed in the anhydrous form. In this case, however, the deviation is much greater. Similarly, the I-TPI molecules in the solvated forms adopt an alternating arrangement, in which equivalent substituents are positioned on opposite sides of the chain, further decreasing steric interactions.

The stability relationship between these polymorphs can be deduced from the conditions under which they form. Following formation of the gel, under the correct conditions, crystals of Form SII appear first, without disturbing the gel phase. When the gel breaks down, these crystals transform spontaneously into Form SI, which according to Ostwald's rule, implies that Form SI is more stable than Form SII. Form SI can also crystallise directly from the gel phase, concomitant with the gel's break-down, bypassing the formation of Form SII. Crystals of Form SIII also transform into Form SI over time, but despite several attempts, could not be re-grown for thermal analysis. The difficulty encountered in re-growing this form, and the fact that it requires heterogeneous nucleation, both imply that it is highly metastable.[75] Given that the packing motif of Form SIII is similar to the other methanol solvates (Figure 4.14), it may represent another step in the sequential crystallisation of the I-TPI gel. The high Z' of 3 and the metastability of this structure suggest it may appear early on in the sequence and rapidly transform into a more stable polymorph, which is consistent with the difficulty encountered in reproducing this form.

To further probe this stability order, the total packing energy of each form was calculated from its crystal structure, using the UNI intermolecular interactions tool in Mercury, an empirical force field calculation.[76, 77] The calculated energies are given in Table 4.5, and correlate with the stability of each crystal form, assuming entropic effects are approximately equal.

Table 4.5: Calculated total packing energies of Forms I-V of I-TPI

	Form SI	Form SII	Form SIII	Form V	Form VI
Total Packing Energy / kJ mol^{-1}	-229.1	-222.8	-225.0	-189.5	-190.0

These results show that Form SI has the lowest packing energy of the three solvates, which is to be expected given that it is the most thermodynamically stable under ambient conditions. Form SII has a higher energy than Form SIII, which is the opposite trend to what would be expected based on the crystallisation observations. However, since both crystal structures have higher R-values, these results will have to be taken with care. Form SII has the highest density of the three solvates, which is unusual given its observed metastability, and following the rule of density, suggests that this crystal form is the most stable of all three methanol solvates at absolute zero.[78] It is possible that forms SI and SII undergo an enantiotropic transition at lower temperatures. The two anhydrous polymorphs, Forms V and VI, have very similar packing energies, which is to be expected, given their extremely close structural similarity.

Relationships between the solvated and anhydrous forms were characterised by DSC (Figure 4.15).
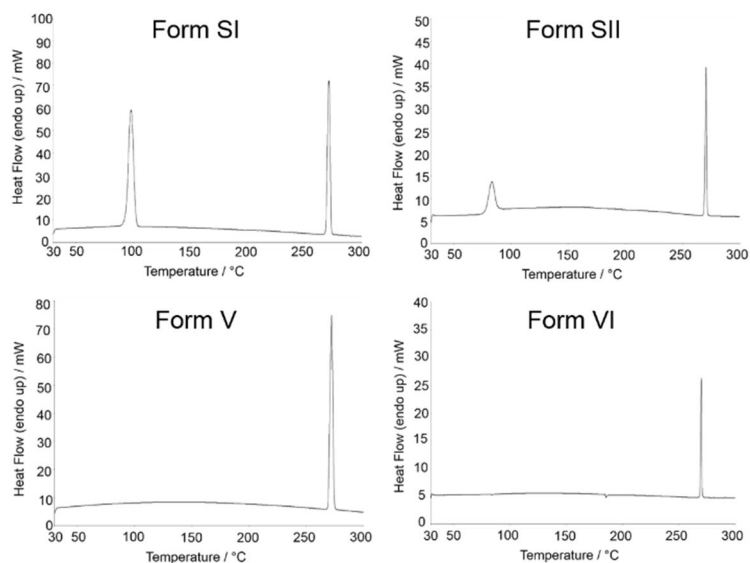
Figure 4.15: DSC thermograms of Forms SI, SII, V and VI. Peak onset temperatures are as follows: Form SI desolvation 93.95 °C, melt 268.82 °C; Form SII desolvation 78.25 °C, melt 269.04 °C; Form V melt 269.17 °C; Form VI melt 268.79 °C.

The DSC thermograms of Forms SI and SII, the two solvates that were stable enough to analyse, show desolvation peaks at 91 °C and 77 °C, respectively. These desolvation temperatures are much greater than the boiling point of methanol (64 °C), which shows that the solvent is strongly bound into the crystal structure. The structure of the desolvated form was characterised using PXRD, by heating a sample of Forms SI and SII above their transition temperatures. Both experiments showed the presence of Form V after desolvation (Figure 4.16). DSC thermograms of Forms SI, SII, and Form V all contain a melting endotherm at 269 °C. The DSC thermograms of Form VI and Form V show no reproducible thermal event before the melting point at 269 ˚C.
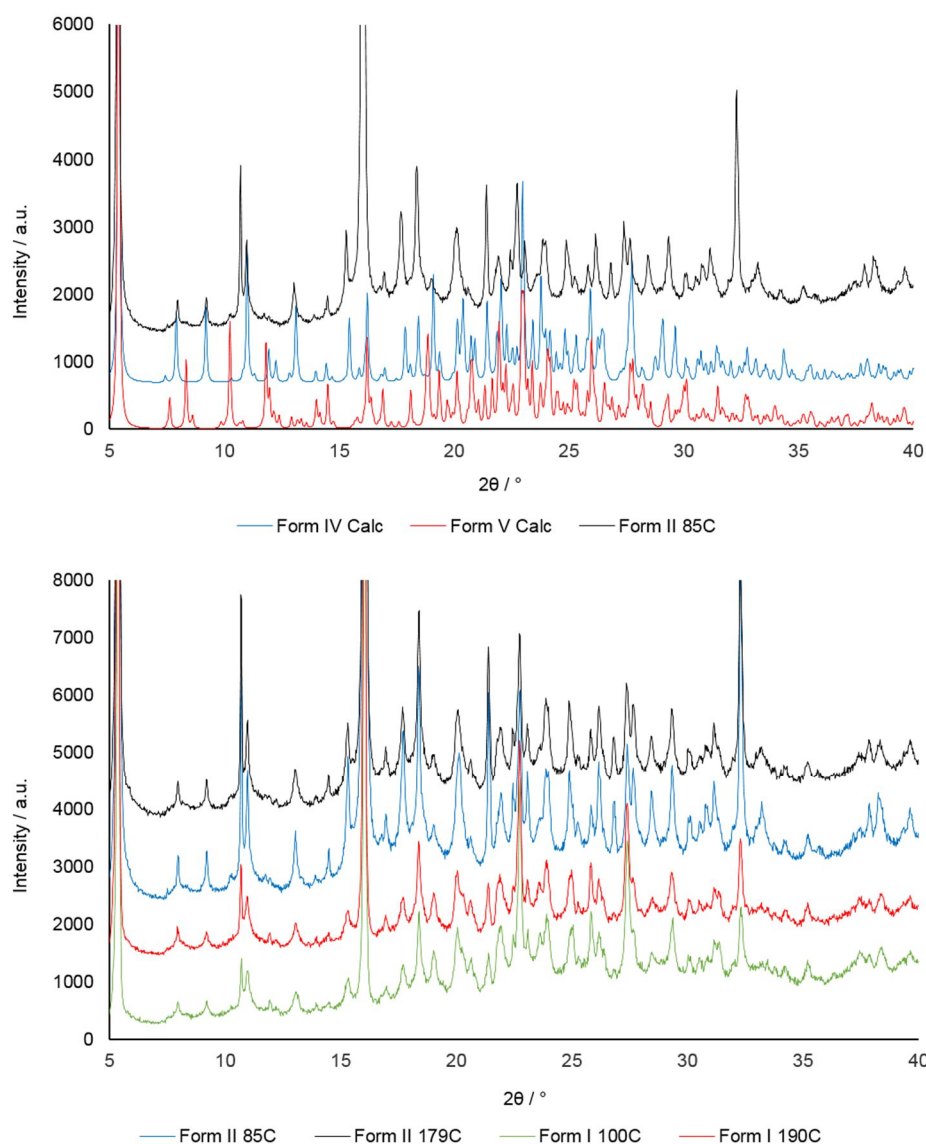
Figure 4.16: Experimental PXRD patterns of Forms I and II after their phase transitions, compared to the calculated patterns of Forms IV and V (top), showing that both forms transform into Form IV after desolvation (bottom). The legends show the temperature each sample was heated to.

The ability of the gel to nucleate the metastable Form SII suggests a small energetic difference, and a potential structural similarity, between the crystal structure of Form SII and the gel fibre.[79] Given the importance of one-dimensional intermolecular interactions in supramolecular gelation,[5] it is likely that the alternating methanol/I-TPI chains comprise the building blocks of gel fibres. Kinetic restrictions on packing molecules orthogonal to these chains promote one-dimensional fibre formation over

three-dimensional crystallisation on a short timescale, leading to the formation of a supramolecular gel. The powder X-ray diffraction pattern of the dried xerogel is most similar to the calculated pattern of Form SI (Figure 4.17).
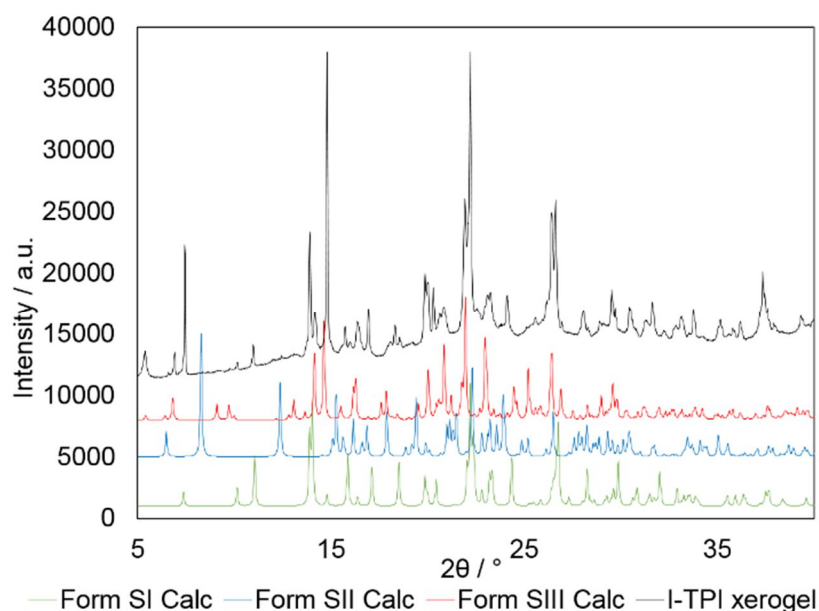
Figure 4.17: Experimental PXRD patterns of the dried I-TPI xerogel, compared with calculated patterns of metastable methanol solvates, Forms SI–SIII.

This is to be expected, as the gel was left to dry overnight, which allowed time for the metastable gel fibres to begin the transformation into Form SI. However, there are several additional peaks that do not correspond to any known form and suggest that the xerogel does not share its structure with any of the known methanol solvates. The unique structure of the gel is consistent with its role as the first step in the crystallisation regime of I-TPI.

4.5   Pharmaceutical Crystallisation

The ability of the I-TPI gel to selectively crystallise a metastable polymorph of a methanol solvate suggests that this property may also be applied to other substrates, and hence that the material may be applicable as a medium for the controlled crystallisation of pharmaceuticals. To investigate this suggestion, diatrizoic acid, DTA, was crystallised within the I-TPI gel (Figure 4.18).
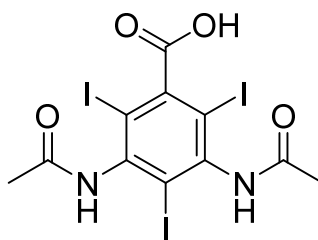
Figure 4.18: Structure of diatrizoic acid (DTA).

Recent work shows that polymorph control can be achieved by matching the structure of a supramolecular gelator to that of the target drug.[79] Whilst there are some structural similarities between DTA and I-TPI, including the iodo- substituent and anti-parallel arrangement of hydrogen bond donor and acceptor groups, I-TPI could not be classed as a "drug-mimicking" gelator.

Previous studies of DTA have resulted in the discovery of two hydrates, nine solvates and three anhydrous polymorphs.[41] The strongest intermolecular interaction in all the crystal structures involves the carboxylic acid.[80] Most commonly, a hydrogen bond is donated to the solvent in an interaction found to be stronger than the halogen bonds in this system. These interactions mirror that of I-TPI, in which hydrogen bonding is dominant. Matching the principal supramolecular motifs of the gelator and drug substrate should further reinforce interactions between the two, in order to facilitate control of solid form.

Various concentrations of DTA, ranging from 1–5 % w/v, were incorporated into a 2 % w/v I-TPI gel in methanol, according to Table 4.6.

Table 4.6: Results of gelation screening of mixtures containing 2 % w/v I-TPI in methanol, and varying concentrations of diatrizoic acid (DTA). G = gel, C = crystals.

Mass of DTA / mg	Amount of DTA / mmol	Result
10	0.016	G then C
15	0.024	G then C
20	0.033	G then C
25	0.041	G then C
30	0.049	G then C
35	0.057	C
40	0.065	C
45	0.073	C
50	0.081	C

The DTA-containing samples were all found to crystallise in a stepwise manner, forming two distinct crystal habits, over a similar timescale to the crystallisation of the pure I-TPI gel. First, all samples grew clusters of small, white needles over the course of one hour to one day. Samples with a higher drug concentration crystallised faster, and those above 3% w/v no longer exhibited gelation but crystallised immediately from solution. If left for a time ranging from four days to two weeks, the gel broke down and these needles were replaced by transparent, block-shaped single crystals (Figure 4.19). This transformation occurred for every concentration of DTA but once again, the rate of the change was faster for gels with a higher drug loading.
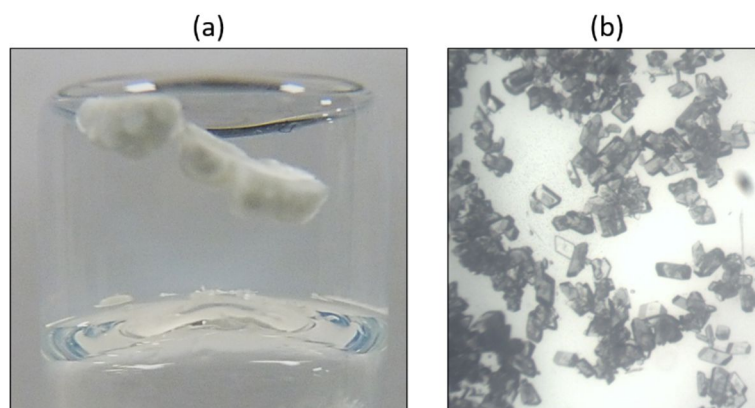
Figure 4.19: (a) Small needle-like crystals initially grown within a 2 % w/v I-TPI gel containing 2% w/v DTA. (b) Block-like single crystals formed after break-down of the same gel.

Attempts to determine the single-crystal structure or PXRD pattern of the needle-like crystals resulted in amorphous background, and it is possible that these crystals are either too small to show diffraction or that they amorphise when removed from the gel. Solution-state ^{1}H NMR spectroscopy showed that these crystals contain a 2:1 ratio of I-TPI and DTA. However, due to the fast exchange of the carboxylate proton, it is not possible to determine by this method whether the structure is a salt or a co-crystal. Solid-state ^{13}C NMR confirmed the presence of both DTA and I-TPI, and also proved that the structure contains methanol, and is therefore another solvate. To confirm that the sample was not simply a mixture of pure crystals of DTA and I-TPI, the IR spectrum was measured and compared to those of the two components. The spectrum of the needles was different to both pure compounds, and was not a sum of the two, which proves that they are a distinct crystalline form containing DTA, I-TPI, and methanol (Figure 4.20).
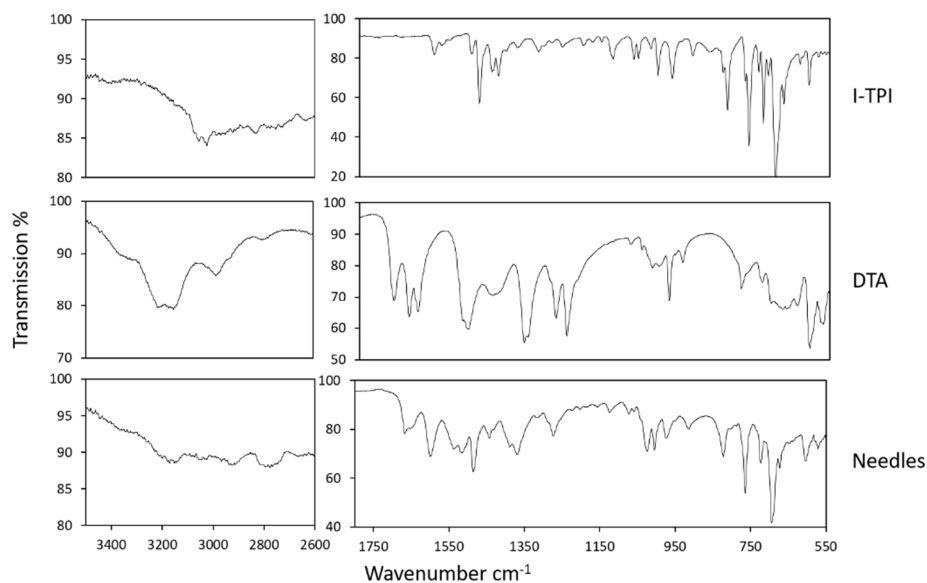
Figure 4.20: IR spectra of pure I-TPI, pure DTA and the needle shaped co-crystals

Formation of the needle-shaped crystals occurred over a few hours to one day, and was accompanied by breakdown of the gel, due to the incorporation of gelator molecules into the crystals. Rheological characterisation of the DTA-containing gels was not possible, due to the fast formation of crystallites under the experimental conditions, which subsequently caused the gel to break down. The larger, block-shaped crystals were more stable and were identified by single-crystal X-ray diffraction as a salt solvate, in which the asymmetric unit contains one molecule of a deprotonated DTA anion, one molecule of a protonated I-TPI cation, and two methanol molecules. Whilst this structure contains the same molecules as the needles, the stoichiometry is different. Selected crystallographic information for this structure can be found in Table 4.7 and the full information can be found in Appendix 7.2.

Table 4.7: Selected crystallographic data for the salt solvate containing I-TPI and DTA.

Crystal Form	TPI-DTA Salt Solvate
Space group	$P\bar{1}$
$a/Å$	9.700(5)
$b/Å$	12.806(6)
$c/Å$	15.467(8)
$\alpha/°$	73.556(2)
$\beta/°$	80.454(2)
$\gamma/°$	82.492(2)
$V/Å^3$	1810.0(16)
Z	4
$\rho_{calc}/g\ cm^{-3}$	2.019

The drug and gelator form hydrogen-bonded chains with an alternating sequence: I-TPI, methanol, DTA (Figure 4.21a). Unlike the I-TPI solvates, these chains are connected via hydrogen bonds from the methanol in one chain to the carboxylate group of the DTA anion in an adjacent chain (Figure 4.21b). The multiple hydrogen-bonding groups in DTA facilitate the formation of stacks of DTA molecules orthogonal to the alternating chains. (Figure 4.22a). This stacking prompts the organisation of I-TPI and DTA into discrete layers (Figure 4.22b). This crystal structure demonstrates the formation of a hydrogen bonded network between I-TPI, DTA and methanol, reinforcing the assumption that structural similarity between drug and gelator encourages them to interact.

(a)

(b)
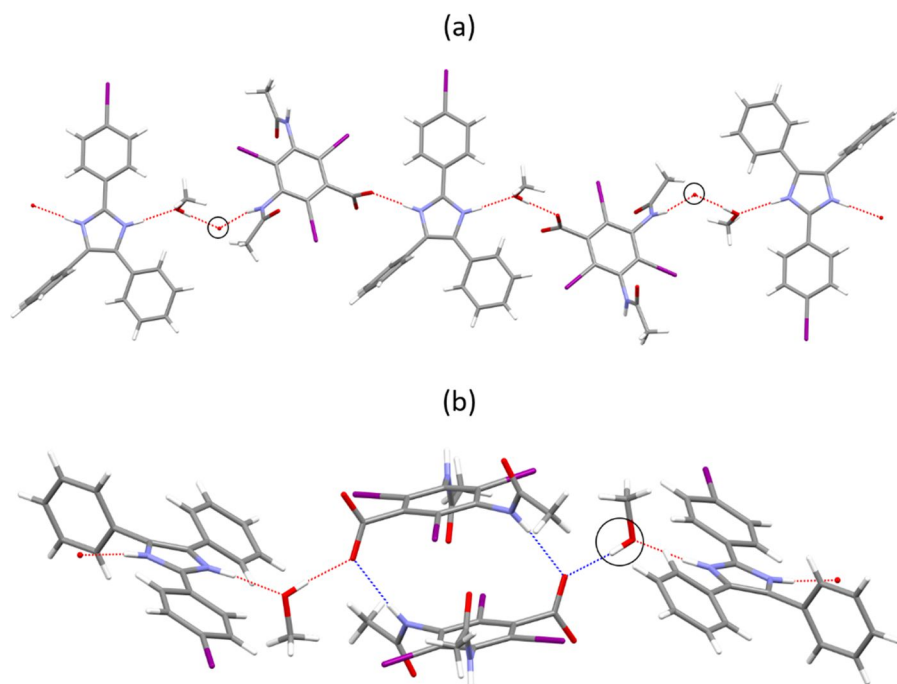
Figure 4.21: (a) Hydrogen-bonded chains in the I-TPI/DTA/MeOH salt solvate. (b) The hydrogen bonding motif between chains in the I-TPI/DTA/MeOH salt solvate. The black circles in both diagrams show points at which the carbonyl oxygen from DTA forms hydrogen bonds between adjacent chains, linking them together. In diagram (b) the red dashed lines show hydrogen bonds within a chain and the blue dashed lines show hydrogen bonds between chains.

(a)   (b)
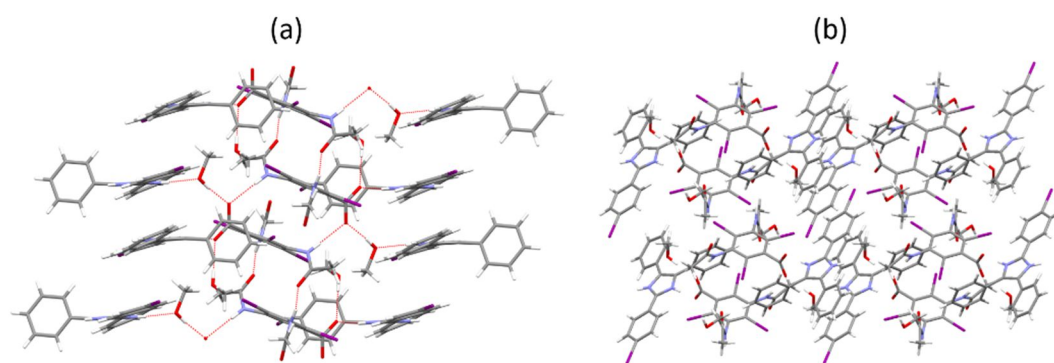
Figure 4.22: (a) Hydrogen-bonded stacks of DTA molecules (b) Layered packing pattern of the salt solvate structure.

There have been numerous recent examples of pharmaceutical polymorph-control techniques in which a gelator selectively nucleates a known solid form, or facilitates the crystallisation of a new one.[55, 79, 81-84] In this case, however, a series of solid forms are produced, in order of increasing thermodynamic stability, obeying Ostwald's rule of stages and mirroring the crystallisation regime of the gelator itself. Gels that can stabilise a metastable polymorph of their gelator may therefore represent a new avenue in the field of pharmaceutical crystallisation, in line with recent suggestions that the function of a supramolecular system is defined more by its energy landscape than by the chemical structure of its components.[85]

4.6   Conclusions

In conclusion, the supramolecular gelation behaviour of a mono-iodinated 2,4,5-triphenyl imidazole derivative was observed at high concentrations in methanol, driven by the formation of hydrogen-bonded chains of imidazole and methanol. Steric interactions between peripheral groups mean that whilst the gel is thermodynamically metastable, it is the most kinetically accessible state in the system. Gelation therefore occurs first, followed by a stepwise crystallisation forming three increasingly stable methanol solvates. Thus, the supramolecular gel can be considered the first stage in the crystallisation regime of the gelator, as described by Ostwald's rule of stages. The incorporation of a pharmaceutical drug within the gel produces a similar stepwise crystallisation, yielding two increasingly stable solid forms of a drug-gelator salt. This behaviour highlights the possibility of using other gelators that crystallise as a metastable crystal form within the gel network, as a crystallisation medium to access metastable pharmaceutical polymorphs.

4.7   References

1.   J. Bernstein, in *Polymorphism in Molecular Crystals*, Clarendon Press, Oxford, 2002, ch. 2, pp. 29-65.

2.   W. Ostwald, *Z. Phys. Chem*, 1897, **22**, 289-330.

3.   J. Thun, L. Seyfarth, J. Senker, R. E. Dinnebier and J. Breu, *Angew. Chem., Int. Ed.*, 2007, **46**, 6729-6731.

4.   A. Levin, T. O. Mason, L. Adler-Abramovich, A. K. Buell, G. Meisl, C. Galvagnion, Y. Bram, S. A. Stratford, C. M. Dobson, T. P. J. Knowles and E. Gazit, *Nat. Commun.*, 2014, **5**, 5219.

5.   K. Hanabusa, M. Yamada, M. Kimura and H. Shirai, *Angew. Chem., Int. Ed.*, 1996, **35**, 1949-1951.

6.   C. D. Jones, S. R. Kennedy, M. Walker, D. S. Yufit and J. W. Steed, *Chem.*, 2017, **3**, 603-628.

7.   F. Fages, F. Vögtle and M. Žinic, in *Low Molecular Mass Gelators*, Springer, Berlin, 2005, ch. 3, pp. 77-131.

8.   P. Dastidar, *Chem. Soc. Rev.*, 2008, **37**, 2699-2715.

9.   D. K. Kumar and J. W. Steed, *Chem. Soc. Rev.*, 2014, **43**, 2080-2088.

10.   I. Ramos Sasselli, P. J. Halling, R. V. Ulijn and T. Tuttle, *ACS Nano*, 2016, **10**, 2661-2668.

11.   D. J. Adams, K. Morris, L. Chen, L. C. Serpell, J. Bacsa and G. M. Day, *Soft Matter*, 2010, **6**, 4144-4156.

12.   J. R. Moffat and D. K. Smith, *Chem. Commun.*, 2008, **19**, 2248-2250.

13.   P. Zhu, X. Yan, Y. Su, Y. Yang and J. Li, *Chem. - Eur. J.*, 2010, **16**, 3176-3183.

14.   P. Terech, N. M. Sangeetha and U. Maitra, *J. Phys. Chem. B*, 2006, **110**, 15224-15233.

15.   O. Lebel, M.-È. Perron, T. Maris, S. F. Zalzal, A. Nanci and J. D. Wuest, *Chem. Mater.*, 2006, **18**, 3616-3626.

16.   K. A. Houton, K. L. Morris, L. Chen, M. Schmidtmann, J. T. A. Jones, L. C. Serpell, G. O. Lloyd and D. J. Adams, *Langmuir*, 2012, **28**, 9797-9806.

17.   B. Roy, P. Bairi and A. K. Nandi, *Soft Matter*, 2012, **8**, 2366-2369.

18. I. Kapoor, E.-M. Schon, J. Bachl, D. Kuhbeck, C. Cativiela, S. Saha, R. Banerjee, S. Roelens, J. J. Marrero-Tellado and D. D. Diaz, *Soft Matter*, 2012, **8**, 3446-3456.

19. H. B. Aiyappa, S. Saha, B. Garai, J. Thote, S. Kurungot and R. Banerjee, *Cryst. Growth Des.*, 2014, **14**, 3434-3437.

20. J. Liu, F. Xu, Z. Sun, Y. Pan, J. Tian, H.-C. Lin and X. Li, *Soft Matter*, 2016, **12**, 141-148.

21. Y. Wang, L. Tang and J. Yu, *Cryst. Growth Des.*, 2008, **8**, 884-889.

22. E. C. Barker, A. D. Martin, C. J. Garvey, C. Y. Goh, F. Jones, M. Mocerino, B. W. Skelton, M. I. Ogden and T. Becker, *Soft Matter*, 2017, **13**, 1006-1011.

23. M. Guo, Q. Yin, Y. Li, Y. Huang, Z. Zhang and L. Zhou, *Chem. Lett.*, 2017, **46**, 1292-1295.

24. Z. Shi, L. Hao, M. Zhang, L. Dang and H. Wei, *J. Cryst. Growth*, 2017, **469**, 8-12.

25. K. Nakashima, *Biomed. Chromatogr.*, 2003, **17**, 83-95.

26. E. H. White and M. J. C. Harding, *J. Am. Chem. Soc.*, 1964, **86**, 5686-5687.

27. D. M. White and J. Sonnenberg, *J. Am. Chem. Soc.*, 1966, **88**, 3825-3829.

28. Y. Kishimoto and J. Abe, *J. Am. Chem. Soc.*, 2009, **131**, 4227-4229.

29. H. Yamashita and J. Abe, *J. Phys. Chem. A*, 2011, **115**, 13332-13337.

30. R. M. Edkins, M. R. Probert, C. M. Robertson, J. A. K. Howard and A. Beeby, *RSC Adv.*, 2014, **4**, 5351-5356.

31. T. Kitchen, C. Melvin, M. N. Mohd Najib, A. S. Batsanov and K. Edkins, *Cryst. Growth Des.*, 2016, **16**, 4531-4538.

32. R. M. Edkins, M. R. Probert, K. Fucke, C. M. Robertson, J. A. K. Howard and A. Beeby, *Phys. Chem. Chem. Phys.*, 2013, **15**, 7848-7853.

33. S. Martinez-Carrera, *Acta Crystallogr.*, 1966, **20**, 783-789.

34. A. Cammers and S. Parkin, *CrystEngComm*, 2004, **6**, 168-172.

35. A. Ballabh, D. R. Trivedi and P. Dastidar, *Chem. Mater.*, 2003, **15**, 2136-2140.

36. S. H. Seo and J. Y. Chang, *Chem. Mater.*, 2005, **17**, 3249-3254.

37. S. J. James, A. Perrin, C. D. Jones, D. S. Yufit and J. W. Steed, *Chem. Commun.*, 2014, **50**, 12851-12854.

38. S. Mondal and K. Ghosh, *ChemistrySelect*, 2017, **2**, 4800-4806.

39. G. Yu, X. Yan, C. Han and F. Huang, *Chem. Soc. Rev.*, 2013, **42**, 6697-6722.

40. C. D. Jones and J. W. Steed, *Chem. Soc. Rev.*, 2016, **45**, 6546-6596.

41.   D. Adams, *Gels*, 2018, **4**, 32-36.

42.   L. L. Mears, E. R. Draper, A. M. Castilla, H. Su, B. Dietrich, M. C. Nolan, G. N. Smith, J. Doutch, S. Rogers and R. Akhtar, *Biomacromolecules*, 2017, **18**, 3531-3540.

43.   K. Almdal, J. Dyre, S. Hvidt and O. Kramer, *Polym. Gels Networks*, 1993, **1**, 5-17.

44.   J. W. Goodwin and R. W. Hughes, *Rheology for chemists: an introduction*, Royal Society of Chemistry, Cambridge, 2008.

45.   A. G. Shtukenberg, S. S. Lee, B. Kahr and M. D. Ward, *Annu. Rev. Chem. Biomol. Eng.*, 2014, **5**, 77-96.

46.   N. Rodríguez-hornedo and D. Murphy, *J. Pharm. Sci.*, 1999, **88**, 651-660.

47.   A. G. Shtukenberg, M. D. Ward and B. Kahr, *Chem. Rev.*, 2017, **117**, 14042-14090.

48.   G. Clydesdale, K. J. Roberts and R. Docherty, *J. Cryst. Growth*, 1994, **135**, 331-340.

49.   R. Dowling, R. J. Davey, R. A. Curtis, G. Han, S. K. Poornachary, P. S. Chow and R. B. H. Tan, *Chem. Commun.*, 2010, **46**, 5924-5926.

50.   J. L. W. Griffin, P. V. Coveney, A. Whiting and R. Davey, *J. Chem. Soc., Perkin Trans. 2*, 1999, **10**, 1973-1981.

51.   S. K. Poornachary, P. S. Chow, R. B. Tan and R. J. Davey, *Cryst. Growth Des.*, 2007, **7**, 254-261.

52.   L. E. Buerkle and S. J. Rowan, *Chem. Soc. Rev.*, 2012, **41**, 6089-6102.

53.   Y. Lan, M. G. Corradini, R. G. Weiss, S. R. Raghavan and M. A. Rogers, *Chem. Soc. Rev.*, 2015, **44**, 6035-6058.

54.   P. Terech, D. Pasquier, V. Bordas and C. Rossat, *Langmuir*, 2000, **16**, 4485-4494.

55.   J. A. Foster, M.-O. M. Piepenbrock, G. O. Lloyd, N. Clarke, J. A. K. Howard and J. W. Steed, *Nat. Chem.*, 2010, **2**, 1037-1043.

56.   G. O. Lloyd, M.-O. M. Piepenbrock, J. A. Foster, N. Clarke and J. W. Steed, *Soft Matter*, 2012, **8**, 204-216.

57.   M.-O. M. Piepenbrock, N. Clarke, J. A. Foster and J. W. Steed, *Chem. Commun.*, 2011, **47**, 2095-2097.

58.   M.-O. M. Piepenbrock, G. O. Lloyd, N. Clarke and J. W. Steed, *Chem. Commun.*, 2008, 2644-2646.

59. L. E. Buerkle, R. Galleguillos and S. J. Rowan, *Soft Matter*, 2011, **7**, 6984-6990.

60. A. E. Way, A. B. Korpusik, T. B. Dorsey, L. E. Buerkle, H. A. von Recum and S. J. Rowan, *Macromolecules*, 2014, **47**, 1810-1818.

61. Y. J. Adhia, T. H. Schloemer, M. T. Perez and A. J. McNeil, *Soft Matter*, 2012, **8**, 430-434.

62. A. M. Brizard, M. C. A. Stuart and J. H. van Esch, *Faraday Discuss.*, 2009, **143**, 345-357.

63. C. A. Offiler, C. D. Jones and J. W. Steed, *Chem. Commun.*, 2017, **53**, 2024-2027.

64. P. Byrne, G. O. Lloyd, L. Applegarth, K. M. Anderson, N. Clarke and J. W. Steed, *New J. Chem.*, 2010, **34**, 2261-2274.

65. T. Becker, C. Yong Goh, F. Jones, M. J. McIldowie, M. Mocerino and M. I. Ogden, *Chem. Commun.*, 2008, **33**, 3900-3902.

66. F. Hofmeister, *Arch. Exp. Path. Pharm.*, 1888, **24**, 247-260.

67. W. Kunz, J. Henle and B. W. Ninham, *Curr. Opin. Colloid Interface Sci.*, 2004, **9**, 19-37.

68. C. J. E. Kempster and H. Lipson, *Acta Crystallogr., Sect. B: Struct. Crystallogr. Cryst. Chem.*, 1972, **28**, 3674.

69. L. Yu, *CrystEngComm*, 2007, **9**, 847-851.

70. T. Ueda, S. Nagatomo, H. Masui, N. Nakamura and S. Hayashi, *Z. Naturforsch. A*, 1999, **54**, 437-442.

71. K. M. Steed and J. W. Steed, *Chem. Rev.*, 2015, **115**, 2895-2933.

72. K. M. Anderson, M. R. Probert, C. N. Whiteley, A. M. Rowland, A. E. Goeta and J. W. Steed, *Cryst. Growth Des.*, 2009, **9**, 1082-1087.

73. A. D. Bond, R. Boese and G. R. Desiraju, *Angew. Chem., Int. Ed.*, 2007, **46**, 618-622.

74. K. Fucke, K. M. Anderson, M. H. Filby, M. Henry, J. Wright, S. A. Mason, M. J. Gutmann, L. J. Barbour, C. Oliver and A. W. Coleman, *Chem. - Eur. J.*, 2011, **17**, 10259-10271.

75. J. D. Dunitz and J. Bernstein, *Acc. Chem. Res.*, 1995, **28**, 193-200.

76. A. Gavezzotti, *Crystallogr. Rev.*, 1998, **7**, 5-121.

77. A. Gavezzotti, *Acc. Chem. Res.*, 1994, **27**, 309-314.

78. A. Burger and R. Ramberger, *Microchim. Acta*, 1979, **72**, 273-316.

79.	J. A. Foster, K. K. Damodaran, A. Maurin, G. M. Day, H. P. G. Thompson, G. J. Cameron, J. C. Bernal and J. W. Steed, *Chem. Sci.*, 2017, **8**, 78-84.

80.	K. Fucke, G. J. McIntyre, M.-H. Lemée-Cailleau, C. Wilkinson, A. J. Edwards, J. A. K. Howard and J. W. Steed, *Chem. - Eur. J.*, 2015, **21**, 1036-1047.

81.	L. Kaufmann, S. R. Kennedy, C. D. Jones and J. W. Steed, *Chem. Commun.*, 2016, **52**, 10113-10116.

82.	C. Ruiz-Palomero, S. R. Kennedy, M. L. Soriano, C. D. Jones, M. Valcarcel and J. W. Steed, *Chem. Commun.*, 2016, **52**, 7782-7785.

83.	J. Buendia, E. Matesanz, D. K. Smith and L. Sanchez, *CrystEngComm*, 2015, **17**, 8146-8152.

84.	F. Aparicio, E. Matesanz and L. Sanchez, *Chem. Commun.*, 2012, **48**, 5757-5759.

85.	F. Tantakitti, J. Boekhoven, X. Wang, R. V. Kazantsev, T. Yu, J. Li, E. Zhuang, R. Zandi, J. H. Ortony, C. J. Newcomb, L. C. Palmer, G. S. Shekhawat, M. O. de la Cruz, G. C. Schatz and S. I. Stupp, *Nat. Mater.*, 2016, **15**, 469.

5. Experimental

5.1 Materials

All solvents and reagents were purchased from standard commercial sources and used without further purification.

5.2 Instrumentation for the Characterisation of Pharmaceutical Solid Forms

Powder X-Ray Diffraction, PXRD

Powder X-ray diffraction, PXRD, was performed using either a Bruker D8 or PANalytical Empyrean powder X-ray diffractometer in Bragg-Brentano geometry. Samples were mounted on a silicon single-crystal wafer and analysed using Cu-Kα radiation at a wavelength of 1.5406 Å. X-rays were produced using an operating voltage of 40 kV and current of 40 mA. Samples were scanned over an angle range of 2-40° 2θ, with a step size of 0.02 ° and a scan rate between 0.5-1.5 s/step.

Single-Crystal X-Ray Diffraction

Ambient pressure X-ray single-crystal data were collected using one of two methods:

1. At a temperature of 120 K, using Mo Kα radiation (λ =0.71073Å), on a Bruker D8 Venture diffractometer (Photon100 CMOS detector, IµS-microsource, focusing mirrors) equipped with a Cryostream 700+ (Oxford Cryosystems) open-flow nitrogen cryostat. Single crystals were coated in perfluoro polyether

oil, mounted on a MiTeGen sample holder and placed directly into the precooled cryostream.

2.   At a temperature of 100 K, on a Rigaku Saturn 724+ diffractometer at station I19 of the Diamond Light Source synchrotron (undulator, $\lambda = 0.6889$ Å, ω-scan, 1.0°/frame).

High-pressure X-ray single-crystal data were obtained by *in situ* compression of crystals grown at ambient pressure, in a Merrill–Bassett diamond anvil cell (DAC), using Fluorinert™ FC-70 as an inert pressure transmitting fluid. A 0.25 mm thickness steel gasket, pre-indented to 0.15 mm, with a precision drilled 300 μm hole created the sample chamber between the two diamond anvils, of culet size 0.8 mm. A ruby chip was included in the sample chamber for pressure determination, using the R_1 ruby fluorescence method.[1] The DAC was directly attached to a goniometer head and mounted onto a XIPHOS II[2, 3] diffractometer, a custom-built four circle Huber diffractometer with an Ag-Kα IμS[4] generator and APEXII CCD detector, located at Newcastle University.

The data were processed using Bruker APEXII software, the structure was solved by direct methods and refined by full-matrix least squares on F^2 against all data using Olex2[5] and SHELXTL[6] software. All non-hydrogen atoms were refined anisotropically, hydrogen atoms in structures were placed in the calculated positions and refined in riding mode.

Infra-red Spectroscopy

Fourier transform infra-red spectroscopy (FTIR) was carried out using either a Perkin Elmer Spectrum 2 or a Perkin Elmer Spectrum 100 spectrometer, fitted with a diamond universal Attenuated Total Reflectance (ATR) accessory. Four scans were collected for each sample at a resolution of 2 cm^{-1} over a wavenumber region of 4000 cm^{-1} to 600 cm^{-1}.

Thermogravimetric Analysis, TGA

Thermogravimetric analysis, TGA, was carried out using a TA Instruments Q 500 TGA analyser. Between 1 and 5 mg of sample was weighed into platinum pans and dry nitrogen was used as the purge gas (flow rate: 60 mL min^{-1}).

Differential Scanning Calorimetry, DSC

Differential scanning calorimetry, DSC, was performed using either a TA Instruments Q2000 calorimeter or a Perkin Elmer 8500 calorimeter, both calibrated using an indium standard (melting point onset = 156.6 °C, heat of fusion = 28.57 J g^{-1}). Between 1 and 3 mg of sample was weighed accurately (±0.01 mg) using a Sartorius microbalance into sealed aluminium pans and dry nitrogen was used as the purge gas (flow rate: 50 mL min^{-1}).

Solid-State Nuclear Magnetic Resonance Spectroscopy, SS NMR

Solid-state ^{13}C NMR spectra were obtained at 100.63 MHz using a Bruker Avance III HD spectrometer and a 4 mm (rotor outside diameter) magic-angle spinning probe. They were recorded using one of two methods:

1. Cross polarisation with TOSS spinning sideband suppression with a 1-7 s recycle delay, 1-7 ms contact time, at a spin rate of 8 kHz and a temperature of 10 or 20 °C, depending on the stability of the sample.

2. Direct excitation with proton decoupling with a 1-7 recycle delay, at a spin rate of 8 kHz and a temperature of 10 or 20 °C, depending on the stability of the sample.

Spectral referencing was with respect to external, neat tetramethylsilane, carried out by setting the high-frequency signal from adamantane to 38.5 ppm.

5.3 Instrumentation for the Structural Characterisation of Gels and Gelators

Nuclear Magnetic Resonance Spectroscopy, NMR

Solution-state NMR spectra were recorded in DMSO-D_6 or $CDCl_3$, without an internal reference, using either a Bruker Avance III-HD-400 spectrometer with operating frequencies of 399.95 MHz for ^1H and 100.57 MHz for ^{13}C, a Bruker Neo-400 spectrometer with operating frequencies of 400.20 MHz for ^1H, and 100.63 MHz for ^{13}C, or a Varian VNMRS-600 spectrometer with operating frequencies of 599.42 MHz for ^1H and 150.72 MHz for ^{13}C.

Mass Spectrometry

Liquid chromatography mass spectrometry was carried out using a Waters SQD mass spectrometer and Acquity UPLC, equipped with an Acquity UPLC BEH C_{18} 1.7 μm (2.1 mm x 50 mm) column. Samples were prepared as dilute solutions (<1 mg mL^{-1}) in either methanol or acetonitrile and the mobile phase was either water containing formic acid (0.1 %v /v):methanol or water containing formic acid (0.1 % v/v):acetonitrile, eluted at a flow rate at 0.6 mL min^{-1}. A solvent gradient was used, changing from 95 % water and 5 % organic solvent to 5 % water and 95 % organic solvent over 4.5 minutes.

Elemental Analysis

Elemental analysis was performed using an Exeter CE-440 Elemental Analyser.

Oscillatory Rheometry

Oscillatory rheometry measurements were performed using a TA Instruments AR 2000, on a rough Peltier plate, with a 25 mm rough plate geometry and 2.5 mm gap. Samples were prepared by heating gelator solutions to the boiling point of the solvent in sealed 7 cm^3 vials. The hot solutions were then poured into a 25 mm cylindrical glass mould on the Peltier plate, which was set to maintain a temperature of either 10 or 0 °C throughout formation and analysis of the gels, in order to minimise evaporation of the solvent. The gels were allowed to form over 30 minutes prior to analysis, after which time the mould was removed. Frequency sweep experiments were performed with a constant applied stress of 1 Pa, and stress sweep experiments with a constant frequency of 1 Hz.

Scanning Electron Microscopy, SEM

SEM samples were prepared on silicon wafers, dried in air for 2 days, and coated with either 2 nm of platinum using a Cressington 328 Ultra High Resolution EM Coating System, or 7 nm of gold-palladium using a Cressington 108 Auto Sputter Coater. The images were obtained using either an FEI Helios NanoLab DualBeam microscope or a Zeiss Sigma 300 VP microscope.

5.4   Chapter 2: The Polymorphism of Mexiletine Hydrochloride

Detailed Crystallisation Procedures

Solvent crystallisations were carried out using one of five methods:

1. Slow cooling: Approximately 20 mg of mexiletine hydrochloride was weighed into a small glass vial. Sufficient solvent was added to dissolve the material when heated to boiling using a heat gun. The sealed vial was left to cool in an insulating wooden block under ambient conditions and monitored for crystallisation.

2. Fast cooling: Approximately 20 mg of mexiletine hydrochloride was weighed into a small glass vial. Sufficient solvent was added to dissolve the material when heated to boiling using a heat gun. The sealed vial was cooled quickly in an ice bath and monitored for crystallisation.

3. Evaporation: Approximately 20 mg of mexiletine hydrochloride was weighed into a small glass vial. Sufficient solvent was added to dissolve the material without heating. The vial was left open on the bench to evaporate under ambient conditions and monitored for crystallisation.

4. Precipitation: Approximately 20 mg of mexiletine hydrochloride was weighed into a large glass vial. Sufficient solvent was added to dissolve the material without heating. A miscible anti-solvent (either hexane or diethyl ether) was gradually added to the vial until small crystallites were visible. The vial was then sealed, left to stand under ambient conditions, and monitored for crystallisation.

5. Vapour Diffusion: Approximately 20 mg of mexiletine hydrochloride was weighed into a small glass vial. Sufficient solvent was added to dissolve the material without heating. The small vial was left unsealed and placed into a larger vial containing a miscible anti-solvent (a range of alkanes and ethers were used). The large vial was then sealed, and the system was left to stand under ambient conditions and monitored for crystallisation.

Sublimation crystallisation was carried out using a microscope hot-stage. A small amount of mexiletine hydrochloride powder was placed on a microscope slide, surrounded by a small O-ring and covered with a glass cover slip. The system was heated using the hot-stage to 150 °C, at which point small crystallites began to appear on the cover slip. The temperature was held constant for 7 hours before being allowed to cool to room temperature and the long, needle-shaped crystals could be collected from the cover slip (Figure 5.1).
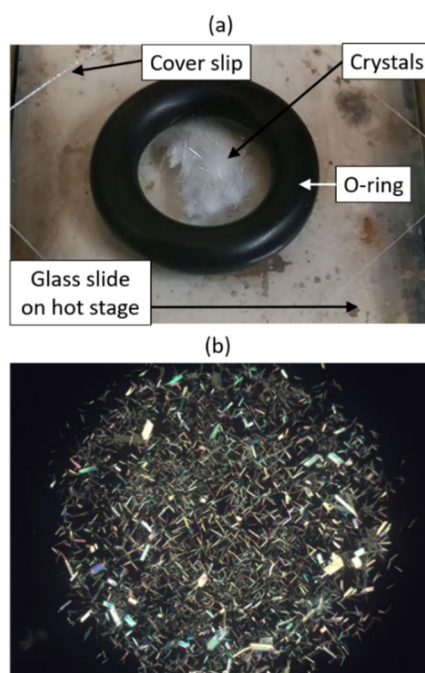
Figure 5.1: (a) Experimental set up for sublimation crystallisation, (b) single crystals of Form 2 of mexiletine hydrochloride grown by sublimation.

PolySNAP Clustering Procedure

Before the PXRD patterns were compared by the software, the backgrounds were removed, and the intensities normalised. The area between 30 and 40 ° was masked in all patterns because it contained only low intensity data that decreased the accuracy of the clustering calculation. A horizontal shift was permitted in each pattern, to allow for the variation in unit cell dimensions between different modifications of same solvate.

CSD-Materials Packing Similarity Calculation

This method is based on the programme COMPACK,[7] which generates a small cluster of molecules, as a representation of the whole crystal structure. The cluster is based on a central molecule and a specified number of its nearest neighbours. Clusters representing the two target crystal structures are then compared, first by searching for

a match for the central molecule, and then by expanding the search to include its nearest neighbours. The two clusters are superimposed to maximise the number of overlapping molecules, within a defined set of tolerances. This calculation yields a root mean square deviation for the atomic positions in the two structures, which can be used to determine whether the two crystal structures represent the same polymorph. Based on previous literature, a group of 20 molecules were compared, using the standard tolerances of 20% on all distances, and 20 ° on the angles.[8] This comparison excluded the smallest components of the crystal structures, which removed any solvent molecules from the solvates, and ensured that only the drug structures were bring compared.

Crystal Structure Prediction

First, one mexiletine cation conformer was extracted from the single-crystal structure of Form 1 of the hydrochloride salt, its geometry was optimised at the B3LYP-D3/6-31G** level of theory, and atomic CHELPG charges were calculated using GAUSSIAN09.[9] The AZ-FF force-field[10] was then generated and applied to produce a number of potential racemic crystal structures of the chloride salt, in the 20 most common space groups, using the GRACE machinery.[11, 12] The 1000 most stable crystal structures were then fully re-optimized and ranked in terms of their relative energies, using dispersion-corrected density functional theory, specifically the PBE functional[13] with Neumann-Perrin dispersion.[10, 11]

5.5 Chapter 3: Tailored Supramolecular Gelators for the Crystallisation of Mexiletine Hydrochloride

Synthesis and characterisation of bis(3,5-diethyl-4-isocyanatophenyl)methane
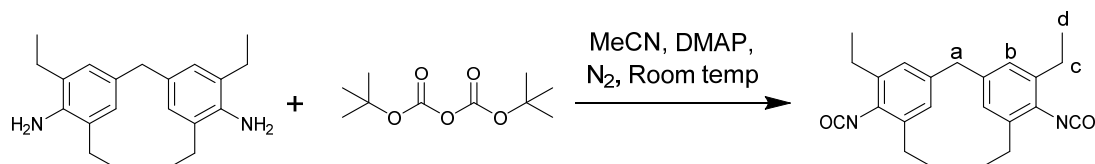
Bis(3,5-diethyl-4-isocyanatophenyl)methane was synthesised according to the literature method.[14] A solution of di-tert-butyl dicarbonate (6.00 g, 34.4 mmol) in dry acetonitrile (20 mL) was slowly added to a solution of 4-DMAP (0.33 g, 2.70 mmol) in dry acetonitrile under a flow of nitrogen. A solution of 4,4'-methylenebis(2,6-diethylaniline) (4.00 g, 12.9 mmol) in dry acetonitrile (20 mL) was slowly added to the previous solution and the resulting mixture was stirred for 2 hours at room temperature under nitrogen. Concentrated H_2SO_4 (2 mL) was slowly added to acetonitrile (3 mL), this solution was added to the reaction mixture and stirred for 5 minutes. The reaction was quenched with water (65 mL) and the solution was extracted with hexane (4 × 100 mL). The combined hexane extracts were dried over $MgSO_4$, filtered and the solvent was removed under vacuum. The crude product was dissolved in DCM (20 mL) and the solution was filtered to remove any solid impurities. The solvent was removed under vacuum, to yield bis(3,5-diethyl-4-isocyanatophenyl)methane as a white solid (1.59 g, 4.39 mmol, 34 %). This compound was used without further purification, for the synthesis of compound **1**. The characterisation data for this compound were consistent with previous literature.[14]

^{1}H NMR (CDCl$_3$, 400 MHz): δ 6.91 (s, 4H, b), 3.90 (s, 2H, a), 2.70 (q, J = 7.6 Hz, 8H, c), 1.26 (t, J = 7.6 Hz, 12H, d).

^{13}C{^{1}H}or NMR (CDCl$_3$, 101 MHz): δ 138.93 (C=O), 138.53 (Ar$\underline{C}$), 127.99 (Ar$\underline{C}$), 126.97 (Ar$\underline{C}$), 123.81 (Ar$\underline{C}$), 41.15 (Ar-$\underline{C}$H$_2$-Ar), 25.73 (Ar-$\underline{C}$H$_2$-CH$_3$), 14.27 (Ar-CH$_2$-$\underline{C}$H$_3$).

m/z ESI-MS (MeCN): retention time 4.05 min 363.4 [M+H]$^+$. The [M+H]$^+$ peak is very low intensity and there are much larger peaks corresponding to the fragment molecule in which one isocyanate group has broken down to an amine: 337.4 [M+H]$^+$.

Synthesis and characterisation of Compound 1
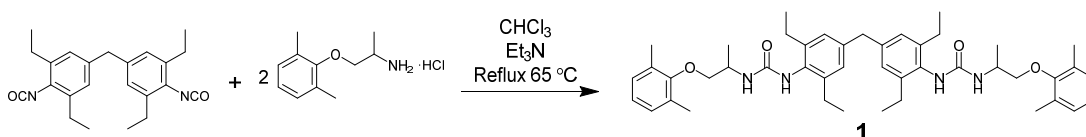
Racemic mexiletine hydrochloride (1.45 g, 6.7 mmol) was suspended in chloroform (100 mL) and dissolved upon the addition of excess triethylamine (1 mL). Bis(3,5-diethyl-4-isocyanatophenyl)methane (1.00 g, 3.06 mmol) was added, and the solution was heated to reflux and stirred for 24 hours. The crude product was collected by filtration, suspended in water (100 mL) and sonicated for 10 minutes to remove water soluble impurities. The precipitate was collected by filtration, washed with water (100 mL) and chloroform (50 mL), and dried under vacuum to yield compound **1** as a white solid (1.90 g, 2.63 mmol, 86 %).
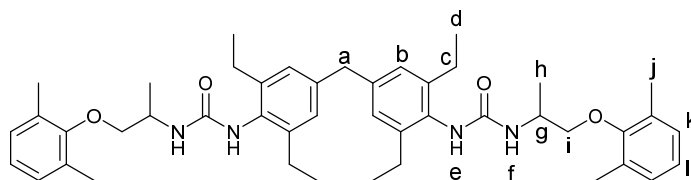
Compound 1 had limited solubility in all common NMR solvents. In cases where sufficient compound dissolved to produce a high-resolution ^{1}H NMR spectrum, the sample gelled (Figure 5.2) and as a result, some multiplicity information was lost due to significant peak broadening. For these reasons, it was not possible to obtain a solution-state ^{13}C NMR spectrum of this molecule, and CP MAS SS NMR was used instead.

^{1}H NMR (CDCl$_3$, 400 MHz): 7.05-6.87 (m, 10H, b, k, l), 5.65 (s br, 2H, e), 4.78 (apparent t, $J = 7.6$ Hz, 2H, f)[†], 4.28-4.17 (m, 2H, g/H$_X$), 3.92 (s, 2H, a), 3.72-3.60 (m, 4H, i/H$_{A,B}$), 2.61 (s br, 8H, c), 2.03 (apparent d, $J = 4.3$ Hz, 12H, j)[†], 1.36 (apparent dd, $J = 6.7, 5.1$ Hz, 6H, h)[†], 1.16 (t, $J = 7.6$ Hz, 12H, d).

† Compound 1 was synthesised using a racemic starting material and the product is therefore a mixture of meso and rac diastereoisomers. As a result, peaks in the ^{1}H NMR spectrum corresponding to environments 'f', 'j' and 'h' have a higher apparent multiplicity due to the overlapping of signals from each diastereoisomer.

Due to the lower resolution of solid-state NMR, many peaks in the ^{13}C spectrum overlap, and the spectrum is also complicated by the presence of multiple diastereoisomers. Tentative peak assignments are given, based on the spectra of other mexiletine-terminated gelators.

^{13}C NMR (CP-MAS SS NMR, 101 MHz): 158.00 (C=O), 154.58 (ArC), 141.05 (ArC), 132.58 (ArC), 130.81 (ArC), 129.78 (ArC), 127.81 (ArC), 125.89 (ArC), 123.91 (ArC), 76.10 (Ar-O-CH$_2$), 45.73 (NH-CH-CH$_3$), 42.74 (Ar-CH$_2$-Ar), 24.30 (AR-CH$_2$-CH$_3$), 23.20 (O-Ar-CH$_3$), 15.88 (NH-CH-CH$_3$), 13.47 (Ar-CH$_2$-CH$_3$).

m/z ESI-MS (MeCN): retention time 3.91 min, 721.7 [M+H]$^+$.

Elemental Analysis: Calc. (%): C 74.96, H 8.39, N 7.77; Found (%): C 74.74, H 8.32, N 7.69.

Figure 5.2: A gelled NMR sample of compound **1** in CDCl$_3$.

Synthesis and characterisation of Compound 2
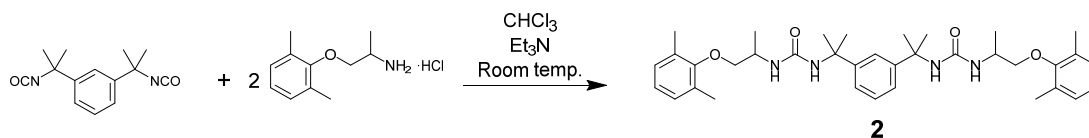
Racemic mexiletine hydrochloride (1.42 g, 6.6 mmol) was suspended in chloroform (80 mL) and dissolved upon the addition of excess triethylamine (1 mL). 1,3-Bis(1-isocyanato-1-methylethyl)benzene (0.69 mL, 3 mmol) was added and the solution was stirred at room temperature for 24 hours. The solvent was removed under vacuum and the crude product was sonicated for 10 minutes in water (100 mL) and then acetonitrile (50 mL), to yield compound **2** as a white solid (1.31 g, 2.18 mmol, 73 %).
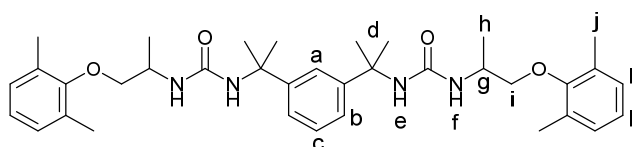
^{1}H NMR (DMSO-d6, 599 MHz): δ 7.33 – 7.29 (m, 1H, c), 7.17 – 7.10 (m, 3H, a, b), 6.97 (d, J = 7.5 Hz, 4H, k), 6.87 (t, J = 7.5 Hz, 2H, l), 6.28 (s, 2H, e), 5.94 (d, J = 8.2 Hz, 2H, f), 3.86 – 3.78 (m, 2H, g/H$_X$)†, 3.58 (ABq, J_{AB} = -9.5 Hz, J_{AX} = 1.61 Hz, 2H, i/H$_A$)†, 3.56 (ABq, J_{AB} = -9.5, J_{BX} = 0.2 Hz, 2H, i/H$_B$)†, 2.19 (s, 12H, j), 1.48 (apparent t, J = 5.6 Hz, 12H, d)*, 1.19 (d, J = 6.7 Hz, 6H, h).

† See Figure 5.3 for further details of the assignment of these peaks.

*See Figure 5.4 for further details of the assignment of these peaks.
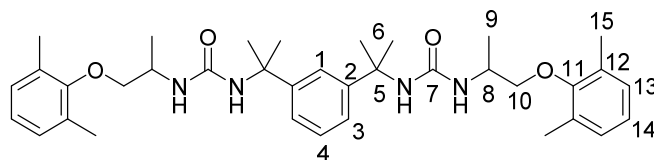
13C {1H} NMR (DMSO-d6, 151 MHz,) δ 157.00 (C7), 155.52 (C12), 148.86 (C2), 130.80 (C11), 129.17 (C13), 127.69 (C1), 124.10 (C14), 122.77 (C3), 121.71 (C4), 75.15 (C10), 54.72 (C5), 45.34 (C8), 30.67 (C6)*, 30.61 (C6)*, 30.52 (C6)*, 30.46 (C6)*, 18.52 (C9), 16.32 (C15).

*See Figure 5.4 for further details of the assignment of these peaks.

m/z ESI-MS (MeCN): retention time 3.40 min, 603.9 [M+H]$^+$, 1205.8 [2M+H]$^+$.

Elemental Analysis: Calc. (%): C 71.73, H 8.36, N 9.29; Found (%): C 71.32, H 8.24, N 9.29.

Protons 'i' and 'g' make up an ABX system as shown in Figure 5.3. The signals corresponding to H_A and H_B (environment i) could be assigned as two AB quartets however, the difference in chemical shift between the two signals is very small, so the central peak overlaps, and the signal contains 7 lines instead of 8. The pure shift signal for protons 'i' is an apparent triplet, in which the central peak is an artefact that indicates strong coupling between the two geminal protons. The proton signal corresponding to H_X (environment g) is further complicated by coupling to protons 'h', so the multiplicity of this peak could not be assigned.
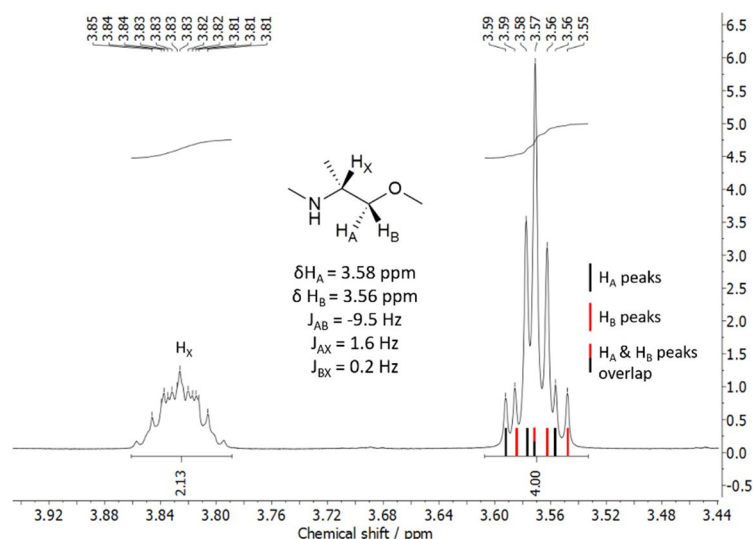
Figure 5.3: Section of the ^{1}H NMR spectrum of compound **2** showing the ABX system: protons in environments 'i' and 'g'

Compound **2** was synthesised using a racemic starting material and the product is therefore a mixture of meso and rac diastereoisomers. As a result, protons 'd' produce 4 separate NMR signals: one from each methyl group in the two diastereoisomers. The two central peaks in this signal overlap, so the signal appears as a triplet in both the pure shift and ^{1}H NMR spectra. Four distinct signals are however visible in the carbon spectrum of these methyl groups (Figure 5.4).
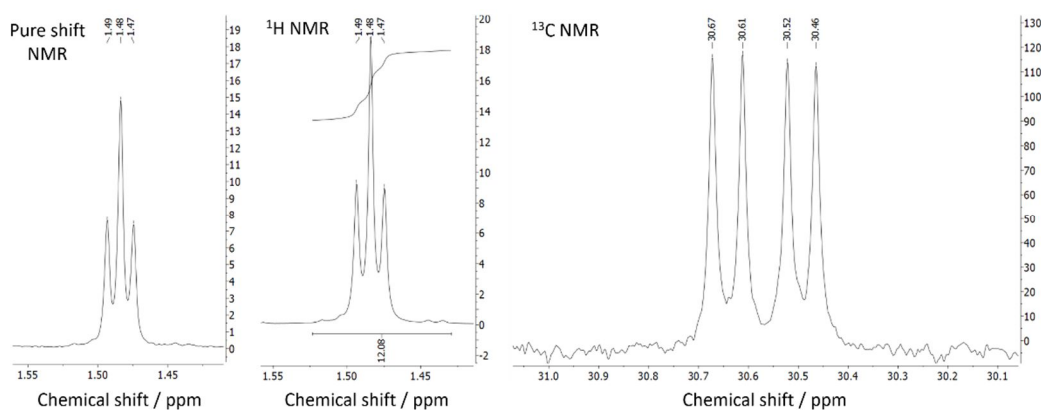
Figure 5.4: Sections of the pure shift, ^{1}H NMR and ^{13}C NMR spectra of compound **2**, corresponding to protons in environment 'd'.

Synthesis and characterisation of Compound 3
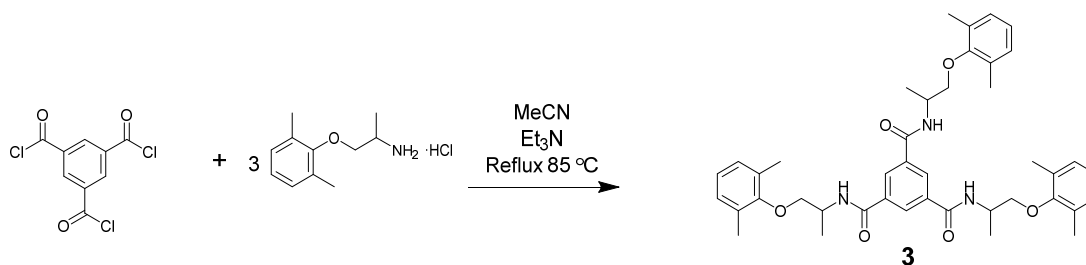
Racemic mexiletine hydrochloride (3.22 g, 13.2 mmol) was suspended in acetonitrile (200 mL) and dissolved upon the addition of excess triethylamine (5 mL). 1,3,5-Benzenetricarbonyl trichloride (1.00 g, 3.77 mmol) was added, the reaction was heated to reflux and stirred for 24 hours. The solvent was removed under vacuum and the crude product was dissolved in DCM (300 mL), washed with water (3 x 200 mL) and recrystallised from THF/diethyl ether to yield compound **3** as a white solid (1.04g, 1.5 mmol, 40 %).
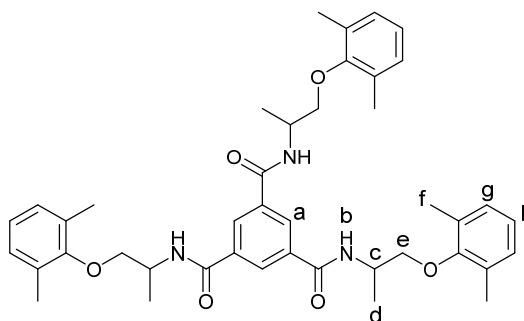
^{1}H NMR (DMSO-d$_6$, 599 MHz): δ 8.66 (d, J = 8.1 Hz, 3H, b), 8.44 (apparent d, J = 3.2 Hz, 3H, a)†, 6.97 (d, J = 7.5 Hz, 6H, g), 6.87 (t, J = 7.5 Hz, 3H, h), 4.47 – 4.37 (m, 3H, c)†, 3.81 – 3.71 (m, 6H, e)†, 2.18 (s, 18H, f), 1.34 (d, J = 6.9 Hz, 9H, d).

† See Figure 5.5 for further details on the assignment of these peaks.
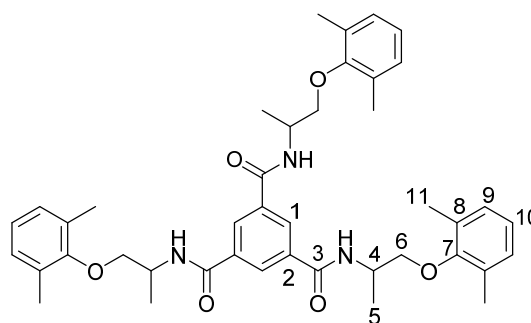
$^{13}C\{^1H\}$ NMR (DMSO-d_6, 151 MHz): δ 165.71 (C3)*, 165.69 (C3)*, 165.67 (C3)*, 155.53 (C8), 135.49 (C2)*, 135.47 (C2)*, 130.74 (C7), 129.20 (C9), 129.16 (C1), 124.18 (C10), 74.37 (C6), 46.08 (C4), 17.61 (C5), 16.33 (C11).

* See Figure 5.6 for further details of the assignment of these peaks

m/z ESI-MS (MeOH): retention time 4.18 min, 694.4 [M+H]$^+$, 716.4 [M+Na]$^+$, 732.3 [M+K]$^+$, 1409.7 [2M+Na]$^+$, 1425.5 [2M+K]$^+$.

Elemental Analysis: Calc. (%): C 72.70, H 7.41, N 6.06; Found (%): C 72.28, H 7.31, N 5.95.

Compound 3 was synthesised using a racemic starting material and the product is therefore a mixture of eight stereoisomers. Six of these are diastereoisomers that produce unique NMR signals. The presence of multiple diastereoisomers leads to overlapping signals in the pure shift spectrum and a higher apparent multiplicity of signals in the proton spectrum, such as the apparent doublet at 8.44 ppm corresponding to protons 'a' (Figure 5.5). Similarly, overlapping signals from multiple isomers mean that the ABX system, corresponding to protons 'c' and 'e', cannot be fully resolved. However, the typical pattern of repeating AB quartets can be observed in the multiplet at 3.81-3.71 ppm. The pure shift signal for the two geminal protons, 'e', also contains several artefact peaks that are indicate strong coupling between the two protons

(Figure 5.5). The presence of multiple diastereoisomers is also evident in the carbon spectrum, where there are multiple peaks corresponding to carbon environments 2 and 3 (Figure 5.6).
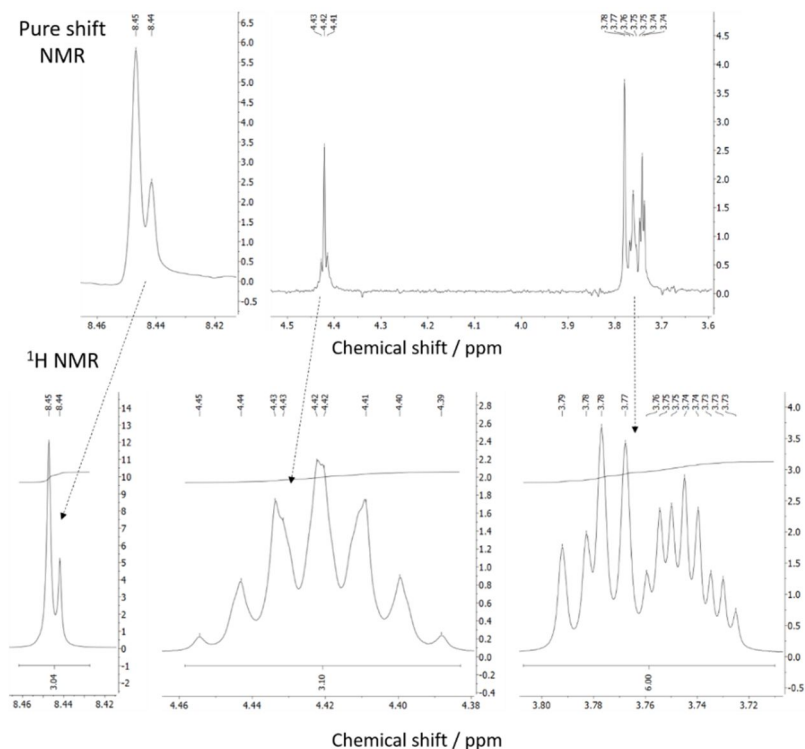
Figure 5.5: Sections of ^{1}H and pure shift NMR spectra of compound 2 showing the effects of multiple stereoisomers on environments 'a', 'c' and 'e'.
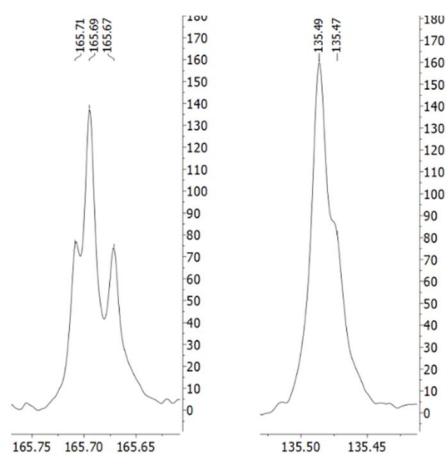
Figure 5.6: Sections of the ^{13}C NMR spectrum of compound **3** showing signals from environments 2 and 3 in multiple diastereoisomers.

Detailed gel screening procedure

The gelation behaviour of compounds **1**, **2** and **3** were investigated in a wide range of solvents. A 2 % w/v solution was produced by dissolving 10 mg of the gelator in 0.5 mL of the required solvent by heating the mixture with a heat gun, in a sealed glass vial. The solution was left to cool to room temperature in an insulating wooden block and was monitored visually for gelation and crystal growth.

5.6   Chapter 5: Supramolecular Gelation as the First Stage in Ostwald's Rule

Synthesis and characterisation of I-TPI
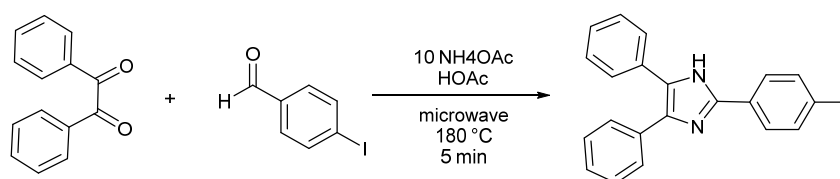
I-TPI was synthesised according to the literature method.[15] Benzil (0.42 g, 2 mmol), 4-iodobenzaldehyde (0.46 g, 2 mmol) and ammonium acetate (1.54 g, 20 mmol) were suspended in acetic acid (10 mL) in a 20 mL microwave reaction vessel containing a PTFE stirrer bar. Using a microwave, the vessel was heated for 5 min at 180 °C and then allowed to cool to room temperature. The mixture was added dropwise to a concentrated ammonium hydroxide solution at 0 °C. The resulting white precipitate was collected, washed with water, and dried in an oven, yielding I-TPI as a white solid (844.5 mg, 92 %). Characterisation data from ^{1}H NMR, ^{13}C{^{1}H} NMR spectroscopy and mass spectrometry conformed to the previous literature.[16, 17]

^{1}H NMR (400 MHz, DMSO-d$_6$) δ 12.78 (s, 1H, N<u>H</u>), 7.95 – 7.78 (m, 4H, Ar<u>H</u>), 7.66 – 7.04 (m, 11H, Ar<u>H</u>).

^{13}C{^{1}H} NMR (101 MHz, DMSO) δ 145.11, 137.95, 137.81, 135.47, 131.38, 130.31, 129.13, 129.07, 128.89, 128.67, 128.33, 127.60, 127.56, 127.08, 94.89.

m/z ESI-MS 423.2 [M+H].

Elemental Analysis: Calc. (%) C 59.73 H 3.58 N 6.63; Found (%) C 59.91 H 3.51 N 6.75.

Detailed gel screening procedure

The gelation behaviour of I-TPI was investigated in a wide range of solvents. A 2 % w/v solution was produced by combining 10 mg of I-TPI and 0.5 mL of methanol in a sealed glass vial and heating with a heat gun until the solid dissolved. The solution was left to cool to room temperature in an insulating wooden block and monitored visually for gelation and crystal growth.

For gels containing solid additives, samples were prepared by combining 10 mg of I-TPI with the required mass of additive and dissolving in 0.5 mL methanol before cooling to room temperature. Gelation of solvent mixtures was also investigated, and in this case the 0.5 mL mixture contained mostly methanol, with 5-70 μL of another solvent.

5.7 References

1. G. J. Piermarini, S. Block, J. D. Barnett and R. A. Forman, *J. Appl. Phys.*, 1975, **46**, 2774-2780.

2. M. R. Probert, J. A. Coome, A. E. Goeta and J. A. Howard, *Acta Crystallogr., Sect. A: Found. Crystallogr.*, 2011, **67**, 528.

3. M. R. Probert, C. M. Robertson, J. A. Coome, J. A. Howard, B. C. Michell and A. E. Goeta, *J. Appl. Crystallogr.*, 2010, **43**, 1415-1418.

4. T. Schulz, K. Meindl, D. Leusser, D. Stern, J. Graf, C. Michaelsen, M. Ruf, G. M. Sheldrick and D. Stalke, *J. Appl. Crystallogr.*, 2009, **42**, 885-891.

5. O. V. Dolomanov, L. J. Bourhis, R. J. Gildea, J. A. Howard and H. Puschmann, *J. Appl. Crystallogr.*, 2009, **42**, 339-341.

6. G. Sheldrick, *Acta Crystallogr., Sect. C: Struct. Chem.*, 2015, **71**, 3-8.

7. J. A. Chisholm and S. Motherwell, *J. Appl. Crystallogr.*, 2005, **38**, 228-231.

8. A. J. Cruz-Cabeza and J. Bernstein, *Chem. Rev.*, 2014, **114**, 2170-2191.

9. M. J. Frisch, G. W. Trucks, H. B. Schlegel, G. E. Scuseria, M. A. Robb, J. R. Cheeseman, G. Scalmani, V. Barone, G. A. Petersson, H. Nakatsuji, X. Li, M. Caricato, A. Marenich, J. Bloino, B. G. Janesko, R. Gomperts, B. Mennucci, H. P. Hratchian, J. V. Ortiz, A. F. Izmaylov, J. L. Sonnenberg, D. Williams-Young, F. Ding, F. Lipparini, F. Egidi, J. Goings, B. Peng, A. Petrone, T. Henderson, D. Ranasinghe, V. G. Zakrzewski, J. Gao, N. Rega, G. Zheng, W. Liang, M. Hada, M. Ehara, K. Toyota, R. Fukuda, J. Hasegawa, M. Ishida, T. Nakajima, Y. Honda, O. Kitao, H. Nakai, T. Vreven, K. Throssell, J. J. A. Montgomery, J. E. Peralta, F. Ogliaro, M. Bearpark, J. J. Heyd, E. Brothers, K. N. Kudin, V. N. Staroverov, T. Keith, R. Kobayashi, J. Normand, K. Raghavachari, A. Rendell, J. C. Burant, S. S. Iyengar, J. Tomasi, M. Cossi, J. M. Millam, M. Klene, C. Adamo, R. Cammi, J. W. Ochterski, R. L. Martin, K. Morokuma, O. Farkas, J. B. Foresman and D. J. Fox, Gaussian 09 (Revision D.01), Gaussian Inc, Wallingford, CT, 2016.

10. A. Broo and S. O. Nilsson Lill, *Acta Crystallogr., Sect. B: Struct. Sci., Cryst. Eng. Mater.*, 2016, **72**, 460-476.

11. M. A. Neumann and M.-A. Perrin, *J. Phys. Chem. B*, 2005, **109**, 15531-15541.

12. M. A. Neumann, F. J. J. Leusen and J. Kendrick, *Angew. Chem., Int. Ed.*, 2008, **47**, 2427-2430.

13. J. P. Perdew, K. Burke and M. Ernzerhof, *Phys. Rev. Lett.*, 1996, **77**, 3865-3868.

14. H. J. Knolker, T. Braxmeier and G. Schlechtingen, *Angew. Chem., Int. Ed.*, 1995, **34**, 2497-2500.

15. S. E. Wolkenberg, D. D. Wisnoski, W. H. Leister, Y. Wang, Z. Zhao and C. W. Lindsley, *Org. Lett.*, 2004, **6**, 1453-1456.

16. G. Nagalakshmi, *J. Chem.*, 2008, **5**, 447-452.

17. A. Puratchikody, S. Gopalakrishnan and M. Nallu, *Indian J. Pharm. Sci.*, 2005, **67**, 725.

6. Concluding Remarks

6.1   Conclusion

This work exemplifies a modern pharmaceutical polymorph screen; using novel crystallisation methods and analytical tools to capture a wider polymorph landscape than traditional, solution-phase screens. Two APIs were studied in this work: mexiletine hydrochloride, an anti-arrhythmic drug, which was reported to have six polymorphs in the literature[1-4], and diatrizoic acid, an X-ray contrast agent, of which two hydrates, nine solvates and three anhydrous polymorphs have been reported to date.[5]

First, a polymorph screen of mexiletine hydrochloride was carried out using traditional crystallisation methods including cooling, evaporation, anti-solvent precipitation and sublimation. Comparing the X-ray diffraction data for each form showed that there are actually seven solid forms of mexiletine: an enantiotropic pair of anhydrous polymorphs that are stable at different temperatures, one anhydrous metastable form, three families of isostructural channel solvates and one further solvate, which requires further study to fully understand its structure. Solid-state NMR was used to characterise the highly disordered solvent that was loosely bound within the channels, leading to the identification of eleven modifications of the Type A and B solvate families. Computational crystal structure prediction identified a low-energy, high-density predicted form, which may be accessible using high-pressure crystallography. When a single crystal of Form 2, which has the same molecular conformation as the predicted form, was compressed to 3.56 GPa, a novel unit cell was observed. Interestingly, this unit cell was different to the predicted form. These

results demonstrate the powerful combination of computational and experimental tools in determining the polymorph landscape of an API.

Gel-phase crystallisation was used to further expand the polymorph screen of mexiletine hydrochloride. Three novel, drug-mimetic supramolecular gelators were synthesised by attaching the free base of the drug to a central gel-forming group. Once self-assembled, the surface of the gel fibres is functionalised with drug-mimetic units, to act as a template for the nucleation and growth of high-energy solid forms. Crystallisation within the two bis-urea gels led to significant changes in solid form, including new routes to known Forms 2, 3 and a Type A solvate, and the crystallisation of two new Type A solvates. Crystallisation within this gel is the only known route to crystallise the high temperature stable Form 2 at room temperature, which demonstrates the profound ability of this gel network to stabilise high-energy solid forms. In several cases, gelation was switched off when a change in polymorphism was observed, which suggests that strong interactions between the drug and gelator are a key driving force for the crystallisation of novel polymorphs in this system.[6]

A second gel-phase crystallisation study showed that structural mimicry is not the only mechanism by which a gelator can interact with a drug molecule and influence the outcome of a crystallisation. When diatrizoic acid (DTA) was crystallised within an iodo-triphenyl imidazole (I-TPI) gel, two solid forms were produced, following the same two-step crystallisation process as the gelator itself. In accordance with Ostwald's rule of stages, the gel formed first and then, a highly metastable solvate containing DTA and I-TPI grew within it. Over time, the gel broke down and the crystals transformed into a more stable salt solvate, also containing DTA and I-TPI. This pattern reflects the crystallisation behaviour of the gelator, in which a metastable

methanol solvate grows within the gel, and then transforms into a more stable methanol solvate after the gel has broken down. The spontaneous crystallisation of these gels suggests that supramolecular gelation should be considered an early stage in the crystallisation regime of the gelator, rather than an entirely separate process. The two-step crystallisation behaviour was transferred to the API, which suggests that the polymorph landscape of the gelator can influence the crystallising drug, and this may provide a new avenue of inquiry in the design of supramolecular gelators for gel-phase crystallisation of pharmaceuticals.

6.2   Further Work

To expand the polymorph screen of mexiletine hydrochloride, further crystallisations should be carried out to record a higher precision crystal structure of a Type B solvate. This task proved extremely difficult due to the highly disordered solvent contained within the channels and the tendency of mexiletine to crystallise in a needle-like habit. To overcome these problems, a precise crystallisation procedure could be developed by calculating the solubility curve of mexiletine in a solvent known to form a Type B solvate, and using that data to ensure that all variables are tightly controlled, so that very few nuclei are produced and they are allowed to grow slowly into a high-quality single crystal. A programmable temperature controller such as the Polar Bear crystallisation reactor would be an ideal tool for this work.[7] A single-crystal structure should also be collected of the Type D nitrobenzene solvate discussed in Chapter 3. Although this form is much easier to crystallise in high quality than the Type B solvates, the data collection will most likely require synchrotron radiation because it crystallises as small needles.

The mexiletine polymorph screen provides a template for further investigations into the polymorph landscape of this drug in unusual solvents and under non-ambient conditions. To extend this work, cooling, evaporation, and anti-solvent crystallisations should be carried out in the rest of the solvents that were used for gel screening. These results will act as a control for further gel-phase crystallisation experiments and are also likely to identify new polymorphs of mexiletine, given the extremely prolific solvate formation observed in this work. Particular attention should be paid to finding new members of the Type C and D solvate families, as there are likely to be more than the two forms identified in Chapter 3. Any new forms could be characterised and compared to the known forms, using the techniques described in Chapter 2. Further experiments should also be undertaken to understand the polymorphism of mexiletine at high pressure, to fully characterise the high-pressure form identified by a unit cell in this work, and to try and find the high-density form that was predicted computationally. As the high-pressure unit cell was not consistent with the predicted form, there is clearly a high potential for further work in this area, which may include compressing crystals of known forms, or recrystalising mexiletine from a solution at high pressure.[8]

Further investigation into the gel-phase crystallisation of mexiletine hydrochloride would involve crystallisations within gels of the three gelators discussed in this work, in all remaining solvents. The design of new gelators should focus on bis-ureas because they displayed significantly more versatile gelation behaviour than the tris-amide. The two linking groups used in this work are widely known to produce effective gelators and it would therefore be prudent to focus future efforts on developing new end groups. There have been several recent works describing drug mimetic end-groups[9-11] and so new mechanisms of creating a drug-gel interaction

should also be considered. Gelators that bind the counterion of a pharmaceutical salt, instead of the drug itself, would be a key development in this area as the same gelator could interact with a large group of drugs, which would drastically increase the scope of this technique. Classical supramolecular chemistry such as ion binding[12, 13] and supramolecular synthons[14] should provide the basis for the design of these end-groups. To extend this work using mexiletine hydrochloride, a salt screen could be carried out to find other salt forms that might be easy targets for new gelators.

As gelation was not discovered in any previous polymorph screens of other TPI derivatives,[15] it is likely that the gelation of I-TPI is unique within this family of molecules and so further study of I-TPI as a gelator is not recommended. Instead, this study highlights the importance of understanding the polymorph landscape of new gelators. Further investigations are required to establish whether gelator polymorphism can be exploited to influence the crystallisation of a substrate within the gel, as observed with I-TPI.

6.3 References

1. J. Sivy, V. Kettmann and E. Fresova, *Acta Crystallogr., Sect. C: Cryst. Struct. Commun.*, 1991, **47**, 2695-2696.

2. M. Kuhnert, D. Seidel and G. Unterkircher, *Sci. Pharm.*, 1987, **55**, 13-25.

3. A. Kiss and J. Repasi, *Analyst*, 1993, **118**, 661-664.

4. A. M. Namespetra, D. A. Hirsh, M. P. Hildebrand, A. R. Sandre, H. Hamaed, J. M. Rawson and R. W. Schurko, *CrystEngComm*, 2016, **18**, 6213-6232.

5. K. Fucke, G. J. McIntyre, M.-H. Lemée-Cailleau, C. Wilkinson, A. J. Edwards, J. A. K. Howard and J. W. Steed, *Chem. - Eur. J.*, 2015, **21**, 1036-1047.

6. A. Dawn, M. Mirzamani, C. D. Jones, D. S. Yufit, S. Qian, J. W. Steed and H. Kumari, *Soft Matter*, 2018, **14**, 9489-9497.

7. D. L. Browne, B. H. Harji and S. V. Ley, *Chem. Eng. Technol.*, 2013, **36**, 959-967.

8. B. A. Zakharov and E. V. Boldyreva, *CrystEngComm*, 2019, **21**, 10-22.

9. S. R. Kennedy, C. D. Jones, D. S. Yufit, C. E. Nicholson, S. J. Cooper and J. W. Steed, *CrystEngComm*, 2018, **20**, 1390-1398.

10. A. Dawn, K. S. Andrew, D. S. Yufit, Y. Hong, J. P. Reddy, C. D. Jones, J. A. Aguilar and J. W. Steed, *Cryst. Growth Des.*, 2015, **15**, 4591-4599.

11. J. A. Foster, K. K. Damodaran, A. Maurin, G. M. Day, H. P. G. Thompson, G. J. Cameron, J. C. Bernal and J. W. Steed, *Chem. Sci.*, 2017, **8**, 78-84.

12. J. W. Steed and J. L. Atwood, in *Supramolecular Chemistry*, John Wiley & Sons, Chichester, 2nd edn., 2009, ch. 3, pp. 105-222.

13. J. W. Steed and J. L. Atwood, in *Supramolecular Chemistry*, John Wiley & Sons, Chichester, 2nd edn., 2009, ch. 4, pp. 223-284.

14. G. R. Desiraju, *Angew. Chem., Int. Ed.*, 1995, **34**, 2311-2327.

15. T. Kitchen, C. Melvin, M. N. Mohd Najib, A. S. Batsanov and K. Edkins, *Cryst. Growth Des.*, 2016, **16**, 4531-4538.

7. Appendices

7.1 Full crystallographic information for the novel polymorphs of mexiletine hydrochloride

Table 7.1: Crystallographic information for Form 2 of mexiletine hydrochloride.

Crystallisation conditions	Sublimation at 150 °C
Empirical formula	$C_{11}H_{18}ClNO$
Formula weight	215.71
Temperature/K	120
Crystal system	orthorhombic
Space group	Pccn
a/Å	17.8741(14)
b/Å	18.6782(15)
c/Å	7.3464(7)
α/°	90
β/°	90
γ/°	90
Volume/Å^3	2452.6(4)
Z	8
ρ_{calc} g/cm^3	1.168
μ /mm^{-1}	0.283
F(000)	928.0
Crystal size/mm^3	0.602 × 0.077 × 0.066
Radiation	MoKα (λ = 0.71073)
2Θ range for data collection/°	4.558 to 52.956
Index ranges	-22 ≤ h ≤ 22, -23 ≤ k ≤ 23, -9 ≤ l ≤ 9
Reflections collected	39104
Independent reflections	2530 [R_{int} = 0.1043, R_{sigma} = 0.0434]
Data/restraints/parameters	2530/114/227
Goodness-of-fit on F^2	1.177
Final R indexes [I>=2σ (I)]	R_1 = 0.0817, wR_2 = 0.1617
Final R indexes [all data]	R_1 = 0.1076, wR_2 = 0.1712
Largest diff. peak/hole / e Å^{-3}	0.38/-0.25

Table 7.2: Crystallographic information for the Type A solvent-free form of mexiletine hydrochloride.

Crystallisation conditions	Slow cooling from a supersaturated solution in DCM
Empirical formula	$C_{11}H_{18}ClNO$
Formula weight	215.71
Temperature/K	100.0
Crystal system	orthorhombic
Space group	Pbcn
a/Å	20.8570(2)
b/Å	17.3783(18)
c/Å	7.5648(8)
α/°	90
β/°	90
γ/°	90
Volume/Å^3	2741.9(5)
Z	8
ρ_{calc} g/cm^3	1.045
μ /mm^{-1}	0.234
F(000)	928.0
Crystal size/mm^3	$0.08 \times 0.01 \times 0.01$
Radiation	synchrotron ($\lambda = 0.6889$)
2Θ range for data collection/°	2.956 to 54.994
Index ranges	$-27 \leq h \leq 27$, $-23 \leq k \leq 23$, $-10 \leq l \leq 10$
Reflections collected	22800
Independent reflections	3462 [$R_{int} = 0.1137$, $R_{sigma} = 0.1464$]
Data/restraints/parameters	3462/0/142
Goodness-of-fit on F^2	1.031
Final R indexes [I>=2σ (I)]	$R_1 = 0.0808$, $wR_2 = 0.2112$
Final R indexes [all data]	$R_1 = 0.1071$, $wR_2 = 0.2346$
Largest diff. peak/hole / e Å^{-3}	0.87/-0.22

Table 7.3: Crystallographic information for the Type A methanol solvate of mexiletine hydrochloride.

Crystallisation conditions	Slow cooling from a supersaturated solution in methanol
Empirical formula	$C_{12}H_{22}ClNO_2$
Formula weight	247.76
Temperature/K	120.0
Crystal system	orthorhombic
Space group	Pbcn
a/Å	20.2427(7)
b/Å	18.7675(6)
c/Å	7.5502(2)
α/°	90
β/°	90
γ/°	90
Volume/Å^3	2868.4(15)
Z	8
ρ_{calc} g/cm^3	1.147
μ /mm^{-1}	2.263
F(000)	1072.0
Crystal size/mm^3	0.33 × 0.12 × 0.1
Radiation	CuKα (λ = 1.54178)
2Θ range for data collection/°	6.42 to 144.98
Index ranges	-24 ≤ h ≤ 21, -23 ≤ k ≤ 23, -9 ≤ l ≤ 9
Reflections collected	31273
Independent reflections	2817 [R_{int} = 0.0300, R_{sigma} = 0.0141]
Data/restraints/parameters	2817/0/150
Goodness-of-fit on F^2	1.072
Final R indexes [I>=2σ (I)]	R_1 = 0.0357, wR_2 = 0.0972
Final R indexes [all data]	R_1 = 0.0385, wR_2 = 0.0993
Largest diff. peak/hole / e Å^{-3}	0.41/-0.38

Table 7.4: Crystallographic information for the Type A diethyl ether solvate of mexiletine hydrochloride.

Crystallisation conditions	Vapour diffusion of diethyl ether into a saturated solution in DMF
Empirical formula	$C_{11}H_{18}ClNO$
Formula weight	215.71
Temperature/K	120
Crystal system	orthorhombic
Space group	Pbcn
a/Å	21.125(2)
b/Å	17.3581(16)
c/Å	7.5625(7)
α/°	90
β/°	90
γ/°	90
Volume/Å^3	2773.1(4)
Z	8
ρ_{calc} g/cm^3	1.033
μ /mm^{-1}	0.250
F(000)	928.0
Crystal size/mm^3	$0.286 \times 0.149 \times 0.075$
Radiation	MoKα (λ = 0.71073)
2Θ range for data collection/°	4.694 to 50
Index ranges	$-25 \leq h \leq 25, -20 \leq k \leq 20, -8 \leq l \leq 8$
Reflections collected	40312
Independent reflections	2442 [R_{int} = 0.0562, R_{sigma} = 0.0269]
Data/restraints/parameters	2442/0/146
Goodness-of-fit on F^2	1.112
Final R indexes [I>=2σ (I)]	R_1 = 0.0397, wR_2 = 0.0953
Final R indexes [all data]	R_1 = 0.0514, wR_2 = 0.1004
Largest diff. peak/hole / e Å^{-3}	0.21/-0.18

Table 7.5: Crystallographic information for the Type A octane solvates of mexiletine hydrochloride.

Crystallisation conditions	Vapour diffusion of octane into a saturated solution in 1PrOH	Vapour diffusion of octane into a saturated solution in 2BuOH
Empirical formula	$C_{11}H_{18}ClNO$	$C_{11}H_{18}ClNO$
Formula weight	215.71	215.71
Temperature/K	120	120
Crystal system	orthorhombic	orthorhombic
Space group	Pbcn	Pbcn
a/Å	21.9358(13)	21.9241(14)
b/Å	17.1061(10)	17.1098(11)
c/Å	7.5214(5)	7.5198(5)
α/°	90	90
β/°	90	90
γ/°	90	90
Volume/Å^3	2822.3(3)	2820.8(3)
Z	8	8
ρ_{calc} g/cm^3	1.015	1.016
μ /mm^{-1}	0.246	0.246
F(000)	928.0	928.0
Crystal size/mm^3	$0.579 \times 0.164 \times 0.091$	$0.474 \times 0.136 \times 0.074$
Radiation	MoKα (λ = 0.71073)	MoKα (λ = 0.71073)
2Θ range for data collection/°	4.762 to 56.56	4.762 to 53.998
Index ranges	$-29 \leq h \leq 29$, $-22 \leq k \leq 22$, $-10 \leq l \leq 10$	$-28 \leq h \leq 28$, $-21 \leq k \leq 21$, $-9 \leq l \leq 9$
Reflections collected	51696	35849
Independent reflections	3495 [R_{int} = 0.1460, R_{sigma} = 0.0701]	3082 [R_{int} = 0.1071, R_{sigma} = 0.0548]
Data/restraints/parameters	3495/0/131	3082/0/188
Goodness-of-fit on F^2	1.033	1.036
Final R indexes [I$>$=2σ (I)]	R_1 = 0.0543, wR_2 = 0.1222	R_1 = 0.0458, wR_2 = 0.0963
Final R indexes [all data]	R_1 = 0.0864, wR_2 = 0.1345	R_1 = 0.0795, wR_2 = 0.1079
Largest diff. peak/hole / e Å^{-3}	0.31/-0.28	0.22/-0.23

Table 7.6: Crystallographic information for the Type A hexane solvates of mexiletine hydrochloride.

Crystallisation conditions	Vapour diffusion of hexane into a saturated solution in 2PrOH	Vapour diffusion of hexane into a saturated solution in DCM
Empirical formula	$C_{11}H_{18}ClNO$	$C_{11}H_{18}ClNO$
Formula weight	215.71	215.71
Temperature/K	120	120
Crystal system	orthorhombic	orthorhombic
Space group	Pbcn	Pbcn
a/Å	21.8754(17)	21.4560(3)
b/Å	17.2112(13)	17.3330(2)
c/Å	7.5109(6)	7.5478(11)
α/°	90	90
β/°	90	90
γ/°	90	90
Volume/Å^3	2827.9(4)	2807.0(7)
Z	8	8
ρ_{calc} g/cm^3	1.013	1.021
μ /mm^{-1}	0.246	0.247
F(000)	928.0	928.0
Crystal size/mm^3	0.425 × 0.147 × 0.062	0.47 × 0.12 × 0.045
Radiation	MoKα (λ = 0.71073)	MoKα (λ = 0.71073)
2Θ range for data collection/°	4.734 to 48.814	4.7 to 61.112
Index ranges	-25 ≤ h ≤ 25, -20 ≤ k ≤ 20, -8 ≤ l ≤ 8	-30 ≤ h ≤ 30, -24 ≤ k ≤ 24, -10 ≤ l ≤ 10
Reflections collected	39413	44762
Independent reflections	2331 [R_{int} = 0.1388, R_{sigma} = 0.0569]	4298 [R_{int} = 0.1687, R_{sigma} = 0.1095]
Data/restraints/parameters	2331/0/131	4298/0/131
Goodness-of-fit on F^2	1.059	1.034
Final R indexes [I>=2σ (I)]	R_1 = 0.0468, wR_2 = 0.1015	R_1 = 0.0970, wR_2 = 0.2423
Final R indexes [all data]	R_1 = 0.0715, wR_2 = 0.1098	R_1 = 0.1721, wR_2 = 0.2763
Largest diff. peak/hole / e Å^{-3}	0.27/-0.21	0.38/-0.64

Table 7.7: Crystallographic information for the Type C 1,2,4-trichlorobenzene solvate of mexiletine.

Crystallisation conditions	Slow cooling from a supersaturated solution in 1,2,4-trichlorobenzene
Empirical formula	$C_{50}H_{75}Cl_7N_4O_4$
Formula weight	1044.29
Temperature/K	100.0
Crystal system	monoclinic
Space group	$P2_1/c$
a/Å	7.538(3)
b/Å	20.972(9)
c/Å	18.043(8)
α/°	90
β/°	93.725(7)
γ/°	90
Volume/Å^3	2846.0(2)
Z	2
ρ_{calc} g/cm^3	1.219
μ /mm^{-1}	0.362
F(000)	1108.0
Crystal size/mm^3	0.14 × 0.015 × 0.005
Radiation	Synchrotron (λ = 0.6889)
2Θ range for data collection/°	2.89 to 42.986
Index ranges	-8 ≤ h ≤ 8, -22 ≤ k ≤ 22, -19 ≤ l ≤ 19
Reflections collected	20500
Independent reflections	3584 [R_{int} = 0.1746, R_{sigma} = 0.2670]
Data/restraints/parameters	3584/3/277
Goodness-of-fit on F^2	0.867
Final R indexes [I>=2σ (I)]	R_1 = 0.0873, wR_2 = 0.2208
Final R indexes [all data]	R_1 = 0.1593, wR_2 = 0.3023
Largest diff. peak/hole / e Å^{-3}	0.35/-0.20

Table 7.8: Crystallographic information for the co-crystal solvate containing mexiletine hydrochloride, iodine, and DCM.

Crystallisation conditions	Vapour diffusion of hexane into an equimolar solution of mexiletine and iodine in DCM
Empirical formula	$C_{11.5}H_{19}Cl_2INO$
Formula weight	385.08
Temperature/K	120.0
Crystal system	triclinic
Space group	P-1
a/Å	8.7220(9)
b/Å	13.6572(14)
c/Å	14.6845(14)
α/°	70.816(4)
β/°	76.280(4)
γ/°	78.824(4)
Volume/Å^3	1592.1(3)
Z	4
ρ_{calc} g/cm^3	1.607
μ /mm^{-1}	2.332
F(000)	760.0
Crystal size/mm^3	0.793 × 0.055 × 0.042
Radiation	MoKα (λ = 0.71073)
2Θ range for data collection/°	4.846 to 54.994
Index ranges	-11 ≤ h ≤ 11, -17 ≤ k ≤ 17, -19 ≤ l ≤ 19
Reflections collected	29037
Independent reflections	7310 [R_{int} = 0.1083, R_{sigma} = 0.1221]
Data/restraints/parameters	7310/7/341
Goodness-of-fit on F^2	1.037
Final R indexes [I>=2σ (I)]	R_1 = 0.0590, wR_2 = 0.1378
Final R indexes [all data]	R_1 = 0.1173, wR_2 = 0.1575
Largest diff. peak/hole / e Å^{-3}	1.62/-1.61

7.2 Full crystallographic information for the novel polymorphs of I-TPI

Table 7.9: Crystallographic information for Form SI of I-TPI.

Crystallisation conditions	Slow cooling from a supersaturated solution in methanol
Empirical formula	$C_{22}H_{19}IN_2O$
Formula weight	454.29
Temperature/K	120
Crystal system	monoclinic
Space group	$P2_1/c$
a/Å	12.6617(9)
b/Å	12.6076(11)
c/Å	12.7502(10)
α/°	90
β/°	109.050(19)
γ/°	90
Volume/Å^3	1923.9(3)
Z	4
ρ_{calc} g/cm^3	1.568
μ /mm^{-1}	1.677
F(000)	904.0
Crystal size/mm^3	$0.325 \times 0.316 \times 0.224$
Radiation	MoKα (λ = 0.71073)
2Θ range for data collection/°	4.676 to 51.996
Index ranges	$-15 \leq h \leq 14$, $-15 \leq k \leq 15$, $-15 \leq l \leq 15$
Reflections collected	22392
Independent reflections	3769 [R_{int} = 0.0459, R_{sigma} = 0.0299]
Data/restraints/parameters	3769/0/237
Goodness-of-fit on F^2	1.075
Final R indexes [I>=2σ (I)]	R_1 = 0.0244, wR_2 = 0.0548
Final R indexes [all data]	R_1 = 0.0351, wR_2 = 0.0601
Largest diff. peak/hole / e Å^{-3}	0.53/-0.65

Table 7.10: Crystallographic information for Form SII of I-TPI.

Crystallisation conditions	Grown from a 2 % w/v gel of I-TPI in methanol
Empirical formula	$C_{22}H_{19}IN_2O$
Formula weight	454.29
Temperature/K	120.0
Crystal system	monoclinic
Space group	$P2_1/c$
a/Å	6.0855(4)
b/Å	11.5907(8)
c/Å	27.2602(16)
α/°	90
β/°	92.094(19)
γ/°	90
Volume/Å^3	1921.5(2)
Z	4
ρ_{calc} g/cm^3	1.570
μ /mm^{-1}	1.679
F(000)	904.0
Crystal size/mm^3	$0.211 \times 0.068 \times 0.062$
Radiation	MoKα ($\lambda = 0.71073$)
2Θ range for data collection/°	4.614 to 53.562
Index ranges	$-7 \leq h \leq 7$, $-14 \leq k \leq 14$, $-34 \leq l \leq 34$
Reflections collected	27504
Independent reflections	4115 [$R_{int} = 0.0971$, $R_{sigma} = 0.0767$]
Data/restraints/parameters	4115/0/311
Goodness-of-fit on F^2	1.080
Final R indexes [I>=2σ (I)]	$R_1 = 0.0558$, $wR_2 = 0.0817$
Final R indexes [all data]	$R_1 = 0.1094$, $wR_2 = 0.0940$
Largest diff. peak/hole / e Å^{-3}	0.60/-0.89

Table 7.11: Crystallographic information for Form SIII of I-TPI.

Crystallisation conditions	A solution of 10 mg I-TPI, 10 μL H_2O and 0.49 mL MeOH, containing paper fibres as nucleation points was stored at room temperature in a sealed vial, for one week
Empirical formula	$C_{22}H_{19}IN_2O$
Formula weight	454.29
Temperature/K	120.0
Crystal system	monoclinic
Space group	$P2_1$
a/Å	14.6682(12)
b/Å	12.0909(10)
c/Å	17.3887(14)
α/°	90
β/°	110.237(3)
γ/°	90
Volume/Å^3	2893.5(4)
Z	6
ρ_{calc} g/cm^3	1.564
μ /mm^{-1}	1.673
F(000)	1356.0
Crystal size/mm^3	0.448 × 0.137 × 0.05
Radiation	MoKα (λ = 0.71073)
2Θ range for data collection/°	4.192 to 56
Index ranges	-19 ≤ h ≤ 19, -15 ≤ k ≤ 15, -22 ≤ l ≤ 22
Reflections collected	52934
Independent reflections	13959 [R_{int} = 0.1016, R_{sigma} = 0.1164]
Data/restraints/parameters	13959/7/707
Goodness-of-fit on F^2	1.029
Final R indexes [I>=2σ (I)]	R_1 = 0.0643, wR_2 = 0.1294
Final R indexes [all data]	R_1 = 0.1161, wR_2 = 0.1459
Largest diff. peak/hole / e Å^{-3}	0.92/-0.95
Flack parameter	0.04(3)

Table 7.12: Crystallographic information for Form V of I-TPI.

Crystallisation conditions	A solution of 10 mg I-TPI, 2 mg 1,4-diiodobenzene and 0.5 ml methanol was stored in a sealed vial at 50 °C for one week
Empirical formula	$C_{21}H_{15}IN_2$
Formula weight	422.25
Temperature/K	120.0
Crystal system	monoclinic
Space group	$P2_1$
a/Å	8.9217(7)
b/Å	32.728(2)
c/Å	11.9118(9)
α/°	90
β/°	94.579(3)
γ/°	90
Volume/Å^3	3467.0(5)
Z	8
ρ_{calc} g/cm^3	1.618
μ /mm^{-1}	1.851
F(000)	1664.0
Crystal size/mm^3	0.585 × 0.19 × 0.146
Radiation	MoKα (λ = 0.71073)
2Θ range for data collection/°	4.238 to 57.998
Index ranges	-12 ≤ h ≤ 12, -44 ≤ k ≤ 44, -16 ≤ l ≤ 16
Reflections collected	69654
Independent reflections	18393 [R_{int} = 0.0656, R_{sigma} = 0.0630]
Data/restraints/parameters	18393/73/866
Goodness-of-fit on F^2	1.048
Final R indexes [I>=2σ (I)]	R_1 = 0.0546, wR_2 = 0.1232
Final R indexes [all data]	R_1 = 0.0667, wR_2 = 0.1296
Largest diff. peak/hole / e Å^{-3}	1.27/-1.23
Flack parameter	0.24(3)

Table 7.13: Crystallographic information for Form VI of I-TPI.

Crystallisation conditions	Sublimation at 250 °C
Empirical formula	$C_{21}H_{15}IN_2$
Formula weight	422.25
Temperature/K	120
Crystal system	triclinic
Space group	P-1
a/Å	8.9006(8)
b/Å	11.9043(11)
c/Å	33.334(3)
α/°	81.404(3)
β/°	82.994(3)
γ/°	85.467(3)
Volume/Å^3	3459.5(5)
Z	8
ρ_{calc} g/cm^3	1.621
μ /mm^{-1}	1.855
F(000)	1664.0
Crystal size/mm^3	0.979 × 0.078 × 0.058
Radiation	MoKα (λ = 0.71073)
2Θ range for data collection/°	3.97 to 58
Index ranges	-12 ≤ h ≤ 12, -16 ≤ k ≤ 16, -45 ≤ l ≤ 45
Reflections collected	63290
Independent reflections	18359 [R_{int} = 0.1075, R_{sigma} = 0.1339]
Data/restraints/parameters	18359/21/866
Goodness-of-fit on F^2	1.038
Final R indexes [I>=2σ (I)]	R_1 = 0.0785, wR_2 = 0.1705
Final R indexes [all data]	R_1 = 0.1333, wR_2 = 0.1903
Largest diff. peak/hole / e Å^{-3}	5.24/-1.29